

Stony Brook University



OFFICIAL COPY

The official electronic file of this thesis or dissertation is maintained by the University Libraries on behalf of The Graduate School at Stony Brook University.

© All Rights Reserved by Author.

Design and Preparation of Polydiacetylenes Using Supramolecular Chemistry

A Dissertation Presented

by

Bo Liu

to

The Graduate School

in Partial Fulfillment of the

Requirements

for the Degree of

Doctor of Philosophy

in

Chemistry

Stony Brook University

August 2013

Stony Brook University

The Graduate School

Bo Liu

We, the dissertation committee for the above candidate for the
Doctor of Philosophy degree, hereby recommend
acceptance of this dissertation.

**Prof. Frank W. Fowler – Dissertation Advisor
Professor, Chemistry**

**Prof. Joseph W. Lauher – Dissertation Advisor
Professor, Chemistry**

**Prof. Nancy S. Goroff – Chairperson of Defense
Professor, Chemistry**

**Prof. Jonathan G. Rudick – Third Member
Professor, Chemistry**

**Dr. Sung Won Kim – Outside Member
Head of Radiotracer Chemistry and Translation
Brookhaven National Laboratory**

This dissertation is accepted by the Graduate School

Charles Taber
Interim Dean of the Graduate School

Abstract of the Dissertation

Design and Preparation of Polydiacetylenes Using Supramolecular Chemistry

by

Bo Liu

Doctor of Philosophy

in

Chemistry

Stony Brook University

2013

This dissertation is focused on the polymerization of diacetylenes through a single-crystal-to-single-crystal transition, which requires a prearrangement of the diacetylene monomers in space. In the first project, we developed a supramolecular host-guest strategy to control the interactions among monomers. The host *N,N'*-oxalyldiglycine and the guest hexa-2,4-diyne-1,6-diyl dinicotinate have been synthesized and characterized. Their polydiacetylenic co-crystal structure has been revealed by single crystal X-ray diffraction. The decomposition of the co-crystal polymer, which could lead to a new polymer, has also been investigated by various characterization methods. The second project of this research is the development of a general strategy for synthesizing supramolecular organic nanotubes via a macrocyclic architecture. A series of macrocyclic diacetylene monomers with different functional groups have been designed and synthesized successfully. Extensive studies have focused on the enhancement of their stability and solubility. The correct packing of the macrocycles has been achieved via π - π stacking. We have obtained the desired tubular structures as shown in the crystal structures. Finally, studies on the effects of hydrogen bonding for the formation of crystal structures have also been explored.

This dissertation is dedicated to my parents:

Kegang Liu and Qiong Liu

Table of Contents

List of Figures	vii
List of Schemes	xi
List of Tables.....	xiii
List of Abbreviations.....	xiv

Chapter One. Introduction

1.1 Supramolecular Chemistry	1
1.2 Strategies in Supramolecular Synthesis.....	3
1.2.1 Self-assembly	3
1.2.2 Host-guest chemistry	6
1.3 Crystal Engineering.....	8
1.3.1 Topochemical polymerization – Application of crystal engineering.....	10
1.4 Hydrogen Bond	13

Chapter Two. Topochemical polymerization of diacetylenic co-crystals – Application of host-guest strategy

2.1 Introduction	17
2.1.1 Preorganization of diacetylenes.....	19
2.1.2 The oxalamide host.....	23
2.1.3 Pyridine-carboxylic acid hydrogen bond.....	25
2.2 Supramolecular design	28
2.3 Molecular Synthesis	29
2.3.1 Guest molecule	29
2.3.2 Host molecule.....	32
2.3.3 Co-crystal	33
2.4 Decomposition Study of the polymerized co-crystals.	36
2.5 Conclusion.....	43

Chapter Three. Design and preparation of macrocyclic diacetylenes toward organic nanotubes

3.1 Introduction	45
3.1.1 Macrocycle.....	45
3.1.2 Diacetylenic macrocycles and their design.....	49
3.1.3 Covalent bonded tubular structures	52

3.2 Research Goal.....	59
3.3 Synthetic methods of macrocycles	61
3.3.1 Background	61
3.3.2 The designed synthetic route to diacetylene macrocycles	63
3.4 Results and Discussion	65
3.4.1 Macrocycles containing ester substituents.....	65
3.4.2 Macrocycles containing amide substituents	77
3.4.3 Macrocycles containing carbamate substituents	79
3.4.4 Macrocycles containing benzoate substituents	82
3.4.5 Macrocycles containing cinnamate substituents.....	84
3.5 General Discussion.....	85
3.5.1 Synthesis.....	85
3.5.2 Solubility	86
3.5.3 Stability	86
3.5.4 Intramolecular self-cyclization	87
3.6 Conclusion.....	92

Chapter Four. Hydrogen bonding in crystal engineering

4.1 Background	95
4.2 A Cambridge Structure Database Survey	99
4.3 Research Goal.....	110
4.4 Synthesis and Structural Analysis	111
4.5 Conclusion.....	122

Chapter Five. Experimental Section

5.1 General Information	124
5.2 Synthesis.....	127

Bibliography	138
---------------------------	------------

Appendix 1. Molecular Structure and Crystallography Data.....	145
Appendix 2. NMR Spectra	208

List of Figures

Figure 1.1. The Waston-Crick base pairs.....	4
Figure 1.2. Preparation of thiol-stabilized gold nanoparticles in water.....	5
Figure 1.3. The host-guest complex between Mg^{2+} and chlorophyll used in oxygenic photosynthesis.....	6
Figure 1.4. A stable host-guest complex formed from the hard acid potassium ion and hard base 18-crown-6 ether.....	7
Figure 1.5. The topochemical cycloaddition of trans-cinnamic acid.....	11
Figure 1.6. The topochemical polymerization of diacetylenes.....	11
Figure 1.7. Alignment of diacetylene guests with oxalamide hosts to achieve the topochemical polymerization.....	13
Figure 1.8. Different hydrogen bond types.....	14
Figure 1.9. π -facial interactions: Examples of weak hydrogen bonds.....	15
Figure 1.10. Different supramolecular structures formed from carboxylic acids.....	16
Figure 2.1. Photopolymerization of 2,5-distyrylpyrazine.....	18
Figure 2.2. Structures of diradicals and dicarbenes theorized to be involved in the topochemical polymerization of diacetylenes.....	19
Figure 2.3. Examples of diacetylene derivatives for topochemical polymerization.....	21
Figure 2.4. The co-crystal built from 4,4'-bipyridyl diacetylene and ureylene dicarboxylic acid.....	23
Figure 2.5. A library of hydrogen bonding host molecules.....	24
Figure 2.6. Co-crystal formed from 6-phenyl-2-amino-4(1H)-pyrimidone and adipic acid.....	27
Figure 2.7. Crystal Structure of hexa-2,4-diyne-1,6-diyl dinicotinate.....	31
Figure 2.8. The structure of co-crystal 3	34
Figure 2.9. Host removal by using saturated $NaHCO_3$ solution.....	37
Figure 2.10. Sublimation of nicotinic acid from the pure diacetylene.....	39
Figure 2.11. Thermogravimetric analysis of the polydiacetylene with a heating rate of $10\text{ }^\circ\text{C}/\text{min}$ under dried nitrogen gas atmosphere.....	40

Figure 2.12. IR spectra. Red: polymerized co-crystal 3 ; Blue: pure polydiacetylene; Black: residue after sublimation of nicotinic acids.....	41
Figure 2.13. Raman spectrum of the black residue.....	42
Figure 2.14. A plausible structure of the black residue with a repeat unit C_6H_2	43
Figure 3.1. Candidates that show different affinity to metals.....	46
Figure 3.2. Different types of macrocycles.....	46
Figure 3.3. Schematic representation of (a) the solution aggregation of hexakis(phenylacetylene) macrocycles and (b) columnar hexagonal order exhibited by hexakis(phenylacetylene) macrocyclic mesogens.....	48
Figure 3.4. The chemical structure and X-ray structure of ivorenolide A.....	49
Figure 3.5. The synthesized acetylenic macrocycles with different substituents.....	50
Figure 3.6. Macrocycles that contain acetylene functionality show self-aggregation capability.....	50
Figure 3.7. The structure of the designed macrocycle containing diacetylenes.....	51
Figure 3.8. Chemical structure of the liquid crystalline “crowned” phthalocyanine.....	52
Figure 3.9. The structure of properly substituted phthalocyanines.....	54
Figure 3.10. Macrocycle 4 containing diacetylene and pyridine functionalities.....	55
Figure 3.11. Macrocycles 5 and 6 that featuring π - π stacking.....	56
Figure 3.12. A plausible copper-diether coordination complex in Hay coupling.....	57
Figure 3.13. Observed molecular stacking of macrocycle 6 and the structure of polymer obtained by slow annealing.....	57
Figure 3.14. The structure of the designed macrocycle for topochemical polymerization.....	58
Figure 3.15. The diacetylene macrocycle that self-assembles into columns via amide hydrogen bonds.....	59
Figure 3.16. The X-ray crystal structure of macrocycle 11 . A single tubular structure oriented by π - π stacking. Side View.....	69
Figure 3.17. The X-ray crystal structure of macrocycle 11 . Top view.....	70
Figure 3.18. The X-ray crystal structure of compound 21 . Side view.....	74
Figure 3.19. The X-ray crystal structure of compound 21 . Top view.....	75
Figure 3.20. The X-ray crystal structure of compound 15 . Side view.....	76
Figure 3.21. The X-ray crystal structure of compound 15 . Top view.....	76

Figure 3.22. The X-ray crystal structure of macrocycle 39 . Top view.....	83
Figure 3.23. The X-ray crystal structure of macrocycle 39 . Side View. π - π interaction.....	84
Figure 3.24. ^1H NMR studies.....	88
Figure 4.1. A hydrogen bond formed from a pyridinium and a carboxylate.....	98
Figure 4.2. A hydrogen bond formed from a pyridine and a carboxylic acid.....	98
Figure 4.3. Crystal structure of EJUNON.....	101
Figure 4.4. Crystal structure of BAPHOQ.....	101
Figure 4.5. Crystal structure of BAPHIK.....	102
Figure 4.6. Crystal structure of XOLCEG.....	102
Figure 4.7. Crystal structure of QIBSEZ.....	103
Figure 4.8. Crystal structure of ISOREN.....	103
Figure 4.9. Crystal structure of QARBIU.....	104
Figure 4.10. Crystal structure of HOFLIY.....	104
Figure 4.11. An example of hydrogen bonding between 1,4-diazabicyclo[2,2,2]octane and carboxylic acids.....	105
Figure 4.12. Crystal structure of APAKOS.....	106
Figure 4.13. Crystal structure of CEJLUZ.....	106
Figure 4.14. Crystal structure of CEJMEK.....	107
Figure 4.15. Crystal structure of DEBALB.....	107
Figure 4.16. Crystal structure of NATGOF.....	108
Figure 4.17. Crystal structure of RIRSEQ.....	108
Figure 4.18. Crystal structure of XUBWEW.....	109
Figure 4.19. Crystal structure of DMANAC.....	110
Figure 4.20. Crystal structure of IDUVAF.....	112
Figure 4.21. Crystal structure of ALEDIE.....	112
Figure 4.22. Crystal structure of compound 46	114
Figure 4.23. Co-crystal structure of 47 , the hydrate of compound 46 and 2- <i>p</i> -tolylacetic acid.....	116
Figure 4.24. Co-crystal structure of 47 . Top view.....	117

Figure 4.25. Co-crystal structure of **48**. A co-crystal from protonated compound **46**, sebacic acid and deprotonated sebacic acid.....120

Figure 4.26. Co-crystal structure of **48**. The network structure.....121

List of Schemes

Scheme 2.1. Reaction scheme for the single-crystal-to-single-crystal [2+2] photo-dimerization of 2,4-dihydroxy-benzaldehyde and 1,4-bis[(E)-2-(4-pyridyl)-ethenyl]-2-fluorobenzene.....	25
Scheme 2.2. The candidates that used to form co-crystals via N···H–O hydrogen bonds.....	26
Scheme 2.3. The preparation of hexa-2,4-diyne-1,6-diyl dinicotinate (1)	30
Scheme 2.4. The preparation of hexa-2,4-diyne-1,6-diyl dinicotinate (2)	30
Scheme 2.5. The preparation of <i>N,N'</i> -oxalyldiglycine.....	32
Scheme 3.1. The synthesis of macrocycle 5	56
Scheme 3.2. The planned topochemical polymerization among the macrocycles.....	61
Scheme 3.3. Diacetylene synthesis.....	62
Scheme 3.4. Synthesis of the macrocycle using Hay coupling.....	62
Scheme 3.5. A suggested synthetic route toward macrocycles.....	63
Scheme 3.6. Synthetic routes of macrocycles containing different functional groups.....	64
Scheme 3.7. Synthesis of macrocycle 11	65
Scheme 3.8. The formation of monomer and dimer macrocycles.....	66
Scheme 3.9. Alternate synthetic route to macrocycle 11	68
Scheme 3.10. Macrocycle candidates with modified ester functional groups.....	71
Scheme 3.11. Synthesis of macrocycles containing glycolic segments.....	72
Scheme 3.12. The separation of monomer, linear dimer, cyclic dimer, and linear trimer in a macrocycle synthesis.....	73
Scheme 3.13. Macrocycle candidates with amide functional groups.....	78
Scheme 3.14. Synthesis of macrocycles containing amides functional groups.....	79
Scheme 3.15. Reduction of ester functional group to primary alcohol.....	80
Scheme 3.16. Synthesis of macrocycles containing carbamate functional groups.....	81
Scheme 3.17. Synthesis of macrocycles containing benzoate functional groups.....	82
Scheme 3.18. Synthesis of macrocycle containing cinnamate functional groups.....	85

Scheme 3.19. The planned host-guest strategy for macrocycle assembly.....	90
Scheme 3.20. An unsuccessful attempt for the hydrolysis of macrocycle 11	91
Scheme 3.21. The designed synthesis toward macrocycle 44	92
Scheme 4.1. Two types of hydrogen bonding.....	96
Scheme 4.2. Synthesis of compound 46	113
Scheme 4.3. Co-crystal growth from compound 46 and phenol or hydroquinone.....	123

List of Tables

Table 2.1. Crystal parameters of the monomer crystal and the polymer crystal.....	35
Table 2.2. The quantitative study of removing host oxalamides.....	37
Table 3.1. The effect of concentration to the yields of macrocycles.....	67
Table 3.2. Chemical shifts of protons in the methylene groups in macrocycles.....	89
Table 4.1. Co-crystal growth from compound 46 and carboxylic acids.....	115
Table 4.2. Co-crystal growth from compound 46 and symmetrical carboxylic acids.....	119

List of Abbreviations

Å	angstrom
AFM	Atomic Force Microscopy
CSD	Cambridge Structural Database
d	repeat distance
DCC	<i>N,N'</i> -dicyclohexylcarbodiimide
DMAP	4-dimethylaminopyridine
DSC	Differential Scanning Calorimetry
ESR	Electron Spin Resonance
IR	Infrared
MS	Mass Spectrometry
NBS	<i>N</i> -bromosuccinimide
NMR	Nuclear Magnetic Resonance
PDA	polydiacetylene
SAM	self-assembled monolayer
SPM	shape-persistent macrocycle
STM	Scanning Tunneling Microscopy
TEA	triethylamine
TGA	Thermogravimetric Analysis
THF	tetrahydrofuran
TLC	Thin Layer Chromatography
TMEDA	<i>N,N'</i> -tetramethylethylenediamine
TMS	trimethylsilyl
XRD	X-ray diffraction
γ	declination angle

Chapter One

Introduction

1.1 Supramolecular Chemistry

For a long time in chemistry history, organic chemists were focused on the molecular level of materials. It was not until the last quarter of the 20th Century that chemists became aware of the chemical environment “beyond the molecule”, in another words, *supramolecular chemistry*.¹ The so-called “supermolecule”, the subject of study in supramolecular chemistry, is an aggregate that is held together by non-covalent interactions among covalent molecules or ions. The overall goal of supramolecular chemistry is to gain control over the intermolecular non-covalent bond. In the past few decades, tremendous efforts have been made on the study of the assemblies, aggregates, and arrays of molecules.

Supramolecular chemistry is highly multidisciplinary. Traditional organic and inorganic chemistry, involving the preparation of molecular structures, are the fundamentals of supramolecular chemistry. Physical chemistry is used in characterization, helping us understand the properties of supramolecular systems. In recent years, computational modeling has played a more important role in understanding supramolecular behavior. As the size of a typical supramolecular structure is on the nanoscale, the development of nanotechnology is ideal for the study of supramolecular chemistry. Last but not least, supramolecular chemistry deals with many biological processes or functions, such as the assembly of a double-stranded DNA helix, the

conformation of proteins, and catalysis by enzymes. Because supramolecular chemistry involves chemistry, biology and material science, it can be very useful for exploiting the structure-function relationship of materials. Many different types of supramolecular structures have been synthesized, which include cyclodextrins², micelles³, vesicles⁴, dendrimers⁵, liquid crystals⁶, and cocrystals.⁷

An important goal of supramolecular chemistry is the preparation of new materials with novel functionalities. Pioneering supramolecular chemists tried to mimic the highly efficient behavior that chemistry has achieved in nature, such as DNA replication and enzyme catalysis. Designing new and unnatural molecules that have similar functionalities is the key to success. As a consequence, supramolecular chemists are able to prepare sensors⁸⁻¹⁰, medicines¹¹, and imaging devices¹², many of which have widespread use today.

It is apparent that the physical, chemical, and biological properties of materials rely on both the nature of the molecular structures and their relative orientations. The relative orientation depends on supramolecular chemistry. Therefore, the preparation of an unknown material must consider both molecular and supramolecular synthesis.

Supramolecular chemistry involves many different non-covalent interactions, such as van der Waals interactions, hydrogen bonding, dispersion interactions and π - π stacking¹³. It remains very difficult to predict the supramolecular structure for a given molecule.

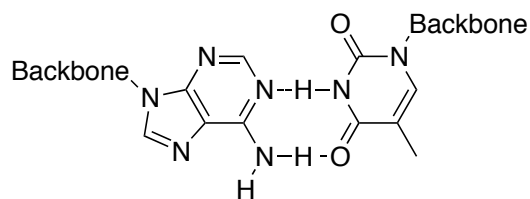
1.2 Strategies in Supramolecular Synthesis

Despite of these difficulties, there are a few strategies that have been developed for the construction of supramolecular systems. In general, they can be split into two broad categories: *self-assembly* and *host-guest chemistry*.

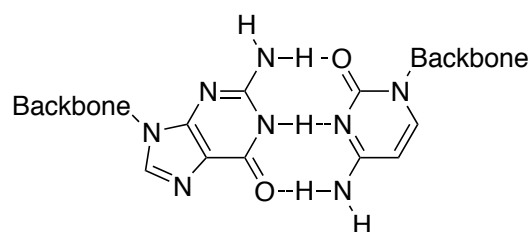
1.2.1 Self-assembly

Under certain conditions, simple molecules with complementary functionalities may interact with one another to form more complex supramolecular structures, held together by non-covalent interactions. This is called the process of self-assembly. Self-assembly means the spontaneous combination of two or more molecules to create a larger aggregate species through some sort of supramolecular interactions. This concept is employed broadly in biochemistry and nanoscience.

Many examples of such processes are found in nature. For instance, the nucleotides of DNA possess all the necessary structural information needed for the self-assembly of a double-stranded DNA helix. The four nucleotides (adenine (A), cytosine (C), guanine (G) and thymine (T)) form two complementary hydrogen bonded pairs, i.e. the Watson-Crick base pairs (**Figure 1.1**), through the topology of the proton donors and proton acceptors of the nucleotides.¹⁴



Adenine-Thymine



Guanine-Cytosine

Figure 1.1. The Watson-Crick base pairs

The Watson-Crick base pairing between the nucleotides leads to the double-helical structure via hydrogen bonds, π - π stacking, and the hydrophobic effect in a self-assembly process. The strands recognize each other, join together, and eventually provide the basis of the genetic code.

In nanoscience, self-assembly is also widely used to form ordered two-dimensional monolayers or even three-dimensional structures.¹⁵ It is achieved by chemisorption of appropriately functionalized molecules onto certain templates or substrate surfaces. The resulting stable, ordered layers could have many applications in sensors, anti-corrosion and wear protection.

As the term *self*-assembly implies, chemists have no direct control over the assembly process. However, it is possible to make intelligent decisions and synthesize appropriate

molecules that may interact well with one another. By studying the existing chemistry, scientists know that certain functional groups or metals have preferences for binding in certain ways. These preferences are often considered to guide the assembly processes.

Self-assembling of thiols on gold surfaces is a typical example in the early work. The thiol-gold interaction has approximately the strength of a hydrogen bond, which stabilizes the self-assembly process. The approach to preparing thiol-gold self-assembled monolayers (SAMs) is relatively simple. A clean substrate with reactive surfaces is immersed into a solution of the coating molecules. Over time, the coating molecules are chemisorbed to the surface and slowly self-assembled to give a stable, ordered monolayer¹⁶ (**Figure 1.2**). Many ionic sensors and nanochemical devices have originated from such studies.¹⁷

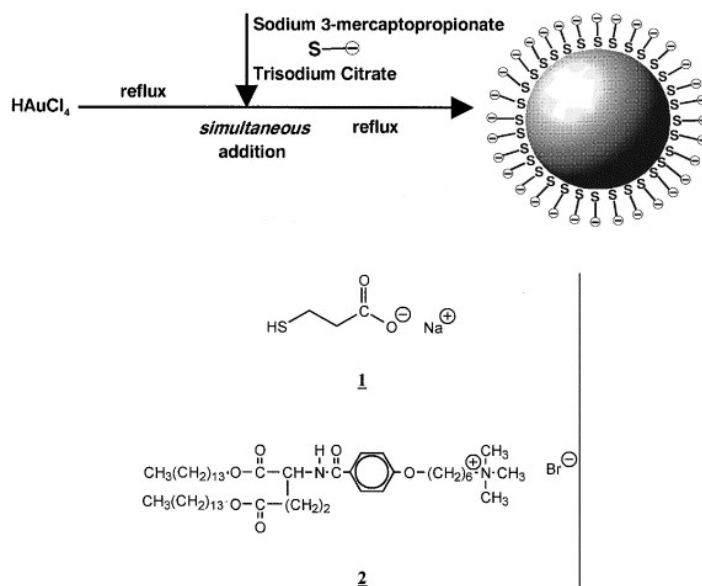


Figure 1.2. Preparation of thiol-stabilized gold nanoparticles in water. Reprinted with permission from Ref. 16. Copyright 2004 American Chemical Society.

1.2.2 Host-guest chemistry

Host-guest chemistry is the study of large “host” molecules that are capable of enclosing smaller “guest” molecules via non-covalent interactions. For a host-guest interaction to occur, the host molecules must have appropriate functional groups, i.e. binding sites for the guest molecules to bind to. Size, geometry and chemical nature all play important roles in host-guest chemistry.

Like the self-assembly process, host-guest interaction also occurs frequently in biological systems. For example, enzymes and their substrates are perfect pairs, with enzymes being the host and the substrates the guest. Metal-ligand complexes can also be considered as host-guest species, with ligands act as hosts for metal cations (**Figure 1.3**).

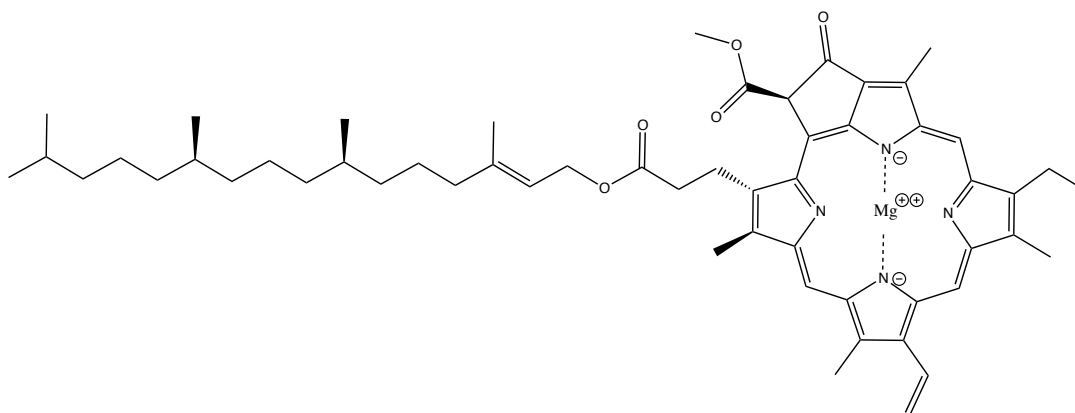


Figure 1.3. The host-guest complex between Mg^{2+} and chlorophyll used in oxygenic photosynthesis.

On the other hand, unlike self-assembly, the host-guest chemistry is much stricter quantitatively. If the host has hydrogen-bond donor functionalities then the guest better contain

an equal number of hydrogen-bond acceptor sites, which allow for multiple interactions between host and guest.

Complementarity is essential in host-guest chemistry. Though an enzyme is generally much larger than its corresponding substrate, only a small percentage of the overall structure, known as the active site of the enzyme, is involved in the binding. In order to recognize each other, host and guest molecules must match in size, shape, conformation and chemical properties.

For example, Lewis acids and bases are used to form complexes via the donation of electron pairs. In terms of the polarizability of the electron density, the acids and bases can either be hard or soft, according to the Lewis theory of acids and bases.¹⁸ Hard acids/bases are non-polarizable while soft acids/bases are easily polarizable. The empirical rule shows that hard-to-hard and soft-to-soft acid-base complexes are stable.¹⁹

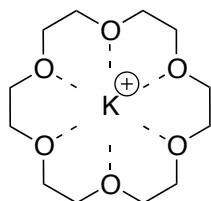


Figure 1.4. A stable host-guest complex formed from the hard acid potassium ion and hard base 18-crown-6 ether

Compared to the traditional organic or inorganic synthesis of the desired molecular components by the formation of strong covalent bonds, supramolecular synthesis consists of one

additional step, which is the association of these components. An ideal supramolecular design depends on the chemical insight of molecular functionalities that could predictably lead to specific favorable intermolecular interactions. However, designs that are reasonable in theory may not be achieved in reality. In some occasions it is simply because of the lack of symmetry requirements in a crystal.

As a rapidly growing field, supramolecular chemistry attracted tremendous attention in the past decades. Complicated architectures can be generated from the weak intermolecular interactions. Consequently, many specialized experimental analytical technologies were developed to apply to the study of supramolecular systems. Diffusion NMR, photophysics and photochemistry, circular dichroism spectroscopy, crystallography, and material science such as Scanning Tunneling Microscopy (STM) and Atomic Force Microscopy (AFM) are all used in the determination of supramolecular structures.

Among all the analytical methods, X-ray crystallography is generally recognized as the most powerful tool for the detailed structural analysis of crystalline supramolecular structures.

1.3 Crystal Engineering

Though a few decades ago a single crystal X-ray diffraction study of a crystal was considered to be very strenuous and time-consuming work performed only by experienced crystallographers, it is now generally accepted as a routine analytical tool for structural analysis. The speed and ease of X-ray diffraction data collection and processing have improved remarkably with the fast development of computing power of personal computers and

development of CCD detectors. Faster computers also speed up the structure solution and refinement. For these reasons even complicated crystal structures can be solved in a reasonable time. Within the development of supramolecular chemistry and crystallographic techniques, a new research area called *Crystal Engineering* was born.

In 1971, the term *Crystal Engineering* was used by G.M.J. Schmidt for the first time in a scientific paper.²⁰ The article postulated that under proper conditions, molecular recognition events, like self-assembly, could be the major factor leading to crystal formation. Since then, a large number of crystal engineering research papers have been published.

Due to the weak intermolecular interactions among the molecules, the formation and growth of a crystal lattice is often a very complex phenomenon. Many issues, such as molecular kinetics, thermal motion, diffusion, adsorption, absorption and viscosity, can affect the crystallization processes. Though most of the conditions leading to crystal growth, *e.g.* temperature and concentrations, can be controlled and monitored, the formation of a good crystal still remains unpredictable.

Crystal engineering involves design and preparation of crystalline materials utilizing supramolecular interactions. For crystal engineering, a careful analysis of the desired supramolecular structures needs to be conducted prior to the traditional synthesis. It is not the same as crystal structure prediction, which is generally considered as a theoretical route to determining crystal symmetry and packing styles for a given molecule. Crystal engineering relies on systematic studies of known structures and thorough understanding of intermolecular interactions. It offers almost unlimited possibilities to successful production of a good quality crystal. It has become a general strategy for the preparation of supramolecular structures.

Both self-assembly and host-guest chemistry, the strategies in supramolecular synthesis, have been widely used in crystal engineering. In many cases they work together, as the design of host-guest chemistry helps the molecules self-assemble in crystals.

1.3.1 Topochemical polymerization – application of crystal engineering

A reaction that occurs under the influence and control of an organized condensed medium is known as a topochemical reaction. The reactivity of molecules in condensed media such as crystals or liquid crystals sometimes appears to be very different from that observed in solution or gas phases. Only reactions that require a minimum of atomic and molecular motion are possible. Topochemical reactions usually possess three characteristics: high regioselectivity, high chemoselectivity, and high stereoselectivity.

A typical topochemical reaction example is the photo-cycloaddition of the crystalline forms of trans-cinnamic acid (**Figure 1.5**), which has been studied for more than a century. There are three different crystalline forms for trans-cinnamic acid, which were called α , β , and γ forms, respectively. In the α and β forms, the double bonds of neighboring cinnamic acids are parallel to each other. The small intermolecular spacing is ideal for the [2+2] cycloaddition.²⁰ The reactive centers in the α and β forms are 3.6-4.1 Å and 3.9-4.1 Å apart, respectively. The photo-cycloaddition occurred in these two forms while not in the γ form because the reactive centers in the γ form are around 4.7-5.1 Å apart, which are too far away.

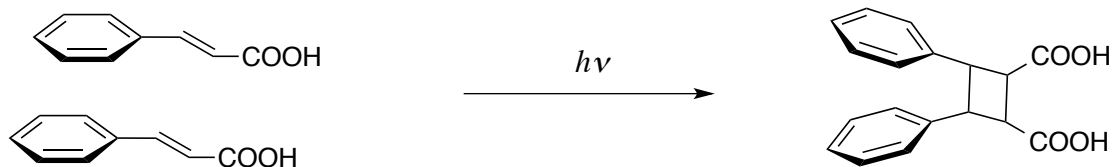


Figure 1.5. The topochemical cycloaddition of trans-cinnamic acid

An attractive application of the topochemical reaction is the topochemically-controlled polymerization of diacetylenes (**Figure 1.6**). This is the focus of our work. The polymerization generates the all-*trans* polydiacetylene polymer via C1-C4 addition between neighboring diacetylene molecules.

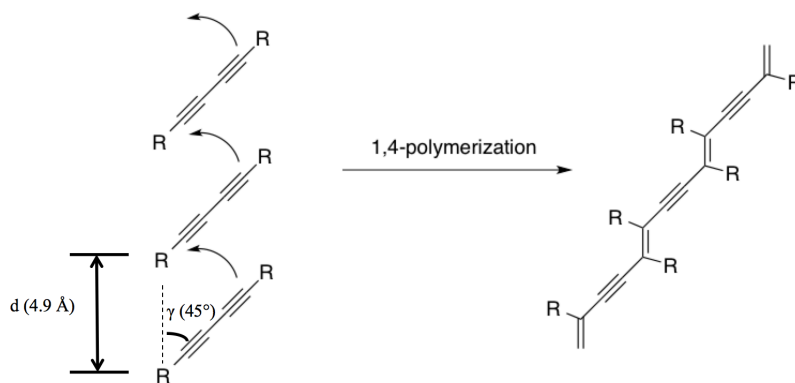


Figure 1.6. The topochemical polymerization of diacetylenes

The generated polymer has a fully conjugated all-carbon backbone, which has been of interest to material scientists as a potential organic optical and electrical conductor. Because of the necessity of controlling the orientation of the precursors, the reaction occurs only in the solid-state. Studies show that the optimal spacing between the neighboring diacetylenes is $\sim 5 \text{ \AA}$.²¹

Moreover, the reactive centers, C1 and C4, are spaced at $\sim 3.5 \text{ \AA}$ and the angle between the stacking axis and the diacetylene chain (γ) should be $\sim 45^\circ$. When the diacetylene functionalities are properly aligned, polymerization can be induced by thermal annealing or high-energy radiation.

A few strategies have been developed for aligning the diacetylene monomers with a molecular repeat distance of $\sim 5 \text{ \AA}$. The *Self-assembly* method has been applied to the synthesis of polydiacetylenes²², while Langmuir-Blodgett films²³⁻²⁵ can also provide the ideal spacing for diacetylenes.

Despite the successful examples in the preparation of the polydiacetylene polymer, many problems remain. The approaches mentioned above rely mainly on the nature of specific diacetylenes. It is difficult to become a common strategy of producing polydiacetylenes, which dramatically limits their applications. In our work, we developed a more general approach for achieving the ideal aligning and spacing, by using a host-guest strategy and hydrogen bonding (**Figure 1.7**). This will be discussed in detail in the next chapter.

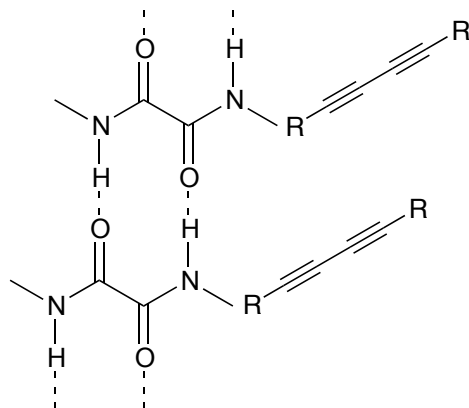


Figure 1.7. Alignment of diacetylene guests with oxalamide hosts to achieve the topochemical polymerization

1.4 Hydrogen Bond

One of the most prominent intermolecular forces that are used in supramolecular chemistry is hydrogen bonding, which is defined as a donor-acceptor interaction involving a hydrogen atom. It was first introduced in 1920 to help describe the internal structure of water. Since that time, the concept has been applied into other systems and has explained many chemical phenomena successfully. A general description is attractive coulombic interaction between a hydrogen atom bound to an electronegative atom D (donor) and another electronegative atom A (acceptor) with one or more pairs of nonbonding electrons.

The strength of a hydrogen bond is highly related to the electronegativity of the donor and acceptor. It can be categorized as strong, moderate, or weak. As indicated in the literature, the strength of a hydrogen bond varies 15-40 kcal/mol for strong interactions, 4-15 kcal/mol for moderate bonds and 1-4 kcal/mol for weak bonds,²⁶ all of which are much stronger than other intermolecular interactions, *e.g.* the van der Waal forces with strength of ~ 0.5 kcal/mol. The

strength of hydrogen bonds can be modified by the appropriate selection of acceptor and donor species. This characteristic makes the hydrogen bond ideal for use in supramolecular synthesis.

Hydrogen bonds can be categorized regarding to the arrangements.

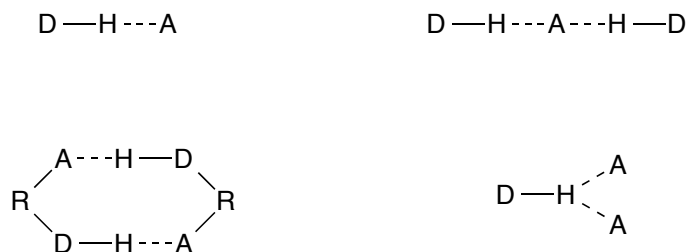


Figure 1.8. Different hydrogen bond types

Compared to other intermolecular interactions, an advantage of hydrogen bonding is that hydrogen bonds are highly oriented. In most cases, the acceptor, hydrogen atom and the donor are arranged linearly or slightly bent to achieve the thermodynamic stable conformation.

The most common hydrogen-bond donors are H atoms bonded to N, O, F, and Cl while acceptors include N, O, P, S, F, Cl, Br and I as well as alkenes, alkynes, aromatic π bonds and even transition metals. Weaker hydrogen bonds, as of the type $C-H \cdots A$ ($A = F, O, N, Cl, Br, I$) also play an important role in supramolecular chemistry. There are a large number of examples of the weak hydrogen bonds collected in the Cambridge Structural Database (CSD).

Another type of weak hydrogen bond involves π -facial interactions, as illustrated in **Figure 1.9**. Though interactions of this type are usually quite weak (1-5 kJ/mol),²⁷ they often act

in a co-operative way with other intermolecular interactions. For example, they help to establish a precise orientation within a given supramolecular structure.

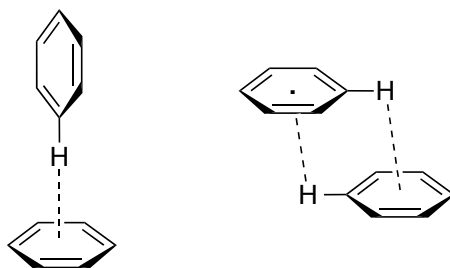


Figure 1.9. π -facial interactions: Examples of weak hydrogen bonds.

Compared to other intermolecular interactions, hydrogen bonding is of greatest interest because the relatively strong and directional properties lead to many possibilities for supramolecular synthesis. For example, carboxylic acids are common organic compounds that contain one hydrogen-bond donor group and one acceptor group. They are self-complementary as hydrogen-bond acceptor-donor pairs and are able to form different types of structures (**Figure 1.10**).

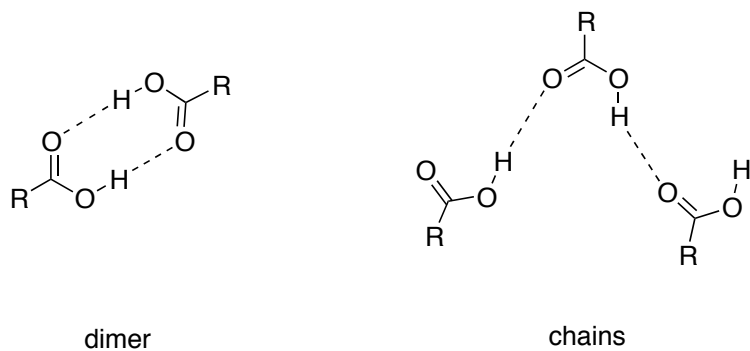


Figure 1.10. Different supramolecular structures formed from carboxylic acids

Amides have similar properties. Overall, due to the flexibility of strength and formation, the hydrogen bond is an ideal tool in supramolecular synthesis. It will be discussed throughout this dissertation.

Chapter Two

Topochemical polymerization of diacetylenic co-crystals – Application of a host-guest strategy

2.1 Introduction

Topochemical polymerization has been well known since the discovery of distyrylpyradine and diacetylene derivatives in the 1960s. In 1967, Wegner²⁸ and Hasegawa²⁹ discovered the thermal-induced topochemical polymerization of diacetylenes and dialkenes respectively, based on Schmidt's pioneering work on the dimerization of cinnamic acid by [2+2] photocycloaddition.^{20,30} In many cases, the topochemical polymerization occurs homogeneously by a single-crystal-to-single-crystal transformation, leading to pure and uniform products.

Conjugated diacetylenes or their derivatives undergo topochemical 1,4-addition polymerization mainly upon thermal annealing to give polydiacetylenes with alternating double and triple bonds. The reaction can be induced by exposure to UV radiation, γ -rays, or high pressure, as well.³¹ As the polymerization proceeds under crystal-lattice control, the resultant polymers are often single crystals, which are otherwise unlikely to be obtained by traditional routine synthesis. The topochemical polymerization appears to be one of the most powerful polymerization approaches in terms of controlling the polymer structure.

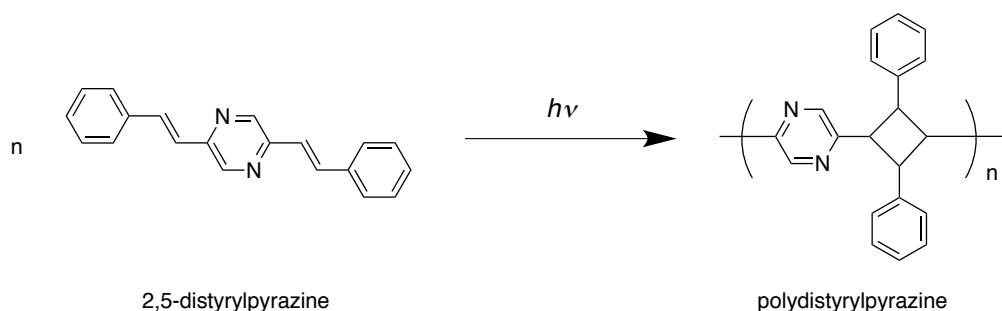


Figure 2.1. Photopolymerization of 2,5-distyrylpyrazine

In the topochemical polymerization of distyrylpyrazine (**Figure 2.1**), the addition of each repeating unit to the chain requires the absorption of a further photon, thus it should be called a stepwise process and not a chain reaction.³² The polymerization of diacetylenes on the other hand proceeds as a classical chain reaction by 1,4-addition, leading to alternating ene-yne polymer chains with all-*trans* selectivity. In general, in the diacetylene crystal, an excited diradical state with an unpaired electron at either end (**Figure 2.2**, left) is generated by thermal or photo treatment.³³ The diradicals (with electron spin $S = \frac{1}{2}$) then undergo thermal addition reactions with neighboring diacetylene moieties and eventually form the polymer.

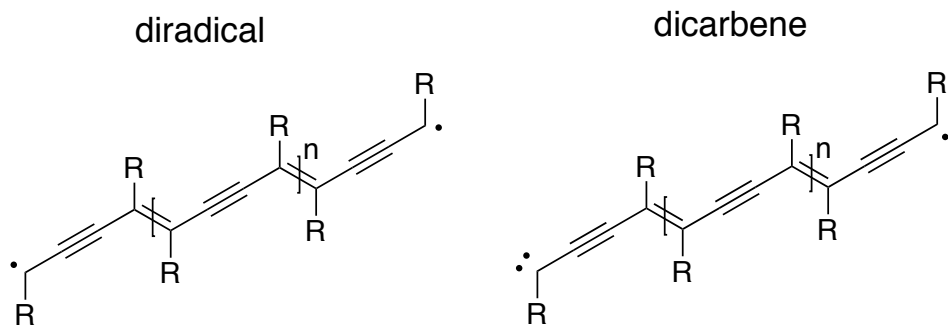


Figure 2.2. Structures of diradicals and dicarbenes theorized to be involved in the topochemical polymerization of diacetylenes.³⁴

It is worth noting that there is other experimental evidence (ESR) in the literature showing dicarbene species (with electron spin $S = 1$, **Figure 2.2**, right) are also involved in the polymerization process, when the chains are longer than seven repeating units.³⁴

Compared to the formation of colorless and nonconjugated polymers attained by the polymerization of dienes, diacetylene derivatives give colored, π -conjugated polymers. It is an exciting feature as a color change accompanies conformational change in conjugated polydiacetylenes, induced by environmental stimuli such as changes in temperature³⁵ or pH³⁶ or by mechanical stress.³⁷ This property has been exploited widely in the fabrication of many sensing devices.³⁸⁻⁴⁰

2.1.1 Preorganization of diacetylenes

Polymerization of diacetylenes in solution usually gives a mixture of 1,2- and 1,4- addition products, providing few applications in synthesis. However, the 1,4- polymerization of diacetylenes can occur successfully in the solid-state by controlling the orientation of the

precursors. It has been demonstrated that an essential prerequisite for the topochemical polymerization of diacetylenes is stacking of the diacetylene functionalities with a molecular repeat distance of $d = 4.7\sim 5.2 \text{ \AA}$ and a tilt angle of about 45° between the diacetylene axis and the packing axis.²⁸ These parameters ensure the minimum motion of atoms during the single-crystal-to-single-crystal polymerization transformation. To achieve defect-free polymer single crystals, the reactions are usually conducted under mild conditions, with a relatively slow rate.

As the spacing among the monomers is an absolute requirement for the polymerization to occur, one of the major difficulties appears to be the design and synthesis of diacetylene monomers. To satisfy the required parameters, the two substituents at either end of the diacetylene monomer should be selected carefully, as they to a large extent provide the spacing-control functionalities. **Figure 2.3** shows some of the successful candidate molecules that have been reported in the literature.

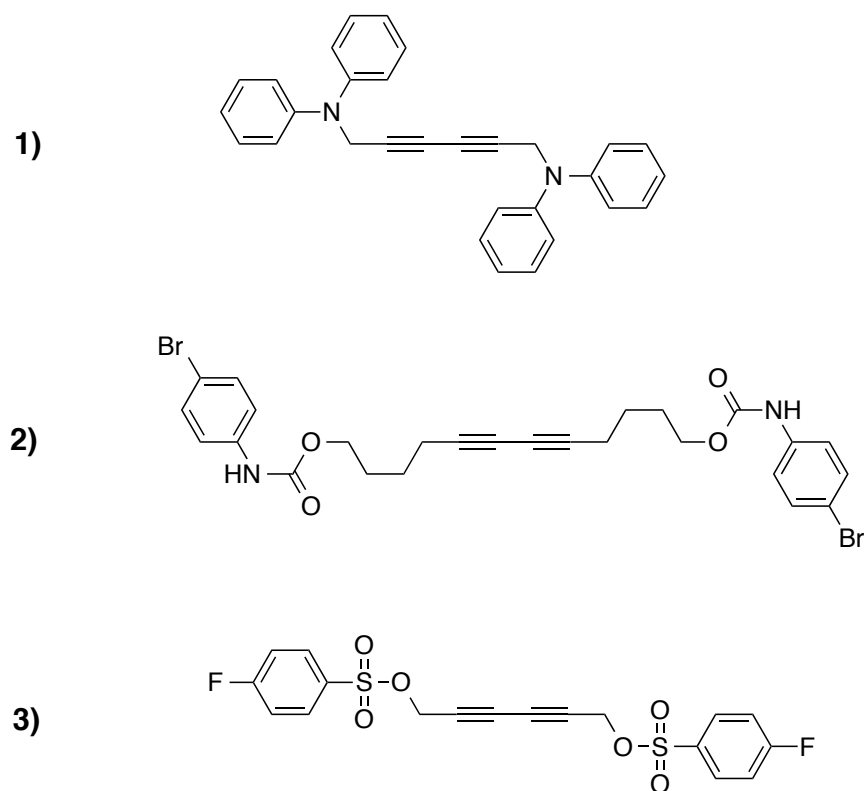


Figure 2.3. Examples of diacetylene derivatives for topochemical polymerization

1) 1,2-bis(diphenylaminomethyl)-1-but-1-en-3-ynylene,⁴¹

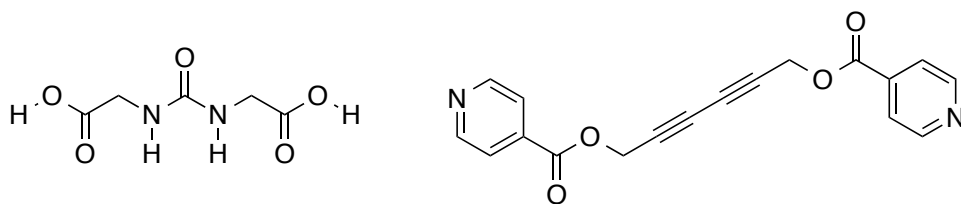
2) 1,2-(4-bis(*p*-bromophenylcarbamoyloxy)butyl)-1-butene-3-yne-ylene,⁴²

3) bis(*p*-fluorobenzenesulfonate)-2,4-hexadiynylene.⁴³

To prepare a diacetylene monomer that has the potential to undergo topochemical polymerization, the monomer cannot have bulky substituents, so the reactive centers can contact to each other within the right distance. In addition, the existence of flexible spacer units on the two sides of the monomer would help provide the necessary molecular flexibility required for the shearing motion of the topochemical polymerization.

An alternative way to pre-organize diacetylenes is to separate the spacing functionality and the diacetylene functionality by using host-guest chemistry. An advantage of this approach is the simplification of molecular synthesis, since the diacetylene functionality and the spacing functionality are divided into two different molecules.

The ureylene⁴⁴ and oxalamide⁴⁵ networks are able to provide the spacing functionality needed for topochemical polymerization. The co-crystal shown in **Figure 2.4** is an example that has been prepared and fully characterized.⁴⁶ The network in the co-crystal is formed through two different hydrogen bonds, which are the urea to urea and the pyridine-carboxylic acid hydrogen bonds. The host ureylene stacks in the crystal to form a network that provides the molecular repeat distance of 4.71 Å. The repeat distance is translated to the guest diacetylene molecule through a pyridine-carboxylic acid hydrogen bond. However, the spacing of 4.71 Å and oriented angle of 56.3° in the diacetylene arrays are not in accordance with the values needed for a successful polymerization.



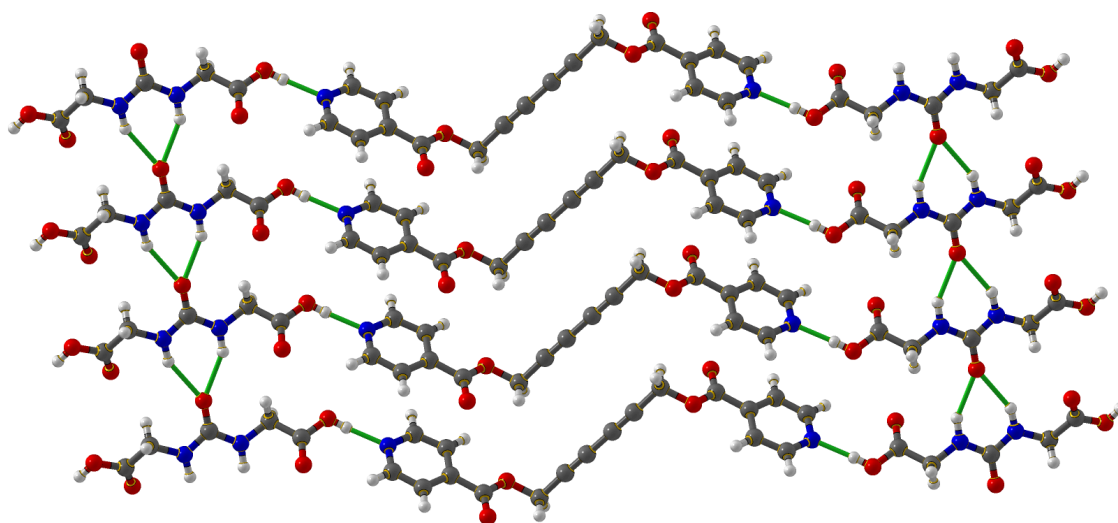


Figure 2.4. The co-crystal built from 4,4'-bipyridyl diacetylene and ureylene dicarboxylic acid⁴⁶

The crystal structure of the pure guest 4,4'-bipyridyl diacetylene has also been examined in the previous study.⁴⁷ Analysis shows that the C1 and C4 reactive centers in the crystal were spaced at 6.23 Å, which implies the incapability of topochemically-controlled polymerization.

2.1.2 The oxalamide host

The pioneering work conducted on ureylene presents a general strategy for controlling the topochemical reactions of diacetylenes, yet the spacing provided by ureylene network (~4.7 Å) is shorter than the optimal polymerization spacing of ~4.9 Å. To better match the desired 4.9 Å spacing, some other functional groups have been introduced and developed.

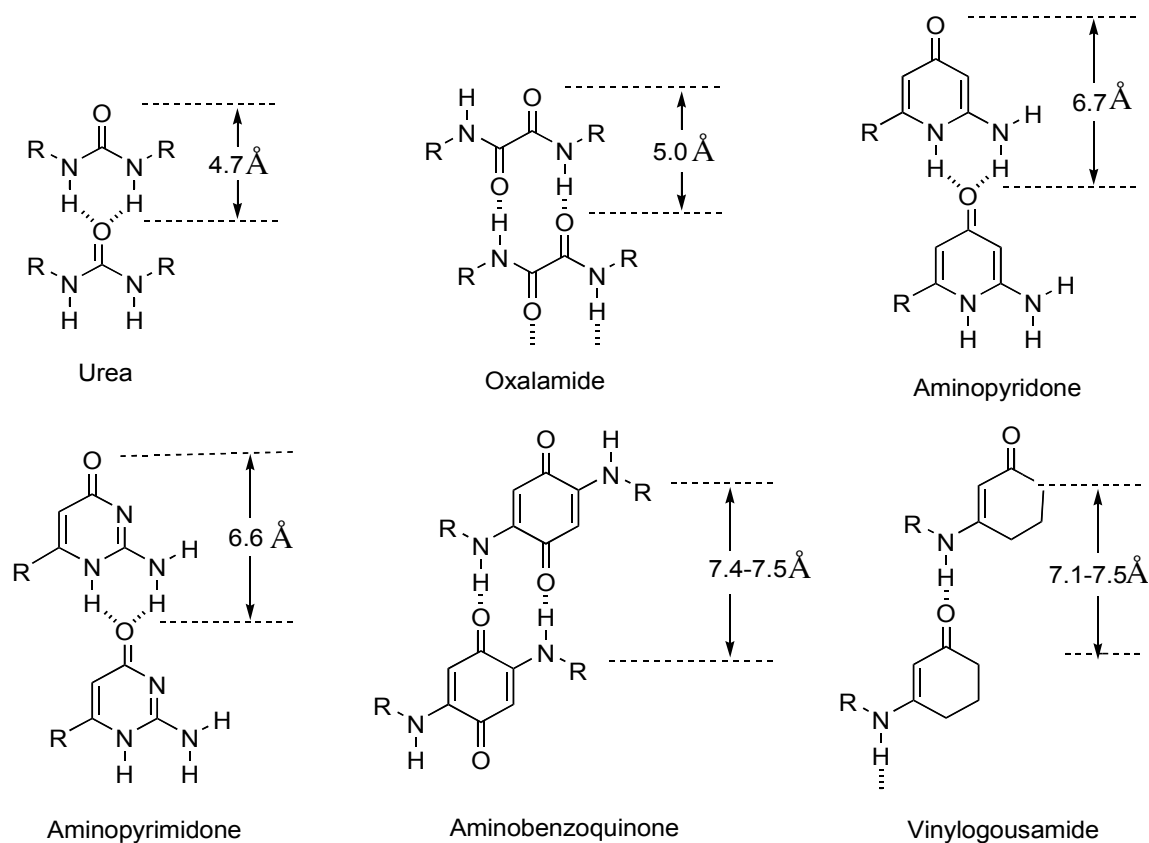


Figure 2.5. A library of hydrogen bonding host molecules^{44,48-50}

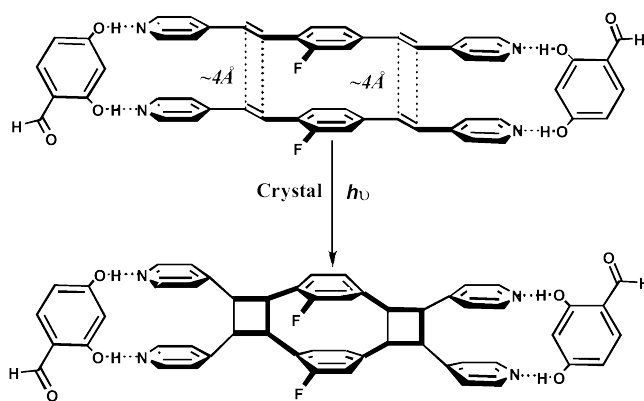
Lauher and Fowler studied a series of hydrogen bonded host molecules, as shown in **Figure 2.5**. Among these candidates, the oxalamide functionality was found to be a reliable unit that will self-assemble into a one-dimensional network via hydrogen bonds, with a repeat distance of about 5 Å. This spacing is consistent with the value required for topochemical polymerization of the diacetylene functionality.

2.1.3 Pyridine-carboxylic acid hydrogen bond

The key to the success of the host-guest strategy is to look for a reliable and predictable interaction between the host and the guest molecules. We have previously indicated in chapter one that the hydrogen bond is such an interaction. In particular, the $N\cdots H-O$ hydrogen bond is of greatest interest because it is strong enough to link the host and guest molecules, yet not so strong to reduce the flexibility and probability for constructing the host-guest network. It has proven to be persistent and could establish networks in crystals as well as discrete assemblies.

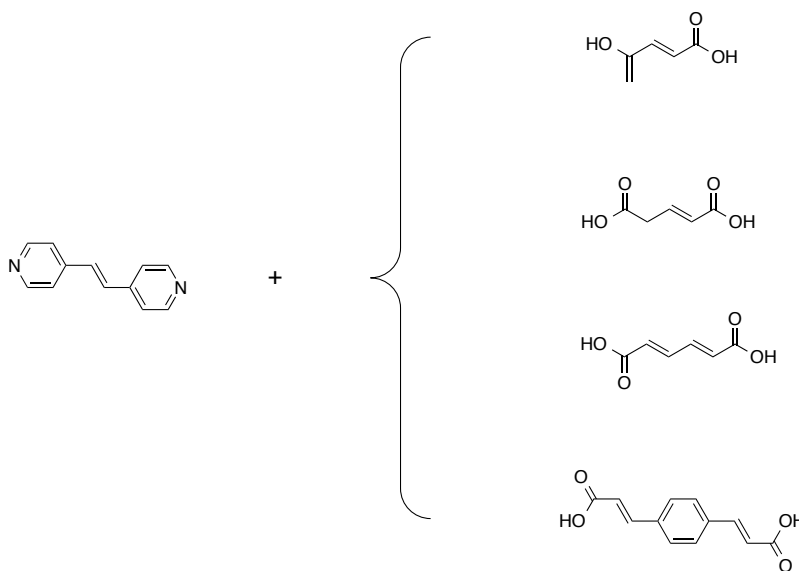
The pyridine-carboxylic acid hydrogen bond is one of the common $N\cdots H-O$ types. Brunklaus and co-workers⁵¹ used the $N\cdots H-O$ hydrogen bond to control the spacing between bipyridine derivatives. (**Scheme 2.1**) The single-crystal-to-single-crystal [2+2] photo-dimerization is successfully conducted in the co-crystals.

Scheme 2.1. Reaction scheme for the single-crystal-to-single-crystal [2+2] photo-dimerization of 2,4-dihydroxy-benzaldehyde and 1,4-bis[(E)-2-(4-pyridyl)-ethenyl]-2-fluorobenzene. Reprinted with permission from ref. 51. Copyright 2009 American Chemical Society.



Michaelides and co-workers reported a series of co-crystals of trans-1,2-bis(4-pyridyl)ethylene with dicarboxylic acids⁵² (**Scheme 2.2**). The [2+2] photo-dimerization was also induced in a few co-crystals.

Scheme 2.2. The candidates that used to form co-crystals via N···H–O hydrogen bonds⁵²



Fowler and Lauher reported the use of aminopyridones and carboxylic acids to form discrete assemblies. In their case, the 2-amino-4(H)-pyrimidone and dicarboxylic acid stack with a molecular repeat distance of 6.5 Å.⁵³

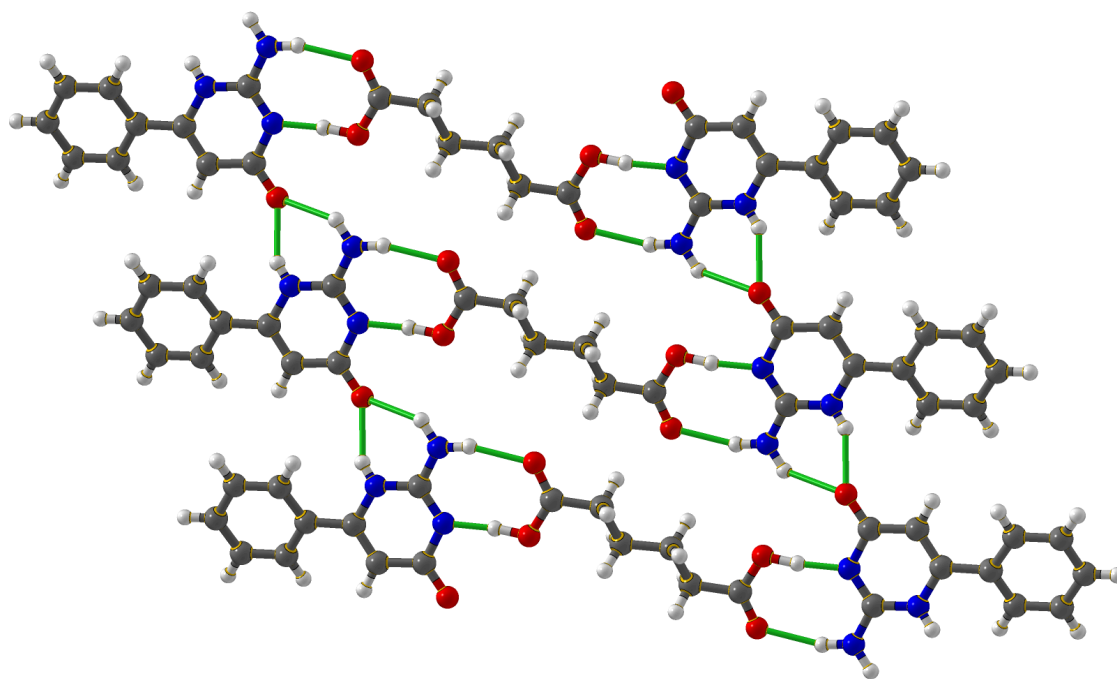
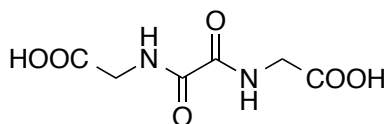


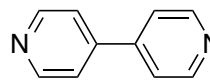
Figure 2.6. Co-crystal formed from 6-phenyl-2-amino-4(1H)-pyrimidone and adipic acid⁵³

Unlike the aminopyridine-to-carboxylic acid hydrogen bond, the pyridine-carboxylic acid hydrogen bond possesses less hydrogen bond donors and acceptors. It would make the formation of uniform network structures more difficult but on the other hand reduce the possibilities of forming complicated and unexpected structures.

As an analogue to urea, the oxalamide functional groups were also used to grow co-crystals with appropriate guest molecules. *N,N'*-Oxalyldiglycine, a suitable oxalamide with two side arms containing carboxylic acids, is one of the simplest examples. It has been used for chelating with transition metals^{54,55} due to its capability to donate electron pairs. In earlier work, it was also shown to form co-crystals with simple bipyridine.⁴⁷



N,N'-oxalyldiglycine



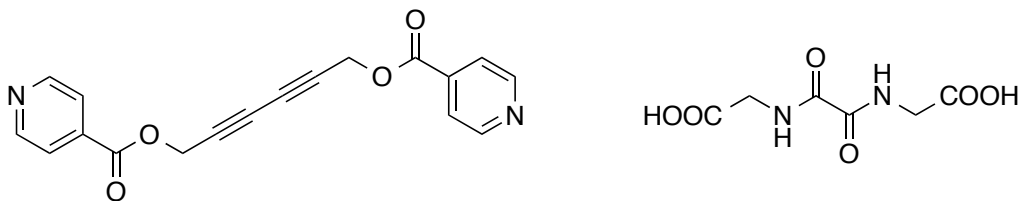
bipyridine

As desired, the molecular repeat distance along the oxalamide network is 5.05 Å.

2.2 Supramolecular design

The success of co-crystallization and network formation between an oxalamide and bipyridine leads to further explorations of their applications in supramolecular chemistry. The combination of the oxalamide, diacetylene, and the pyridine-carboxylic acid hydrogen bond was shown to achieve the prerequisite needed for topochemical polymerization. The host-guest strategy should be applicable to the synthesis of many different co-crystal polymers and open a new horizon on the synthesis of conducting polymers. In addition, investigation of the properties of the obtained co-crystal polymers has been relatively limited. The goal of this project is also to better understand the structural properties of these polymers.

The diacetylene candidate that successfully formed a network structure with the ureylene host was also used to grow co-crystals with the oxalamide host.



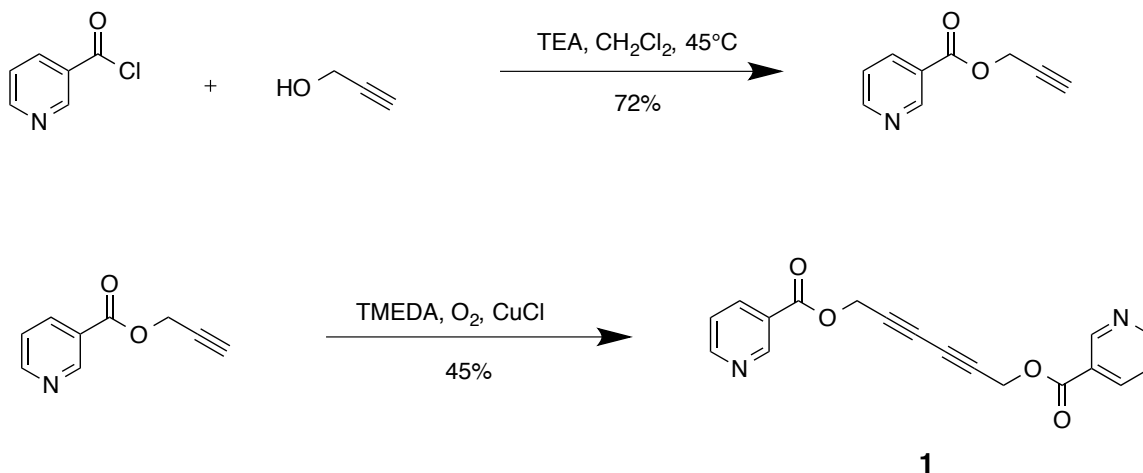
Nguyen reported the co-crystal formed from an oxalamide host and the diyne dinicotinate guest.⁴⁷ X-ray crystallography shows the ratio of the diacetylene to the oxalamide in the crystal is 3 to 1. Instead of forming a network through oxalamide to oxalamide hydrogen bonds, the carbonyl of the carboxylic acid forms hydrogen bonds to the anti-hydrogen atom of the nitrogen, and the anti-hydrogen atom of the nitrogen of one oxalamide forms hydrogen bonds to the carbonyl of the neighboring oxalamides. The network generated from the unexpected hydrogen bonding gives a translational repeat distance of 6.157 Å and an orientation angle of 43.9°, which are not the appropriate values for topochemical polymerization.

2.3 Molecular Synthesis

2.3.1 Guest molecule

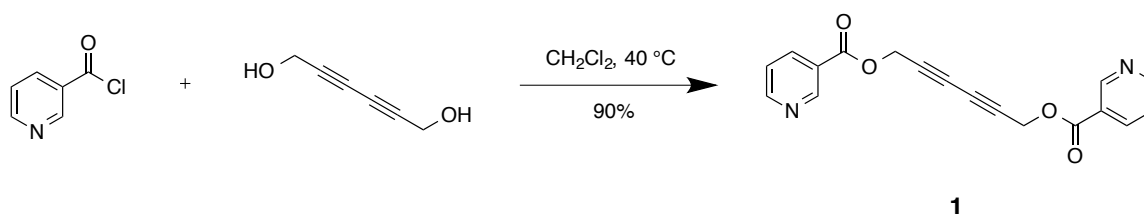
Nguyen⁴⁷ and Tran⁵⁶ designed and synthesized a few symmetrical diacetylenes that terminated with pyridine functionalities, such as hexa-2,4-diyne-1,6-diyl dinicotinate (**1**). Previous synthesis involves two steps, starting from nicotinoyl chloride:

Scheme 2.3. The preparation of hexa-2,4-diyne-1,6-diyl dinicotinate (**1**)⁵⁶



The self-coupling of terminal acetylene (Hay coupling^{57,58}) generates relatively low yields of diacetylenes. To avoid Hay coupling, nicotinoyl chloride is used to react directly with hexa-2,4-diyne-1,6-diol (commercially available) under mild conditions. This gives the desired target molecule in one step:

Scheme 2.4. The preparation of hexa-2,4-diyne-1,6-diyl dinicotinate (**1**)



The crude product obtained can be purified by column chromatography to yield a pale yellow solid in a high percent yield (90%). Recrystallization in methanol can further purify the product as white crystals.

Single crystal X-ray diffractography shows that the crystal structure of hexa-2,4-diyne-1,6-diyl dinicotinate is well organized in a zigzag arrangement. The pyridine rings stack with a distance of ~ 3.45 Å. This π - π interaction, in which the vector between the ring centroids forms an angle of about 20° relative to the normal of the ring planes, is a typical *slipped interaction* (parallel displaced) that are commonly found among the aromatic nitrogen-containing systems.⁵⁹

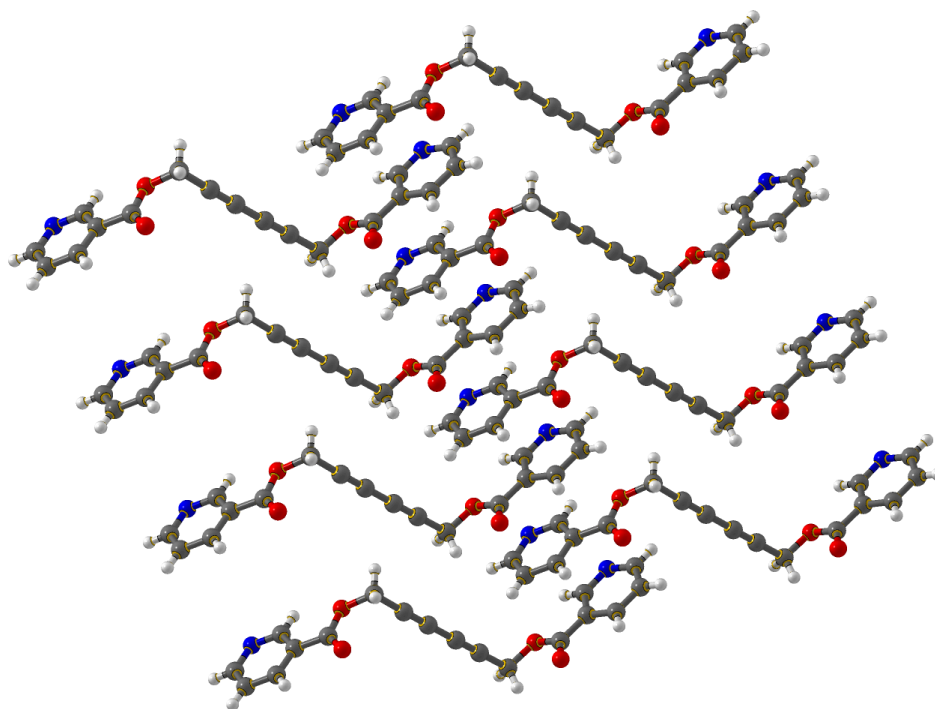


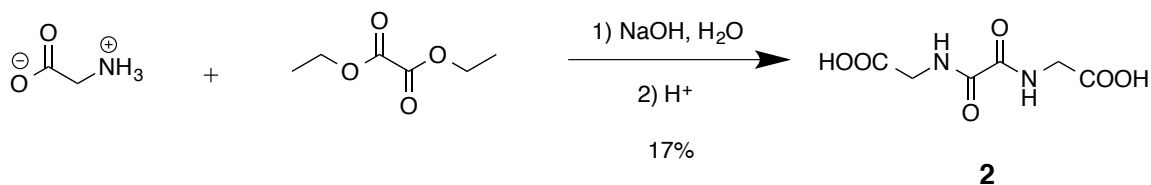
Figure 2.7. Crystal Structure of hexa-2,4-diyne-1,6-diyl dinicotinate

Mainly due to the π - π interactions among the pyridine rings, the repeat spacing of diacetylene functionality is 6.91 Å, much lengthier than the desired \sim 4.9 Å. The distance of C1 and C4 between neighboring molecules is 4.21 Å. These parameters are clearly not suitable for 1,4-topochemical polymerization.

2.3.2 Host molecule

The host molecule **2** used in this experiment is synthesized by reacting glycine with diethyl oxalate in aqueous NaOH solution, and recrystallized from water.⁵⁶

Scheme 2.5. The preparation of *N,N'*-oxalyldiglycine⁵⁶



Previous studies showed there are two different polymorphs for the oxalamide.⁵⁶ The one obtained from crystallization from acidic aqueous solution has a melting point of 252-256 °C, which has the desired hydrogen bonding networks.

2.3.3 Co-crystal

The co-crystallization of oxalamide and diacetylene is supposed to be achieved with ease. However, many attempts failed. In general, the oxalamide is insoluble in common organic solvents due to its high polarity. Thus methanol and water are the only choices that can be used to dissolve the oxalamide for growing the co-crystal, water being a better choice for dissolution. On the other hand, excess use of water drives the diacetylene out of solution.

For these reasons pure methanol and methanol/water mixed solvents are used to grow the co-crystal. Pink crystals are observed from both of the solutions at room temperature or at freezing point, yet none of them are of X-ray quality. In the previous work, Tran⁵⁶ obtained the co-crystal with a dark-red color from MeOH/H₂O. X-ray analysis reveals that the co-crystal is in the $P2_1/n$ space group with a repeat distance of 4.931 Å. In crystallography, the residue factor (R factor) is an indicator used to describe the quality of a crystal. With an R factor of 0.17, the co-crystal data are relatively poor and a better data set is needed.

From the experiments that we carried out, one of the possibilities for the poor crystal data is that the monomer co-crystal tends to polymerize once it forms, generating partially polymerized co-crystal.

For one thing, the host and guest molecules in methanol or water are all colorless. The colored crystals precipitated in solution should be polymerized co-crystals. On the other hand, in general, one of the important features of topochemical polymerization is the reaction occurs via slow motion of atoms in the crystal lattice. To avoid destroying the crystal, the polymerization transformation usually takes place under a mild condition, with a relatively low temperature and slow reaction rate. It is reasonable to assume partially polymerized co-crystals are formed due to

the slow reaction rate. Therefore, different co-crystalline states (polymerized and unpolymerized) cause the obstacle of obtaining good crystals for single crystal X-ray diffraction.

Interestingly, the complete polymerized co-crystal **3** of the oxalamide and diacetylene can be obtained directly from hot methanol via slow evaporation. The co-crystal has a shining metallic gold color and stays unchanged at room temperature. X-ray diffraction analysis confirms the structure of the polymerized co-crystal.

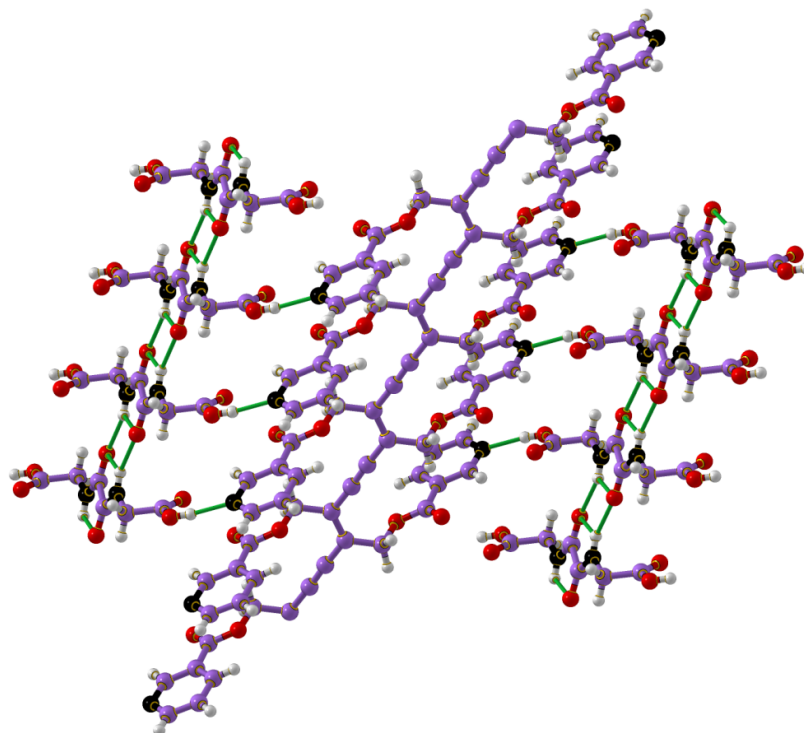


Figure 2.8. The structure of co-crystal **3**

In the co-crystal network, two separate sets of hydrogen bonds are generated from oxalamide to oxalamide and from pyridine to carboxylic acid, respectively. Compared to the

monomer crystal, the symmetry ($P2_1/n$) is retained in the polymer crystal, mainly due to the shearing and slow motion in the transformation (**Table 2.1**). The crystal parameters are very similar as well in the monomer and polymer crystals. The volume size decreases by a small amount after the transformation, indicating a more compact arrangement in the polymer crystal structure.

Table 2.1. Crystal parameters of the monomer crystal and the polymer crystal

Crystal Parameter	Monomer Crystal ⁵⁶	Polymer Crystal
Space Group	$P2_1/n$	$P2_1/n$
a (Å)	4.931	4.902
b (Å)	12.865	13.064
c (Å)	19.273	18.669
β	90.60°	91.04°
Volume (Å ³)	1222.5	1195.3
R factor	0.17	0.13

2.4 Decomposition Study of the polymerized co-crystals.

By using the host-guest strategy, we can quickly produce the polymerized co-crystals in large quantities. This makes it much easier to further investigate the characteristics that the polymer may have.

The polarized optical reflectance spectra of the co-crystal as a function of temperature has been reported in the previous study.⁶⁰ It suggests that the co-crystal possesses relatively good stability, as it is not likely to have any sudden structural modification with temperature. However, when we look at the polymerized co-crystals, the polydiacetylene backbone is formed along the length of the crystal. The host oxalamide molecules are arrayed on both sides and connected to the polydiacetylene backbone via hydrogen bonds. It has been proved to be practical to remove the host molecules from the co-crystals with a suitable reactant, leading to pure polydiacetylene⁵⁶, providing an approach to fabricating polydiacetylenes for those who couldn't polymerize by themselves and producing novel conducting nanomaterials.

The obtained polymerized co-crystal is purified by washing with water and dried at room temperature. Saturated aqueous NaHCO_3 solution is then used to extract the oxalamide carboxylic acid host from the co-crystal at room temperature for 8 hours (**Figure 2.9**). The residue is further washed with distilled water to remove leftover NaHCO_3 . The isolated crystals change color from metallic gold to dark red, losing its metallic shine.

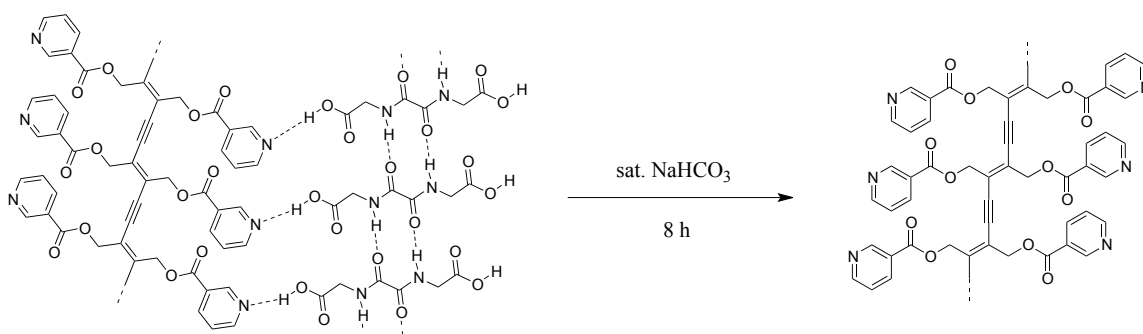


Figure 2.9. Host removal by using saturated NaHCO₃ solution

Table 2.2. The quantitative study of removing host oxalamides

	1	2	3
Polymerized co-crystal 3 (total weight of Host + Guest)	0.0402g	0.0228g	0.0168g
Weight of Host	0.0156g	0.0089g	0.0065g
Filter paper	50.8033g	53.3520g	59.8894g
Filter cake + filter paper	50.9597g	53.3633g	59.9004g
Filter cake (weight of Guest)	0.0232g	0.0113g	0.0110g
Weight loss of Host	0.0170g	0.0115g	0.0058g
Percent loss of Host	109%	129%	89%

The experiments were conducted by calculating the percent loss of host molecules. We at first weighed a certain amount of co-crystal and rinsed it with saturated NaHCO₃ thoroughly, followed by a filtration. The guest molecule (polymer) could not dissolve in solution so it stayed

on the filter paper. The filter paper and filter cake were dried both before and after the filtration in order to get more precise weights. The weight of guest molecules was obtained by comparison of the two values, as indicated in **Table 2.2**.

Due to the tiny amounts of materials used in the experiments, the weighing errors could not be ignored. However, the data we obtained clearly showed that the host oxalamides were extracted in almost quantitatively.

Although the co-crystal remains in good shape during and after the extracting process, X-ray diffraction only shows a few spots for the base-washed crystal, indicating that it loses most of its crystallinity during the loss of host molecules.

Both the polymerized co-crystal and the pure polydiacetylene are insoluble in common organic solvents. We attempted to slowly heat them for the melting point measurements, but neither of them melts. However, an interesting phenomenon is detected when the polydiacetylene is heated up. The polydiacetylene further decomposes. A colorless sublimate is observed from the polymer by Tran.⁵⁶ He then identified the sublimate to be pure nicotinic acid by using ¹H NMR, ¹³C NMR and IR spectrum. The residue turns to black solids, and stays unchanged up to 300 °C.

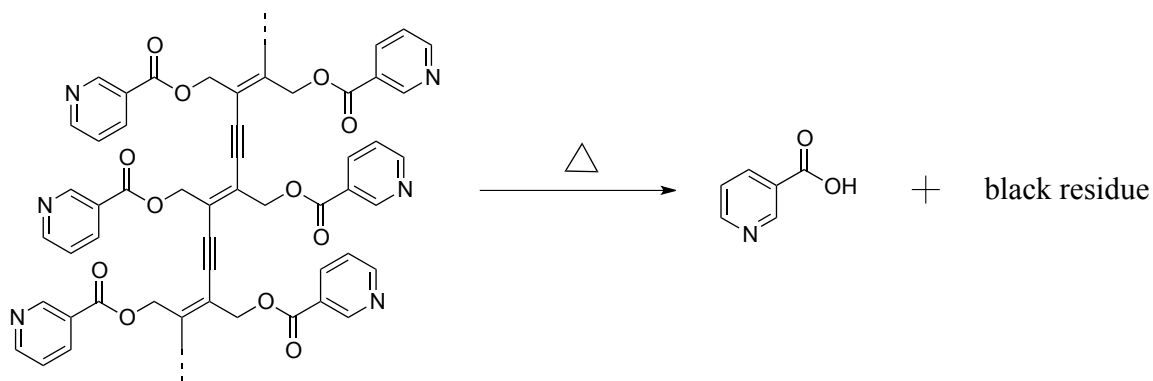


Figure 2.10. Sublimation of nicotinic acid from the pure diacetylene

Thermogravimetric analysis (TGA) is a powerful tool to discover the relationship between the structure and its properties. In the field of crystallography, it is usually operated to measure the crystal-to-crystal transition temperature as well as the melting and crystallization temperatures.⁶¹ In our experiment, TGA was used to investigate the decomposition of the polydiacetylene. The experiments were carried out at a heating and cooling rate of 10 °C/min under dried nitrogen gas. As showed in **Figure 2.11**, the weight loss of the polymer began at ~165 °C, indicating the initiation of sublimation.

The empirical formula of the polydiacetylene is $C_{18}H_{12}O_4N_2$ (molecular weight 320.30), while that for two molecules of nicotinic acids is $C_{12}H_{10}O_4N_2$ (molecular weight 246.22). Theoretically, the complete removal of nicotinic acids would give a 77% loss of the polymer, suggesting the sublimation process be completed around 350 °C. When the temperature reached to 600 °C, the polydiacetylene lost all its weight.

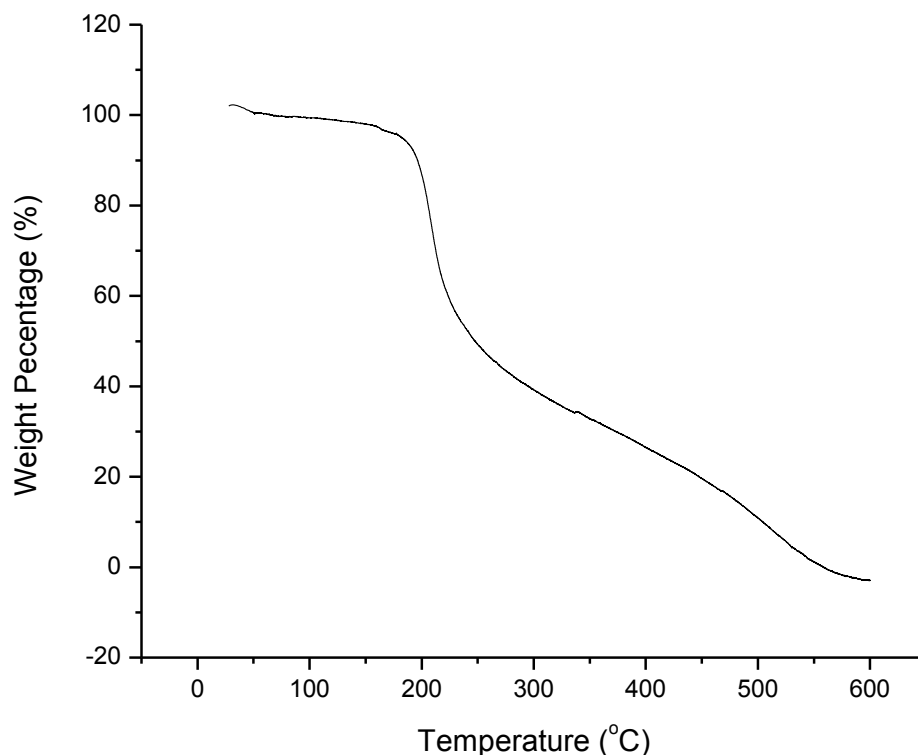


Figure 2.11. Thermogravimetric analysis of the polydiacetylene with a heating rate of 10 °C/min under dried nitrogen gas atmosphere

IR spectra further confirmed the decomposition process. As shown in **Figure 2.12**, the red line represents the IR spectrum of the polymerized co-crystals. A broad peak at 3272 cm^{-1} is attributed to the stretch of O-H bond in the carboxylic acid of the oxalamide host. From the structure of the polymerized co-crystal, we see three different carbonyl functional groups: one carbonyl in the guest polydiacetylene molecules and two carbonyls in the host oxalamide molecules. However, there are only two peaks, located at 1723 cm^{-1} and 1660 cm^{-1} respectively, assigned to carbonyls. It is because IR absorptions from the carbonyl in nicotinate and that in the carboxylic acid are almost the same (at $\sim 1723 \text{ cm}^{-1}$) and these peaks overlap to each other. On

the other hand, the peak at 1660 cm^{-1} should be attributed to the carbonyl in the amide (oxalamide).

After the polymerized co-crystals are washed by NaHCO_3 , the peaks at 3272 cm^{-1} and 1660 cm^{-1} disappear (shown in blue line in **Figure 2.12**), indicating that the host *N,N'*-oxalyldiglycine has been removed completely from the co-crystals.

In addition, as a result of sublimation of nicotinic acid, the residue mostly lost its peaks in the fingerprint region (shown in black line in **Figure 2.12**).

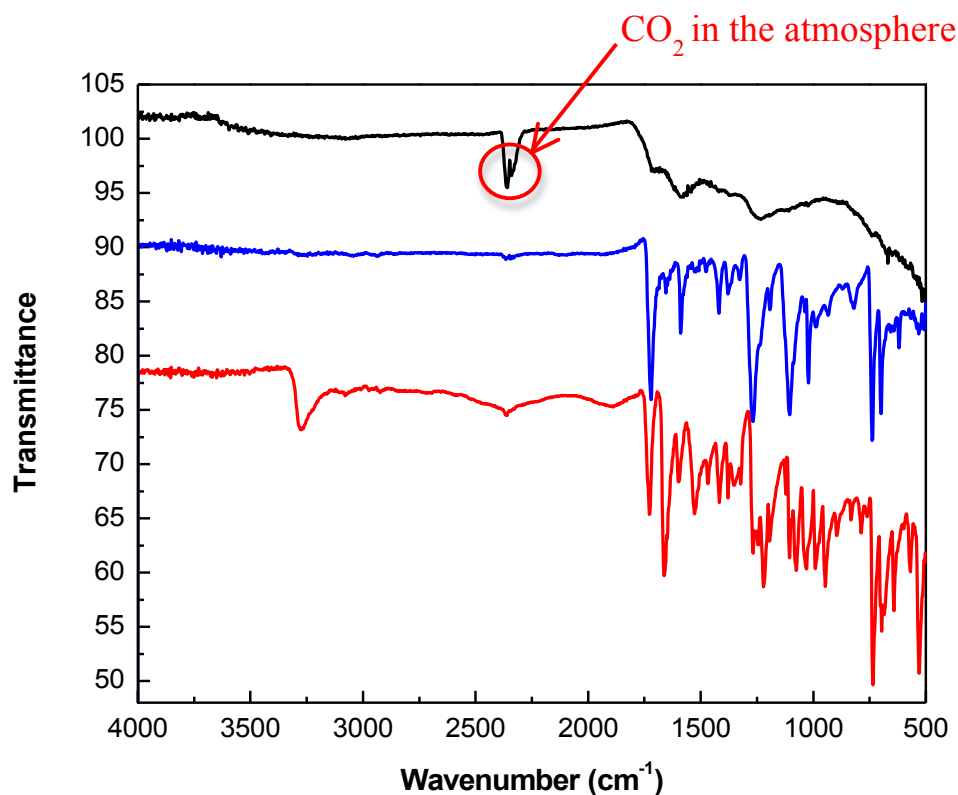


Figure 2.12. IR spectra. **Red:** polymerized co-crystal **3**; **Blue:** pure polydiacetylene; **Black:** residue after sublimation of nicotinic acids

The structure of the black residue is currently unknown. What we do know is that after nicotinic acid is sublimed, the polydiacetylene is expected to have a molecular empirical formula of $(C_6H_2)_n$, a carbon-rich material. Due to the insolubility to all solvents and the inertness to common chemical reactions, characterizations to the black residue are very limited. Raman spectrum of the black residue (**Figure 2.13**) suggests that carbon-carbon double bonds are present, while carbon-carbon triple bonds are not. The peak at 1580 cm^{-1} is consistent with the G band of graphitic carbon, while the peak at 1380 cm^{-1} indicates the disordered sp^2 -hybridized carbon D band.⁶² The peak style implies that there are both ordered and disordered materials in the black residue.

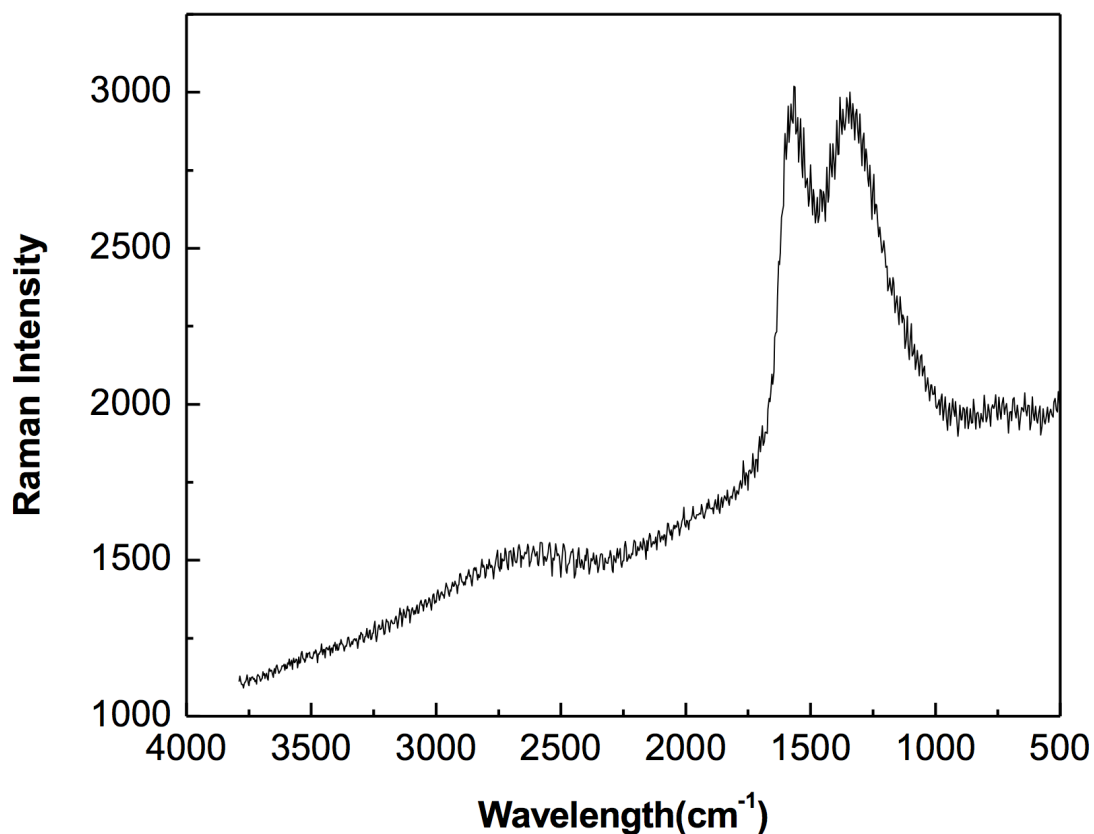


Figure 2.13. Raman spectrum of the black residue

The formation of ordered materials is plausible, mainly because it is formed from the decomposition of highly ordered diacetylene polymers under a relatively mild condition. A reasonable assumption is that it is a graphene analogue or a carbon nanotube analogue. A possible structure is shown in **Figure 2.14**.

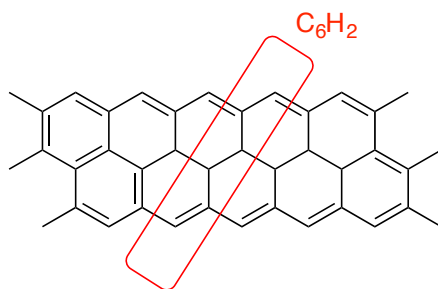


Figure 2.14. A plausible structure of the black residue with a repeat unit C_6H_2

2.5 Conclusion

The successful co-crystallization and polymerization of hexa-2,4-diyne-1,6-diyl dinicotinate and *N,N'*-oxalyldiglycine demonstrate that the host-guest strategy is a reliable and efficient approach to synthesizing polydiacetylenes. By using *N,N'*-oxalyldiglycine as the host molecule, diacetylene functionality can be introduced into the network with a desired molecular repeat spacing of ~ 5 Å and a stacking angle $\sim 45^\circ$, for topochemical polymerization. X-ray analysis reveals the fully conjugate, all-*trans* carbon backbone of the polydiacetylene.

This study can have a broad impact as it leads the supramolecular synthesis into a rational process. Various combinations of different host and guest molecules create more possibilities and make it much easier to design and synthesize novel functional supramolecular structures. The main distinction of this approach is materials produced by using host-guest strategy for topochemical polymerization are highly ordered and organized, as proved by the obtained single crystals.

The properties of the as-prepared polydiacetylenic co-crystal **3** have also been explored. Removal of host molecules in the co-crystal is proved to be an uncomplicated task, which leads to the pure polydiacetylene. In addition, removal of host molecules and sublimation of nicotinic acids from the leftover polymer are both demonstrated to be quantitatively. This feature may be applied to the design of new polydiacetylene conductors. Though the structure of the black residue remains unknown at this point, it could be the potential ordered framework, such as the graphene or carbon nanotube analogue.

Chapter Three

Design and preparation of macrocyclic diacetylenes toward organic nanotubes

3.1 Introduction

3.1.1 Macrocycle

In the 1960s, Charles J. Pedersen at du Pont discovered a compound that came to be known as dibenzo-18-crown-6.⁶³ He isolated it in a 0.4% yield while attempting to prepare a completely different compound. This lucky discovery later led to a new field of chemistry that we now see as *macrocyclic chemistry*. Following his pioneering work, researchers worldwide synthesized and characterized a variety of macrocyclic structures. In 1987, the Nobel Prize was awarded to Pedersen along with Donald J. Cram and Jean-Marie Lehn “for their development and use of molecules with structure-specific interactions of high selectivity”.⁶⁴

These crown ethers gained great attention for their ability to form stable complexes with alkali metal and alkaline earth metal cations within their central cavity.^{65,66} Ring size variation could dramatically affect the binding capability. Also, their derivatives, the nitrogen-containing crown ethers (azacrowns) and sulfur-containing crown ethers (thiacrowns) display different ionic selectivity than the original oxygen-containing crown ethers due to differences in polarizability. For example, three crown ethers (**Figure 3.1**) show decreasing affinity for K^+ in the order $O >$

NH > S while an enhancing binding of Ag^+ .¹³ This is in good accordance with the magnitude of the cation-dipole interactions and Lewis theory of acids and bases. These characteristics make crown ethers very useful on the selectivity and efficiency of metal cation detection as well as transport.^{67,68}

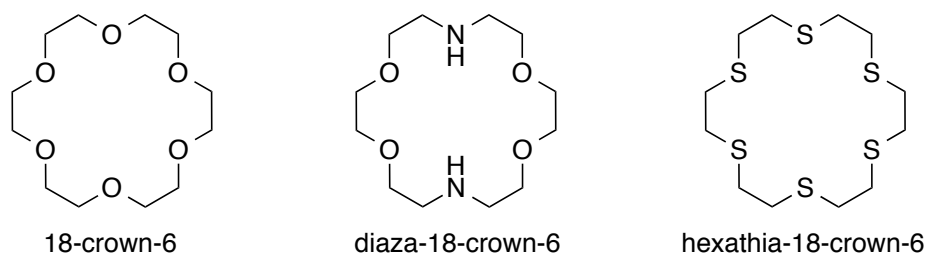


Figure 3.1. Candidates that show different affinity to metals

Many other types of macrocycles have also been synthesized and developed, such as calixarenes, calixpyrroles, cyclophanes, cyclodextrins, and porphyrins. Like crown ethers, these macrocycles also have had a great impact on supramolecular chemistry due to their unique size, shape, and recognition abilities.^{69,70}

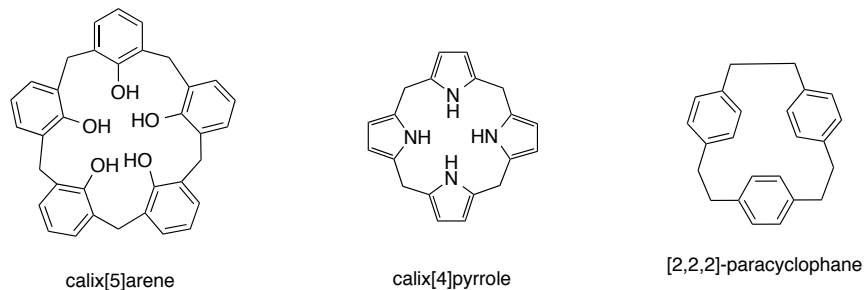


Figure 3.2. Different types of macrocycles

Our group has been focused on diacetylene topochemical polymerization for almost 20 years. It is of interest and a long-term goal to apply diacetylene functionality into a macrocycle and achieve the topochemical polymerization. By this way we should be able to obtain a stable tubular structure.

However, the difficulty is that a diacetylene has 4 *sp* hybridized carbon atoms. In general, the presence of *sp* hybridized carbon atoms makes the macrocycles very rigid. To consist of the diacetylene functionality, a *supracycle* should be designed properly. It is not surprising that the likely conformations of macrocycles containing *sp* hybridized carbon atoms would be remarkably reduced compared to a single bond framework. Also, there are no *cis*- or *trans*-isomers compared to a double bond framework. The inception of diacetylene functionality could dramatically simplify the conformation of macrocyclic systems and make it much easier to investigate the relationship between the structures and properties. In addition, steric hindrance among the macrocycles is mainly reduced since there are no branches for the acetylene linkage.

These shape-persistent macrocycles (SPMs)^{71,72} have attracted great attention for their ability to be building blocks in supramolecular chemistry. Nanoscale materials or devices can be tailored from appropriate aggregation of macrocycles (**Figure 3.3**). In particular, simple stacking of macrocycles forms tubular supramolecular structures, which can be applicable in material, electrical, and medical sciences.⁷³

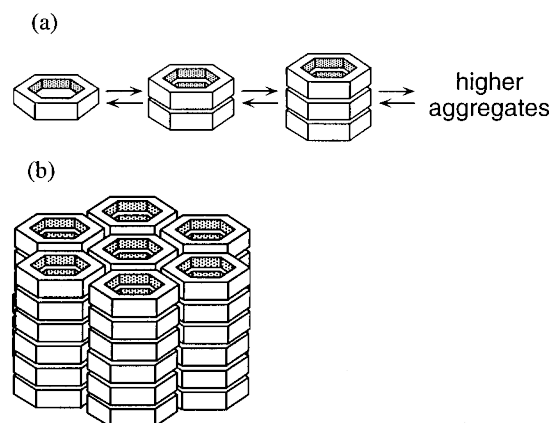


Figure 3.3. Schematic representation of (a) the solution aggregation of hexakis(phenylacetylene) macrocycles and (b) columnar hexagonal order exhibited by hexakis(phenylacetylene) macrocyclic mesogens. Reprinted with permission from ref. 71. Copyright 1997 American Chemical Society.

Though it was rarely seen before, studies showed that the structural template of macrocycles containing acetylene functional groups could also be applied in drug discovery. In 2012, Ivorenolida A, an 18-membered macrolide (**Figure 3.4**) that featuring diacetylenic functionality and five chiral centers, was isolated as a major compound from the crude extract of the stem bark of plant *K. ivorensis* by Zhang and co-workers.⁷⁴ Because of the conjugated acetylenes in it, the configuration of the macrolide is nearly flat. Based on the properties of the crude extract, ivorenolide A could be potentially used for anti-inflammatory medicines. The authors achieved the total synthesis of the enantiomer of ivorenolide A and demonstrated its potent and selective immunosuppressive activities, as measured by T-cell and B-cell proliferation assay *in vitro*. This novel structural template could bring some new thoughts in the development of drug discovery.

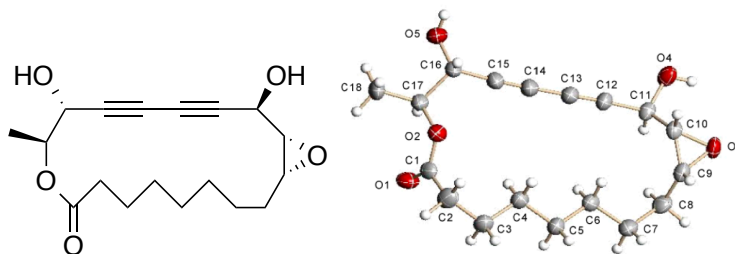


Figure 3.4. The chemical structure and X-ray structure of ivorenolide A. Reprinted with permission from ref. 74, Copyright 2012 American Chemical Society.

3.1.2 Diacetylenic macrocycles and their design

Macrocycles can be functionalized by various approaches. Electron donating and electron withdrawing groups, as well as hydrogen-bonding units, are some common functional groups that can be incorporated into macrocycles. Supramolecular intermolecular interactions, such as hydrogen bonding, π - π stacking, are often involved in the design of macrocycles.

In the 1990s, Moore and Tobe investigated the properties of phenylacetylene macrocycles and phenyldiacetylene macrocycles, respectively. A series of macrocycles with different substituents on the phenyl rings were synthesized successfully (**Figure 3.5**). Moore and co-workers⁷⁵ observed the aromatic π - π stacking that could induce the self-association of certain phenylacetylene macrocycles via ^1H NMR spectra and vapor pressure osmometry measurements. They demonstrated that the electronic properties and orientation of the substituents on the macrocycles could considerably affect the self-associating tendency. In particular, electron-withdrawing ester group assists the aggregation while electron-donating groups such as alkoxy or alkanoate hinder the aggregation. The π - π stacking can also be influenced by the geometry and the size of the macrocycles. It shows that a more planar and rigid structure strengthens the

interaction while a flexible nonplanar framework disfavors it. All of the observations suggest that these macrocycles involve face-to-face π - π stacking in solution.

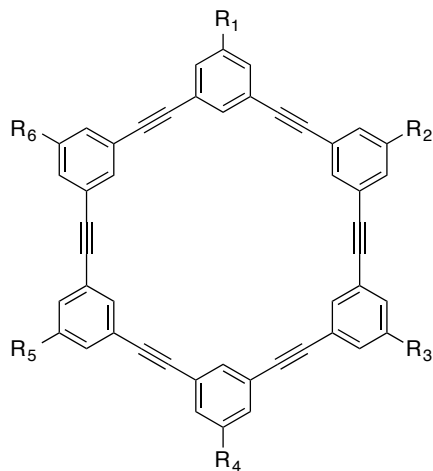


Figure 3.5. The synthesized acetylenic macrocycles with different substituents⁷⁵

Other analogues have also been reported to self-aggregate in the literature.^{76,77}

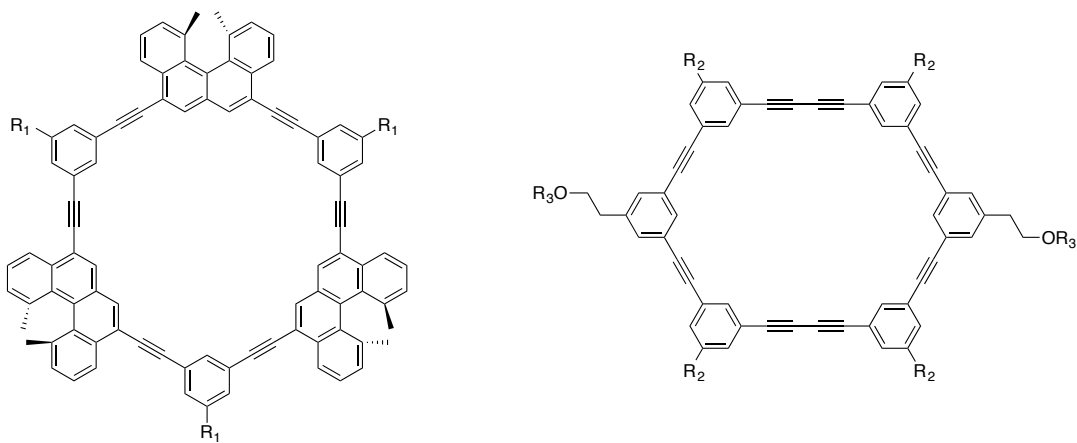


Figure 3.6. Macrocycles that contain acetylene functionality show self-aggregation capability.^{76,77}

Based on Moore and other people's work on the phenylacetylene macrocycles, Tobe and co-workers later designed and synthesized the phenyldiacetylene macrocycles (**Figure 3.7**), and confirmed their association behavior.^{78,79} In their work, cyano groups introduced in the interior of the macrocyclic framework. They also demonstrated the ability for the macrocycles to bind metal cations, as well as tropylium and guanidinium cations.

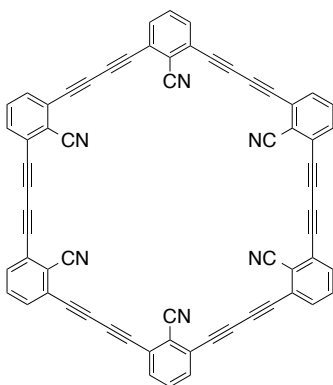


Figure 3.7. The structure of the designed macrocycle containing diacetylenes⁷⁸

Based on the chelation and other properties of the cavity, one can envision that the arrangement of macrocycles in an axial stack would form a tubular structure that could be potentially used as a reaction chamber, ion channel, or nanotube, if functionalized properly. Considering the self-aggregation and π - π stacking, it is not surprising that these macrocycles are valuable candidates for the formation of hollow columns.

Lehn and co-workers examined the tubular mesophases formed from liquid crystals consisting of macrocyclic molecules.⁸⁰ The researchers synthesized *N*-acylated derivatives of saturated macrocyclic hexamines and other similar macrocyclic polyamines and found the

structural information is consistent with a hexagonal columnar mesomorphic order by use of X-ray diffraction patterns.

Similarly, the liquid crystalline “crowned” phthalocyanine (**Figure 3.8**) has been designed and synthesized.⁸¹ The units are stacked to form channels from the observation of X-ray powder diffraction studies, reaching a length of several micrometers.

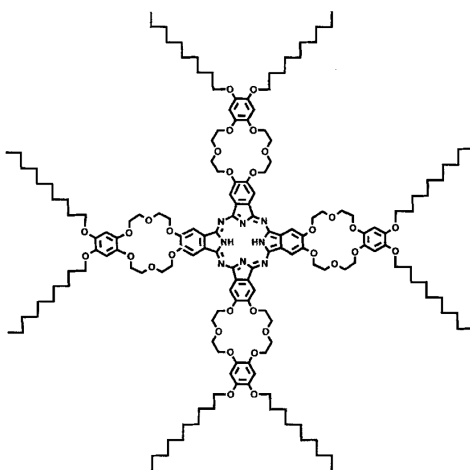


Figure 3.8. Chemical structure of the liquid crystalline “crowned” phthalocyanine. Reprinted with permission from ref. 81. Copyright 1996 Verlag GmbH & Co. KGaA, Weinheim

3.1.3 Covalent bonded tubular structures

The macrocycles stack together through intermolecular interactions such as ion-ion interactions, dipole-dipole attractions, π - π interactions or hydrogen bonding. These weak intermolecular forces help the appropriately functionalized macrocycles form the desired tubular structures. However, the dilemma is that weak forces cannot provide the strong linkage needed to stabilize the formed tubular structures, to a large extent limiting the applications of the tubes.

In general, the strongest interaction among atoms is covalent bonding. While it is relatively difficult to synthesize tubular structures via covalent bonding directly, it is a reasonable assumption to divide supramolecular synthesis into two steps: stacking the functionalized macrocycles in a column via weak intermolecular interactions and then linking every unit in the column via covalent bonds.

This idea is not new. Drenth and co-workers⁸² designed and functionalized phthalocyanine macrocycles with *n*-alkoxy chains (**Figure 3.9**). After introducing polymerizable groups at the end of the aliphatic chains, they attempted to fix the tubular structures. In their experiments, the photopolymerization didn't succeed, but the thermal polymerization product was formed at a temperature of 93 °C in vacuum. The polymers were completely insoluble in organic solvents or concentrated sulfuric acid.

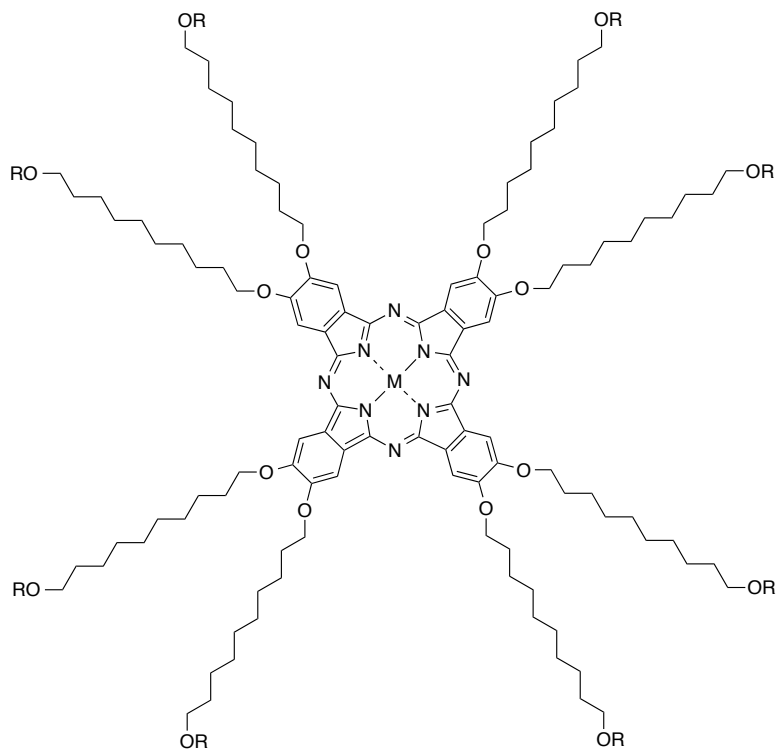


Figure 3.9. The structure of properly substituted phthalocyanines.⁸² The substituents at the end of the aliphatic chains contain carbon-carbon double bonds for polymerization.

For the design of a tubular structure, the polymerization can take place either on the exterior of the macrocycle columns or in the macrocycles. In our group, macrocycles containing diacetylene functionality have also been attempted to topochemically polymerize to establish a covalently bonded tubular structures. It is known that the requirement of diacetylene polymerization is the prearrangement of diacetylene functionality with a repeat distance of ~ 4.9 Å.

Wang⁸³ designed the macrocycle **4** that contained diacetylenes, along with pyridine functionalities, the structure being shown in **Figure 3.10**. In macrocycle **4**, the nitrogen atoms of the pyridines are pointing out of the ring. This feature is supposed to pre-organize the

macrocycles with a proper oxalamide host via hydrogen bonding, in order to achieve the ideal spacing ~ 4.9 Å between the neighboring macrocycles for topochemical polymerization. In addition, hexa-2,4-diyne-1,6-diol functionality in macrocycle **4** is commonly found to be able to provide the desired 4.9 Å spacing in the crystal.²⁸ Another advantage of the design is that after the tubular structures are formed, the host oxalamides can be removed gently, and the pyridinyl tubular polymers can further connect to other molecules or devices via hydrogen bonds or ion-pairs, providing more application possibilities.

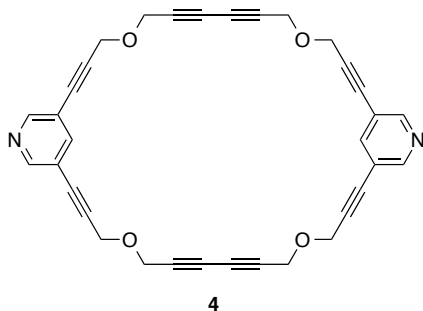


Figure 3.10. Macrocycle **4** containing diacetylene and pyridine functionalities⁸³

Macrocycle **4** has been successfully synthesized by Wang. X-ray crystallographic analysis shows that the spacing distance between the neighboring macrocycles is 4.13 Å, with the contact distance 4.29 Å.⁸³ These parameters are not favorable for the desired 1,4-topochemical polymerization.

The attempt to apply host-guest strategy between macrocycle **4** and certain oxalamides turned out to be very difficult due to extremely poor solubility of **4**. However, though the packing distance in the crystal of **4** (4.13 Å) is not ideal for polymerization, it demonstrated that π - π stacking among the aromatic rings could also be used to form the desired packing style.

Chow⁸⁴ and Hsu⁸⁵ later designed macrocycles **5** and **6** for testing the π - π stacking in crystals (**Figure 3.11**).

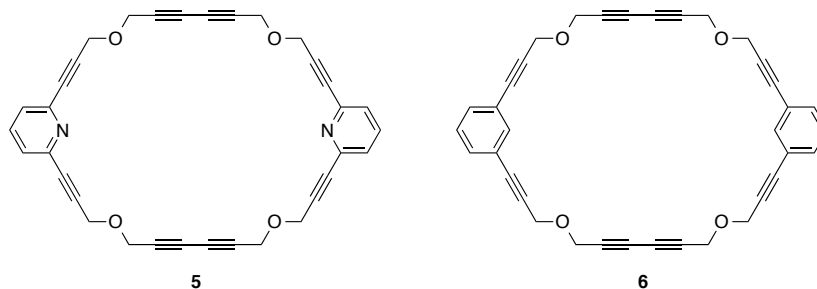
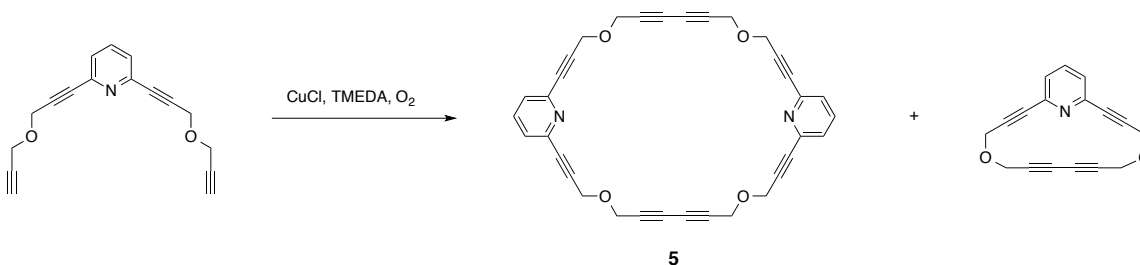


Figure 3.11. Macrocycles **5** and **6** that featuring π - π stacking

Attempts to synthesize macrocycle **5** were unsuccessful, as described by Chow.⁸⁴ Instead of obtaining the desired macrocycle, an unexpected intramolecular self-cyclization product was isolated from the crude products, as shown in **Scheme 3.1**.

Scheme 3.1. The synthesis of macrocycle **5**⁸⁴



According to the result, Chow suggested that a coordination complex containing copper metal may induce the formation of intramolecular self-cyclization during Hay coupling.

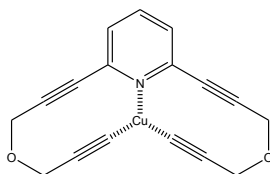


Figure 3.12. A plausible copper-diether coordination complex in Hay coupling⁸⁴

Hsu⁸⁵ successfully synthesized macrocycle **6**. The packing distance in crystal is 4.84 Å, very close to the ideal value for topochemical polymerization.

Thermal annealing experiments (**Figure 3.13**) brought about the polymerization as a single-crystal-to-single-crystal transformation, leading to a synthetic organic nanotube.

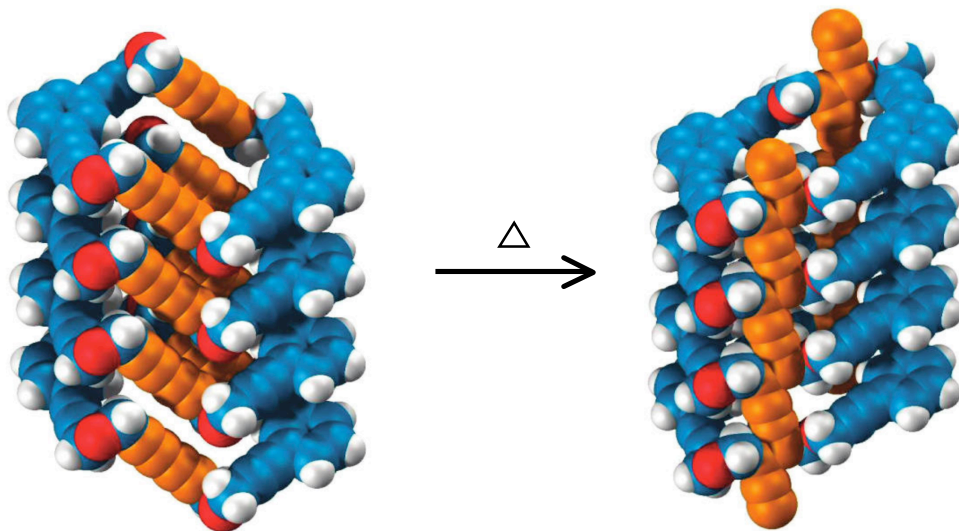


Figure 3.13. Observed molecular stacking of macrocycle **6** and the structure of polymer obtained by slow annealing. Reprinted with permission from ref. 85, Copyright 2012 American Chemical Society.

Macrocycle **6** is the first successful example for the formation of tubular addition polymer with a fully characterized structure. It confirms that 1,4-topochemical polymerization could be potentially developed to a general strategy for synthesizing tubular polymers. However, like macrocycle **4**, macrocycle **6** also shows very poor solubility in most organic solvents.

Other research groups also aimed at the design and synthesis of macrocycles containing diacetylene functionality. Vollhardt and Youngs⁸⁶ synthesized 1,2:5,6:9,10-Tribenzo-3,7,11,13-tetradehydro[14]annulene (**Figure 3.14**) and attempted to conduct its polymerization in crystal. X-ray diffraction studies showed that the distance between the neighboring diacetylenes is 6.3 Å, much longer than the ideal distance of ~4.9 Å for topochemical polymerization.

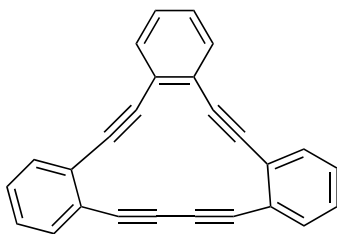


Figure 3.14. The structure of the designed macrocycle for topochemical polymerization⁸⁶

Recently, Shimizu and co-workers synthesized a macrocycle containing diacetylene functionality, which self-assembles into columns via amide hydrogen bonds (**Figure 3.15**).⁸⁷ The repeat distance of the macrocycles in this crystal is 4.98 Å. Topochemical polymerization was observed by heating or UV irradiation. However, the crystal lost its crystallinity after the polymerization.

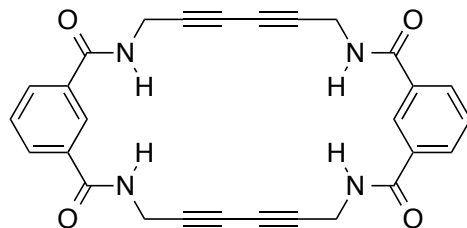


Figure 3.15. The diacetylene macrocycle that self-assembles into columns via amide hydrogen bonds. The diacetylene units may undergo a topochemical polymerization to yield polydiacetylenes via thermal annealing.⁸⁷

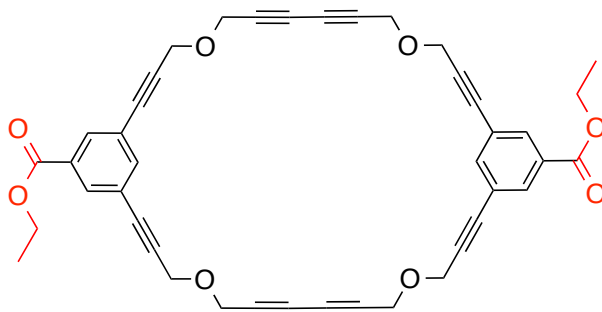
3.2 Research Goal

The beautifully designed macrocycles have demonstrated their capabilities to form tubular structures via self-aggregation in solution or in crystal state. While many macrocycles have been synthesized, the existing methods lack flexibility, as every synthetic route of macrocycles needs to be redesigned. Thus synthesis of macrocycles is very inefficient and time-consuming.

Following the work mentioned above, we want to develop a general synthetic route that can be used to generate a series of macrocycles with ease. Consequently, their ability to form covalently bonded tubular structures via 1,4-topochemical polymerization and the relationship between their structures and properties can be investigated systematically. Considering the disadvantages of previously obtained macrocycles, our design is mainly focused on improving the solubility as well as controlling the spacing between the macrocycles.

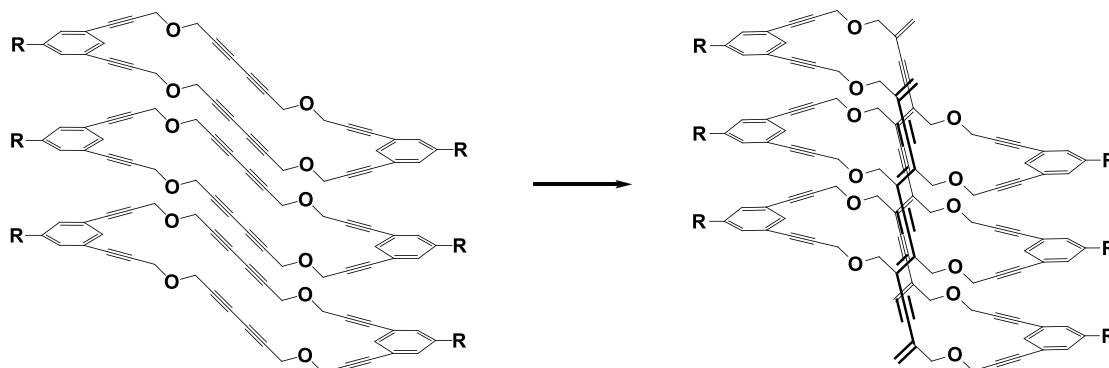
The pyridine-containing macrocycles **4** and **5** and macrocycle **6** may not be good parent compounds since they are insoluble in most solvents. For macrocycle **6**, it lacks the

functionalities for potential reactions or applications. In this project, we in the first time introduce the ester functional group to the macrocycles.



Ester is one of the most common functional groups in organic compounds. Many natural fats and essential oils are esters of fatty acids. It is also widely used in organic synthesis as a protecting group for carboxylic acids. The ester functional group appears relatively stable in a neutral environment but chemically reactive in acidic or basic solutions. By introducing ester groups into the macrocycles, we can easily modify the structure of the existing macrocycles and synthesize a number of new macrocycles. In addition, an ester has the potential to form hydrogen bonds with other molecules. We wish to examine the influence of the ester functional group and other substituents on the packing in crystals and on the formation of synthetic organic nanotubes. Their topochemical polymerization, as shown in **Scheme 3.2**, will also be studied.

Scheme 3.2. The planned topochemical polymerization among the macrocycles



3.3 Synthetic methods of macrocycles

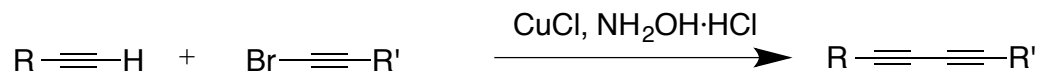
3.3.1 Background

The traditional approach to synthesizing macrocycles is to carry out the ring closing reactions in an extremely diluted solution to form the ring and avoiding other side products. Our strategy is to use an oxidative coupling reaction of acetylenes to achieve the ring closing. A typical value of concentration used in our experiments is ~ 5 micromolar.

In general, there are two types of copper coupling reactions for synthesizing diacetylenes. Cadiot-Chodkiewicz⁸⁸ coupling can be used to synthesize unsymmetrical disubstituted diacetylenes while Glaser⁸⁹ coupling is used to synthesize symmetrical disubstituted diacetylenes. Hay^{57,58} later modified the Glaser coupling condition by using copper (I)/TMEDA, a catalyst system that has a wider range solubility in many solvents.

Scheme 3.3. Diacetylene synthesis

(a) Cadiot-Chodkiewicz Coupling

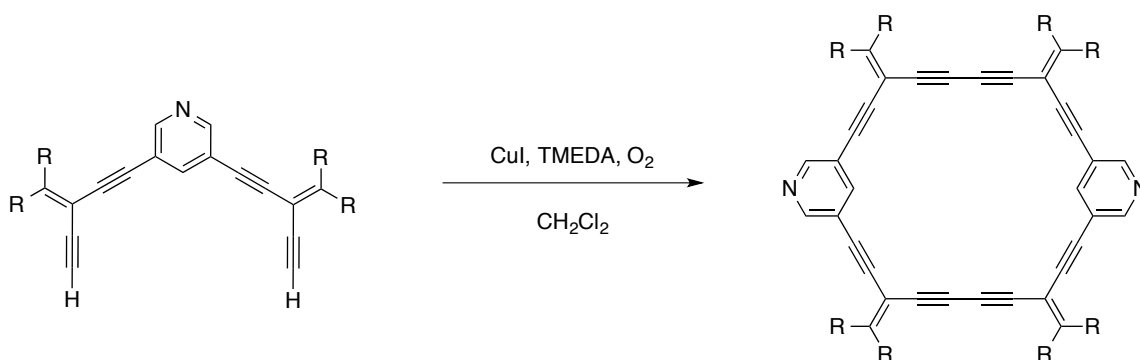


(b) Hay Coupling



Because of the symmetrical structures of the desired macrocycles, Hay coupling is widely used for the ring closing of macrocycles. For example, Tykwinski and co-workers⁹⁰ used Hay coupling to achieve their desired macrocycle. (**Scheme 3.4**)

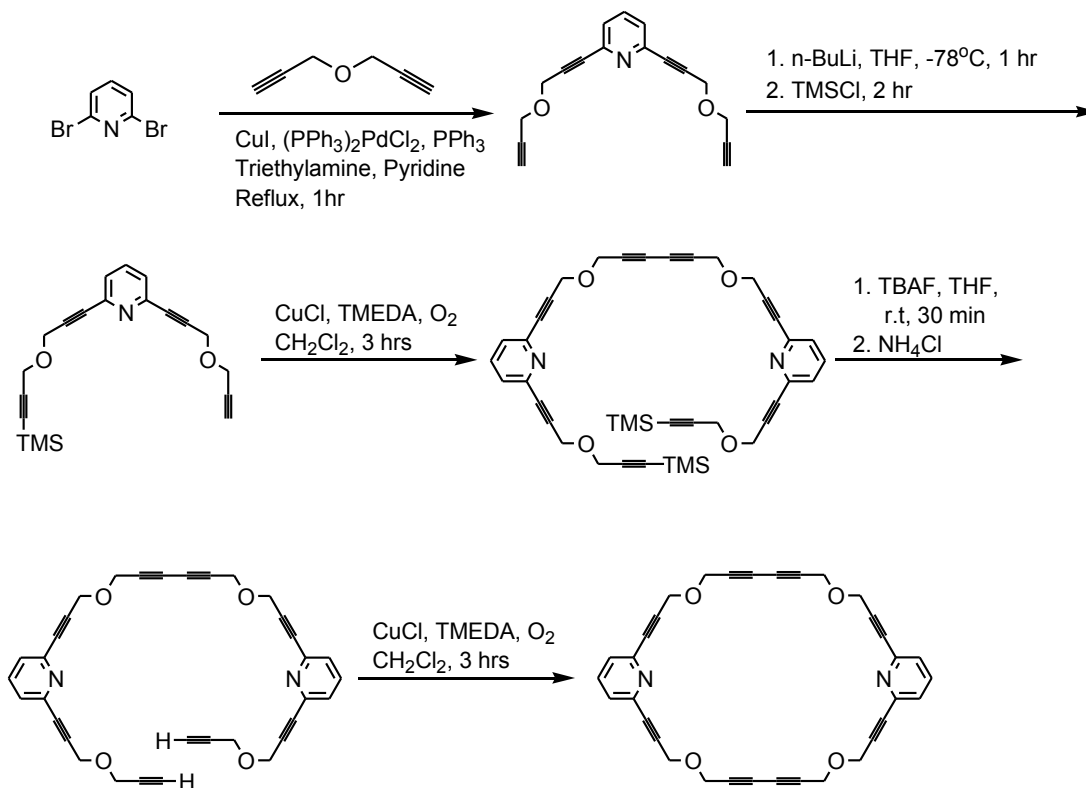
Scheme 3.4. Synthesis of the macrocycle using Hay coupling⁹⁰



3.3.2 The designed synthetic route to diacetylene macrocycles

One synthetic route (**Scheme 3.5**) toward diacetylene macrocycles was suggested by Chow⁸⁴ in order to avoid the formation of the intramolecular self-cyclization product.

Scheme 3.5. A suggested synthetic route toward macrocycles. Reprinted with permission from ref. 84. Copyright 2008 Stony Brook University.

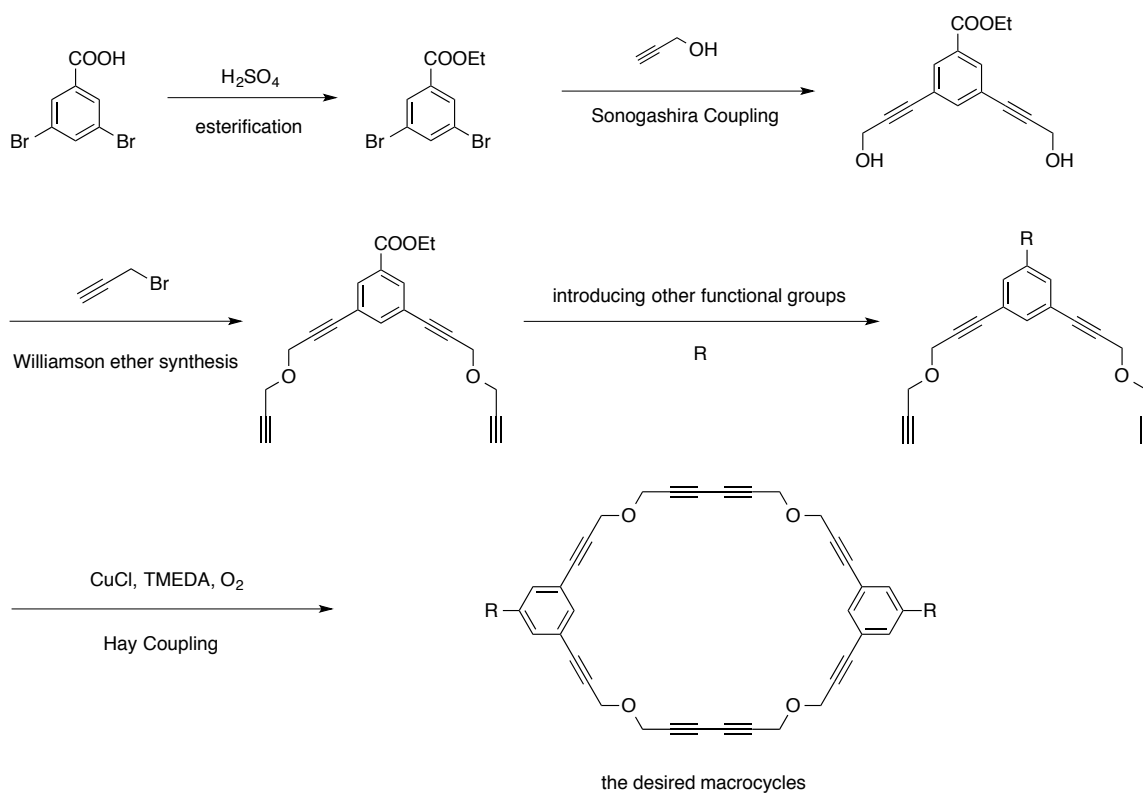


According to Chow's description, there are two issues in the above synthesis. In the second step, the yield of TMS monosubstituted compound was pretty low due to a competition reaction with the disubstituted compound. In addition, the last step (Hay coupling) did not go

smoothly either. Chow found that the reactant might also undergo Hay coupling with each other and form oligomers or polymers, which made it almost impossible to obtain the pure macrocycle.

The general synthetic route to the diacetylene macrocycles that used in this project is shown in **Scheme 3.6**.

Scheme 3.6. Synthetic routes of macrocycles containing different functional groups



In general, 3,5-dibromobenzoic acid or its derivatives couple with propargyl alcohol by Sonogashira coupling to afford the diol. The diol then reacts with propargyl bromide to give the

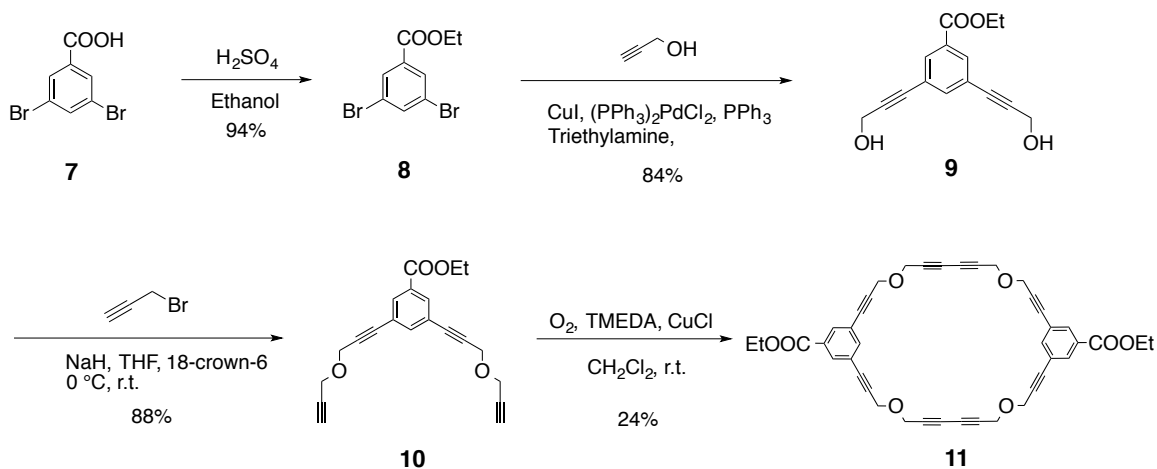
diether via a simple S_N2 Williamson ether formation. The obtained diether undergo dimerization under Hay coupling in a relatively diluted solution to yield the desired diacetylenic macrocycle.

3.4 Results and Discussion

3.4.1 Macrocycles containing ester substituents

We started the project with the synthesis of macrocycle that contains ethyl ester substituents. The synthetic route is shown in **Scheme 3.7**.

Scheme 3.7. Synthesis of macrocycle **11**

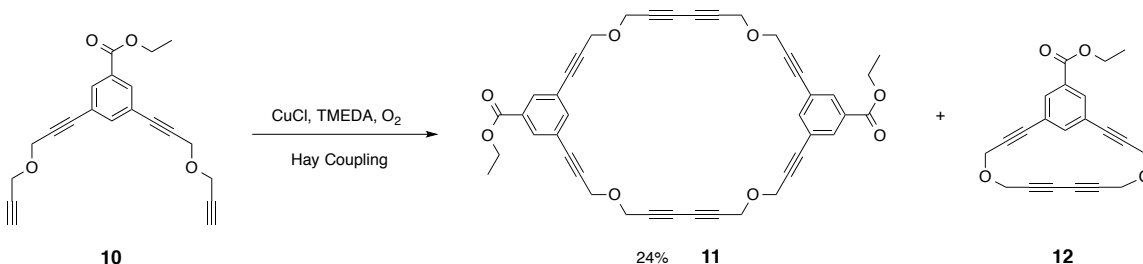


The synthesis starts from the esterification of 3,5-dibromobenzoic acid. Sonogashira Coupling is then used to add propargyl alcohol to the ester **8** and afford the diol **9**. Followed by a

propargyl addition reaction, the obtained diether **10** finally dimerizes under Hay coupling condition to yield the desired macrocycles **11**.

The yield is not excellent in Hay coupling, although many different conditions (varying reaction concentrations, temperature, and the amount of catalyst) have been tested. This is mainly because competition reactions occur among the products. Similar to what Chow⁸⁴ observed, other than forming a dimerized macrocycle, the diether **10** can also undergo intramolecular self-cyclization to form a small macrocycle product **12** (**Scheme 3.8**).

Scheme 3.8. The formation of monomer and dimer macrocycles



By TLC we observed a spot very close to the spot of the desired macrocycle **11**. Due to the small amount, it was insufficient to obtain a meaningful ¹H NMR spectrum. However, because of the high similarity to the macrocycle in terms of polarity, we think it is probably the intramolecular self-cyclization product **12**.

From this point of view, a concentrated solution should help reduce the intramolecular self-cyclization and give more desired dimerization product. We studied the influence of concentrations of the starting material (**Table 3.1**) by TLC tests. The results showed that when

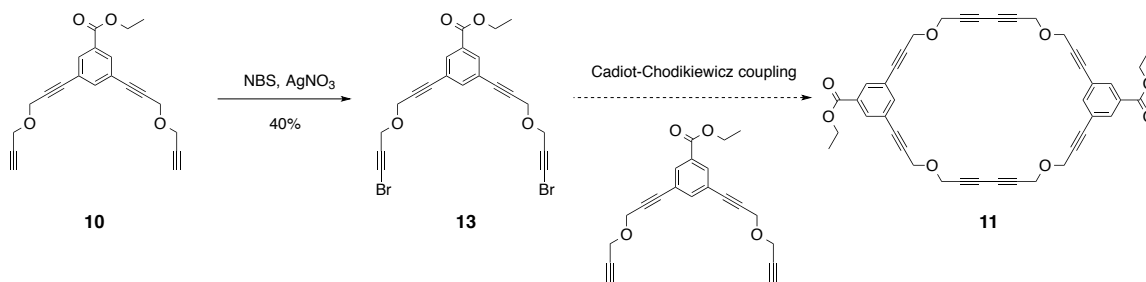
the solution was too concentrated, more side products were generated, such as oligomers or polymers. No pure compounds could be separated from the crude product. However, if the solution is very dilute, the yields of desired macrocycle also decreased.

Table 3.1. The effect of concentration to the yields of macrocycles

Solvent / 1 mmol starting material 10	Monomer 12	Dimer 11
50mL	None	None
100mL	Trace	Trace
250mL	Minor	Major (24%)
500mL	Minor	Minor

To avoid the intramolecular self-cyclization and increase the yield of the desired macrocycle, we attempted to conduct Cadiot-Chodikiewicz coupling for the ring closing. In this case, diether **10** with two bromine substituents has been synthesized by using compound **10** to react with AgNO₃ in the presence of NBS.

Scheme 3.9. Alternate synthetic route to macrocycle **11**



The dibromo diether **13** has been synthesized successfully with a yield of 40%. However, the predicted Cadiot-Chodkiewicz coupling does not go smoothly. No desired macrocycle could be separated from the solution. We only observed a trace amount of the macrocycle, monitored by TLC. The crude products mainly stayed on the starting point after running a TLC test, implying most of the products in the reaction were by-products.

A needle-like crystal of macrocycle **11** was obtained from CH₂Cl₂ solution at 0 °C (**Figure 3.16**). As expected, the macrocycles stack to each other forming a tubular structure, with a repeat distance of 4.23 Å. This repeat spacing is clearly shorter than the ideal 4.9 Å for topochemical polymerization. In fact, the crystal showed very good stability at room temperature. This colorless crystal turned pale yellow after a few months at r.t. or after being heated at 40 °C for 10 days, yet the crystal structure remained the same with no polymerization occurring, as demonstrated by single crystal X-ray diffraction. The crystal was then heated at 40 °C for two months, showing no structural reorganization.

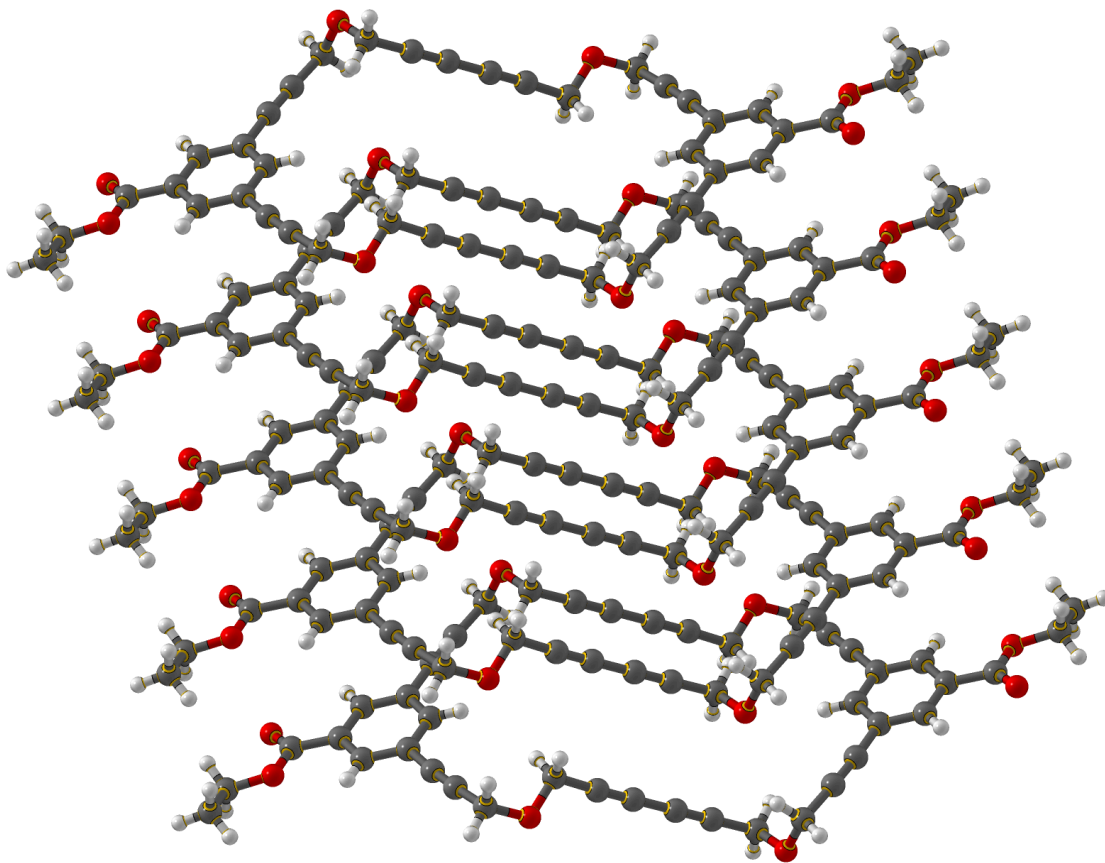


Figure 3.16. The X-ray crystal structure of macrocycle **11**. A single tubular structure oriented by π - π stacking. Side View.

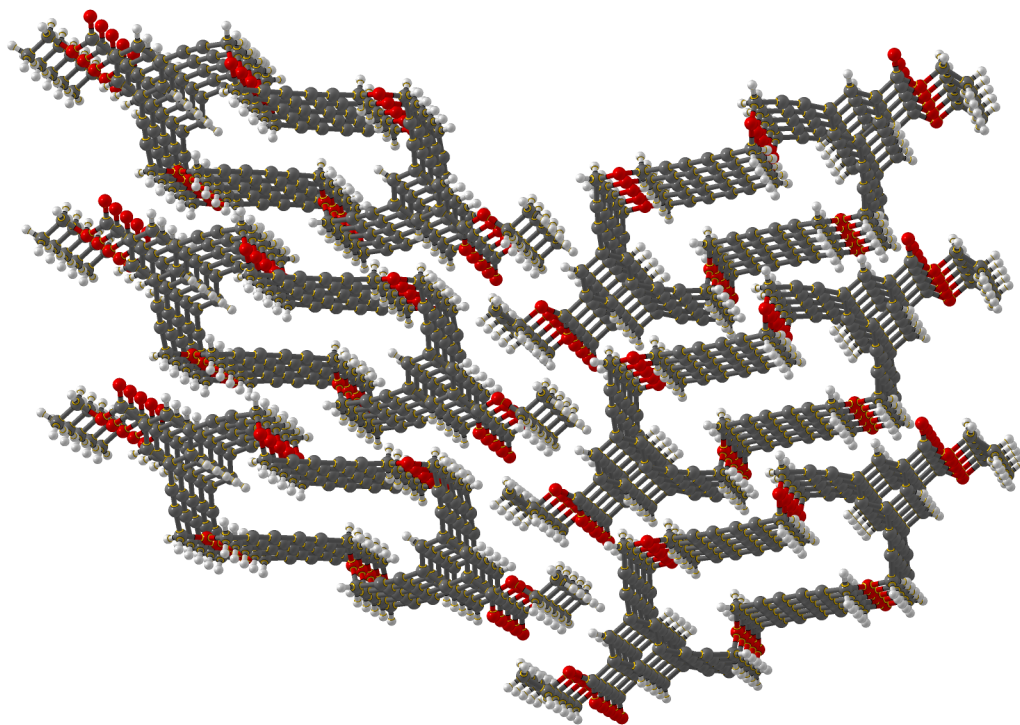


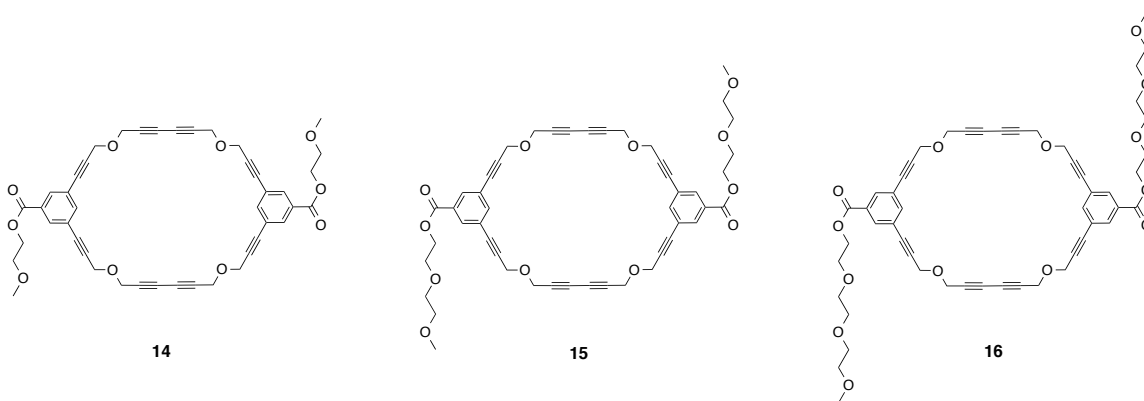
Figure 3.17. The X-ray crystal structure of macrocycle **11**. Top view.

We attempted to measure the melting point of the crystal. When the crystal is heated up to 110 °C gradually, its color turned brown and suddenly black, indicating the polymerization or decomposition taking place, with an uncontrollable rate. As a consequence, it lost all crystallinity.

Compared to macrocycles **4** and **6**, reported by Wang⁸³ and Hsu⁸⁵ respectively, macrocycle **11** does not show any improved solubility. As a matter of fact, it has very poor solubility in most common organic solvents and is only slightly soluble in methylene chloride.

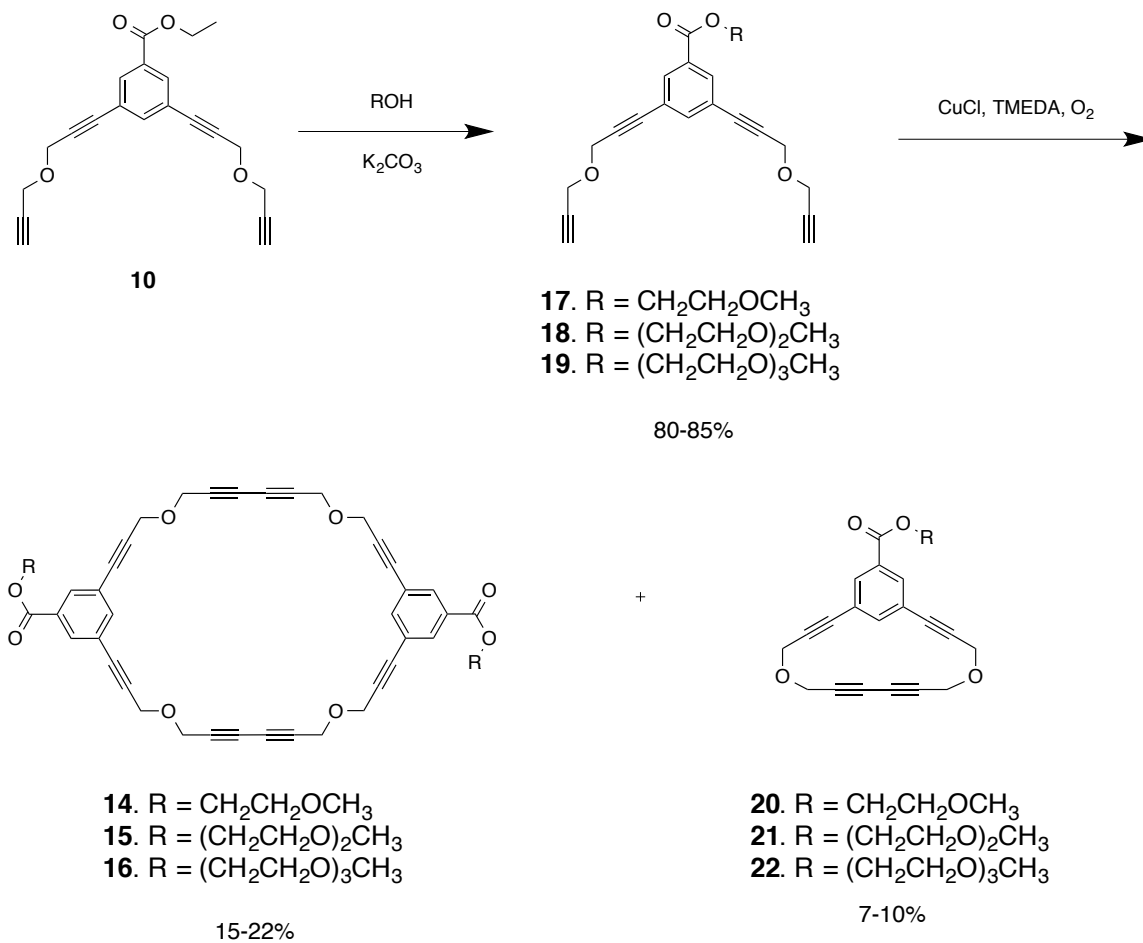
It is known that the existence of glycolic segments can dramatically enhance the solubility of molecules in polar organic solvents due to the interactions between oxygen atoms and solvents.⁹¹ To achieve larger spacing distance in crystals as well as increase the solubility of the macrocycles, we designed and prepared the following macrocycles (**Scheme 3.10**), by introducing glycolic segments with different lengths.

Scheme 3.10. Macrocycle candidates with modified ester functional groups.



Since the macrocycle **11** is insoluble in most organic solvents, it is very difficult to conduct any chemical reactions on it and further modify the macrocycle. The introduction of glycolic segments must be carried out before the ring closing.

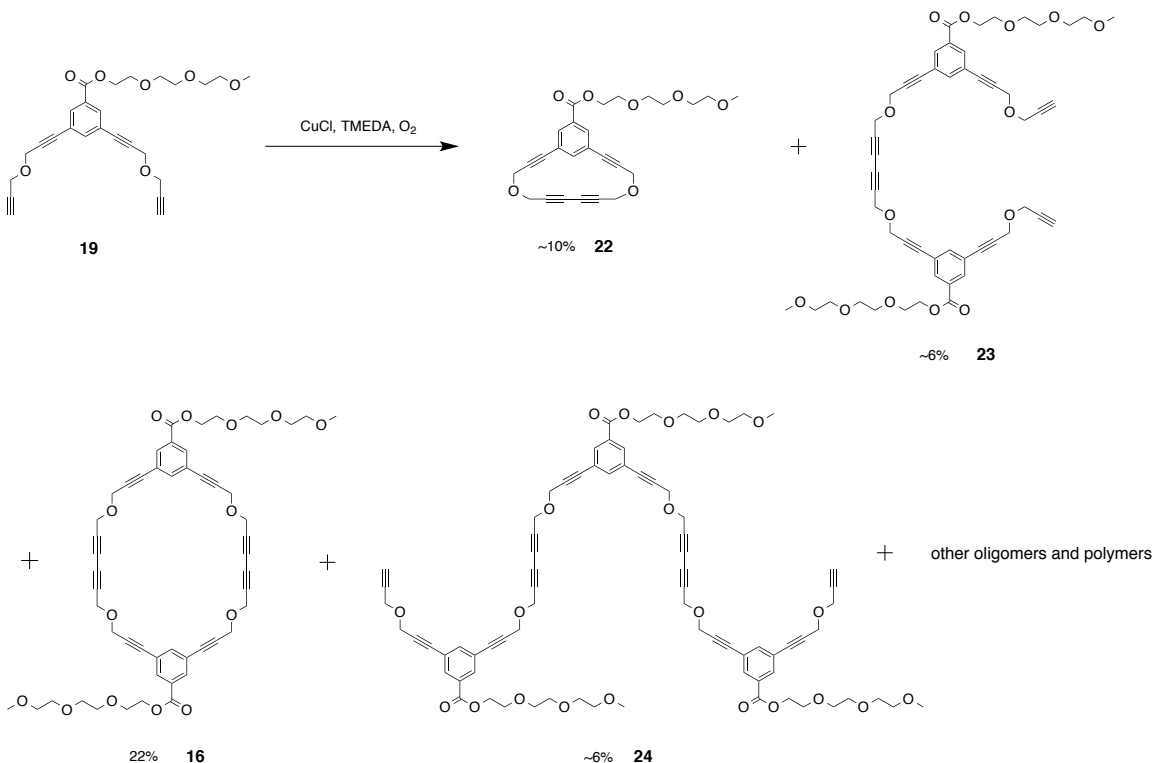
Scheme 3.11. Synthesis of macrocycles containing glycolic segments



We successfully obtained all three macrocycles, as well as the intramolecular self-cyclization macrocycles, as shown in **Scheme 3.11**. As expected, there is increasing solubility as we go from the macrocycle **14** to **16**. Macrocycle **16** is very soluble in methylene chloride. It also shows moderate solubility in other polar aprotic solvents, such as ethyl acetate.

The reaction yields for Hay coupling are relatively low, which is not a surprising result. In the reaction of Hay coupling for macrocycle **16**, we carefully separated all products (**Scheme 3.12**). They were later confirmed as monomer **22**, linear dimer **23**, cyclic dimer **16** (the desired macrocycle) and linear trimer **24**, respectively, via ^1H NMR and mass spectrometry. This result further proved the complexity of the reaction system.

Scheme 3.12. The separation of monomer, linear dimer, cyclic dimer, and linear trimer in a macrocycle synthesis



Among all of these products the crystal of cyclic monomer **21** has been obtained via slow evaporation from a mixed solvent of ethyl acetate and methanol (ratio 1:2/volume) at room temperature. X-ray diffraction studies show the crystal lattice is triclinic, with space group P-1

(**Figure 3.18**). In the crystal, the macrocycles are nearly flat and form a layer-by-layer structure. From the top view of the crystal (**Figure 3.19**), the phenyl rings stack to each other via π - π interactions in almost perfect conformation. The π - π stacking appears to be the driving force for the formation of the crystal structure. The repeat distance between diacetylene functionalities is 8.89 Å, which shows little potential to polymerize topochemically.

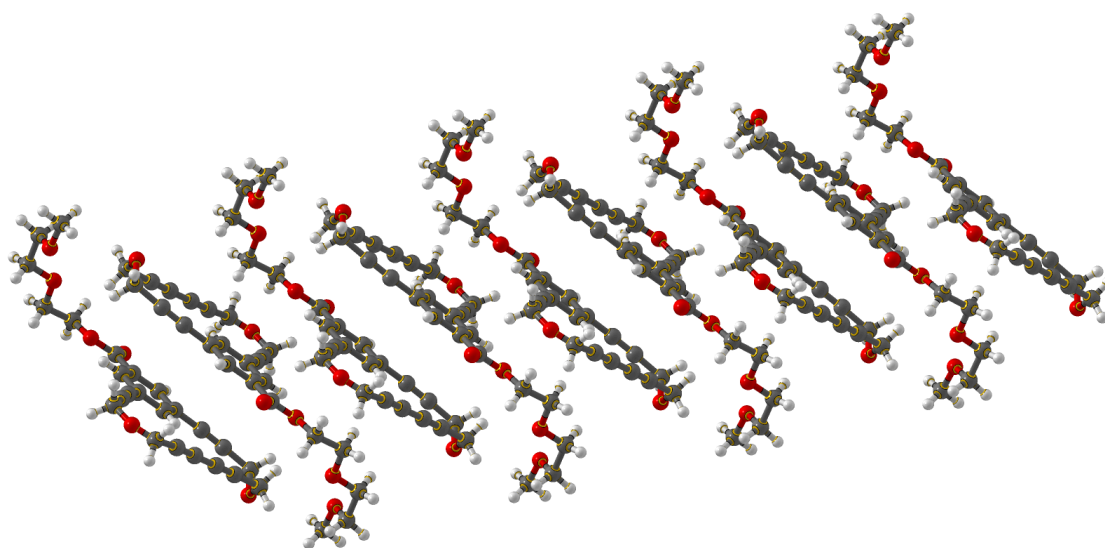


Figure 3.18. The X-ray crystal structure of compound **21**. Side view.

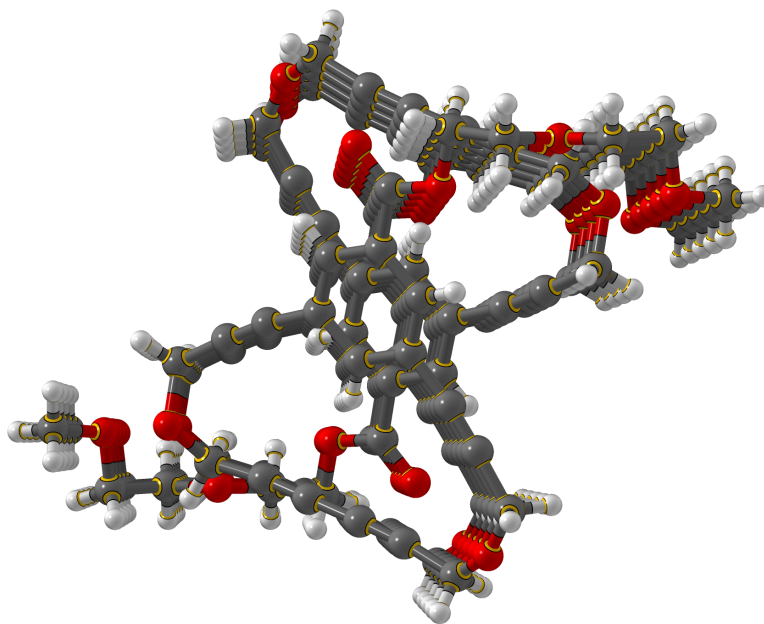


Figure 3.19. The X-ray crystal structure of compound **21**. Top view.

Similarly, the crystal of macrocycle **15** has been obtained via slow evaporation from a mixed solvent of ethyl acetate and methanol (ratio 1:1/volume) at room temperature. X-ray studies confirmed that the macrocycles packed to form a tubular structure, with a repeat distance of 4.43 Å (**Figure 3.20**).

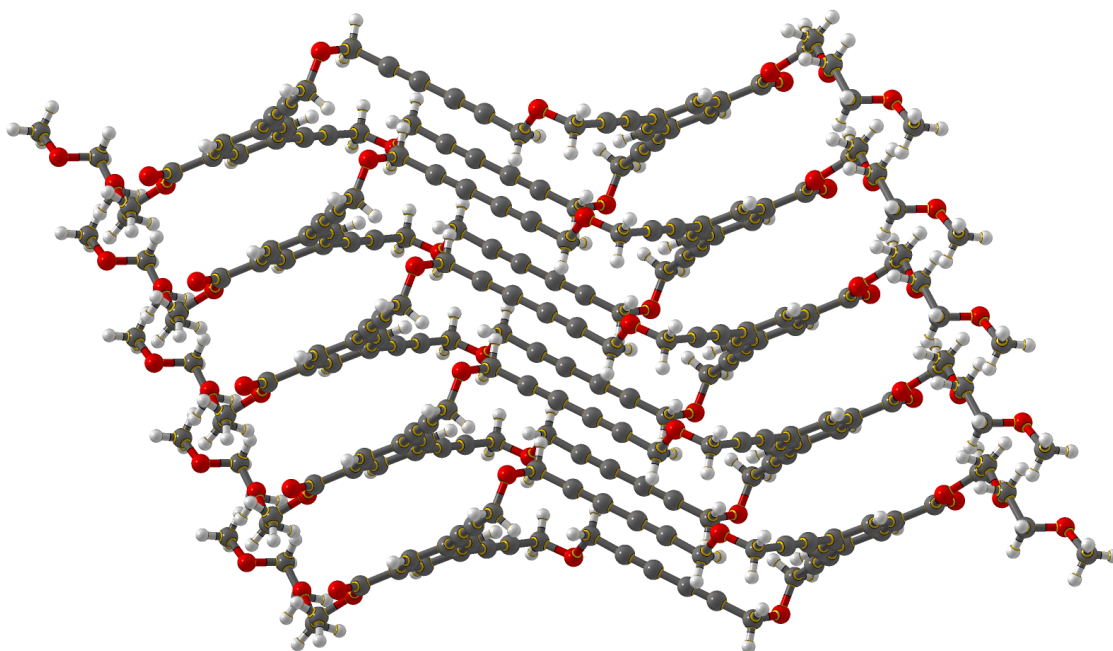


Figure 3.20. The X-ray crystal structure of compound **15**. Side view.

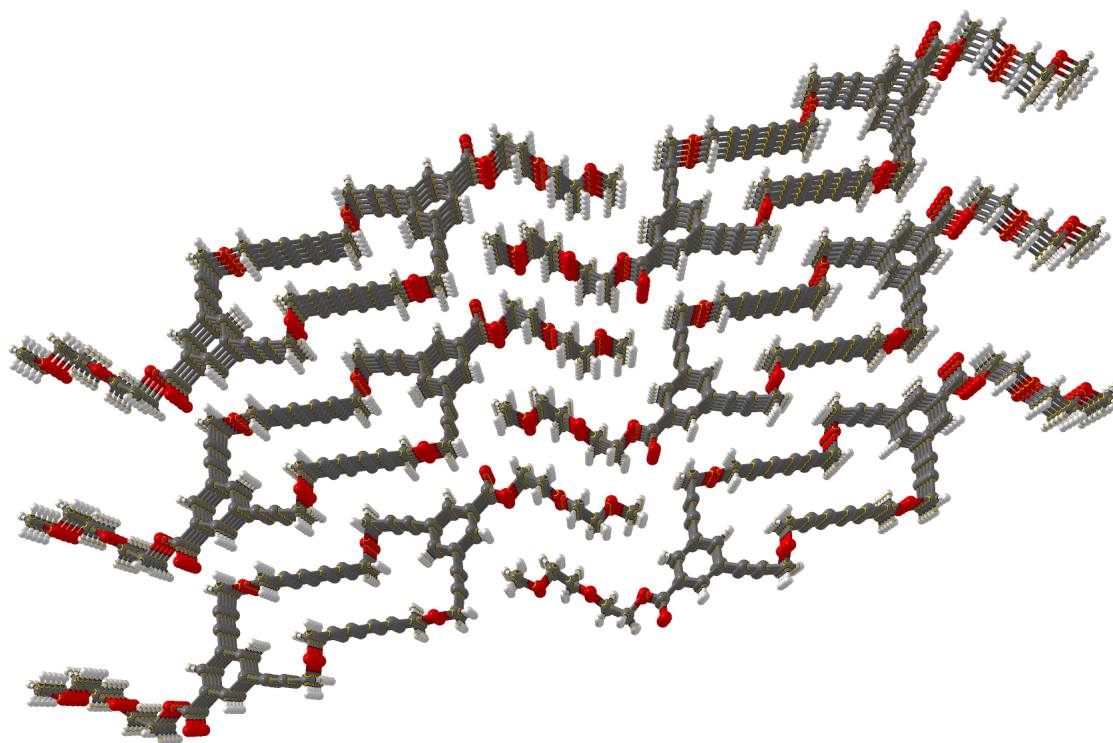


Figure 3.21. The X-ray crystal structure of compound **15**. Top view.

The white crystal of macrocycle **15** turned brown in a few days after crystallization, showing less stability than macrocycle **11**. However, X-ray diffraction confirmed that the crystal still contained unpolymerized diacetylene.

When the crystal is heated up to ~ 150 °C, it turns black instantly, indicating the occurrence of polymerization or decomposition. The compound does not melt up to 300 °C.

We also conducted crystal growth experiments for other macrocycles. However, no X-ray quality crystals have been obtained so far. Though macrocycle **16** is soluble in some solvents, experiments showed that it was likely to precipitate from solution in an amorphous state. This is probably because the long and soft side arms at either end in the macrocycle prohibit it from forming a rigid and consistent structure.

Macrocycles **14**, **15** and **16** all show good stability. These white solids turn light yellow in a few days, yet ^1H NMR spectra show no difference. None of the macrocycle crystals melt.

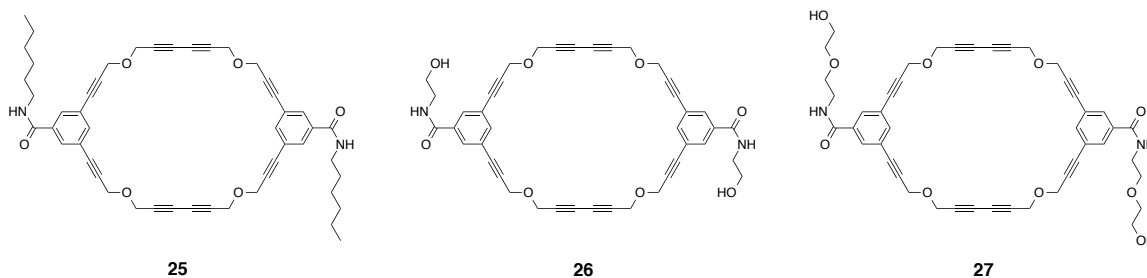
3.4.2 Macrocycles containing amide substituents

The studies of macrocycles containing ester functional groups did not give perfect results in terms of packing in crystal. In this section, we continue our modifications on these macrocycles by converting esters to amides.

Three macrocycles containing amide functional groups were targeted (**Scheme 3.13**). In these macrocycles, the amides at either end could potentially provide hydrogen bonding when forming crystals. Because the molecular spacing for macrocycle **11** is shorter than the ideal parameter for topochemical polymerization, we plan to add the hexamine tails (shown in

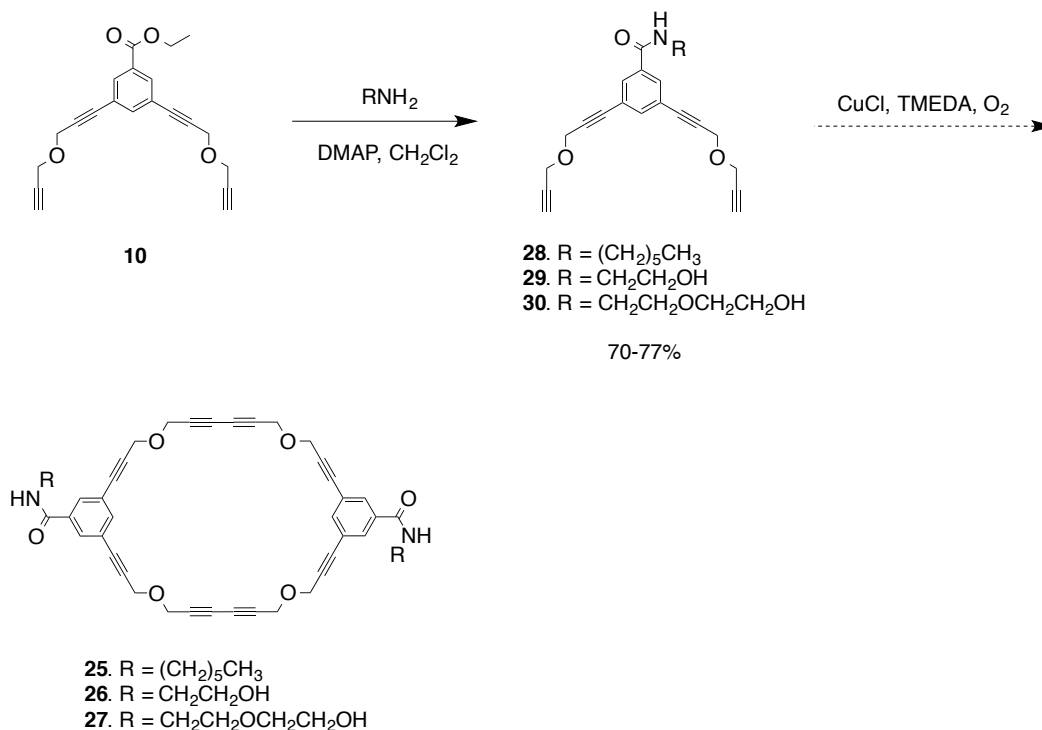
macrocycle **25**) in order to increase the packing distance. In addition, in macrocycles **26** and **27**, the existence of glycol segments could also help enhance the solubility of the macrocycles in solution.

Scheme 3.13. Macrocycle candidates with amide functional groups



We obtained the uncoupled amides by reacting compound **10** with the corresponding amines in the presence of DMAP (**Scheme 3.14**). These reactions went smoothly. However, the separation of Hay coupling products was unsuccessful. In the synthesis of macrocycle **26**, by monitoring the TLC measurements (solvent: ethyl acetate/hexanes 5:1/v), we found that most of the products stayed at the base line and could not be separated. It is probably due to the formation of oligomers or polymers. We carefully obtained a small amount of the potential macrocycle that precipitated in the test tube as tiny white crystals. The white crystals turned purple very quickly and no longer dissolved in any solvents. Thus we could not obtain an NMR spectrum for its structure analysis. Due to the small size of the crystal, attempts at an X-ray diffraction study were also a failure.

Scheme 3.14. Synthesis of macrocycles containing amides functional groups

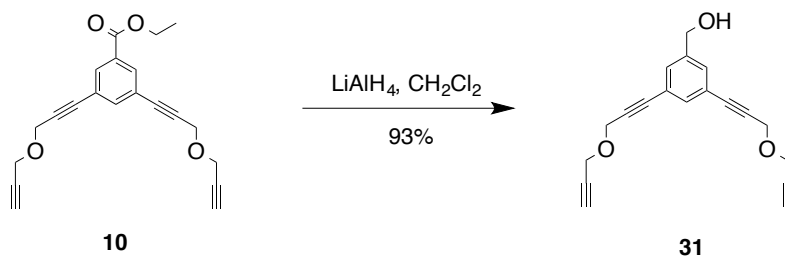


3.4.3 Macrocycles containing carbamate substituents

The amide-to-amide hydrogen bond in carbamate or its derivatives can establish a molecular repeat distance of $\sim 5 \text{ \AA}$, very close to the requirement for topochemical polymerization of diacetylenes. A large number of diacetylenes used for polymerization are actually carbamate derivatives.⁹² Because the introduction of carbamate functionality into macrocycles might help establish the ideal spacing in crystal, we also designed a few macrocycles that contained carbamate substituents.

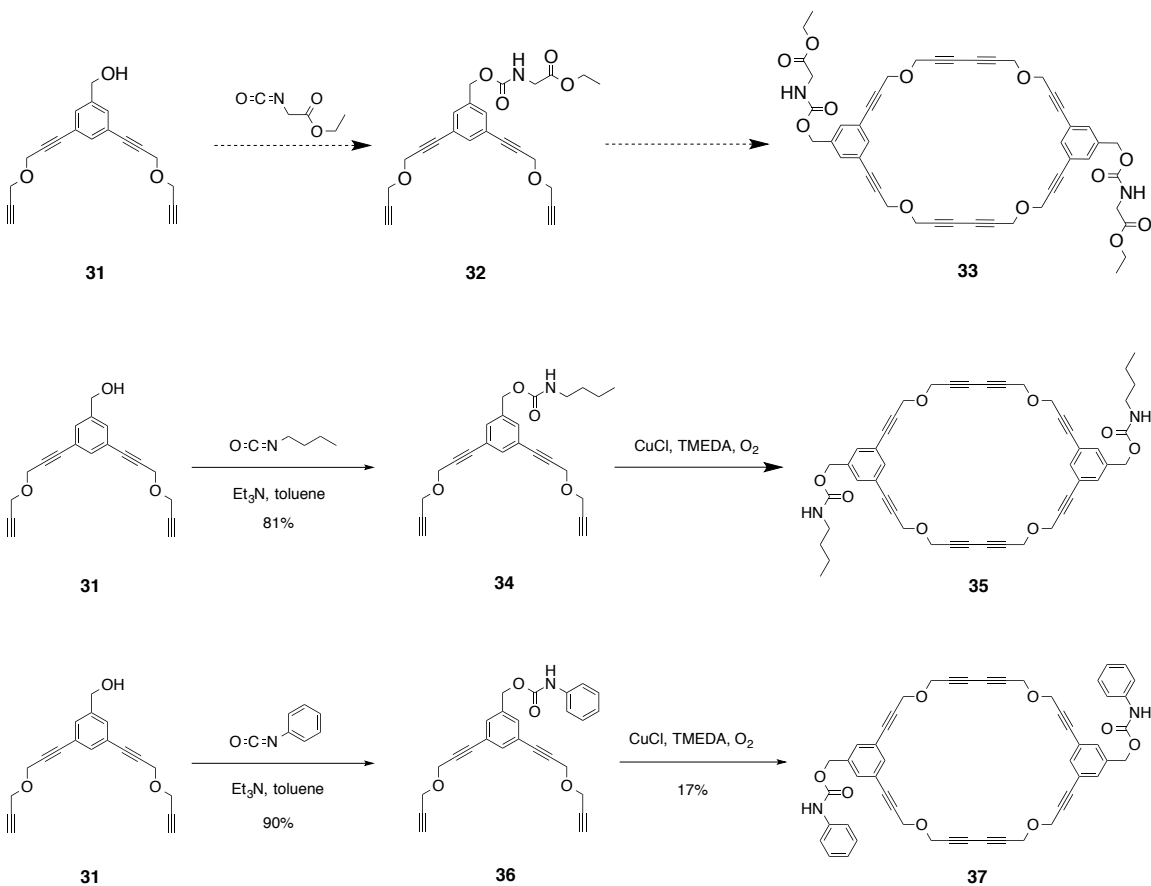
The synthesis involves two steps based on compound **10**. The first step is to reduce the ester functional group to its alcohol by using LiAlH_4 (**Scheme 3.15**).

Scheme 3.15. Reduction of ester functional group to primary alcohol



The second step is to use compound **31** to react with isocyanides, providing its carbamate derivatives.

Scheme 3.16. Synthesis of macrocycles containing carbamate functional groups



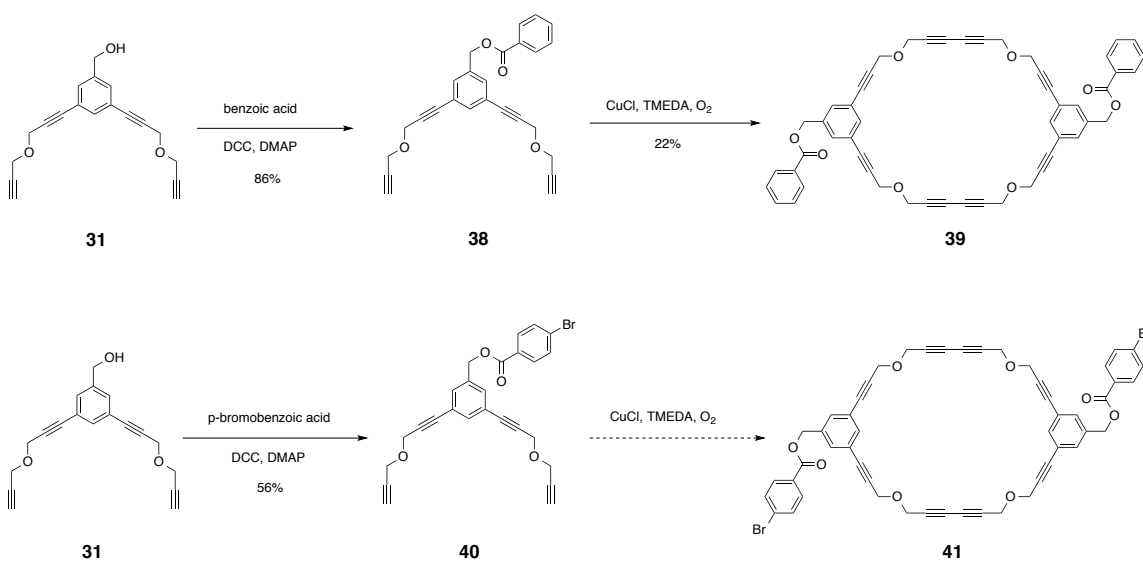
As shown in Scheme 3.16, the synthesis of macrocycle **33** failed due to unknown reasons. Hay coupling for macrocycle **35** gives a pretty low yield. We only successfully obtained the pure macrocycle **37**.

The purple macrocycle **37** crystals precipitate from mixed solvents methylene chloride and ethyl acetate (2:1/v). However, the small size of the crystals prohibits a full X-ray diffraction study. Like other macrocycles we have obtained, macrocycle **37** does not melt.

3.4.4 Macrocycles containing benzoate substituents

In general, large substituents could increase the spacing between molecules. It is why we want to introduce benzoate functional groups in the macrocycles. By allowing compound **31** to react with certain carboxylic acids, we can easily obtain the precursors for the macrocycles containing benzoate substituents. Two trials related to this thought are listed in **Scheme 3.17**. We successfully synthesized macrocycle **39** and obtained the pure product. In contrast, the reaction toward synthesizing macrocycle **41** is a failure for unknown reasons. No desired macrocycle was observed in the synthesis.

Scheme 3.17. Synthesis of macrocycles containing benzoate functional groups



The crystal of macrocycle **39** was obtained from methylene chloride at room temperature via slow evaporation. This structure is completely different from the crystal structures of

macrocycles we previously obtained. Instead of forming a tubular structure, the macrocycles in the crystal intertwine to each other, as shown in **Figure 3.22**. The side arms (benzoate substituents) insert into the interior of the neighboring macrocycles and occupy the hollow space. From the side view of the crystal (**Figure 3.23**) we can conclude that the π - π stacking between the phenyl rings in benzoates, which helps stabilize the structure, induces this “strange” packing style.

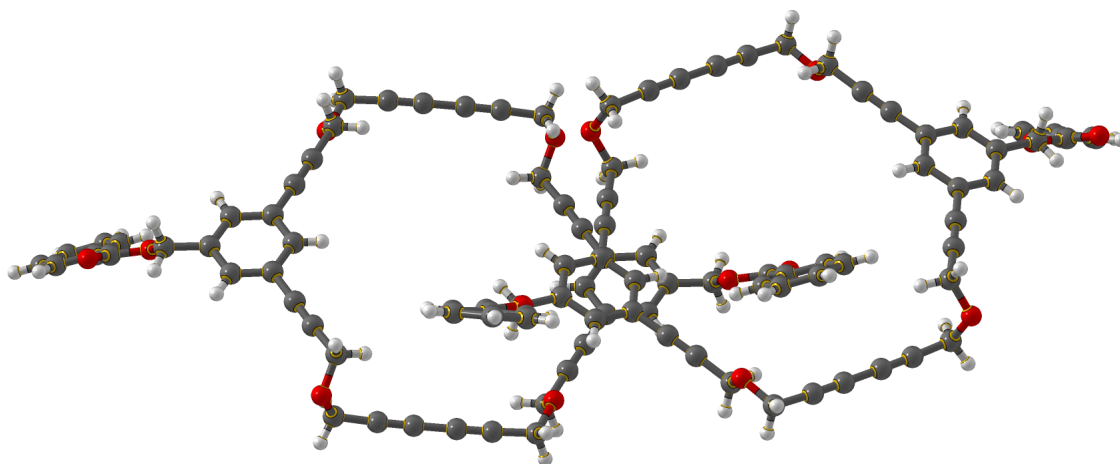


Figure 3.22. The X-ray crystal structure of macrocycle **39**. Top view.

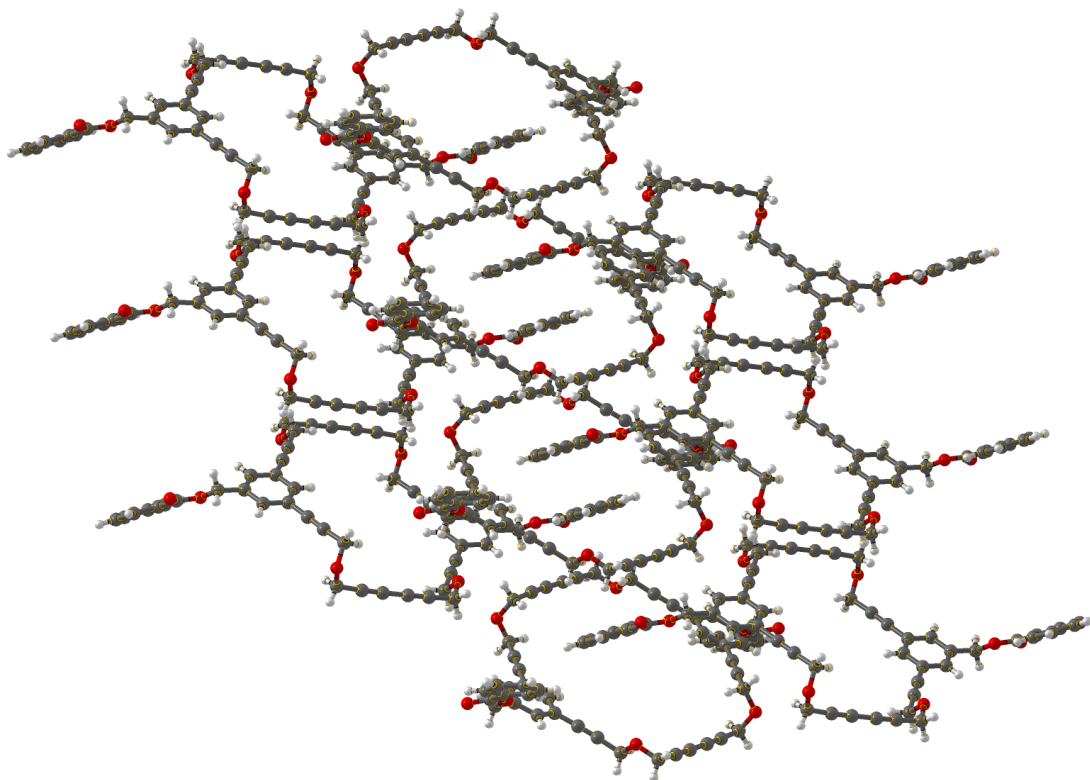
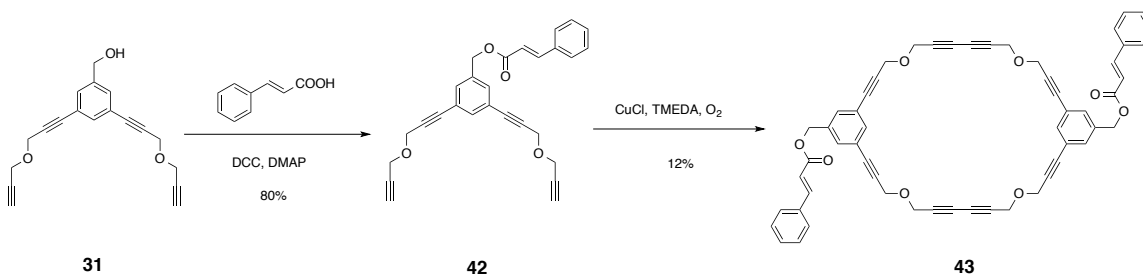


Figure 3.23. The X-ray crystal structure of macrocycle **39**. Side View. π - π interaction.

3.4.5 Macrocycles containing cinnamate substituents

As mentioned in Chapter 1, [2+2] photodimerization (**Figure 1.5**) between cinnamic acids was thoroughly investigated in the past. We think the tubular packing style of macrocycles could also provide an ideal environment for [2+2] photodimerization, if the side arms in the macrocycles are appropriated functionalized. It is an interesting study as it would broaden what we know about the macrocycles. To investigate the possibility of [2+2] photodimerization, we designed and synthesized macrocycle **43**.

Scheme 3.18. Synthesis of macrocycle containing cinnamate functional groups



Macrocycle **43** is soluble in methylene chloride and methanol. A yellow crystal of **43** was obtained from mixed solvents methanol and ethyl acetate (1:1/v) at room temperature via slow evaporation. However, the crystal is not of X-ray quality.

3.5 General Discussion

3.5.1 Synthesis

We have synthesized a series of diacetylenic macrocycles containing different functional groups. The Hay coupling reaction was used for the cyclizations throughout the project. Overall, the synthesis is very challenging, mainly due to the structural characteristics of the precursors of macrocycles. Two arms in the precursors could have many different possibilities to link molecules together, generating a complex that including monomer, dimer, trimer, and other oligomers.

Cadiot-Chodkiewicz coupling has been attempted to synthesize the macrocycles, but it was unsuccessful. Despite of the relatively low yields of Hay coupling, our approach to synthesizing macrocycles containing diacetylene functionalities is by far the simplest and most efficient.

3.5.2 Solubility

Another issue in the syntheses is the poor solubility of some macrocycles. Sometimes the poor solubility made the separation and purification very difficult to be accomplished. Increasing the solubility of the macrocycles is one of our aims. We demonstrated that the introduction of glycolic segments could increase the solubility of the macrocycles. Other functional groups that can provide large polarity or hydrogen bonding may help enhance the solubility in polar protic solvents, as well. With better solubility, there are more opportunities for the crystal growth and applications of macrocycles.

3.5.3 Stability

A few macrocycles obtained in this project appeared unstable, as they changed color quickly after they were purified from column chromatography, which prohibited us from characterizing the pure products. However, this phenomenon is very promising. It shows the relatively high reactivity of the macrocycles. The color change at room temperature usually implies the occurrence of polymerization of diacetylenes, instead of decomposition, although we do not know at this point whether these materials polymerize partially or fully. Unfortunately,

because of the small size of the crystals, so far we could not confirm the polymerization via X-ray diffraction.

3.5.4 Intramolecular self-cyclization

Intramolecular self-cyclization takes place in the synthesis of almost every macrocycle and acts as the biggest competition reaction. Adjustment of concentration of the macrocycle precursors in the Hay coupling could reduce the formation of the intramolecular self-cyclization products (monomers). Among the accomplished experiments, we successfully separated some intramolecular self-cyclization products. In general, they have similar polarity to the corresponding dimer macrocycles, as they are very close to the desired macrocycles on TLC plates. Due to the similarity of chemical environments, it is not surprising that these two types of macrocycles have almost identical chemical shifts in ^1H NMR spectra. However, we interestingly found that the chemical shifts of protons in the methylene groups, as shown in **Figure 3.24**, are distinguishable.

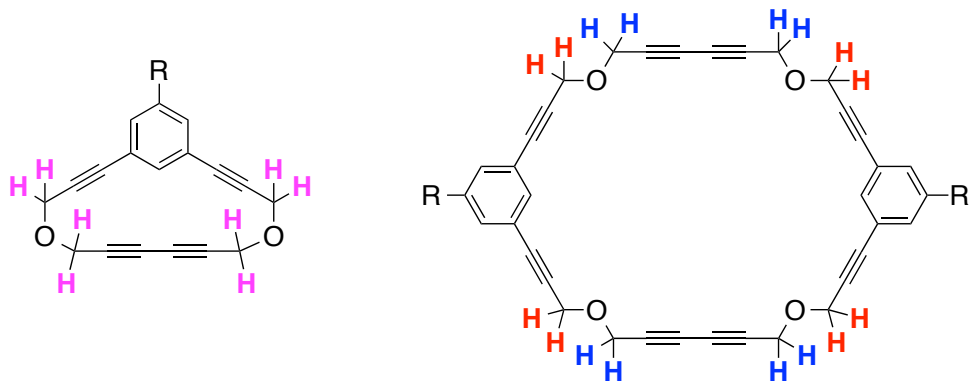
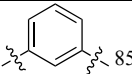
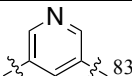
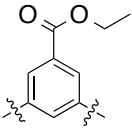
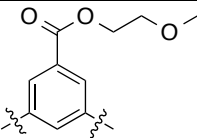
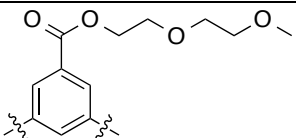
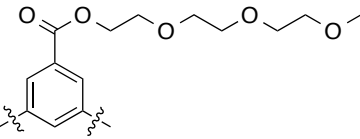
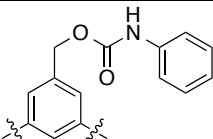
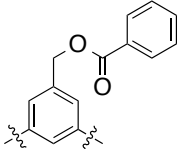
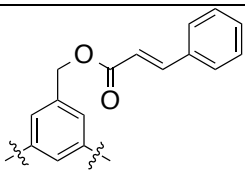


Figure 3.24. ^1H NMR studies. In the monomer, protons (purple) have the same chemical shifts, representing as a singlet in ^1H NMR spectra. In the dimer, protons (blue and red) have different chemical shifts, representing as a pair of singlets in ^1H NMR spectra.

In the dimers (**Figure 3.24**, right), there are two different types of protons in the methylene groups in terms of chemical environment (Shown in blue and red, respectively). Consequently, we observed a pair of strong singlets, having chemical shifts ~ 4.4 and ~ 4.5 ppm, respectively. On the other hand, though there are two different types of protons in the monomer as well, we only observed a strong singlet for the protons (**Figure 3.24**, left, protons are shown in purple).

Table 3.2 lists all the data we obtained from ^1H NMR experiments.

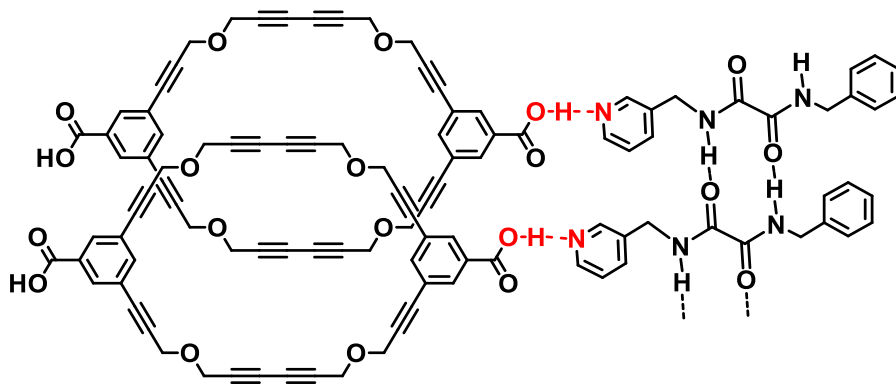
Table 3.2. Chemical shifts of protons in the methylene groups in macrocycles (ppm). The compound numbers are shown in the parentheses.

Structures of Macrocycles	Monomer (singlet)	Dimer (2 singlets)	
	4.41	4.41	4.49
	4.42	4.41	4.50
	Not separated	4.41 (11)	4.50 (11)
	4.41 (20)	4.41 (14)	4.49 (14)
	4.42 (21)	4.41 (15)	4.50 (15)
	4.41 (22)	4.40 (16)	4.49 (16)
	Not separated	4.41 (37)	4.48 (37)
	Not separated	4.41 (39)	4.49 (39)
	Not separated	4.41 (43)	4.49 (43)

All the synthesized monomers and dimers satisfy the “*singlet/2 singlets*” empirical rule. This can be used to quickly determine if a separated compound is the monomer or dimer in our future experiments, in the absence of mass spectrometry and X-ray diffraction. (In fact, mass spectrometry is not always a reliable approach to determining the structure because sometimes the molecular ion peak cannot be observed in mass spectrometry analysis. In addition, as we found in the spectra, the dimer may generate a fragment that has similar molecular weight to the corresponding monomer, depending on the stability of the dimer.)

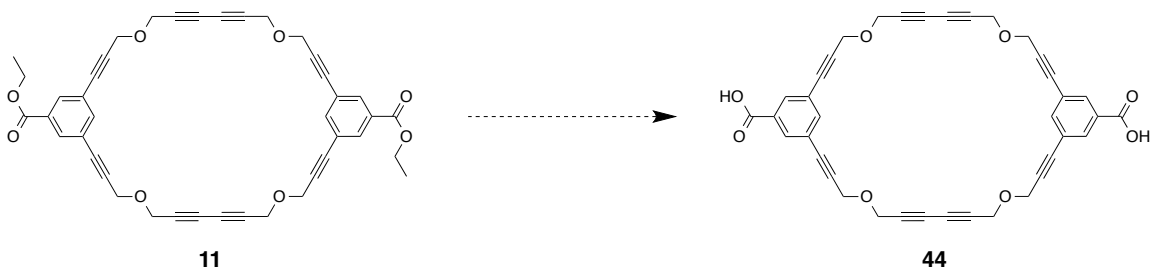
The crystal structures obtained imply that achieving the ideal molecular spacing for topochemical polymerization is not an easy task. Because the host-guest strategy has proven to be powerful to control the distance between the diacetylene functionalities, we also attempted to apply host-guest strategy to the substituted macrocycle systems. Similar to what we introduced in Chapter 2, the N \cdots H–O hydrogen bond was designed to link the host and guest molecules, as shown in **Scheme 3.19**.

Scheme 3.19. The planned host-guest strategy for macrocycle assembly



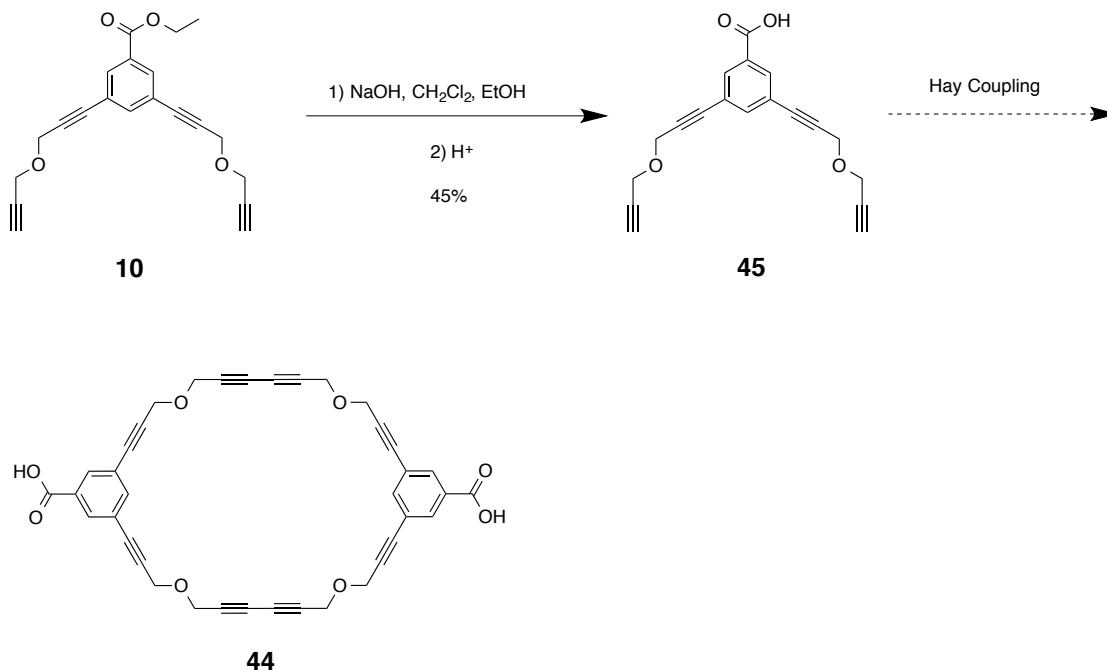
Due to poor solubility of macrocycle **11**, the direct hydrolysis was not achieved.

Scheme 3.20. An unsuccessful attempt for the hydrolysis of macrocycle **11**



As an alternative synthesis, we first converted diether **10** to the corresponding carboxylic acid. This reaction proceeded smoothly, with a yield of 45% (**Scheme 3.21**). However, in the crude products from Hay coupling of compound **45**, we could not separate the pure macrocycle **44**. It might also be a solubility problem.

Scheme 3.21. The designed synthesis toward macrocycle **44**



3.6 Conclusion

In this project, we developed a general strategy to synthesize macrocycles containing diacetylene functionalities, based on the pioneering work that was done by group members Wang, Chow and Hsu. Esters, amides, carbamate, benzoate, and cinnamate functional groups were introduced as substituents on the macrocycles. These synthesized macrocycles display many different properties, such as polarity, solubility, stability, and so on. Most macrocycles showed relatively good stability in solution, while some of them appeared unstable as they changed color rapidly when exposed to the atmosphere or in solid state, implying partial polymerization.

Previous studies revealed that similar macrocycles usually have poor solubility in solution, which made it very difficult to obtain their crystal structures or further explore their applications. We demonstrated that the introduction of glycol segments could largely enhance their solubility. By using this method, more soluble macrocycles can be synthesized in the future. Moreover, introduction of other polar substituents to the macrocycles could also increase the solubility in polar aprotic solvents.

Due to poor solubility or inappropriate crystal growth conditions, many macrocycles cannot be achieved as good crystals. Among these desired macrocycles, we obtained three crystals that were fully characterized by X-ray diffractometry. Two of them (macrocycles **11** and **15**) have the appropriate packing and form tubular structures, while the third one (macrocycle **39**) has an unexpected packing in the crystal. The most promising macrocycles for topochemical polymerization would be those with amide substituents because the hydrogen bonding between amides could provide a molecular spacing that is very close to the ideal 4.9 Å needed for topochemical polymerization. In addition, the color change of the final products observed during the separation implies the polymerization process in crystals. More work should focus on these macrocycles or their analogues.

Because the macrocycles possess many different conformations and one of the main driving forces for the packing in crystals is the weak π - π interaction, it is not hard to understand the relatively small chances for crystal growth. Future work will be focused on crystal growth in different conditions, such as at gradually increasing temperatures. For one thing, topochemical polymerization and other applications are based on the ideal packing of macrocycles in crystals. For another, this whole study provides a great opportunity to investigate certain effects in crystal

growth, such as the framework of molecules, polarity, and sizes of substituents. The research could present further important development in the field of *Crystal Engineering*.

Chapter Four

Hydrogen bonding in crystal engineering

4.1 Background

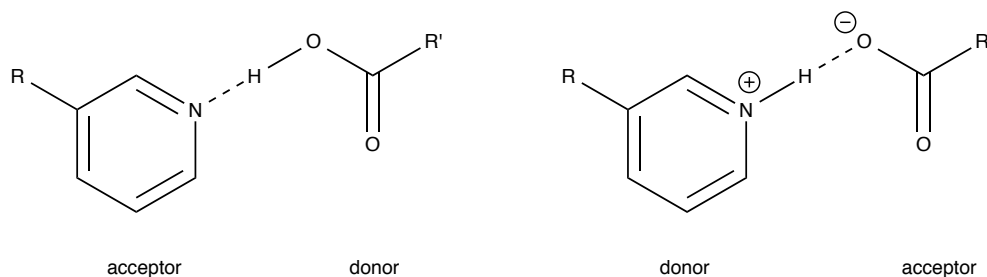
The hydrogen bond is the most important non-covalent interaction in the design of supramolecular structures, because of its strength and high degree of orientation. It is a special dipole-dipole interaction between a proton donor and a proton acceptor. Many natural species, such as amino acids, carbohydrates and nucleobases are a rich source of hydrogen-bond donors and acceptors.

The strength of hydrogen bond mainly depends on the electronegativity of the atoms to which the hydrogen atom is attached and the geometry of the hydrogen bond (*e.g.* linear or bent). Hydrogen bonds can be divided into three broad categories: strong, moderate, and weak, in terms of bond energy. A strong interaction is by some means similar to a covalent bond, where the donor atom, hydrogen atom, and acceptor atom are practically linear. Examples of strong interaction usually involve atoms with strong electronegativity, such as F and O. This type of hydrogen bonds could be found in HF complexes or carboxylic acids to carboxylate anions. Moderate-strength hydrogen bonds have a bond angle $\sim 130\text{-}180^\circ$ and are usually formed between neutral donor and neutral acceptor groups. Examples include the self-association of

carboxylic acids or alcohols. In comparison, weak hydrogen bonds are less likely to be seen. The bond angle ranges from 90° to 180° . A typical weak-strength interaction usually contains carbon atoms or π electron systems, in the forms of $C-H\cdots A$ (acceptor) and $\pi\cdots H-D$ (donor).

Among the three categories, the moderate interaction is of most interest to us because it has been seen most widely and used in crystal engineering. We have successfully applied the moderate-strength $O-H\cdots N$ hydrogen bonds in our host-guest strategy, as discussed in Chapter 2. We have obtained the desired co-crystals via hydrogen bonding between a pyridine and a carboxylic acid. A reasonable consideration is that there could be two possibilities of hydrogen bonding between the host and guest molecules, which are the $O-H\cdots N$ type and $O\cdots H-N$ type, respectively. In the first case (**Scheme 4.1**, left), there is no formal proton transfer and we have a co-crystal. In the second case (**Scheme 4.1**, right), there is a proton transfer and we have a salt.

Scheme 4.1. Two types of hydrogen bonding



Can we predict what kind of hydrogen bonding will be applied for crystal growth in a certain system? We do not always know. In co-crystal **3** (**Figure 2.8**), the position of hydrogen atoms in the hydrogen bonds was located and refined in the SHELXTL program. It reveals that

the bond length between oxygen and hydrogen atoms is 0.820 Å, while that between nitrogen and hydrogen atoms is 1.840 Å. These parameters clearly suggest that there is a covalent bond between oxygen and hydrogen atoms, and a hydrogen bond between nitrogen and hydrogen atoms. The hydrogen bond in co-crystal **3** can be presented as the O–H···N type, with a bond angle of 171.7°.

From the point of view of classical acid-base theory, the pK_a of typical carboxylic acids is around 4.5, while the pK_a of pyridinium is around 5. The acidity of a carboxylic acid and a pyridinium is very close. Previous studies showed that pyridines and carboxylic acids could form both co-crystals and salts.⁹³ A Cambridge Structure Database (CSD) survey reveals that there are hundreds of examples for the formation of hydrogen bonds from a pyridinium and a carboxylate (one of the examples is shown in **Figure 4.1**) as well as that from a pyridine and a carboxylic acid (one of the examples is shown in **Figure 4.2**). However, the proton transfer does not occur in co-crystal **3**. Because of the lack of pK_a values of carboxylic acid and pyridinium in solid phase as well as the complexity of co-crystal formation, it is not easy to predict the patterns of hydrogen bonding in solid state even for a simple acid-base system.

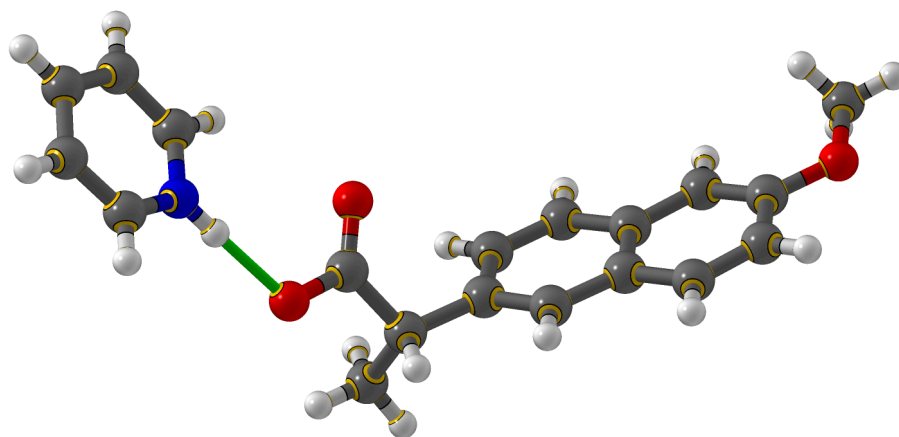


Figure 4.1. A hydrogen bond formed from a pyridinium and a carboxylate⁹⁴

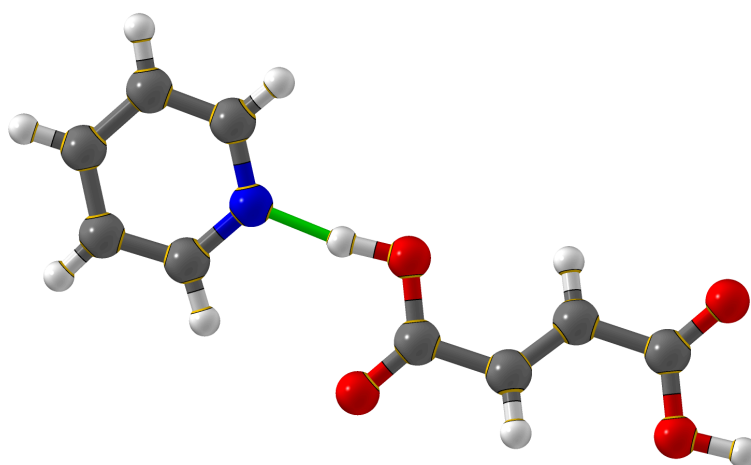


Figure 4.2. A hydrogen bond formed from a pyridine and a carboxylic acid⁹³

4.2 A Cambridge Structure Database Survey

The goal of crystal engineering is to analyze known structures and thoroughly understand the intermolecular interactions, in order to produce desired crystals in good quality. To further explore the hydrogen bond formation, we conducted a CSD survey for the hydrogen bonds involving nitrogen, hydrogen, and oxygen atoms.

Our group has been focused on the hydrogen bond formation for a long time. Compared to a pyridinium, an ammonium group is a much weaker acid with pK_a of ~ 9 , implying an amine should more readily form salts with a carboxylic acid via proton transfer. The crystallization between carboxylic acids and primary amines has been explored by Zhong and co-workers, who conducted more than 10 experiments and demonstrated that the primary amines form salts with carboxylic acids in every case.⁹⁵ In particular, we are interested in tertiary amines. Would they also form co-crystals or salts with carboxylic acids?

In the CSD survey, there are two phenomena that attracted our attention. On the nitrogen atom side, the number of examples involving tertiary ammonium groups is much fewer than that of primary and secondary ammonium groups even though the pK_a s are very similar. This could be easily understood since primary and secondary ammonium ions are much less hindered, and thus the formation of hydrogen bonds can be achieved more easily compared to tertiary ammonium groups. In addition, primary and secondary ammonium ions have more protons, which should increase the opportunity of forming hydrogen bonds in crystals.

On the oxygen atom side, the carboxylate tends to form two hydrogen bonds with other molecules by using both of its oxygen atoms. This is also understandable as more hydrogen bonds could lower the energy of the carboxylate and stabilize the crystal structures. As a matter

of fact, a carboxylate that forms only one hydrogen bond is relatively unstable. The number of examples in the CSD with a single hydrogen-bonded carboxylate is very small.

Considering these two facts, is it possible to form a hydrogen bond between a tertiary ammonium and a single hydrogen-bonded carboxylate? Although it is very unlikely, we did find some examples in the CSD survey.

In general, these examples can be divided into two categories. Because a carboxylate has a tendency to form two hydrogen bonds, a single hydrogen-bonded carboxylate is obtained when other effects, *e.g.* electron distribution, can stabilize it.

The typical carboxylate that forms only one hydrogen bond is trifluoroacetate. Because of the strong electron withdrawing effect from three fluorine atoms, trifluoroacetate has a much lower electron density on the oxygen atoms, making them less likely to form two hydrogen bonds. Examples are shown in **Figure 4.3** to **Figure 4.6**. The crystals are represented with their six-letter ref codes, which can be used to retrieve their structural diagrams in CSD.

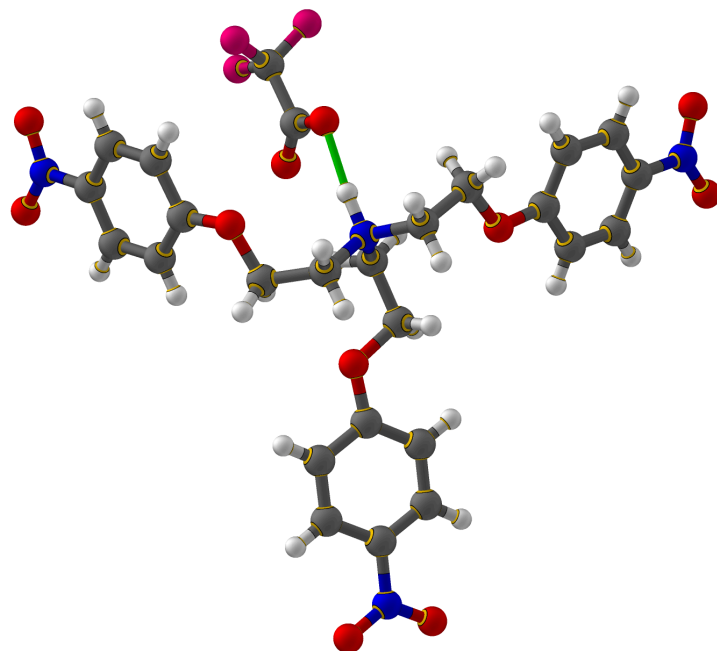


Figure 4.3. Crystal structure of EJUNON⁹⁶

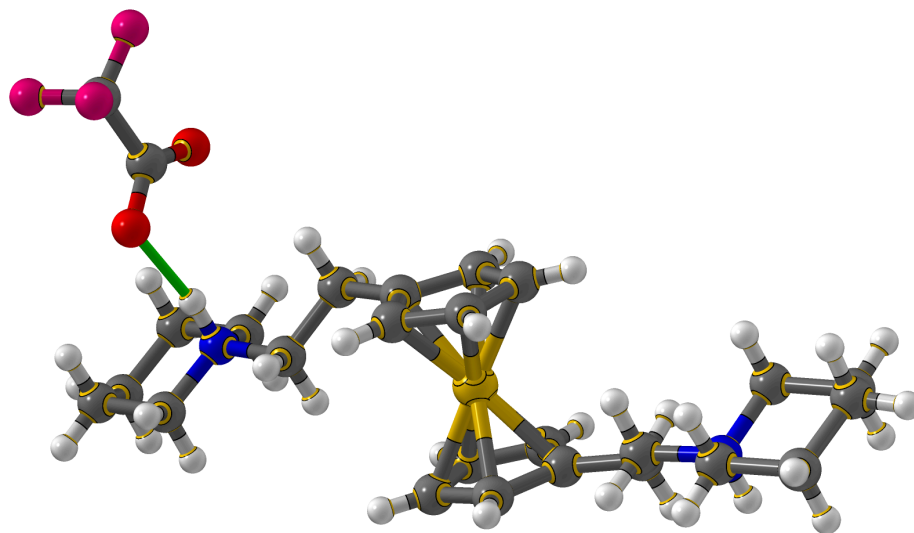


Figure 4.4. Crystal structure of BAPHOQ⁹⁷

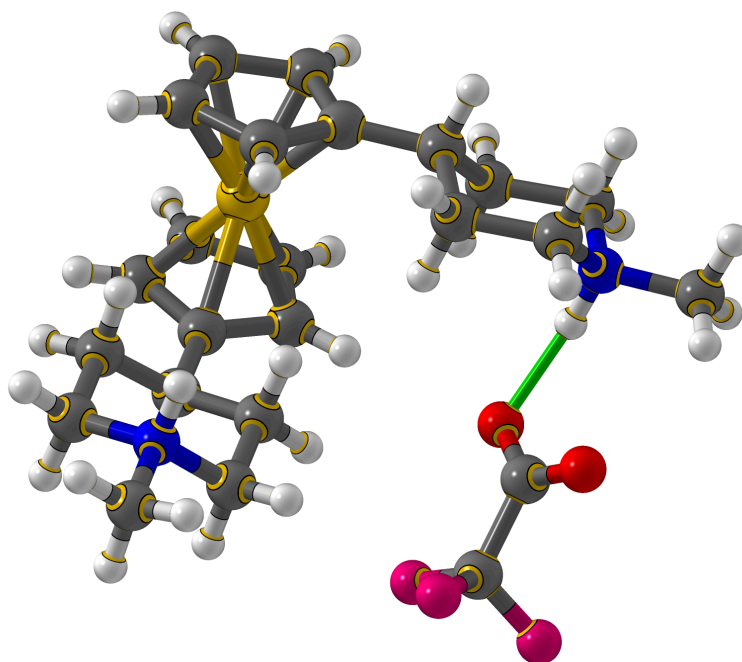


Figure 4.5. Crystal structure of BAPHIK⁹⁷

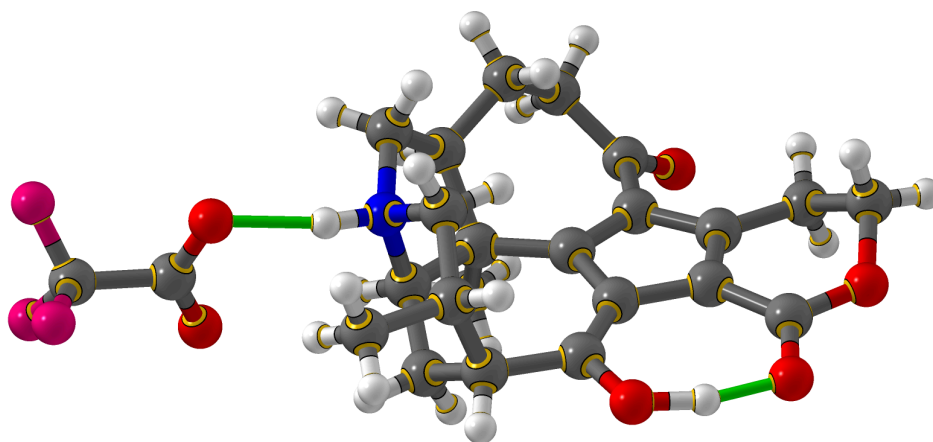


Figure 4.6. Crystal structure of XOLCEG⁹⁸

Similar to trifluoroacetate, the nitrobenzoates are also weak bases due to the electron withdrawing effect from nitro substituents via the phenyl rings. A few examples of

nitrobenzoates with only a single hydrogen bond on the carboxylates are also found in the literature (**Figure 4.7** to **Figure 4.9**).

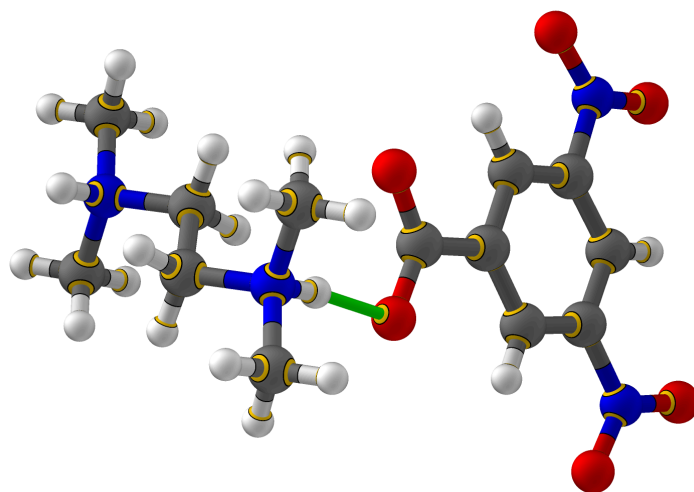


Figure 4.7. Crystal structure of QIBSEZ⁹⁹

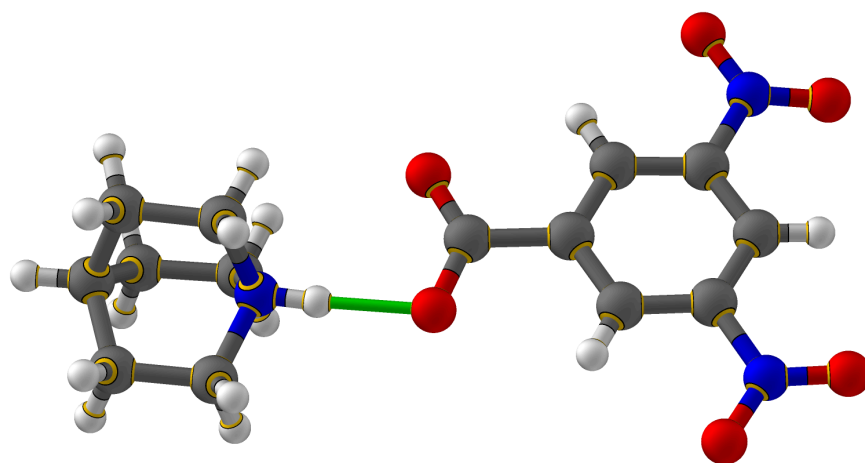


Figure 4.8. Crystal structure of ISOREN¹⁰⁰

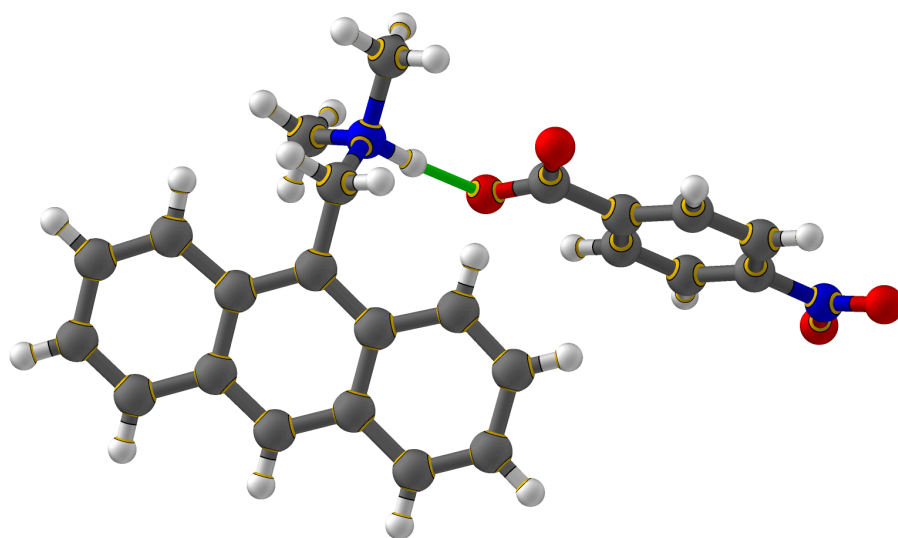


Figure 4.9. Crystal structure of QARBIU¹⁰¹

Like nitrobenzoates, terephthalate (**Figure 4.10**) is also found to be able to form single hydrogen bonds for both of its carboxylates with protonated 1,4-diazabicyclo[2,2,2]octanes. However, this is the only example that involved terephthalate.

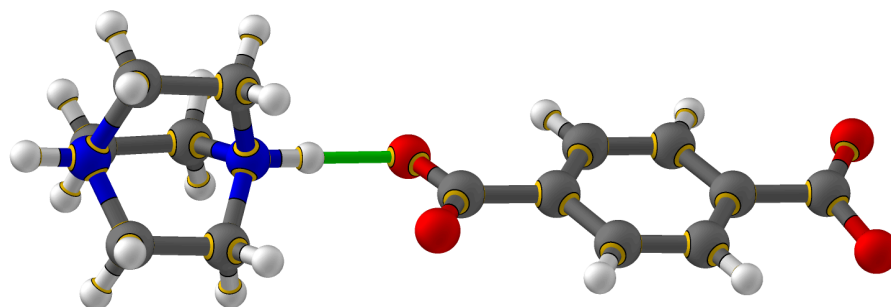


Figure 4.10. Crystal structure of HOFLIY¹⁰²

It is worth noting that the structure shown in **Figure 4.10**¹⁰² is somehow abnormal, because 1,4-diazabicyclo[2,2,2]octane with two protons is very unlikely to be stable in crystal. Braga and co-workers¹⁰³ investigated the co-crystallization from 1,4-diazabicyclo[2,2,2]octane and a series of dicarboxylic acids (**Figure 4.11**). In all their cases, 1,4-diazabicyclo[2,2,2]octane forms co-crystals with dicarboxylic acids, not the salts. Thus the type of the hydrogen bond is N \cdots H–O. These conclusions have been confirmed by X-Ray diffraction as well as solid-state NMR studies.

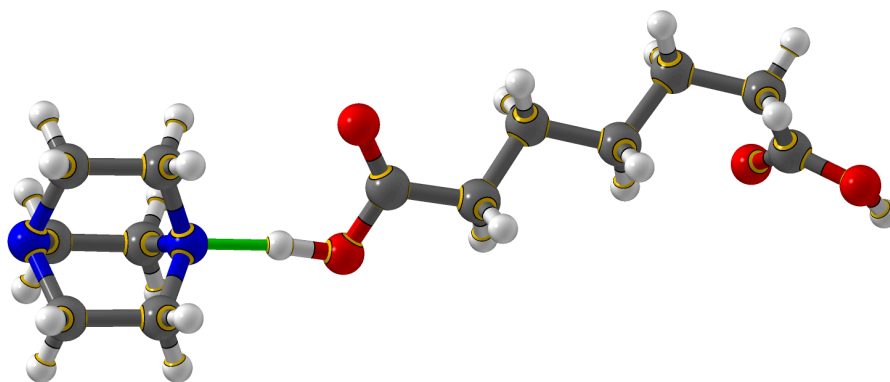


Figure 4.11. An example of hydrogen bonding between 1,4-diazabicyclo[2,2,2]octane and carboxylic acids.¹⁰³

The other effect that prohibits a carboxylate from forming two hydrogen bonds is steric hindrance. If there are one or more bulky substituents on the ammonium ions, sometimes there is no space for the carboxylates to form the second hydrogen bond. The CSD survey contains several examples illustrating steric hindrance, as shown in **Figure 4.12** to **Figure 4.18**.

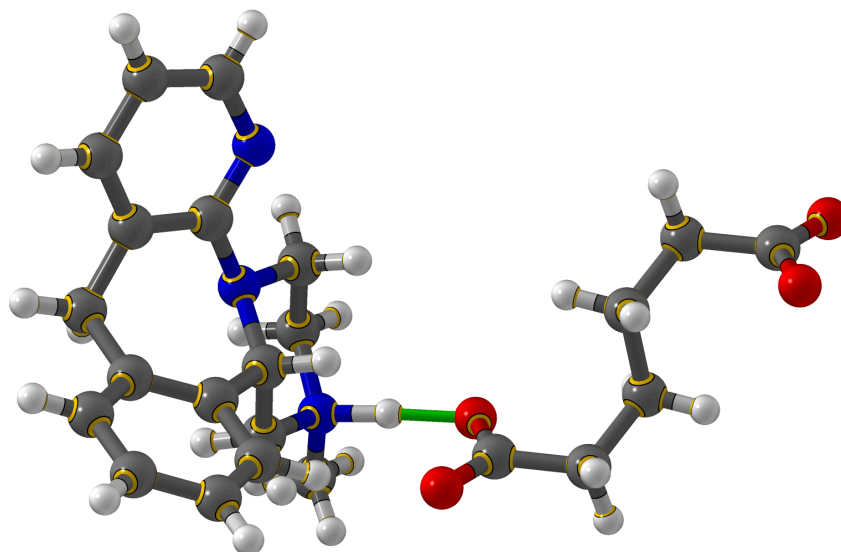


Figure 4.12. Crystal structure of APAKOS¹⁰⁴

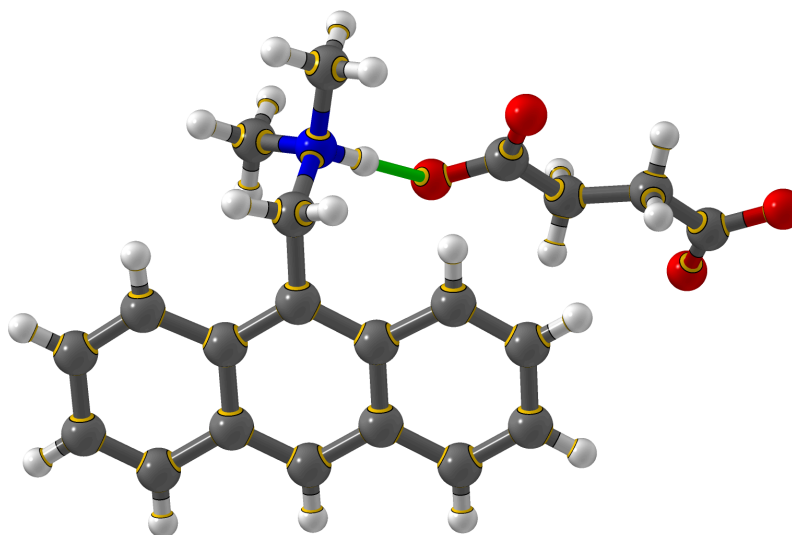


Figure 4.13. Crystal structure of CEJLUZ¹⁰⁵

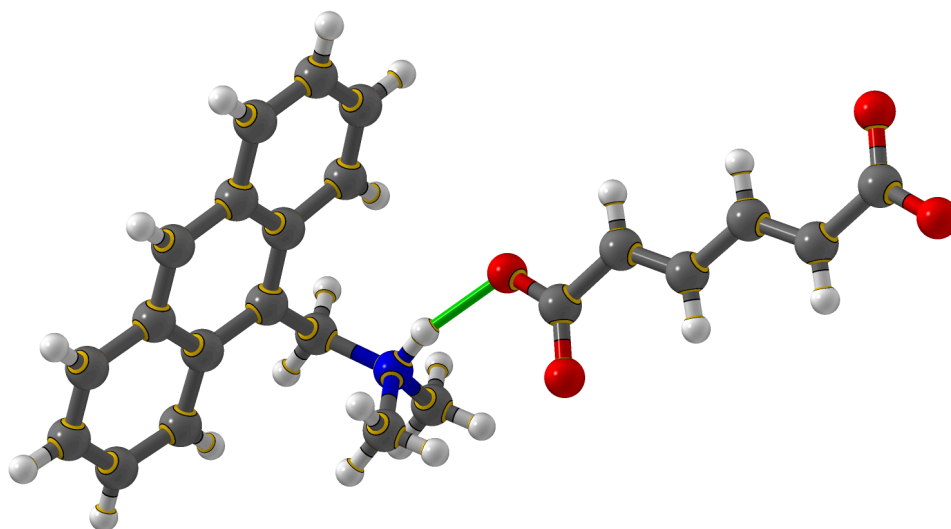


Figure 4.14. Crystal structure of CEJMEK¹⁰⁵

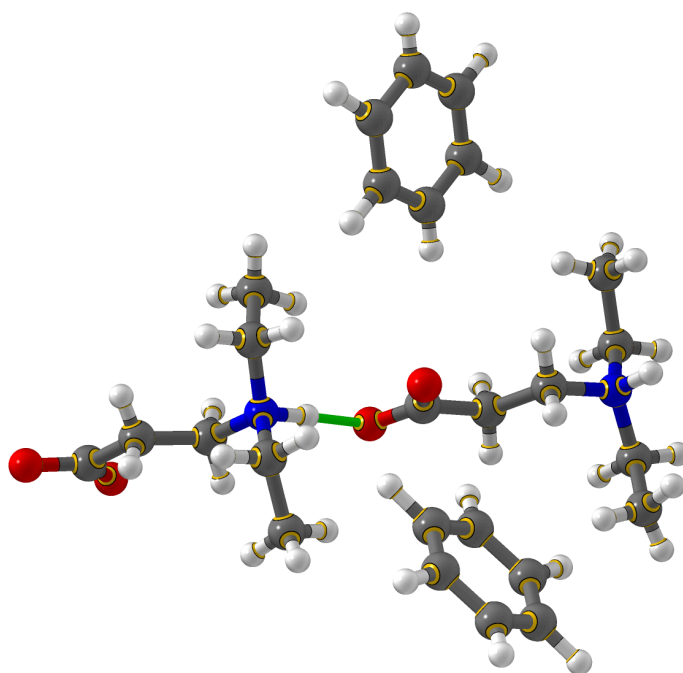


Figure 4.15. Crystal structure of DEBALB¹⁰⁶

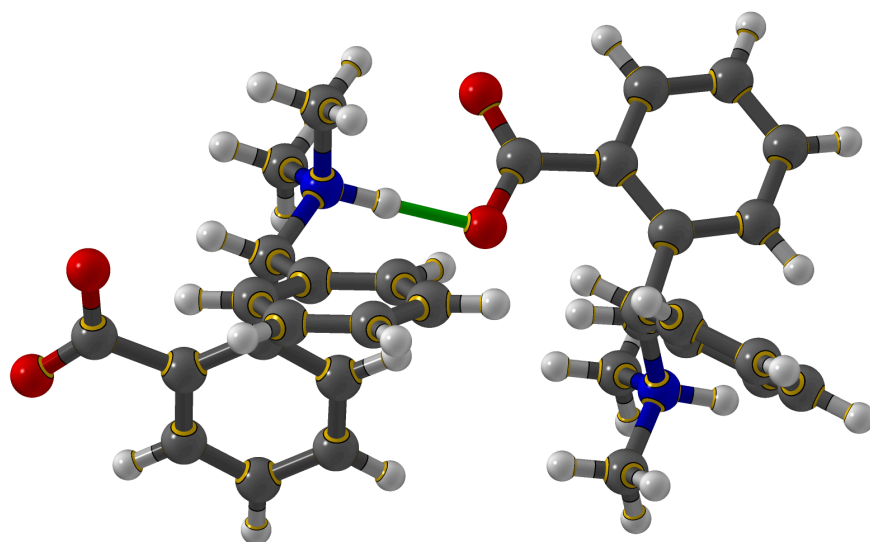


Figure 4.16. Crystal structure of NATGOF¹⁰⁷

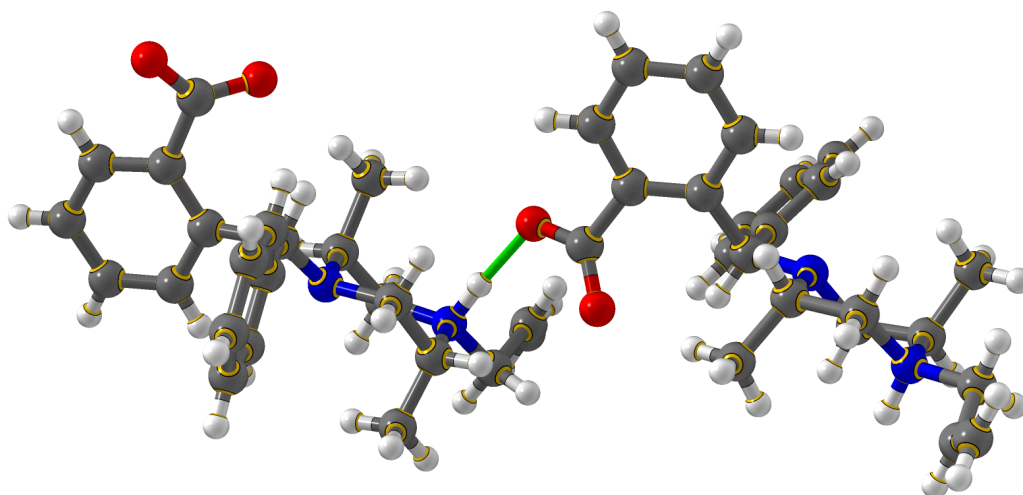


Figure 4.17. Crystal structure of RIRSEQ¹⁰⁸

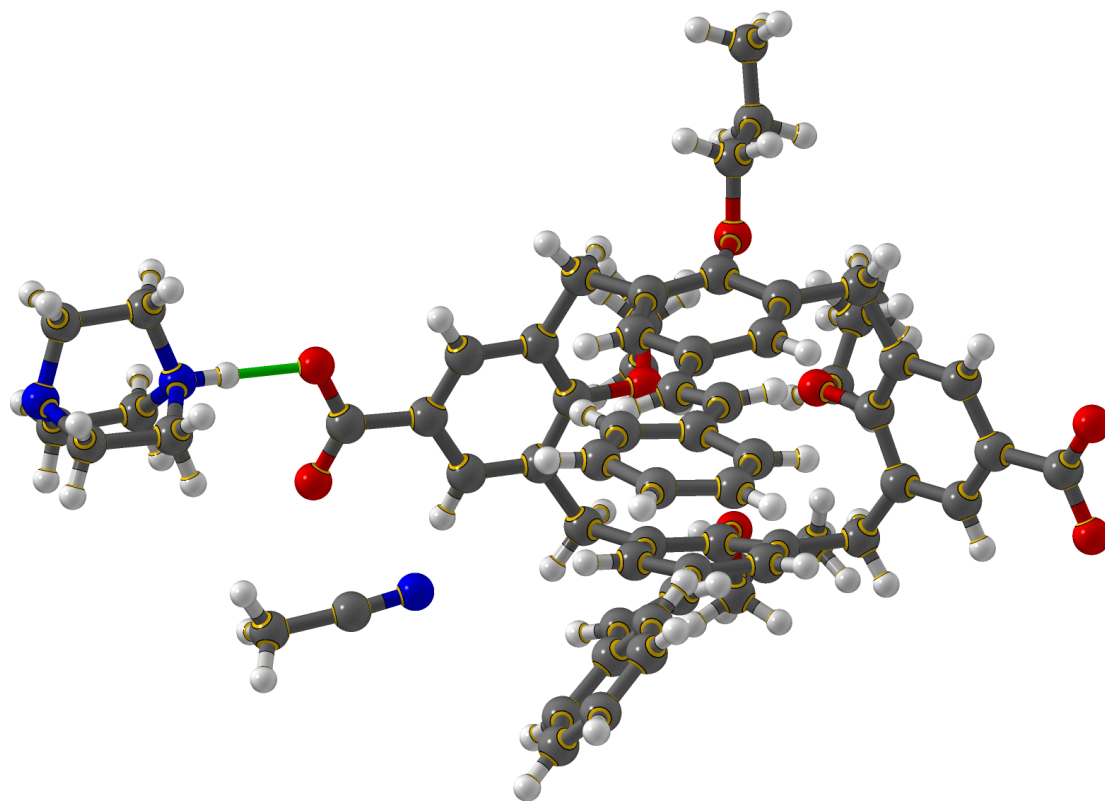


Figure 4.18. Crystal structure of XUBWEW¹⁰⁹

One example of the intramolecular hydrogen bond was also found (**Figure 4.19**). Unlike the previous examples involving steric hindrance, the favorable stereo conformation in **Figure 4.19** helps establish the intramolecular hydrogen bonding.

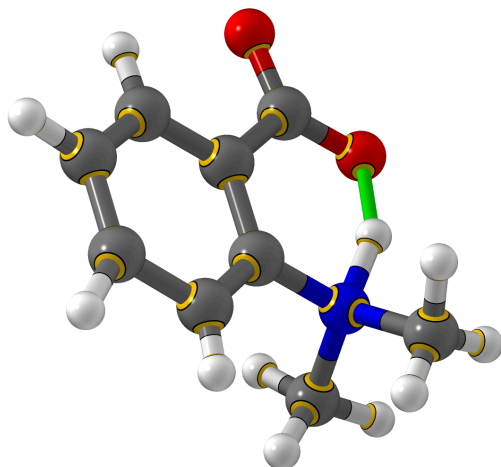
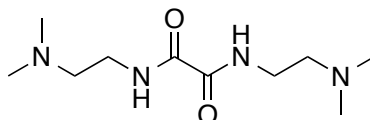


Figure 4.19. Crystal structure of DMANAC¹¹⁰

The listed examples above are all crystals that contain hydrogen bonds from a tertiary ammonium and a single hydrogen-bonded carboxylate, except a few examples with poor X-ray data. We can conclude that this type of hydrogen bonding rarely occurs in crystals.

4.3 Research Goal

The research goal of this project is to give us some insight on the hydrogen bond formation, as well as host-guest chemistry and co-crystal growth. To further explore the formation of hydrogen bond involving the tertiary amine, we designed and synthesized the molecule N^1,N^2 -bis(2-(dimethylamino)ethyl)oxalamide, which consists of both oxalamide functionality and tertiary amines.



46

In the molecule, the oxalamides are proved to be able to form hydrogen bonds and establish a network structure with a repeat distance of ~ 4.9 Å. They are generally recognized as the host molecules. The tertiary amines (ammoniums) are suggested to form hydrogen bonds with carboxylic acids (carboxylates), which should be the guest molecules in this situation. Though tertiary amines are usually sterically hindered, the introduction of two methyl groups should to some extent reduce the steric hindrance, and increase the opportunity of forming hydrogen bonds.

4.4 Synthesis and Structural Analysis

The designed compound **46** is not new. The first synthesis was published in 1950.¹¹¹ However, its crystal structure was never reported. Only two crystals involving it were discovered after a CSD survey.

The first one is a co-crystal from compound **46** and nitrate ions, as shown in **Figure 4.20**.¹¹² Two oxygen atoms in the nitrate ion form two hydrogen bonds with protons from the oxalamide and the tertiary ammonium, respectively. Because of the existence of the nitrate ion, compound **46** does not build a layer-by-layer network structure in the co-crystal.

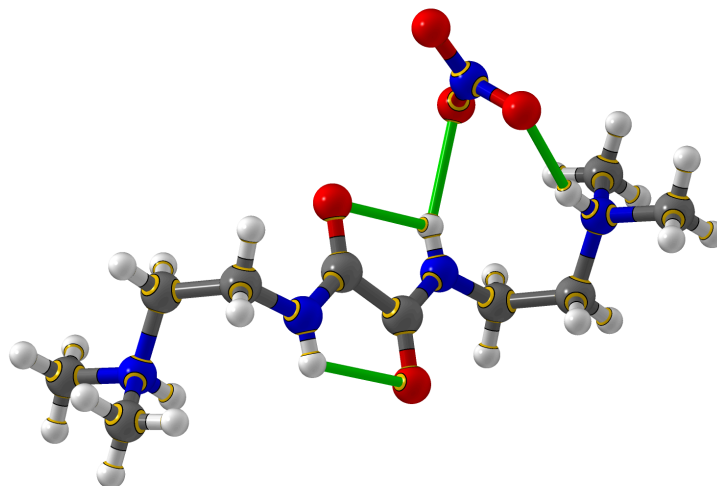


Figure 4.20. Crystal structure of IDUVAF¹¹²

The second crystal structure that contains compound **46** is its platinum(II) complex, [Pt₂-*N,N'*-bis(2-dimethyl-aminoethyl oxamide)Cl₄].¹¹³ In this case, compound **46** binds to two platinum ions as an oxalamide ligand (**Figure 4.21**).

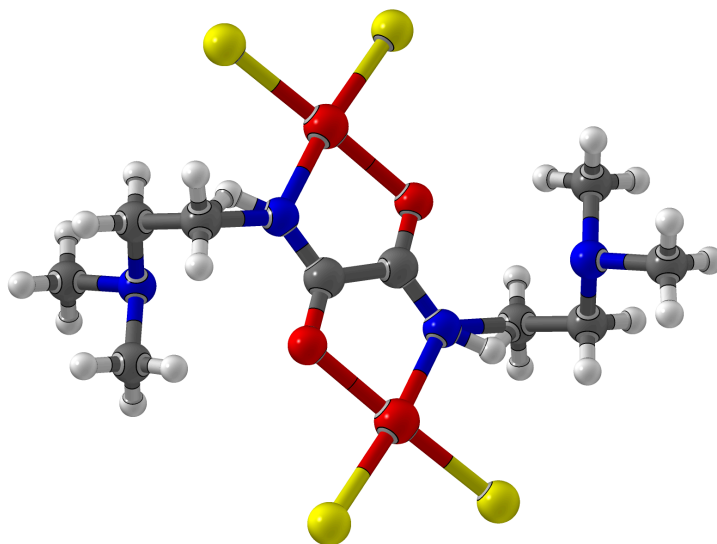
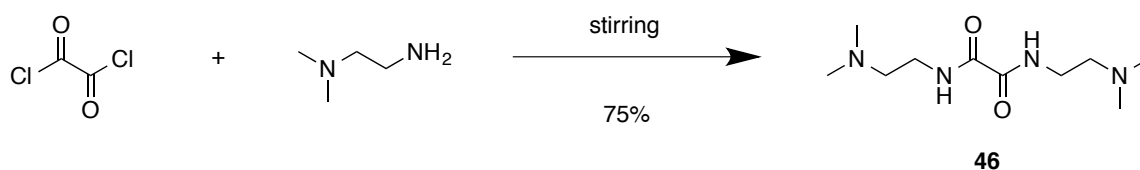


Figure 4.21. Crystal structure of ALEDIE¹¹³

Compound **46** can be synthesized by simply mixing oxalyl dichloride and *N,N'*-dimethylethane-1,2-diamine in solution, as shown in **Scheme 4.2**.

Scheme 4.2. Synthesis of compound **46**



We successfully obtained a single crystal of compound **46** from methanol at room temperature (**Figure 4.22**). X-ray diffraction study shows the length of hydrogen bonds for the linkage of each layer is 2.139 Å. Moreover, compound **46** forms a network structure that has a repeat spacing of 5.116 Å, slightly longer than the values found in typical oxalamides (~4.9-5.0 Å), implying hydrogen bonding in compound **46** is a relatively weak interaction, which is probably due to the moderate repulsion between the ending tertiary amines in the molecules.

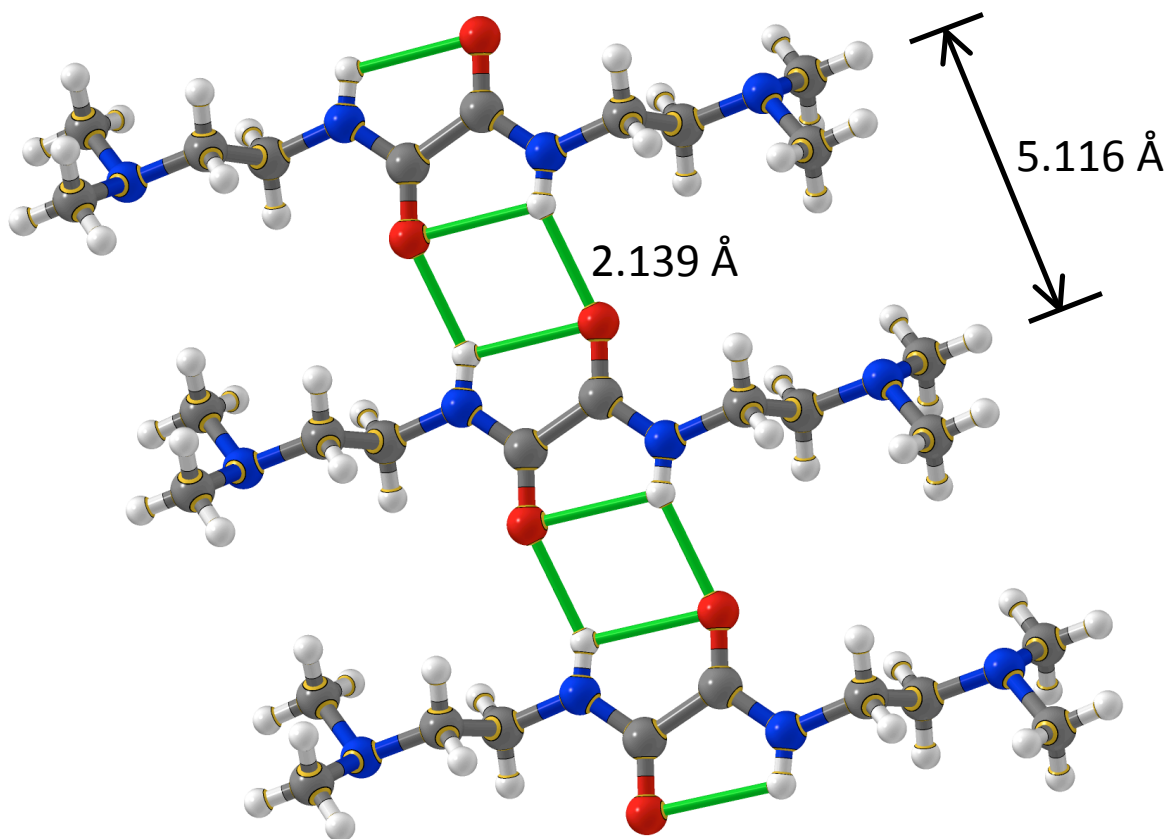
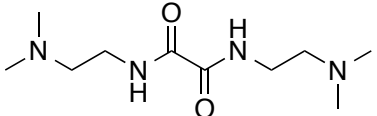
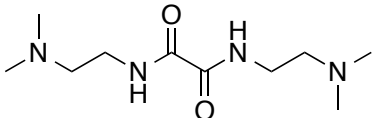
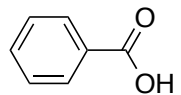
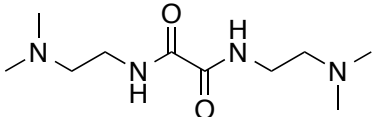
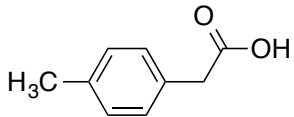
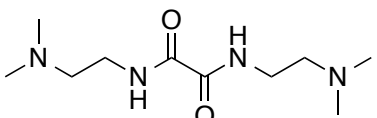
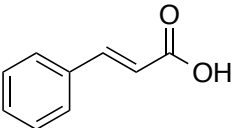


Figure 4.22. Crystal structure of compound 46

We conducted a series of experiments to test the capability of compound **46** forming co-crystals with different carboxylic acids. Several candidates were chosen to grow co-crystals with compound **46**.

Table 4.1. Co-crystal growth from compound **46** and carboxylic acids. Solvent: methanol.

	Tertiary amine	Carboxylic acid	Co-crystal growth result
Entry 1		CH ₃ COOH	Negative
Entry 2			Negative
Entry 3			47
Entry 4			Negative

As shown in **Table 4.1**, most experiments for co-crystal growth gave negative results, as crystals obtained from the mixed solution are the individual crystals of the starting materials. The results are unusual because it should be very easy for amines and carboxylic acids to form co-crystals or salts in every case. Probably because of the disruption caused by the steric hindrance of the tertiary amines, the formation of stable co-crystal structures is prohibited.

A colorless crystal **47** was separated from the solution of entry **3**. It was later demonstrated by X-ray diffraction as the hydrate from compound **46** and 2-*p*-tolylacetic acid. The crystal structure is shown in **Figure 4.23** and **4.24**. The hydrogen atoms on the water molecule were located in electron density map.

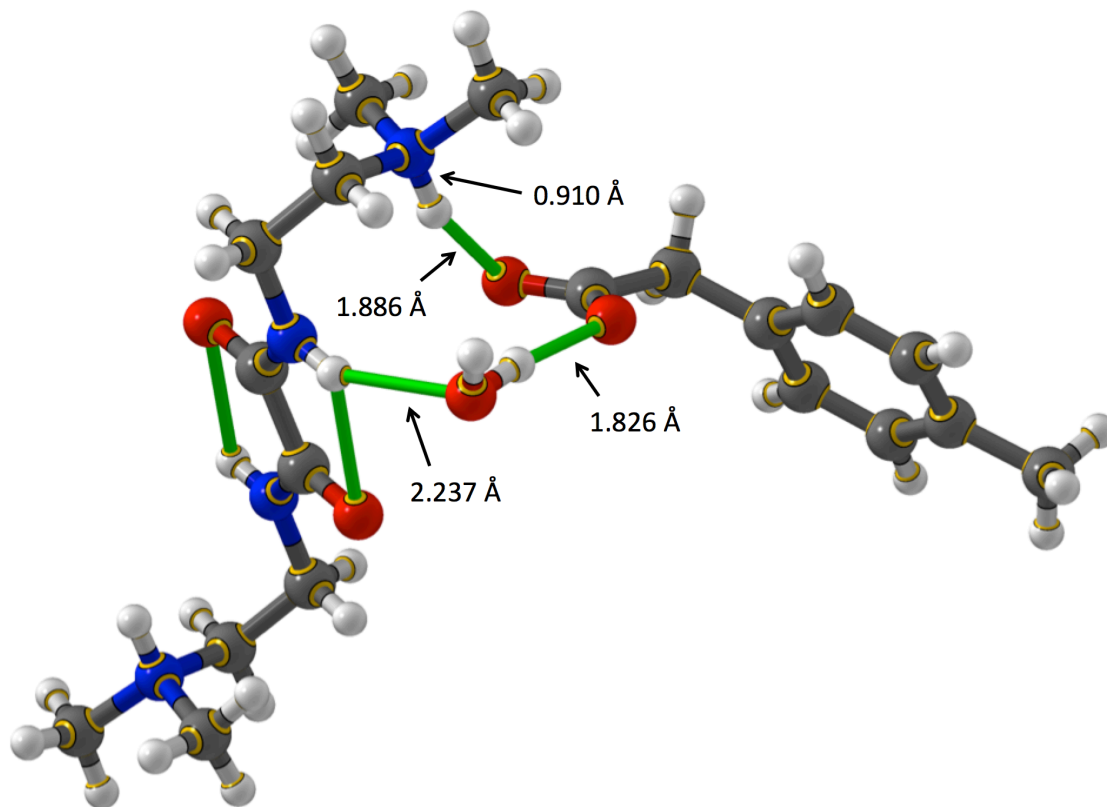


Figure 4.23. Co-crystal structure of **47**, the hydrate of compound **46** and 2-*p*-tolylacetic acid

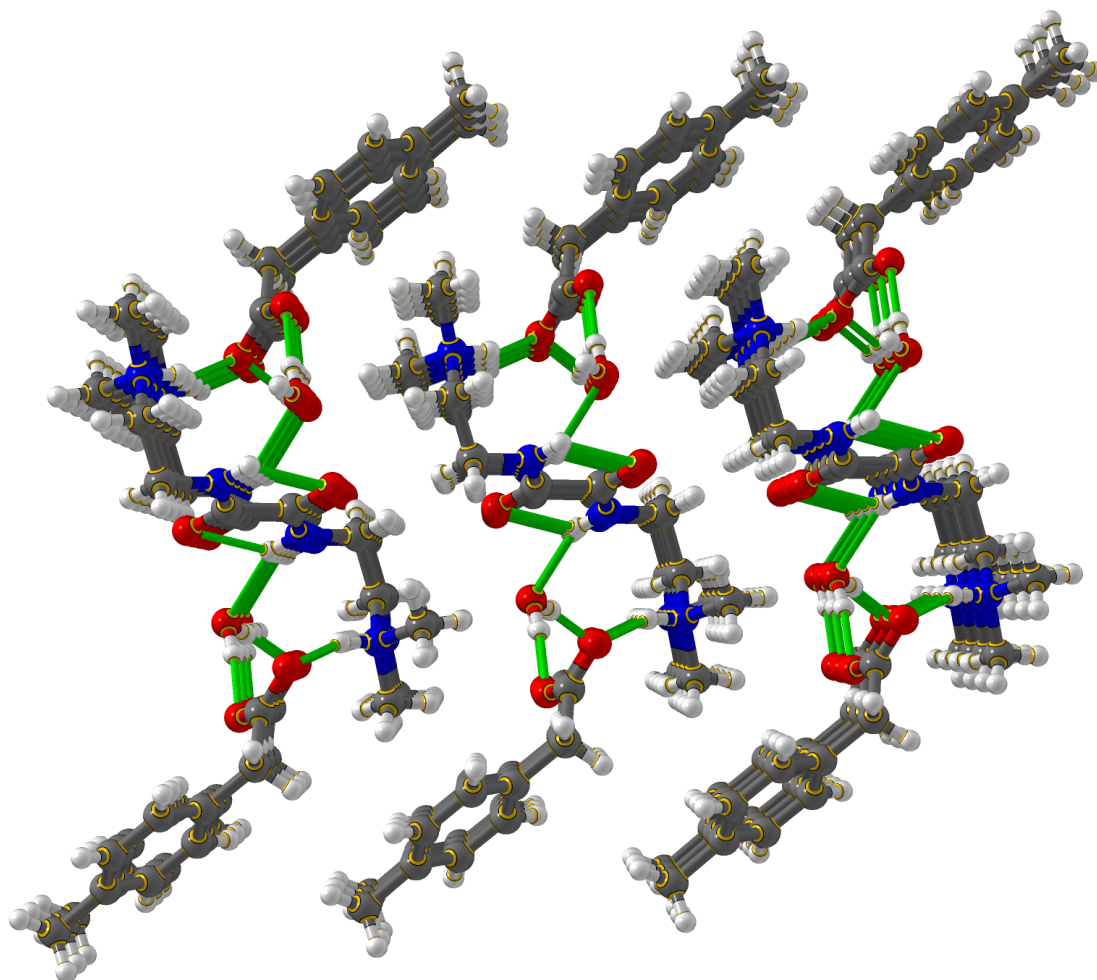


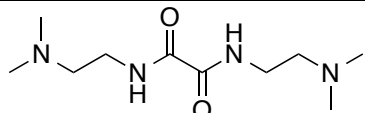
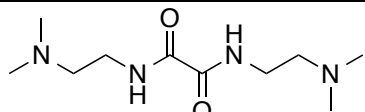
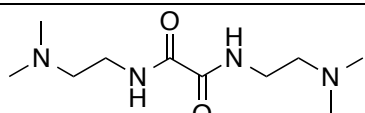
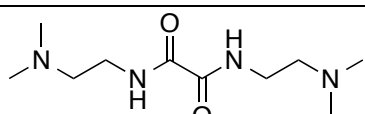
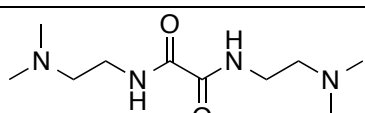
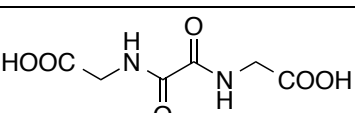
Figure 4.24. Co-crystal structure of **47**. Top view.

Different from co-crystal **3** we obtained in Chapter 2, which forms the hydrogen bonds from two neutral species, in co-crystal **47**, 2-*p*-tolylacetic acids protonate the tertiary amines in compound **46** and form the ion-ion pairs with them. This result is confirmed by the bond lengths of N–H 0.910 Å and O–H 1.886 Å (**Figure 4.23**). The produced carboxylate group is stabilized by forming two hydrogen bonds with the tertiary ammonium ion and a water molecule, respectively. The length of the hydrogen bond between the carboxylate and the ammonium is

1.886 Å, with an angle of 151.3°. In contrast, the hydrogen bond between the carboxylate and water molecule is shorter than that, at 1.826 Å. The almost linear direction (173.8°) of the latter hydrogen bond suggests that it contributes more to the stabilization of the carboxylate. Probably due to the strong interactions among compound **46**, 2-*p*-tolylacetate, and water, compound **46** in co-crystal **47** does not form the expected network structure that we have seen in **Figure 4.22**.

Because of the symmetrical characteristic of compound **46**, a reasonable consideration is that it could be easier to form the desired co-crystals with dicarboxylic acids that are also symmetric. Based on this assumption, we attempted to grow the co-crystals from compound **46** and symmetrical carboxylic acids in methanol.

Table 4.2. Co-crystal growth from compound **46** and symmetrical carboxylic acids

	Tertiary amine	Carboxylic acid	Co-crystal growth Result
Entry 5		HOOC-COOH	Negative
Entry 6		HOOC(CH ₂) ₂ COOH	Negative
Entry 7		HOOC(CH ₂) ₄ COOH	Negative
Entry 8		HOOC(CH ₂) ₈ COOH	48
Entry 9			Negative

Most of the experiments that we conducted resulted in single crystals of the starting materials or potential co-crystals with poor X-ray crystal data. We only successfully obtained a co-crystal from the solution of compound **46** and sebacic acid (decanedioic acid), and confirmed its structure by X-ray diffraction (**Figure 4.25**).

Interestingly, there are three species, protonated compound **46**, sebacic acid, and deprotonated sebacic acid (decanedioate) in co-crystal **48**. As seen in **Figure 4.25**, the carboxylic acid group in sebacic acid forms only one hydrogen bond with another decanedioate, while the carboxylate group in decanedioate forms two hydrogen bonds with another sebacic acid and the

ammonium ion from protonated compound **46**, respectively. This observation further confirms the point we previously made in this chapter that a carboxylate requires at least 2 hydrogen bonds for stabilization.

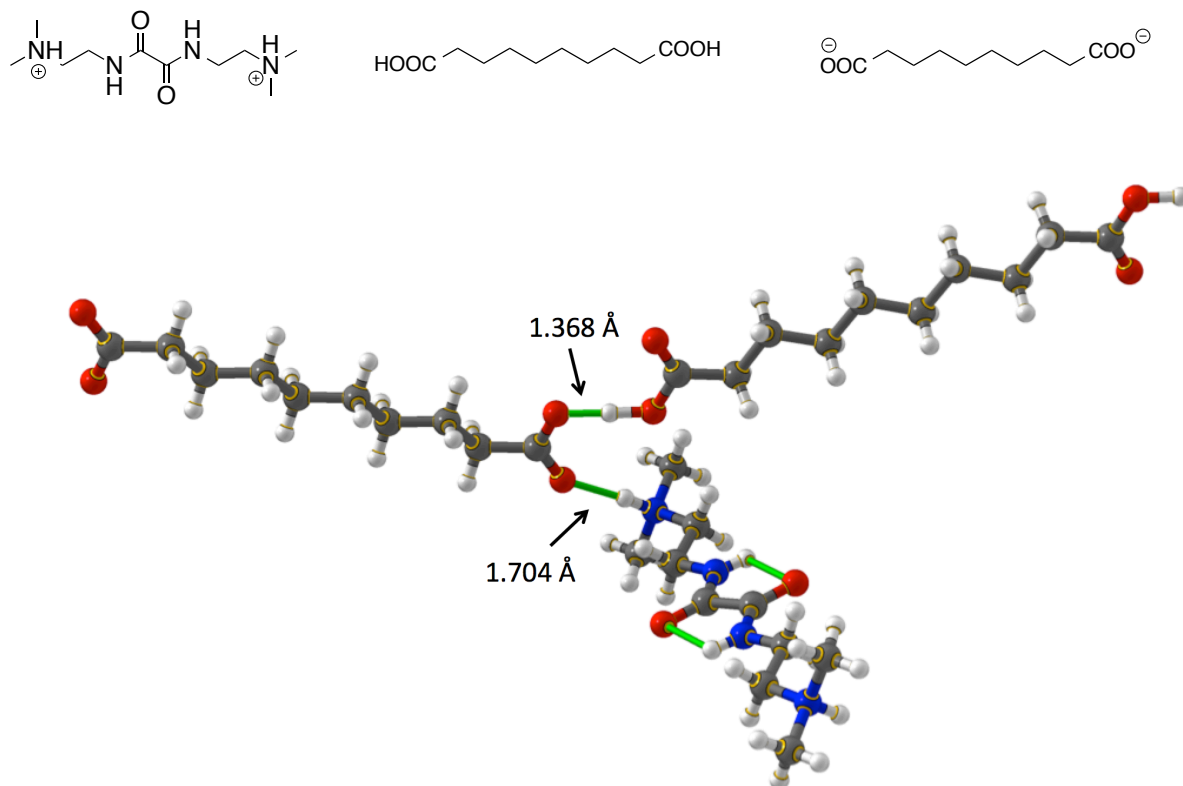


Figure 4.25. Co-crystal structure of **48**. A co-crystal from protonated compound **46**, sebacic acid and deprotonated sebacic acid

The expected network structure is successfully built via the oxalamide functional groups in co-crystal **48**. However, the repeat distance of the network structure in co-crystal **48** is 5.466 Å, much larger than that in crystal of compound **46** (Figure 4.22, 5.116 Å). This is likely due to the steric effect of the tertiary amines formed in co-crystal **48**, as shown in Figure 4.26.

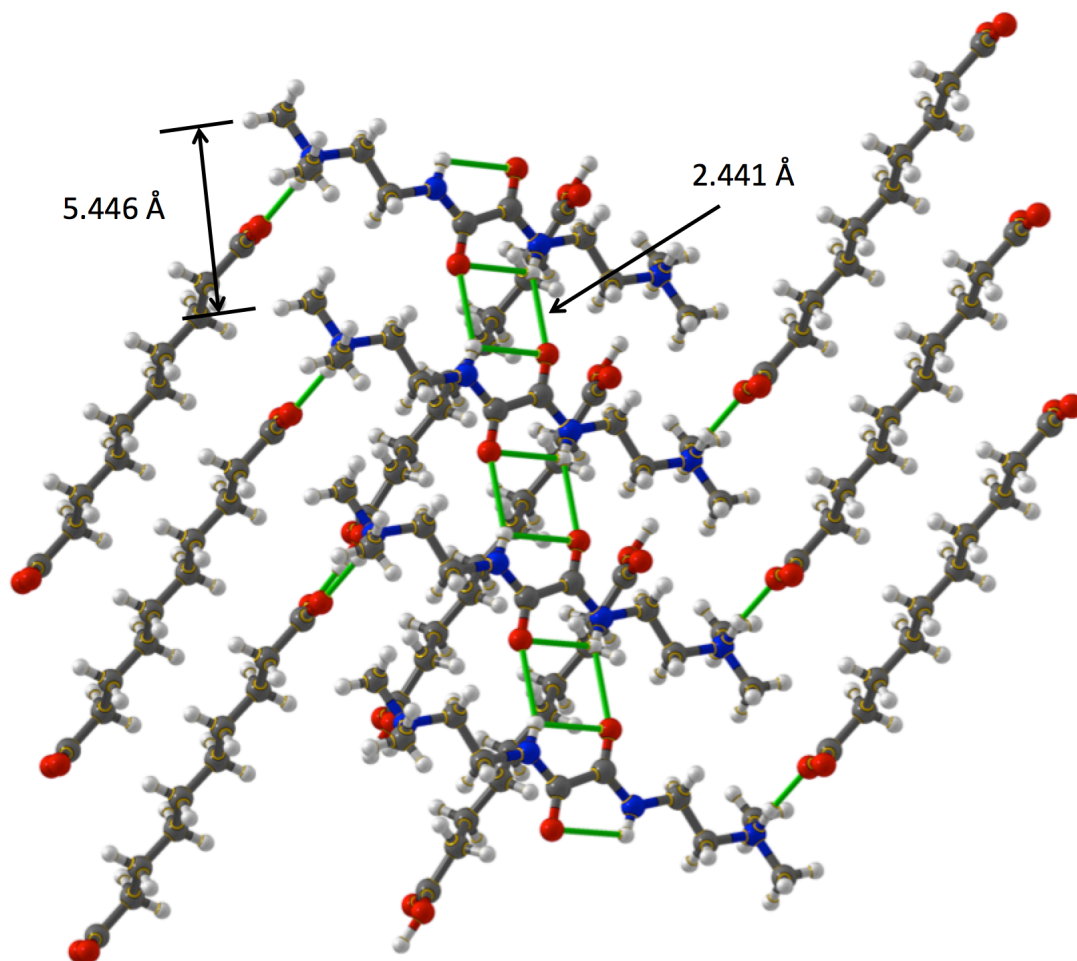


Figure 4.26. Co-crystal structure of **48**. The network structure.

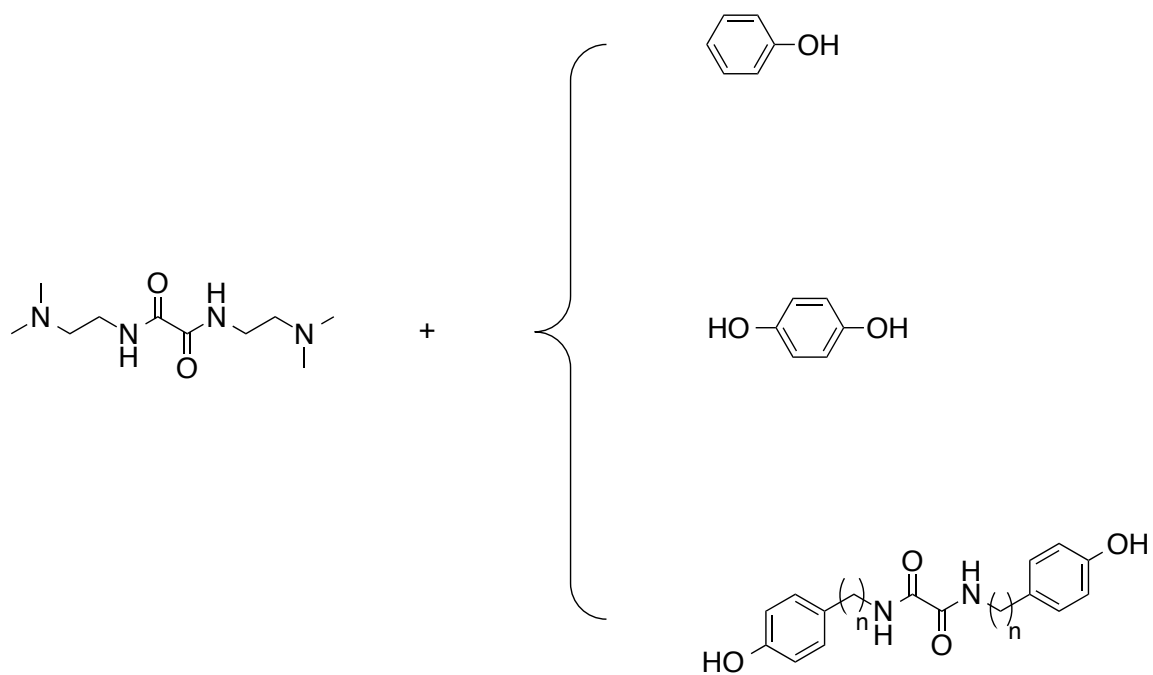
4.5 Conclusion

We have obtained the single crystal of compound **46**, confirmed its crystal structure via X-ray diffraction, and studied its capability to form co-crystals with different carboxylic acids. Two co-crystals **47** and **48** were successfully produced in our experiments. Though there could be two types of hydrogen bonds, presented as $N\cdots H-O$ and $N-H\cdots O$ respectively, in both of the co-crystal cases, the carboxylic acids protonate the tertiary amines in compound **46** and form the ion-ion pairs. The hydrogen bonds in both of the co-crystals are proved to be $N-H\cdots O$ type, which is different from the co-crystals we obtained in Chapter 2.

In both co-crystals **47** and **48**, each carboxylate functional group establishes two hydrogen bonds to make it more stable. This is in accordance with our CSD survey, as in our systems there are no significant electronic effects, *e.g.* existence of strong electron withdrawing groups, to stabilize the carboxylate, nor large steric effects prohibiting it from forming two hydrogen bonds.

Future work will be focused on the co-crystal growth from compound **46** and phenol or its derivatives, or hydroquinone or its derivatives. Phenol and hydroquinone, with pK_a of around 10, are weaker acids compared to carboxylic acids. It is more difficult to protonate amines with phenol or hydroquinone in solution. Although proton affinity in the solid state is different from that in solution, it is of interest to test whether the phenol or hydroquinone could protonate the tertiary amines and what structures and organizations would be generated from the designed complex. This work will help us choose the appropriate functional groups for establishing the desired host-guest strategy and provide a deeper understanding of hydrogen bonding in crystal engineering.

Scheme 4.3. Co-crystal growth from compound **46** and phenol or hydroquinone



Chapter Five

Experimental Section

5.1 General Information

The chemicals were purchased from Acros Organics, Aldrich Co. or Fisher Scientific Company, and used without purification unless otherwise stated.

TLC

Thin layer chromatography was performed on Whatman AL SIL G/UV254 and visualization was accomplished with UV light. Column chromatography was performed using Merck silica gel 60, 230-400 mesh.

Thermal Analysis

Thermal property was studied by using a Perkin-Elmer DSC 7 differential scanning calorimeter (DSC) and TGA 7 Thermogravimetric Analysis (TGA) with a heating and cooling rate of 10 °C/min under dried nitrogen gas atmosphere.

NMR

¹H NMR spectra were recorded on a Varian Gemini-300 MHz, Inova-400 MHz, or Inova-500 MHz spectrometer in deuterated solvents using residual protons as an internal reference. All

chemical shifts are reported in parts per million (ppm). Coupling constants are reported in hertz (Hz) and are described as being either singlet (s), doublet (d), doublet of doublets (dd), doublet of doublet of doublets (ddd), triplet (t), doublet of triplets (dt), quartet (q), or multiplet (m). Proton decoupled ^{13}C NMR spectra were recorded on an Inova-400 (100 MHz) or Inova-500 (125 MHz) spectrometer and are reported in ppm using solvent as internal standard.

MS

Mass Spectrometry was carried out on an Agilent LC-MSD that consists of an 1100 HPLC and a G1956A mass spectrometer. The 1100 HPLC provides liquid solvent delivery to the electrospray ionization (ESI) source of the mass spectrometer. The mass analyzer is a single quadrupole providing MS capabilities with unit resolution over the m/z range 50-1500Da.

IR

Infrared spectroscopy was performed using a Thermo Nicolet 380 FTIR spectrometer. The data were collected using pure solid samples.

Raman

Raman spectroscopy was performed using a Thermo Nicolet Almega dispersive Raman spectrometer coupled with an infinity corrected, confocal design microscope. The spectrometer uses a 785-nm class I laser, and the data were collected in the reflection mode of the microscope at a slit width of 25 μm . The data were collected and analyzed using the Omnic software suite (Nicolet, USA).

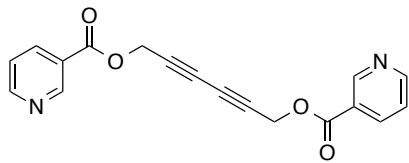
X-Ray Diffraction

Crystals were selected and mounted on glass fibers using epoxy glue. The crystals were optically centered and data were collected on an Oxford Gemini A diffractometer. X-ray data were collected using monochromated Cu radiation. The structures were solved and refined with standard SHELX procedures. The graphics of crystals were drawn in *Chem-Ray* program.

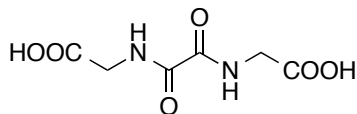
Preparation of silylated flask

An Erlenmeyer flask was treated with 5% HF solution for 2 hours, rinsed with distilled water thoroughly, and dried, and silylated with 2% of dimethyldichlorosilane in methylene chloride for 2 hours.

5.2 Synthesis

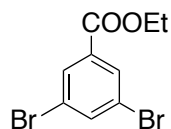


Hexa-2,4-diyne-1,6-diyl dinicotinate (1). To 0.18g (1.6 mmol) hexa-2,4-diyne-1,6-diol in CH_2Cl_2 at 40 °C was added 0.45 g (3.2 mmol) nicotinoyl chloride. The reaction mixture was stirred and maintained at 40 °C for 4 hours. The solvent was then removed in *vacuo* evaporation. The crude product was purified by flash chromatography (3:1 hexanes/EtOAc) to yield 0.43 g (84%) of product as white powders. m.p. 106-109 °C (Lit.⁵⁶ m.p. 107-109 °C); ^1H NMR (400 MHz, CDCl_3) δ 5.03 (4H, s), 7.43 (ddd, 2H, $J = 8$ Hz, 4.8 Hz, 0.8 Hz), 8.32 (ddd, 2H, $J = 8$ Hz, 2Hz, 1.6 Hz), 8.80 (dd, 2H, $J = 4.8$ Hz, 1.6 Hz), 9.23 (dd, 2H, $J = 2.4$ Hz, 0.8 Hz); ^{13}C NMR (125 MHz, CDCl_3) δ 164.5, 154.0, 151.2, 137.5, 125.4, 123.6, 73.6, 71.0, 53.3; IR (cm^{-1}) 1722, 1587, 1480, 1422, 1375, 1273, 1101.

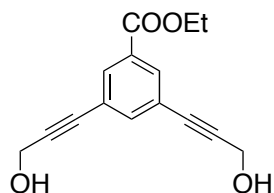


***N,N'*-Oxalyldiglycine (2).** 17 mL of 6.25 M NaOH was diluted in 75 mL H_2O . To the solution was added 8.25 g (110 mmol) glycine and 8.04 g (55 mmol) diethyl oxalate. The reaction mixture was stirred and maintained at 40 °C for 2 h, allowed to cool to r.t., acidified to pH=2 with 1 M HCl and refrigerated overnight. The oxalamide precipitate was collected by filtration and washed with a small amount of cold water, yielding 2.47 g (22%) white crystals.⁵⁶ m.p. 252-255 °C (Lit.¹¹⁴ m.p. 250-255 °C); ^1H NMR (400 MHz, D_2O , in the presence of two drops NaOD) δ 3.91 (4H, s); ^{13}C NMR (100 MHz, D_2O , in the presence of two drops NaOD) δ 176.3, 161.4, 43.8; IR (cm^{-1}) 3295, 1706, 1651, 1530, 1404, 1235.

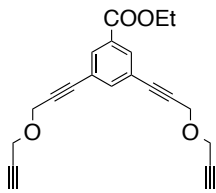
Co-crystal (3). Dissolve 0.32 g (1 mmol) diacetylene **1** and 0.20 g (1 mmol) oxalamide **2** in 60 mL hot methanol in a silylated Erlenmeyer flask. The solution was allowed to slowly evaporate to dryness at ~60 °C. Needle-like gold metallic crystals were found at the bottom of the flask. IR (cm^{-1}) 3272, 1723, 1660, 1597, 1524, 1217.



Compound (8). A solution of 3,5-dibromobenzoic acid (2.8g, 10 mmol) and conc. H₂SO₄ (1.5 mL) in ethanol (22 mL) was heated to reflux under N₂. After 12 hours the solvent was removed in *vacuo* evaporation. Water (20 mL) was added to the residue, followed by an extraction with diethyl ether. The organic layer was washed with saturated NaHCO₃ (20 mL), saturated NaCl (20 mL) and then dried with MgSO₄. After filtration the solvent was removed, yielding 2.89g (88%) yellow solids. m.p. 55-57 °C (Lit.¹¹⁵ m.p. 51 °C); ¹H NMR (400 MHz, CDCl₃) δ 1.39 (t, 3H, J = 7.2 Hz), 4.38 (q, 2H, J = 7.2 Hz), 7.83 (t, 1H, J = 1.6 Hz), 8.10 (d, 2H, J = 1.6 Hz). ¹³C NMR (100 MHz, CDCl₃) δ 164.2, 138.3, 133.8, 131.5, 123.1, 62.0, 14.4.



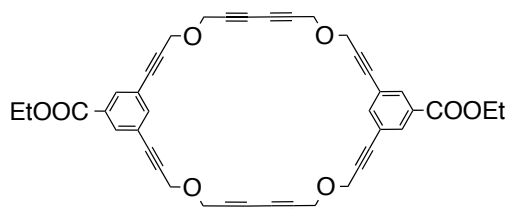
Compound (9). Pd(PPh₃)₂Cl₂ (0.08g, 0.12 mmol) and propargyl alcohol (4.0 mL, 71 mmol) were added under N₂ to a solution of Ph₃P (0.22g, 0.86 mmol), CuI (0.08g, 0.40 mmol) and compound **8** (2.2g, 7.1 mmol) in 60 mL of dry TEA. The solution was stirred and heated to reflux. After 4 hours the mixture was cooled to room temperature and filtered to remove the insoluble triethylamine hydrobromide. The salt was washed with diethyl ether several times until the ether solution was clear. The filtrates were concentrated in *vacuo* evaporation and purified by column chromatography (Hexanes/EtOAc 1:3), yielding 1.54g light yellow oil (yield: 84%). ¹H NMR (400 MHz, CDCl₃) δ 1.38 (t, 3H, J = 7.2 Hz), 2.01 (s, 2H), 4.35 (q, 2H, J = 7.2 Hz), 4.50 (s, 4H), 7.61 (t, 1H, J = 1.6 Hz), 8.02 (d, 2H, J = 1.6 Hz); ¹³C NMR (100 MHz, CDCl₃) δ 165.4, 138.5, 132.7, 131.3, 123.6, 89.1, 84.0, 61.7, 51.7, 14.5.



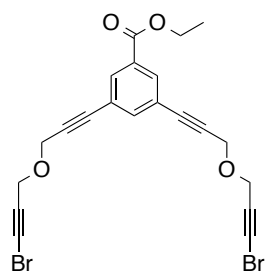
Compound (10). A solution of compound **9** (0.52g, 2.0 mmol) in 10 mL dried THF was added slowly to a suspension of sodium hydride (60% dispersion in mineral oil, 1.5g, 62.5 mmol) in 15 mL dried THF under nitrogen in ice bath. After 20 min 18-crown-6 (1.4g, 5.4 mmol) was added to the solution. The mixture was stirred for another 20 min. Then propargyl bromide (0.9 mL, 10 mmol) was added dropwise, and the ice bath was removed. The reaction mixture was allowed to

warm to room temperature and stirred for 4 hours. The excess sodium hydride was removed by filtration with caution. (Destroying the residual NaH with water or aqueous NH₄Cl in the solution will also destroy the product.) The filtrate was then concentrated and purified by column chromatography (Hexanes/EtOAc 3:1), yielding 0.59g (88%) yellow cream solid. ¹H NMR (400 MHz, CDCl₃) δ 1.39 (t, 3H, J = 7.2 Hz), 2.49 (t, 2H, J = 2.4 Hz), 4.31 (d, 4H, J = 2.4 Hz), 4.34 (q, 2H, J = 7.2 Hz), 4.48 (s, 4H), 7.66 (t, 1H, J = 1.6 Hz), 8.05 (d, 2H, J = 1.2 Hz); ¹³C NMR (100 MHz, CDCl₃) δ 165.1, 138.6, 132.7, 131.3, 123.3, 86.0, 85.0, 78.9, 75.4, 61.6, 57.2, 56.8, 14.4.

General procedure for diacetylenic macrocycle synthesis (A): To a stirred solution of corresponding diether (0.50 mmol) in 100 mL methylene chloride was added copper (I) chloride (CuCl) (0.35g, 3.5 mmol) and 0.8 mL (9.1 mmol) *N,N'*-tetramethylethylenediamine (TMEDA). O₂ was bubbled into this solution. After 3-6 hours methylene chloride was removed in *vacuo*. The crude product was purified by column chromatography.

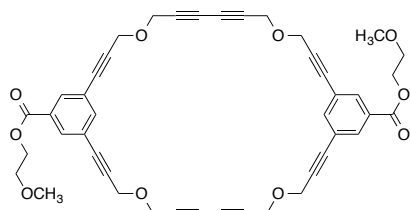


Compound (11). Following **general procedure A**, 0.16g (0.50 mmol) compound **10** yields 0.038g (24%) of white solid. The eluent for column chromatography (Hexanes/EtOAc 1:1, 1% TEA). ¹H NMR (300 MHz, CDCl₃) δ 1.39 (t, 3H, J = 7.2 Hz), 4.37 (q, 2H, J = 7.5 Hz), 4.41 (s, 8H), 4.50 (s, 8H), 7.72 (d, 2H, J = 1.5 Hz), 8.05 (d, 4H, J = 1.5 Hz).

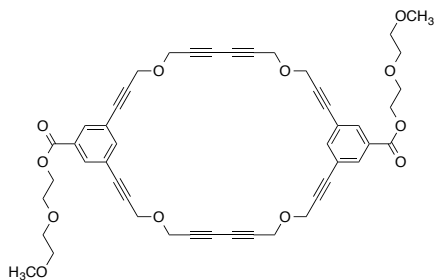


Compound (13). To the solution of compound **10** (0.27g, 0.5 mmol) in acetone, NBS (0.11g, 0.6 mmol, recrystallized out of H₂O before use) was added. At the end AgNO₃ (0.01g, 0.06 mmol) was added to the mixture. The solution turned cloudy in 10 min. The reaction was stirred for 8 hours. Acetone was removed in *vacuo* before ice water was added. After extracted with ether for 3 times, the organic layer was concentrated and purified by column

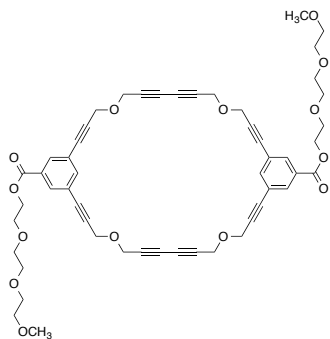
chromatography (Hexanes/EtOAc 3:1), yielding 0.10g (40%) yellow solid. ^1H NMR (300 MHz, CDCl_3) δ 1.40 (t, 3H, $J = 7.0$ Hz), 4.35-4.41 (m, 6H), 4.48 (s, 4H), 7.68 (t, 1H, $J = 1.5$ Hz), 8.06 (d, 2H, $J = 1.8$ Hz).



Compound (14). Following **general procedure A**, 0.18g (0.50 mmol) compound **17** yields 0.043g (24%) of white solid. The eluent for column chromatography (Hexanes/EtOAc 1:1, 1% TEA). ^1H NMR (400 MHz, CDCl_3) δ 3.42 (s, 6H), 3.71 (t, 4H, $J = 4.8$ Hz), 4.41 (s, 8H), 4.45-4.48 (m, 4H), 4.49 (s, 8H), 7.72 (s, 2H), 8.07 (d, 4H, $J = 1.2$ Hz). ^{13}C NMR (100 MHz, CDCl_3) δ 165.2, 139.3, 132.9, 131.0, 123.4, 85.8, 85.5, 74.9, 71.3, 70.6, 64.7, 59.2, 57.4, 57.2.

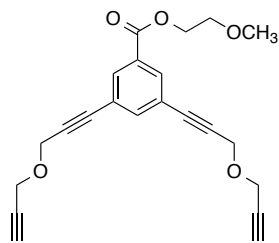


Compound (15). Following **general procedure A**, 0.21g (0.50 mmol) compound **18** yields 0.04g (20%) of white solid. The eluent for column chromatography (Hexanes/EtOAc 1:1, 1% TEA). ^1H NMR (300 MHz, CDCl_3) δ 3.39 (s, 6H), 3.56-3.58 (m, 4H), 3.67-3.70 (m, 4H), 3.81-3.84 (m, 4H), 4.41 (s, 8H), 4.46-4.50 (a singlet overlapping a multiplet, 12H), 7.72 (t, 2H, $J = 1.5$ Hz), 8.07 (d, 4H, $J = 1.5$ Hz).

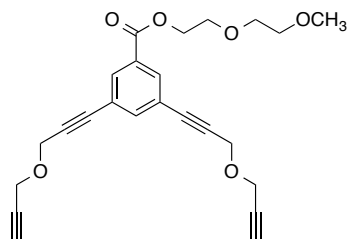


Compound (16). Following **general procedure A**, 0.23g (0.50 mmol) compound **19** yields 0.05g (22%) of white solid. The eluent for column chromatography (Hexanes/EtOAc 1:1, 1% TEA). ^1H NMR (400 MHz, CDCl_3) δ 3.35 (s, 6H), 3.51-3.53 (m, 4H), 3.62-3.70 (m, 12H), 3.80-3.83 (m, 4H), 4.40 (s, 8H), 4.45-4.47 (m, 4H), 4.49 (s, 8H), 7.71 (t, 2H, $J = 1.6$ Hz), 8.05 (d, 4H, $J = 1.6$ Hz); ^{13}C NMR (100 MHz, CDCl_3) δ 57.2, 57.4, 59.2, 64.8, 69.2, 70.8, 70.8, 70.8, 71.3,

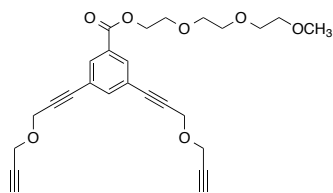
72.1, 74.9, 85.5, 85.8, 123.4, 131.0, 132.9, 139.3; MS m/z $[M + H]^+$ calculated for $[C_{52}H_{52}O_4 + H]^+$ 901.3, found 901.3.



Compound **(17)**. 2-methoxyethanol (0.75g, 10 mmol) and 0.5g (4.7 mmol) anhydrate Na_2CO_3 was added to the solution of compound **10** (0.33g, 1.0 mmol) in CH_2Cl_2 . The mixture was stirred vigorously at room temperature overnight. The crude product was concentrated in *vacuo* and purified by column chromatography (Hexanes/EtOAc 3:1 then 1:1), yielding 0.29g (80%) colorless oil. 1H NMR (300 MHz, $CDCl_3$) δ 2.49 (t, 2H, $J = 2.4$ Hz), 3.41 (s, 3H), 3.70 (t, 2H, $J = 4.8$ Hz), 4.30 (d, 4H, $J = 2.4$ Hz), 4.45 (t, 2H, $J = 4.8$ Hz), 4.47 (s, 4H), 7.66 (t, 1H, $J = 1.5$ Hz), 8.06 (d, 2H, $J = 1.5$ Hz).

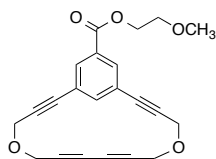


Compound **(18)**. 2-(2-methoxyethoxy)ethanol (1.2g, 10 mmol) and 0.5g (4.7 mmol) anhydrate Na_2CO_3 was added to the solution of compound **10** (0.33g, 1.0 mmol) in CH_2Cl_2 . The mixture was stirred vigorously at room temperature overnight. The crude product was concentrated in *vacuo* and purified by column chromatography (Hexanes/EtOAc 3:1 then 1:1), yielding 0.35g (85%) colorless oil. 1H NMR (300 MHz, $CDCl_3$) δ 2.49 (t, 2H, 2.4 Hz), 3.39 (s, 3H), 3.56-3.85 (m, 6H), 4.32 (d, 4H, $J = 2.4$ Hz), 4.48 (d, 6H, $J = 6$ Hz), 7.68 (s, 1H), 8.07 (d, 2H, $J = 1.5$ Hz).

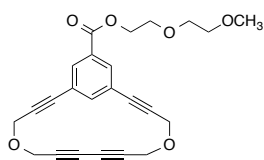


Compound **(19)**. 2-(2-(2-methoxyethoxy)ethoxy)ethanol (1.6g, 10 mmol) and 0.5g (4.7 mmol) anhydrate Na_2CO_3 was added to the solution of compound **10** (0.33g, 1.0 mmol) in CH_2Cl_2 . The mixture was stirred vigorously at room temperature overnight. The crude product was concentrated in *vacuo* and purified by column chromatography (Hexanes/EtOAc 3:1 then 1:1), yielding 0.36g (80%) colorless oil. 1H NMR (300 MHz, $CDCl_3$) δ 2.49 (t, 2H, $J = 2.4$

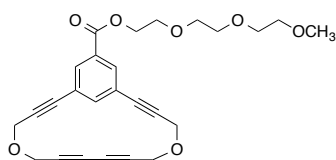
Hz), 3.35 (s, 3H), 3.52-3.81 (m, 10H), 4.31 (m, 4H), 4.47 (m, 6H), 7.67 (d, 1H, $J = 1.5$ Hz), 8.05 (d, 2H, $J = 1.8$ Hz).



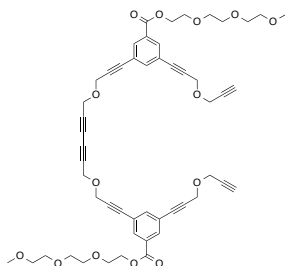
Compound (**20**). This white solid is a side product in the synthesis of **14**. ^1H NMR (400 MHz, CDCl_3) δ 3.42 (s, 3H), 3.72 (t, 2H, $J = 4.8$ Hz), 4.41 (d, 8H, $J = 1.6$ Hz), 4.46 (t, 2H, $J = 4.8$ Hz), 7.95 (d, 2H, $J = 1.6$ Hz), 8.29 (t, 1H, $J = 1.6$ Hz). ^{13}C NMR (100 MHz, CDCl_3) δ 165.5, 141.3, 130.8, 130.1, 123.6, 87.5, 86.9, 70.9, 70.6, 64.6, 61.2, 60.0, 59.3, 29.9.



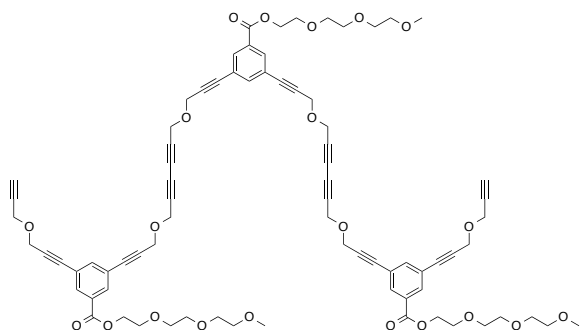
Compound (**21**). This white solid is a side product in the synthesis of **15**. ^1H NMR (300 MHz, CDCl_3) δ 3.39 (s, 3H), 3.55-3.58 (m, 2H), 3.67-3.70 (m, 2H), 3.81-3.84 (m, 2H), 4.42 (s, 8H), 4.46-4.50 (m, 2H), 7.95 (d, 2H, $J = 1.5$ Hz), 8.29 (t, 1H, $J = 1.5$ Hz).



Compound (**22**). This white solid is a side product in the synthesis of **16**. ^1H NMR (300 MHz, CDCl_3) δ 3.37 (s, 3H), 3.52-3.55 (m, 2H), 3.64-3.71 (m, 6H), 3.81-3.84 (m, 2H), 4.41 (s, 8H), 4.45-4.49 (m, 2H), 7.94 (d, 2H, $J = 1.8$ Hz), 8.29 (t, 1H, $J = 1.5$ Hz). MS m/z [$\text{M} + \text{H}^+$] calculated for $[\text{C}_{26}\text{H}_{26}\text{O}_7 + \text{H}]^+$ 451.1, found 451.1.

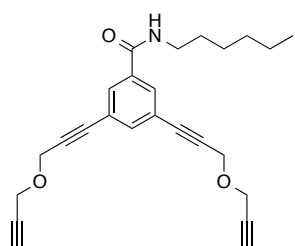


Compound (**23**). This white solid is a side product in the synthesis of **16**. ^1H NMR (300 MHz, CDCl_3) δ 2.49 (t, 2H), 3.36 (s, 6H), 3.52-3.55 (m, 4H), 3.63-3.71 (m, 12H), 3.81-3.84 (m, 4H), 4.32 (d, 4H, $J = 2.4$ Hz), 4.40 (s, 4H), 4.48 (d, 12H, $J = 2.4$ Hz), 7.68 (t, 2H, $J = 1.5$ Hz), 8.06 (d, 4H, $J = 1.5$ Hz).

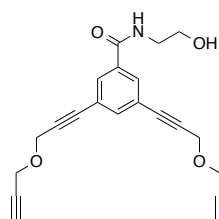


Hz), 8.07 (d, 6H, 1.5 Hz).

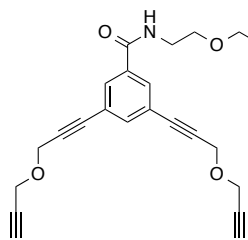
Compound (**24**). This white solid is a side product in the synthesis of **16**. ^1H NMR (300 MHz, CDCl_3) δ 2.49 (t, 2H, $J = 2.4$ Hz), 3.36 (s, 9H), 3.52-3.55 (m, 6H), 3.63-3.71 (m, 18H), 3.81-3.84 (m, 6H), 4.32 (d, 4H, $J = 2.4$ Hz), 4.40 (s, 8H), 4.49 (d, 18H, $J = 2.4$ Hz), 7.68 (t, 3H, $J = 1.5$



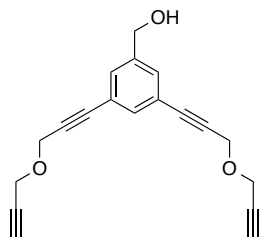
Compound (**28**). *n*-Hexamine (0.10g, 10 mmol) and 0.025g (0.2 mmol) DMAP was added to the solution of compound **10** (0.33g, 1.0 mmol) in CH_2Cl_2 . The mixture was heated to reflux and stirred vigorously overnight. The crude product was concentrated in *vacuo* and purified by column chromatography (Hexanes/EtOAc 1:2), yielding 0.27g (70%) yellow oil. ^1H NMR (300 MHz, CDCl_3) δ 0.88 (t, 3H, $J = 6.6$ Hz), 1.28-1.38 (m, 6H), 1.55-1.68 (m, 2H), 2.49 (t, 2H, $J = 2.4$ Hz), 3.39-3.45 (m, 2H), 4.30 (d, 4H, $J = 2.4$ Hz), 4.47 (s, 4H), 6.19 (t, 1H, $J = 5.7$ Hz), 7.60 (t, 1H, $J = 1.5$ Hz), 7.76 (d, 2H, $J = 1.5$ Hz).



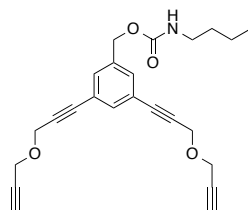
Compound (**29**). 2-aminoethanol (0.12g, 20 mmol) and 0.05g (0.4 mmol) DMAP was added to the solution of compound **10** (0.33g, 1.0 mmol) in CH_2Cl_2 . The mixture was heated to reflux and stirred vigorously overnight. The crude product was concentrated in *vacuo* and purified by column chromatography (Hexanes/EtOAc 1:3), yielding 0.27g (77%) yellow oil. ^1H NMR (400 MHz, CDCl_3) δ 2.49 (t, 2H, $J = 2.8$ Hz), 2.88 (s, 1H), 3.59 (q, 2H, $J = 5.2$ Hz), 3.81 (t, 2H, $J = 5.2$ Hz), 4.29 (d, 4H, $J = 2.4$ Hz), 4.45 (s, 4H), 7.01 (s, 1H), 7.57 (s, 1H), 7.76 (d, 2H, $J = 1.6$ Hz). ^{13}C NMR (100 MHz, CDCl_3) δ 166.9, 137.2, 134.8, 130.3, 123.2, 86.0, 85.0, 78.8, 75.6, 61.6, 57.2, 56.8, 42.9.



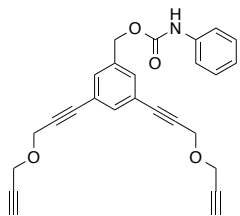
Compound (**30**). 2-(2-aminoethoxy)ethanol (0.21g, 20 mmol) and 0.05g (0.4 mmol) DMAP was added to the solution of compound **10** (0.33g, 1.0 mmol) in CH_2Cl_2 . The mixture was heated to reflux and stirred vigorously overnight. The crude product was concentrated in *vacuo* and purified by column chromatography (Hexanes/EtOAc 1:3), yielding 0.28g (72%) yellow oil. ^1H NMR (300 MHz, CDCl_3) δ 2.50 (m, 2H), 3.61-3.68 (m, 6H), 3.78 (t, 2H, $J = 4.2$ Hz), 4.32 (d, 4H, $J = 2.4$ Hz), 4.48 (s, 4H), 6.73 (s, 1H), 7.61 (t, 1H, $J = 1.8$ Hz), 7.80 (d, 2H, $J = 1.5$ Hz).



Compound (**31**). 0.114g (0.34 mmol) compound **10** in dried THF was added dropwise to LiAlH_4 (cooled in ice water). Bubbles are generated. After 10 min water was added dropwise to the solution to quench the reaction. Then 10% H_2SO_4 was added to dissolve the solids. Crude product was extracted out from the solution by ethyl ether. The ether solution was concentrated in *vacuo*, followed by column chromatography (Hexanes/EtOAc 2:1), yielding 0.09g (93%) light yellow oil. ^1H NMR (400 MHz, CDCl_3) δ 1.84 (s, 1H), 2.48 (t, 2H, $J = 2.4$ Hz), 4.31 (d, 4H, $J = 2.4$ Hz), 4.47 (s, 4H), 4.64 (s, 2H), 7.40 (t, 2H, $J = 1.2$ Hz), 7.44 (d, 1H, $J = 1.2$ Hz). ^{13}C NMR (125 MHz, CDCl_3) δ 141.4, 133.8, 130.0, 122.8, 85.7, 84.8, 78.8, 75.1, 64.0, 57.1, 56.5.

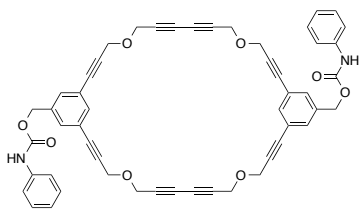


Compound (**34**). 0.029g (0.10 mmol) compound **31** was added dropwise to a mixture of 0.020g (0.20 mmol) *n*-butyl isocyanate and triethylamine (catalytic amount) in toluene. The solution was heated up to reflux. After reaction toluene was removed in *vacuo* and the crude product was purified by column chromatography (Hexanes/EtOAc 2:1), yielding 0.032g (81%) yellow oil. ^1H NMR (300 MHz, CDCl_3) δ 0.92 (t, 3H, $J = 7.2$ Hz), 1.25 (s, 4H), 2.48 (t, 2H, $J = 2.4$ Hz), 3.20 (q, 2H), 4.31 (t, 4H, $J = 1.2$ Hz), 4.48 (s, 4H), 5.03 (s, 2H), 7.39 (s, 2H), 7.46 (s, 1H).



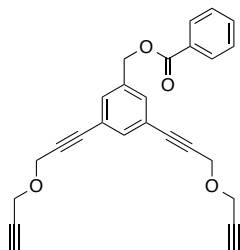
Compound (**36**). 0.7g (2.4 mmol) compound **31** was added dropwise to a mixture of 1.0 mL (9 mmol) phenyl isocyanate and triethylamine (catalytic amount) in 50 mL dry toluene. The solution was heated at reflux for 4 hours.

After reaction toluene was removed in *vacuo* and the crude product was purified by column chromatography (Hexanes/EtOAc 2:1), yielding 0.89g (90%) yellow solid. ^1H NMR (400 MHz, CDCl_3) δ 2.48 (t, 2H, $J = 2.4$ Hz), 4.31 (d, 4H, $J = 2.4$ Hz), 4.48 (s, 4H), 5.13 (s, 2H), 6.73 (s, 1H), 7.06-7.13 (m, 1H), 7.29-7.33 (m, 2H), 7.38-7.41 (m, 2H), 7.43 (d, 2H, $J = 1.6$ Hz), 7.48 (t, 1H, $J = 1.6$ Hz). ^{13}C NMR (125 MHz, CDCl_3) δ 153.3, 137.6, 136.8, 134.3, 130.9, 130.2, 129.6, 128.8, 124.3, 123.4, 122.9, 120.5, 118.6, 85.3, 85.1, 78.7, 75.4, 65.4, 57.0, 56.4.



Compound (**37**). Following **general procedure A**, 0.25g (0.60 mmol) compound **36** yields 0.042g (17%) of white solid. Note:

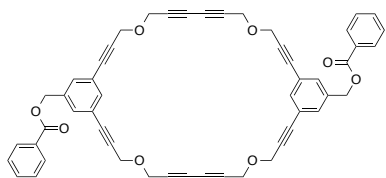
Two column chromatography processes were conducted. All solids were removed from the solution in the first column chromatography by using pure EtOAc as the eluent. The crude product was further purified by the second column chromatography (Hexanes/EtOAc 2.5:1) to give the pure compound **37** as purple crystal. ^1H NMR (500 MHz, CDCl_3) δ 4.41 (s, 8H), 4.48 (s, 8H), 5.14 (s, 4H), 6.75 (s, 2H), 7.25-7.53 (m, 16H). MS m/z $[\text{M} + \text{NH}_4]^+$ calculated for $[\text{C}_{52}\text{H}_{38}\text{N}_2\text{O}_8 + \text{NH}_4]^+$ 836.3, found 836.2.



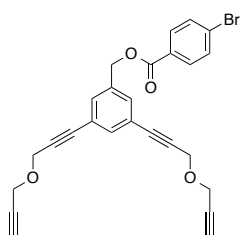
Compound (**38**). A solution of DCC (0.21g, 1.0 mmol) was added dropwise to a solution of compound **31** (0.29g, 1.0 mmol), DMAP (0.05g, 0.4 mmol), and benzoic acid (0.15g, 1.2 mmol) in methylene chloride at 0 °C under N_2 protection. The mixture was allowed to warm up to room temperature and stirred for 12 hours. After reaction the precipitate was filtered. The filtrate

was concentrated in *vacuo*. The crude product was purified by column chromatography (Hexanes/EtOAc 2:1), yielding 0.34g (86%) white solids. ^1H NMR (400 MHz, CDCl_3) δ 2.48 (t, 2H, $J = 2.4$ Hz), 4.30 (d, 4H, $J = 2.4$ Hz), 4.47 (s, 4H), 5.29 (s, 2H), 7.42-7.50 (m, 5H), 7.57 (t,

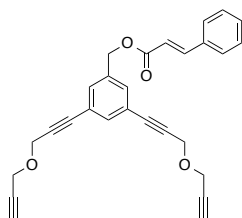
1H, J = 7.6 Hz), 8.06 (d, 2H, J = 7.2 Hz). ¹³C NMR (100 MHz, CDCl₃) δ 166.3, 137.0, 134.8, 133.4, 131.4, 129.9, 128.6, 123.4, 85.7, 85.5, 79.0, 75.0, 75.2, 65.6, 57.3, 56.8.



Compound (**39**). Following **general procedure A**, 0.16g (0.40 mmol) compound **38** yields 0.035g (22%) of white solid. ¹H NMR (300 MHz, CDCl₃) δ 4.41 (s, 8H), 4.49 (s, 8H), 5.30 (s, 4H), 7.43-7.48 (m, 8H), 7.54-7.60 (m, 4H), 8.05 (d, 2H, J = 1.5 Hz), 8.08 (m, 2H); MS *m/z* [M + NH₄]⁺ calculated for [C₅₂H₃₆O₈ + NH₄]⁺ 806.3, found 806.3.

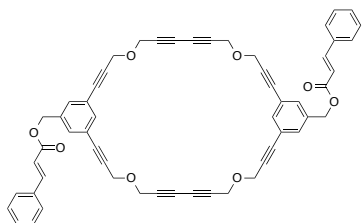


Compound (**40**). A solution of DCC (0.11g, 0.5 mmol) in 20 mL CH₂Cl₂ was added dropwise to a solution of compound **31** (0.14g, 0.5 mmol), DMAP (0.025g, 0.2 mmol), and 4-bromobenzoic acid (0.12g, 0.6 mmol) in 40 mL CH₂Cl₂ at 0 °C under N₂ protection. The mixture was allowed to warm up to room temperature and stirred for 12 hours. After reaction the precipitate was filtered. The filtrate was concentrated in *vacuo*. The crude product was purified by column chromatography (Hexanes/EtOAc 3:1), yielding 0.13g (56%) white solids. ¹H NMR (300 MHz, CDCl₃) δ 2.48 (t, 2H, J = 2.4 Hz), 4.31 (d, 4H, J = 2.4 Hz), 4.48 (s, 4H), 5.28 (s, 2H), 7.46 (d, 2H, J = 1.5 Hz), 7.50 (t, 1H, J = 1.5 Hz), 7.59 (dt, 2H, J = 9 Hz, 2.1 Hz), 7.92 (dt, 2H, J = 9 Hz, 2.1 Hz). ¹³C NMR (125 MHz, CDCl₃) δ 165.3, 136.4, 134.6, 131.7, 131.2, 131.1, 128.5, 128.3, 123.1, 85.3, 85.3, 78.8, 75.1, 65.6, 57.0, 56.5.

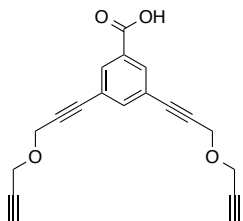


Compound (**42**). Cinnamic acid (0.09g, 0.6 mmol), DMAP (0.03g, 0.2 mmol) and compound **31** (0.14g, 0.5 mmol) were dissolved in 60 mL solvents of CH₂Cl₂ and toluene (1:1) at 0 °C under N₂. The solution of DCC (0.1g, 0.5 mmol) in 10 mL CH₂Cl₂ was added dropwise into mixture. The reaction was allowed to warm to room temperature and stirred for 4 hours. After reaction the solids were removed by filtration. The crude product was concentrated in *vacuo* and purified by column chromatography (Hexanes/EtOAc 3:1), yielding 0.17g (80%) white solids. ¹H NMR (300

MHz, CDCl₃) δ 2.49 (t, 2H, J = 2.4 Hz), 4.31 (d, 4H, J = 2.4 Hz), 4.48 (s, 4H), 5.18 (s, 2H), 6.48 (d, 1H, J = 16.2 Hz), 7.38-7.40 (m, 3H), 7.45 (d, 2H, J = 1.2 Hz), 7.49 (t, 1H, J = 1.2 Hz), 7.52-7.55 (m, 2H), 7.73 (d, 1H, J = 16.2 Hz); ¹³C NMR (100 MHz, CDCl₃) δ 166.6, 145.7, 137.0, 134.6, 131.4, 130.5, 129.0, 128.1, 123.3, 117.6, 85.5, 79.0, 75.3, 65.2, 57.0, 32.8, 31.1, 26.4, 25.5, 24.8.



Compound (**43**). Following **general procedure A**, 0.21g (0.50 mmol) compound **42** yields 0.025g (12%) of white solid. ¹H NMR (300 MHz, CDCl₃) δ 4.41 (s, 8H), 4.49 (s, 8H), 5.18 (s, 4H), 6.48 (d, 2H, J = 15.9 Hz), 7.38-7.40 (m, 6H), 7.44 (s, 4H), 7.52-7.55 (m, 6H), 7.73 (d, 2H, J = 15.6 Hz). MS *m/z* [M + NH₄]⁺ calculated for [C₅₆H₄₀O₈ + NH₄]⁺ 858.3, found 858.3.



Compound (**45**). 0.17g (0.5 mmol) compound **10** in ethanol was added to 20 mL 1 mol/L NaOH aqueous solution. The reaction was stirred at room temperature for 4 hours. Excess 6 mol/L HCl was then added to the solution to pH = 1. The crude mixture was extracted with diethyl ether for 3 times. The ether layer was collected and concentrated in *vacuo*. The crude material was purified by column chromatography (Hexanes/EtOAc 1:5), yielding 0.07g (45%) compound **45** as white solids. ¹H NMR (300 MHz, CDCl₃) δ 2.50 (t, 2H, J = 2.4 Hz), 4.31 (d, 4H, J = 2.4 Hz), 4.48 (s, 4H), 7.69 (t, 1H, J = 1.5 Hz), 8.08 (d, 2H, J = 1.5 Hz), 11.60 (s, 1H). ¹³C NMR (100 MHz, CDCl₃) δ 170.5, 139.4, 133.2, 130.0, 123.5, 86.2, 84.8, 78.9, 75.5, 57.1, 56.8.

Bibliography

- (1) Lehn, J. M. *Supramolecular chemistry : concepts and perspectives*; VCH: Weinheim ; New York, 1995.
- (2) Chen, G.; Jiang, M. Cyclodextrin-based inclusion complexation bridging supramolecular chemistry and macromolecular self-assembly; *Chemical Society Reviews* **2011**, *40*, 2254.
- (3) Gohy, J.-F.; Lohmeijer, B. G. G.; Schubert, U. S. Reversible Metallo-Supramolecular Block Copolymer Micelles Containing a Soft Core; *Macromolecular Rapid Communications* **2002**, *23*, 555.
- (4) Zhang, X.; Rehm, S.; Safont-Sempere, M. M.; Würthner, F. Vesicular perylene dye nanocapsules as supramolecular fluorescent pH sensor systems; *Nature Chemistry* **2009**, *1*, 623.
- (5) Zeng, F.; Zimmerman, S. C. Dendrimers in Supramolecular Chemistry: From Molecular Recognition to Self-Assembly; *Chemical Reviews* **1997**, *97*, 1681.
- (6) Chuard, T.; Deschenaux, R. Design, mesomorphic properties, and supramolecular organization of [60]fullerene-containing thermotropic liquid crystals; *Journal of Materials Chemistry* **2002**, *12*, 1944.
- (7) Wuest, J. D. Molecular solids: Co-crystals give light a tune-up; *Nat Chem* **2012**, *4*, 74.
- (8) Palacios, M. A.; Nishiyabu, R.; Marquez, M.; Anzenbacher, P. Supramolecular Chemistry Approach to the Design of a High-Resolution Sensor Array for Multianion Detection in Water; *Journal of the American Chemical Society* **2007**, *129*, 7538.
- (9) Joyce, L. A.; Shabbir, S. H.; Anslyn, E. V. The uses of supramolecular chemistry in synthetic methodology development: examples of anion and neutral molecular recognition; *Chemical Society Reviews* **2010**, *39*, 3621.
- (10) Thomas, S. W.; Joly, G. D.; Swager, T. M. Chemical sensors based on amplifying fluorescent conjugated polymers; *Chemical Reviews* **2007**, *107*, 1339.
- (11) Liu, Z.; Sun, X.; Nakayama-Ratchford, N.; Dai, H. Supramolecular Chemistry on Water-Soluble Carbon Nanotubes for Drug Loading and Delivery; *ACS Nano* **2007**, *1*, 50.
- (12) Srinivasan, S.; Babu, P. A.; Mahesh, S.; Ajayaghosh, A. Reversible Self-Assembly of Entrapped Fluorescent Gelators in Polymerized Styrene Gel Matrix: Erasable Thermal Imaging via Recreation of Supramolecular Architectures; *Journal of the American Chemical Society* **2009**, *131*, 15122.
- (13) Steed, J. W.; Atwood, J. L. *Supramolecular chemistry*; 2nd ed.; Wiley: Chichester, UK, 2009.
- (14) Horton, H. R. *Principles of biochemistry*; 3rd ed.; Prentice Hall: Upper Saddle River, NJ, 2002.
- (15) O'Reilly, R. K. In *Supramolecular Chemistry*; John Wiley & Sons, Ltd: 2012.
- (16) Daniel, M. C.; Astruc, D. Gold nanoparticles: Assembly, supramolecular chemistry, quantum-size-related properties, and applications toward biology, catalysis, and nanotechnology; *Chemical Reviews* **2004**, *104*, 293.
- (17) Saha, K.; Agasti, S. S.; Kim, C.; Li, X.; Rotello, V. M. Gold Nanoparticles in Chemical and Biological Sensing; *Chemical Reviews* **2012**, *112*, 2739.

- (18) Lewis, G. N. *Valence and the structure of atoms and molecules*; Chemical Catalog Company, Inc.: New York,, 1923.
- (19) Pearson, R. G. Hard and Soft Acids and Bases; *Journal of the American Chemical Society* **1963**, *85*, 3533.
- (20) Schmidt, G. M. Photodimerization in the Solid State; *Pure and Applied Chemistry* **1971**, *27*, 647.
- (21) Lauher, J. W.; Fowler, F. W.; Goroff, N. S. Single-crystal-to-single-crystal topochemical polymerizations by design; *Accounts of Chemical Research* **2008**, *41*, 1215.
- (22) Zhou, W.; Li, Y.; Zhu, D. Progress in polydiacetylene nanowires by self-assembly and self-polymerization; *Chemistry-an Asian Journal* **2007**, *2*, 222.
- (23) Tieke, B.; Enkelmann, V.; Kapp, H.; Lieser, G.; Wegner, G. Topochemical Reactions in Langmuir-Blodgett Multilayers; *Journal of Macromolecular Science: Part A - Chemistry* **1981**, *15*, 1045.
- (24) Cheong, D.-W.; Kim, W.-H.; Samuelson, L. A.; Kumar, J.; Tripathy, S. K. Oriented Z-Type Langmuir-Blodgett Films from a Soluble Asymmetrically Substituted Polydiacetylene; *Macromolecules* **1996**, *29*, 1416.
- (25) Carpick, R. W.; Sasaki, D. Y.; Marcus, M. S.; Eriksson, M. A.; Burns, A. R. Polydiacetylene films: a review of recent investigations into chromogenic transitions and nanomechanical properties; *Journal of Physics-Condensed Matter* **2004**, *16*, R679.
- (26) Jeffrey, G. A. *An introduction to hydrogen bonding*; Oxford University Press: New York, 1997.
- (27) Adams, H.; Harris, K. D. M.; Hembury, G. A.; Hunter, C. A.; Livingstone, D.; McCabe, J. F. How strong is a [small pi]-facial hydrogen bond?; *Chemical Communications* **1996**, 2531.
- (28) Wegner, G. Topochemical Reactions of Monomers with Conjugated Triple Bonds .I. Polymerization of 2.4-Hexadiyn-1.6-Diols Deivatives in Crystalline State; *Zeitschrift Fur Naturforschung Part B-Chemie Biochemie Biophysik Biologie Und Verwandten Gebiete* **1969**, *B 24*, 824.
- (29) Hasegawa, M.; Suzuki, Y. Four-center type photopolymerization in the solid state: Poly-2,5-distrylpyrazine; *Journal of Polymer Science Part B: Polymer Letters* **1967**, *5*, 813.
- (30) Cohen, M. D.; Schmidt, G. M. J. Topochemistry .I. Survey; *Journal of the Chemical Society* **1964**, 1996.
- (31) Wilhelm, C.; Boyd, S. A.; Chawda, S.; Fowler, F. W.; Goroff, N. S.; Halada, G. P.; Grey, C. P.; Lauher, J. W.; Luo, L.; Martin, C. D.; Parise, J. B.; Tarabrella, C.; Webb, J. A. Pressure-induced polymerization of diiodobutadiyne in assembled cocrystals; *Journal of the American Chemical Society* **2008**, *130*, 4415.
- (32) Hasegawa, M. Photopolymerization of diolefin crystals; *Chemical Reviews* **1983**, *83*, 507.
- (33) Bubeck, C.; Sixl, H.; Neumann, W. ESR analysis of the initial reaction products in the solid state photopolymerization of diacetylenes; *Chemical Physics* **1980**, *48*, 269.
- (34) Sixl, H. Spectroscopy of the Intermediate States of the Solid-State Polymerization Reaction in Diacetylene Crystals; *Advances in Polymer Science* **1984**, *63*, 49.
- (35) Yarimaga, O.; Im, M.; Choi, Y.-K.; Kim, T. W.; Jung, Y. K.; Park, H. G.; Lee, S.; Kim, J.-M. A Color Display System Based on Thermochromic Conjugated Polydiacetylene Supramolecules; *Macromolecular Research* **2010**, *18*, 404.

- (36) Kew, S. J.; Hall, E. A. H. pH response of carboxy-terminated colorimetric polydiacetylene vesicles; *Analytical Chemistry* **2006**, *78*, 2231.
- (37) Lee, J.; Kim, H.-J.; Kim, J. Polydiacetylene liposome arrays for selective potassium detection; *Journal of the American Chemical Society* **2008**, *130*, 5010.
- (38) McQuade, D. T.; Pullen, A. E.; Swager, T. M. Conjugated polymer-based chemical sensors; *Chemical Reviews* **2000**, *100*, 2537.
- (39) Ahn, D. J.; Kim, J.-M. Fluorogenic polydiacetylene supramolecules: Immobilization, micropatterning, and application to label-free chemosensors; *Accounts of Chemical Research* **2008**, *41*, 805.
- (40) Lee, J.; Yarimaga, O.; Lee, C. H.; Choi, Y.-K.; Kim, J.-M. Network Polydiacetylene Films: Preparation, Patterning, and Sensor Applications; *Advanced Functional Materials* **2011**, *21*, 1032.
- (41) Enkelmann, V.; Schleier, G. Poly[1,2-Bis(Diphenylaminomethyl)-1-Buten-3-Ynylene]; *Acta Crystallographica Section B* **1980**, *36*, 1954.
- (42) Spinat, P.; Brouty, C.; Whuler, A.; Sichere, M. C. Structural Determination at 205 K of 1,2-Poly (4-Bis[Para-Bromophenylcarbamoxy]Butyl-1-Butene-3-Yne-Ylene), (C₂₆H₂₆Br₂N₂O₄)_n; *Acta Crystallographica Section C* **1985**, *41*, 1452.
- (43) Yee, K. C. Synthesis and thermal solid-state polymerization of a new diacetylene: 2,4-hexadiynylene bis(p-fluorobenzenesulfonate); *The Journal of Organic Chemistry* **1979**, *44*, 2571.
- (44) Zhao, X. Q.; Chang, Y. L.; Fowler, F. W.; Lauher, J. W. An Approach to the Design of Molecular-Solids - the Ureylenedicarboxylic Acids; *Journal of the American Chemical Society* **1990**, *112*, 6627.
- (45) Schauer, C. L.; Matwey, E.; Fowler, F. W.; Lauher, J. W. Controlled spacing of metal atoms via ligand hydrogen bonds; *Journal of the American Chemical Society* **1997**, *119*, 10245.
- (46) Kane, J. J.; Liao, R. F.; Lauher, J. W.; Fowler, F. W. Preparation of Layered Diacetylenes as a Demonstration of Strategies for Supramolecular Synthesis; *Journal of the American Chemical Society* **1995**, *117*, 12003.
- (47) Nguyen, T. L. Ph.D. Dissertation, The Preparation of Designed Two Dimensional Hydrogen Bonded Networks. Application in Material Science, Stony Brook University, **1998**.
- (48) Chang, Y. L.; West, M. A.; Fowler, F. W.; Lauher, J. W. An Approach to the Design of Molecular-Solids - Strategies for Controlling the Assembly of Molecules into 2-Dimensional Layered Structures; *Journal of the American Chemical Society* **1993**, *115*, 5991.
- (49) Toledo, L. M.; Lauher, J. W.; Fowler, F. W. Design of Molecular-Solids - Application of 2-Amino-4(1h)-Pyridones to the Preparation of Hydrogen-Bonded Alpha-Networks and Beta-Networks; *Chemistry of Materials* **1994**, *6*, 1222.
- (50) Toledo, L. M.; Musa, K. M.; Lauher, J. W.; Fowler, F. W. Development of Strategies for the Preparation of Designed Solids - an Investigation of the 2-Amino-4(1h)-Pyrimidone Ring-System for the Molecular Self-Assembly of Hydrogen-Bonded Alpha-Networks and Beta-Networks; *Chemistry of Materials* **1995**, *7*, 1639.
- (51) Khan, M.; Enkelmann, V.; Brunklau, G. O-H...N Heterosynthon: A Robust Supramolecular Unit For Crystal Engineering; *Crystal Growth & Design* **2009**, *9*, 2354.

- (52) Tsaggeos, K.; Masiera, N.; Niwicka, A.; Dokorou, V.; Siskos, M. G.; Skoulika, S.; Michaelides, A. Crystal Structure, Thermal Behavior, and Photochemical Reactivity of a Series of Co-Crystals of trans-1,2-Bis(4-pyridyl) Ethylene with Dicarboxylic Acids; *Crystal Growth & Design* **2012**, *12*, 2187.
- (53) Liao, R. F.; Lauher, J. W.; Fowler, F. W. The application of the 2-amino-4-pyrimidones to supramolecular synthesis; *Tetrahedron* **1996**, *52*, 3153.
- (54) Lloret, F.; Sletten, J.; Ruiz, R.; Julve, M.; Faus, J.; Verdaguer, M. Oxamidato complexes. 2. Copper(II) and nickel(II) complexes with oxamide-N,N'-diacetic acid: solution study, synthesis, crystal structures, and magnetic properties; *Inorganic Chemistry* **1992**, *31*, 778.
- (55) Jian-Fang, L.; Yan-Tuan, L.; Zhi-Yong, W.; Da-Qi, W.; Jian-Min, D. trans--Oxamido-N, N-diethanoato-bis[diacuacopper(II)] dihydrate; *Acta Crystallographica Section C* **2005**, *61*, m400.
- (56) Tran, T. M.S. Dissertation, The Preparation of Polydiacetylenes Using Supramolecular Chemistry, Stony Brook University, **2001**.
- (57) Hay, A. S. Oxidative Coupling of Acetylenes; *The Journal of Organic Chemistry* **1960**, *25*, 1275.
- (58) Hay, A. S. Oxidative Coupling of Acetylenes .2.; *The Journal of Organic Chemistry* **1962**, *27*, 3320.
- (59) Janiak, C. A critical account on pi-pi stacking in metal complexes with aromatic nitrogen-containing ligands; *Journal of the Chemical Society, Dalton Transactions* **2000**, 3885.
- (60) Pigos, J. M.; Zhu, Z.; Musfeldt, J. L. Optical Properties of a Supramolecular Assembly Containing Polydiacetylene; *Chemistry of Materials* **1999**, *11*, 3275.
- (61) Dei, S.; Matsumoto, A.; Matsumoto, A. Thermochromism of Polydiacetylenes in the Solid State and in Solution by the Self-Organization of Polymer Chains Containing No Polar Group; *Macromolecules* **2008**, *41*, 2467.
- (62) Luo, L.; Wilhelm, C.; Young, C. N.; Grey, C. P.; Halada, G. P.; Xiao, K.; Ivanov, I. N.; Howe, J. Y.; Geohegan, D. B.; Goroff, N. S. Characterization and Carbonization of Highly Oriented Poly(diiododiacetylene) Nanofibers; *Macromolecules* **2011**, *44*, 2626.
- (63) Pedersen, C. J. Cyclic Polyethers and Their Complexes with Metal Salts; *Journal of the American Chemical Society* **1967**, *89*, 7017.
- (64) Press Release: The 1987 Nobel Prize in Chemistry.
http://www.nobelprize.org/nobel_prizes/chemistry/laureates/1987/press.html (accessed August 7, 2013)
- (65) Lindoy, L. F. *The chemistry of macrocyclic ligand complexes*; Cambridge University Press: Cambridge Cambridgeshire ; New York, 1989.
- (66) Inoue, Y.; Gokel, G. W. *Cation binding by macrocycles : complexation of cationic species by crown ethers*; M. Dekker: New York, 1990.
- (67) Yoshio, M.; Noguchi, H. Crown ethers for chemical analysis: A Review; *Analytical Letters* **1982**, *15*, 1197.
- (68) Tsukanov, A.; Dubonosov, A.; Bren, V.; Minkin, V. Organic chemosensors with crown-ether groups (review); *Chemistry of heterocyclic compounds* **2008**, *44*, 899.
- (69) Steed, J. W.; Atwood, J. L. *Supramolecular chemistry*; 2nd ed.; Wiley: Chichester, UK, 2009.

- (70) Davis, F.; Higson, S. *Macrocycles : construction, chemistry and nanotechnology applications*; Wiley: Chichester, West Sussex, U.K., 2011.
- (71) Moore, J. S. Shape-Persistent Molecular Architectures of Nanoscale Dimension; *Accounts of Chemical Research* **1997**, *30*, 402.
- (72) Höger, S. Highly efficient methods for the preparation of shape-persistent macrocyclics; *Journal of Polymer Science Part A: Polymer Chemistry* **1999**, *37*, 2685.
- (73) Bong, D. T.; Clark, T. D.; Granja, J. R.; Ghadiri, M. R. Self-assembling organic nanotubes; *Angewandte Chemie International Edition* **2001**, *40*, 988.
- (74) Zhang, B.; Wang, Y.; Yang, S.-P.; Zhou, Y.; Wu, W.-B.; Tang, W.; Zuo, J.-P.; Li, Y.; Yue, J.-M. Ivorenolide A, an Unprecedented Immunosuppressive Macrolide from *Khaya ivorensis*: Structural Elucidation and Bioinspired Total Synthesis; *Journal of the American Chemical Society* **2012**, *134*, 20605.
- (75) Shetty, A. S.; Zhang, J.; Moore, J. S. Aromatic π -Stacking in Solution as Revealed through the Aggregation of Phenylacetylene Macrocyclics; *Journal of the American Chemical Society* **1996**, *118*, 1019.
- (76) Nakamura, K.; Okubo, H.; Yamaguchi, M. Synthesis and Self-aggregation of Cyclic Alkynes Containing Helicene; *Organic Letters* **2001**, *3*, 1097.
- (77) Lin, C.-H.; Tour, J. Hydrogen-Bond-Assisted π -Stacking of Shape-Persistent Cyclophanes; *The Journal of Organic Chemistry* **2002**, *67*, 7761.
- (78) Tobe, Y.; Utsumi, N.; Nagano, A.; Naemura, K. Synthesis and Association Behavior of [4.4.4.4.4.4]Metacyclophanedodecayne Derivatives with Interior Binding Groups; *Angewandte Chemie International Edition* **1998**, *37*, 1285.
- (79) Tobe, Y.; Utsumi, N.; Kawabata, K.; Nagano, A.; Adachi, K.; Araki, S.; Sonoda, M.; Hirose, K.; Naemura, K. m-Diethynylbenzene Macrocyclics: Syntheses and Self-Association Behavior in Solution; *Journal of the American Chemical Society* **2002**, *124*, 5350.
- (80) Lehn, J.-M.; Malthete, J.; Levelut, A.-M. Tubular mesophases: liquid crystals consisting of macrocyclic molecules; *Journal of the Chemical Society, Chemical Communications* **1985**, 1794.
- (81) van Nostrum, C. F. Self-assembled wires and channels; *Advanced Materials* **1996**, *8*, 1027.
- (82) Van der Pol, J. F.; Neeleman, E.; Van Miltenburg, J. C.; Zwicker, J. W.; Nolte, R. J. M.; Drenth, W. A polymer with the mesomorphic order of liquid crystalline phthalocyanines; *Macromolecules* **1990**, *23*, 155.
- (83) Wang, T. M.S. Dissertation, The Topochemical Polymerization of Diacetylenes Using Supramolecular Host-Guest Chemistry, Stony Brook University, **2005**.
- (84) Chow, S. K. M.S. Dissertation, Synthesis of 2,6-Pyridine-Based Diacetylene Macrocyclic and its Possible Formation to a Covalent Bonded Tubular Structure via Topochemical Polymerization, Stony Brook University, **2008**.
- (85) Hsu, T. J.; Fowler, F. W.; Lauher, J. W. Preparation and Structure of a Tubular Addition Polymer: A True Synthetic Nanotube; *Journal of the American Chemical Society* **2012**, *134*, 142.
- (86) Baldwin, K. P.; Matzger, A. J.; Scheiman, D. A.; Tessier, C. A.; Vollhardt, K. P. C.; Youngs, W. J. Synthesis, Crystal Structure, and Polymerization of 1,2:5,6:9,10-Tribenzo-3,7,11,13-tetrahydro[14]annulene; *Synlett* **1995**, *1995*, 1215.

- (87) Xu, Y.; Smith, M. D.; Geer, M. F.; Pellechia, P. J.; Brown, J. C.; Wibowo, A. C.; Shimizu, L. S. Thermal Reaction of a Columnar Assembled Diacetylene Macrocycle; *Journal of the American Chemical Society* **2010**, *132*, 5334.
- (88) Chodkiewicz, W.; Cadiot, P. Nouvelle Synthèse De Composés Polyacétyléniques Conjugués Symétriques Et Dissymétriques; *Comptes Rendus Hebdomadaires Des Seances De L Academie Des Sciences* **1955**, *241*, 1055.
- (89) Glaser, C. Beiträge zur Kenntniss des Acetylnylbenzols; *Berichte der deutschen chemischen Gesellschaft* **1869**, *2*, 422.
- (90) Campbell, K.; McDonald, R.; Tykwinski, R. R. Functionalized Macrocyclic Ligands for Use in Supramolecular Chemistry; *The Journal of Organic Chemistry* **2002**, *67*, 1133.
- (91) Barton, A. F. M. Solubility parameters; *Chemical Reviews* **1975**, *75*, 731.
- (92) Spagnoli, S.; Berrehar, J.; LapersonneMeyer, C.; Schott, M.; Rameau, A.; Rawiso, M. gamma-ray polymerization of urethane-substituted diacetylenes: Reactivity and chain lengths; *Macromolecules* **1996**, *29*, 5615.
- (93) Mohamed, S.; Tocher, D. A.; Vickers, M.; Karamertzanis, P. G.; Price, S. L. Salt or Cocrystal? A New Series of Crystal Structures Formed from Simple Pyridines and Carboxylic Acids; *Crystal Growth & Design* **2009**, *9*, 2881.
- (94) O'mahony, J.; Karlsson, B. C. G.; Mizaikoff, B.; Nicholls, I. A. Correlated theoretical, spectroscopic and X-ray crystallographic studies of a non-covalent molecularly imprinted polymerisation system; *Analyst* **2007**, *132*, 1161.
- (95) Li, Z.; Fowler, F. W.; Lauher, J. W. Weak Interactions Dominating the Supramolecular Self-Assembly in a Salt: A Designed Single-Crystal-to-Single-Crystal Topochemical Polymerization of a Terminal Aryldiacetylene; *Journal of the American Chemical Society* **2009**, *131*, 634.
- (96) Dey, S. K.; Ojha, B.; Das, G. A subtle interplay of C-H hydrogen bonds in complexation of anions of varied dimensionality by a nitro functionalized tripodal podand; *Crystengcomm* **2011**, *13*, 269.
- (97) Bradley, S.; Camm, K. D.; Liu, X. M.; McGowan, P. C.; Mumtaz, R.; Oughton, K. A.; Podesta, T. J.; Thornton-Pett, M. Synthesis and structural studies of 1,1'-bis-amino-functionalized ferrocenes, ferrocene salts, and ferrocenium salts; *Inorganic Chemistry* **2002**, *41*, 715.
- (98) Kobayashi, J.; Inaba, Y.; Shiro, M.; Yoshida, N.; Morita, H. Daphnicyclidins A-H, novel hexa- or pentacyclic alkaloids from two species of *Daphniphyllum*; *Journal of the American Chemical Society* **2001**, *123*, 11402.
- (99) Burchell, C. J.; Glidewell, C.; Lough, A. J.; Ferguson, G. Salts of 3,5-dinitrobenzoic acid with organic diamines: hydrogen-bonded supramolecular structures in one, two and three dimensions; *Acta Crystallographica Section B* **2001**, *57*, 201.
- (100) Chantrapromma, S.; Usman, A.; Fun, H. K.; Poh, B. L.; Karalai, C. Structural and spectroscopic studies of the adducts of quinuclidine and 3,5-dinitrobenzoic acid; *Journal of Molecular Structure* **2004**, *688*, 59.
- (101) Ihmels, H.; Leusser, D.; Pfeiffer, M.; Stalke, D. Solid-State Photolysis of Anthracene-Linked Ammonium Salts: The Search for Topochemical Anthracene Photodimerizations; *Tetrahedron* **2000**, *56*, 6867.
- (102) Yang, E.; Song, X.-C.; Zhu, J.-W. 1,4-Diazoniabicyclo[2.2.2]octane terephthalate; *Acta Crystallographica Section E* **2008**, *64*, o1764.

- (103) Braga, D.; Maini, L.; de Sanctis, G.; Rubini, K.; Grepioni, F.; Chierotti, M. R.; Gobetto, R. Mechanochemical Preparation of Hydrogen-Bonded Adducts Between the Diamine 1,4-Diazabicyclo[2.2.2]octane and Dicarboxylic Acids of Variable Chain Length: An X-ray Diffraction and Solid-State NMR Study; *Chemistry – A European Journal* **2003**, *9*, 5538.
- (104) Sarma, B.; Thakuria, R.; Nath, N. K.; Nangia, A. Crystal structures of mirtazapine molecular salts; *Crystengcomm* **2011**, *13*, 3232.
- (105) Horiguchi, M.; Ito, Y. Unsymmetrical photodimerization of a 9-aminomethylanthracene in the crystalline salt; *The Journal of Organic Chemistry* **2006**, *71*, 3608.
- (106) Peterson, M. A.; Hope, H.; Nash, C. P. Hydrogen-Bonding in N-Substituted Amino-Acids - Crystal-Structure of the N,N-Diethyl-Beta-Alanine-Benzene Inclusion Compound; *Journal of the American Chemical Society* **1979**, *101*, 946.
- (107) Dann, Y. L.; Cowley, A. R.; Anderson, H. L. 2-[(Dimethylamino)(phenyl)methyl]benzoic acid; *Acta Crystallographica Section E* **2005**, *61*, o2502.
- (108) Katsura, Y.; Zhang, X. Y.; Homma, K.; Rice, K. C.; Calderon, S. N.; Rothman, R. B.; Yamamura, H. I.; Davis, P.; FlippenAnderson, J. L.; Xu, H.; Becketts, K.; Foltz, E. J.; Porreca, F. Probes for narcotic receptor-mediated phenomena .25. Synthesis and evaluation of N-alkyl-substituted (alpha-piperazinylbenzyl)benzamides as novel, highly selective delta opioid receptor agonists; *Journal of Medicinal Chemistry* **1997**, *40*, 2936.
- (109) Krebs, F. C.; Jorgensen, M. Calix[4]arene-5,17-dicarboxylic acids and their interactions with aliphatic amines. Part 2. A crystal engineering approach; *Journal of the Chemical Society-Perkin Transactions 2* **2000**, 1935.
- (110) Dhaneshw.Nn; Pant, L. M. Structure of N,N-Dimethylantranilic Acid; *Acta Crystallographica Section B* **1973**, *29*, 2980.
- (111) Phillips, A. P. Dicarboxylic Acid Bis-(β -Tertiaryaminoalkyl) Amides as Curare Substitutes; *Science* **1950**, *112*, 536.
- (112) Sun, W.; Li, Y.-T.; Wu, Z.-Y.; Song, Y.-L. N,N'-Bis[2-(dimethylammonio)ethyl]oxamide dinitrate; *Acta Crystallographica Section E* **2006**, *62*, o3023.
- (113) Messori, L.; Shaw, J.; Camalli, M.; Mura, P.; Marcon, G. Structural features of a new dinuclear platinum(II) complex with significant anti proliferative activity; *Inorganic Chemistry* **2003**, *42*, 6166.
- (114) Hearn, W. R.; Hendry, R. A. Stereoisomerism of N,N'-Oxalylbis-(alanine) Derivatives1; *Journal of the American Chemical Society* **1957**, *79*, 5213.
- (115) Sudborough, J. J. K., D.D. Studies on Alcoholysis III. The Alcoholysis of Aromatic Esters and the inhibiting influence of Ortho-substituents; *Journal of the Indian Institute of Science* **1920**, *3*, 1.

Appendix 1. Molecular Structure and Crystallography Data

Molecular Structure and Crystallography Data for Compound 1

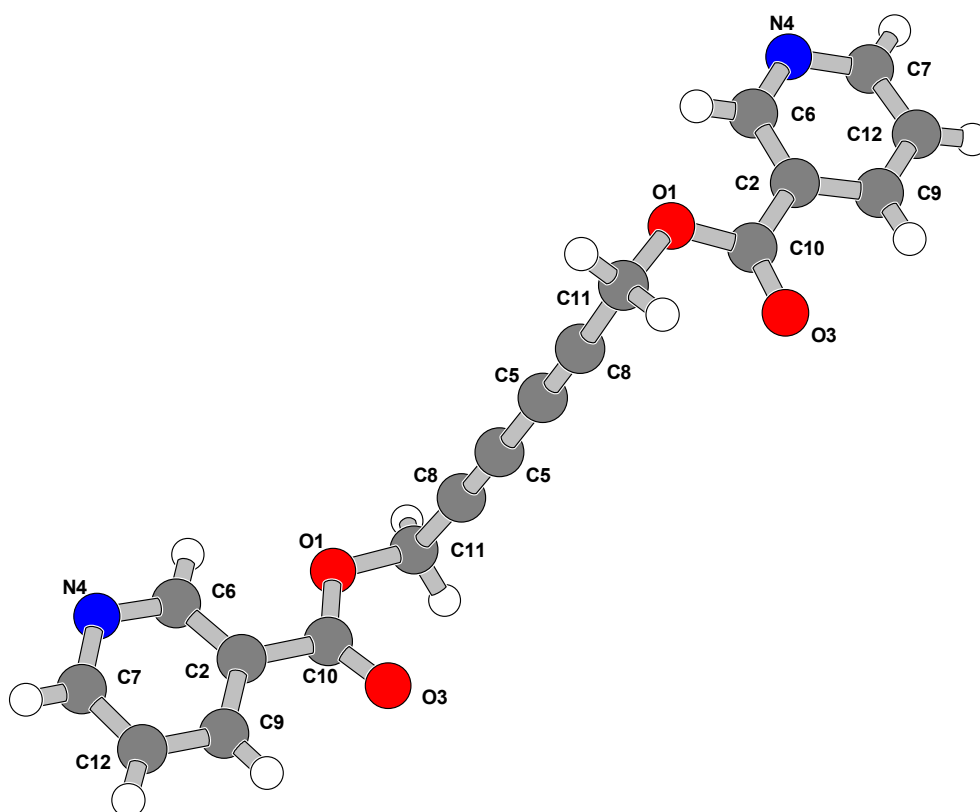


Table 1. Crystal data and structure refinement for Compound 1.

Identification code	hexa-2,4-diyne-1,6-diyl dinicotinate	
Empirical formula	C ₁₈ H ₁₂ N ₂ O ₄	
Formula weight	320.30	
Temperature	293(2) K	
Wavelength	1.54178 Å	
Crystal system	Monoclinic	
Space group	C2/c	
Unit cell dimensions	a = 6.9120(3) Å	a = 90°
	b = 19.1280(8) Å	b = 93.593(4)°
	c = 11.5173(5) Å	g = 90°
Volume	1519.74(11) Å ³	
Z	4	
Density (calculated)	1.400 Mg/m ³	
Absorption coefficient	0.839 mm ⁻¹	
F(000)	664	
Crystal size	1 x 0.5 x 0.5 mm ³	
Theta range for data collection	4.62 to 61.68°.	
Index ranges	-7<=h<=7, -21<=k<=17, -13<=l<=13	
Reflections collected	5113	
Independent reflections	1174 [R(int) = 0.0342]	
Completeness to theta = 61.68	98.7 %	
Refinement method	Full-matrix least-squares on F ²	
Data / restraints / parameters	1174 / 0 / 109	
Goodness-of-fit on F ²	1.092	
Final R indices [I>2sigma(I)]	R1 = 0.0490, wR2 = 0.1063	
R indices (all data)	R1 = 0.0631, wR2 = 0.1151	
Largest diff. peak and hole	0.297 and -0.461 e. ⁻³	

Table 2. Atomic coordinates ($\times 10^4$) and equivalent isotropic displacement parameters (2×10^3) for Compound 1. $U(\text{eq})$ is defined as one third of the trace of the orthogonalized U^{ij} tensor.

	x	y	z	$U(\text{eq})$
O(1)	1535(2)	1464(1)	212(1)	56(1)
C(2)	2405(2)	1230(1)	2176(2)	44(1)
O(3)	1976(2)	343(1)	739(1)	75(1)
N(4)	2956(2)	2202(1)	3465(1)	63(1)
C(5)	4184(3)	1187(1)	-2183(2)	53(1)
C(6)	2514(3)	1936(1)	2410(2)	51(1)
C(7)	3282(3)	1740(1)	4329(2)	62(1)
C(8)	2777(3)	1200(1)	-1634(2)	55(1)
C(9)	2752(3)	771(1)	3092(2)	56(1)
C(10)	1964(2)	954(1)	989(2)	51(1)
C(11)	1042(3)	1243(1)	-973(2)	63(1)
C(12)	3190(3)	1031(1)	4189(2)	59(1)

Table 3. Bond lengths (Å) and angles (°) for Compound 1.

O(1)-C(10)	1.344(2)
O(1)-C(11)	1.449(2)
C(2)-C(6)	1.379(2)
C(2)-C(9)	1.382(3)
C(2)-C(10)	1.479(3)
O(3)-C(10)	1.204(2)
N(4)-C(6)	1.335(2)
N(4)-C(7)	1.338(3)
C(5)-C(8)	1.194(3)
C(5)-C(5)#1	1.381(4)
C(7)-C(12)	1.368(3)
C(8)-C(11)	1.462(3)
C(9)-C(12)	1.373(3)
C(10)-O(1)-C(11)	116.40(15)
C(6)-C(2)-C(9)	117.91(17)
C(6)-C(2)-C(10)	122.39(17)
C(9)-C(2)-C(10)	119.70(17)
C(6)-N(4)-C(7)	116.33(17)
C(8)-C(5)-C(5)#1	178.83(14)
N(4)-C(6)-C(2)	123.90(18)
N(4)-C(7)-C(12)	124.26(19)
C(5)-C(8)-C(11)	177.8(2)
C(12)-C(9)-C(2)	119.34(18)
O(3)-C(10)-O(1)	123.33(19)
O(3)-C(10)-C(2)	124.25(19)
O(1)-C(10)-C(2)	112.42(15)
O(1)-C(11)-C(8)	110.77(15)
C(7)-C(12)-C(9)	118.25(19)

Symmetry transformations used to generate equivalent atoms:

#1 -x+1,y,-z-1/2

Table 4. Anisotropic displacement parameters ($\times 10^3$) for Compound 1. The anisotropic displacement factor exponent takes the form: $-2p^2[h^2 a^* U^{11} + \dots + 2 h k a^* b^* U^{12}]$

	U ¹¹	U ²²	U ³³	U ²³	U ¹³	U ¹²
O(1)	65(1)	52(1)	53(1)	-7(1)	4(1)	-1(1)
C(2)	37(1)	41(1)	55(1)	0(1)	11(1)	1(1)
O(3)	90(1)	47(1)	88(1)	-19(1)	-9(1)	2(1)
N(4)	86(1)	52(1)	51(1)	-6(1)	7(1)	7(1)
C(5)	71(1)	44(1)	45(1)	-1(1)	-3(1)	0(1)
C(6)	60(1)	45(1)	50(1)	1(1)	8(1)	3(1)
C(7)	69(1)	69(1)	49(1)	-4(1)	13(1)	10(1)
C(8)	70(1)	45(1)	50(1)	-2(1)	-4(1)	0(1)
C(9)	50(1)	44(1)	75(1)	4(1)	12(1)	0(1)
C(10)	40(1)	45(1)	68(1)	-7(1)	6(1)	-1(1)
C(11)	65(1)	68(1)	55(1)	-12(1)	-3(1)	-3(1)
C(12)	59(1)	63(1)	57(1)	13(1)	16(1)	7(1)

Table 5. Hydrogen coordinates ($\times 10^4$) and isotropic displacement parameters (2×10^3) for Compound 1.

	x	y	z	U(eq)
H(6)	2265	2246	1797	61
H(7)	3592	1913	5072	74
H(9)	2689	291	2968	67
H(11A)	137	1573	-1346	75
H(11B)	416	789	-968	75
H(12)	3419	732	4820	71

Molecular Structure and Crystallography Data for Co-crystal 3

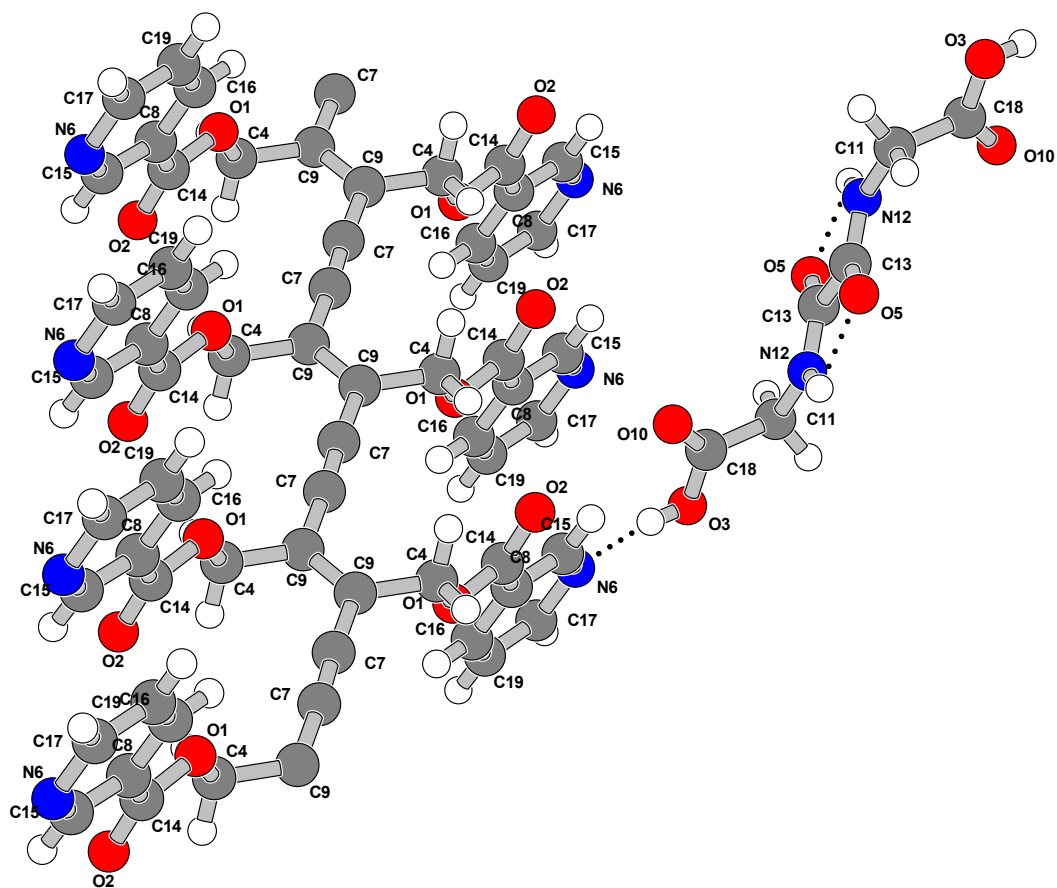


Table 1. Crystal data and structure refinement for Co-crystal 3.

Identification code	Co-crystal 3	
Empirical formula	C ₂₄ H ₂₀ N ₄ O ₁₀	
Formula weight	524.44	
Temperature	293(2) K	
Wavelength	1.54178 Å	
Crystal system	Monoclinic	
Space group	P2(1)/n	
Unit cell dimensions	a = 4.8999(5) Å	a = 90°
	b = 13.0738(13) Å	b = 91.016(11)°
	c = 18.642(3) Å	g = 90°
Volume	1194.1(2) Å ³	
Z	2	
Density (calculated)	1.459 Mg/m ³	
Absorption coefficient	0.989 mm ⁻¹	
F(000)	544	
Crystal size	6 x 0.3 x 0.3 mm ³	
Theta range for data collection	4.13 to 61.92°.	
Index ranges	-5 ≤ h ≤ 5, -14 ≤ k ≤ 14, -21 ≤ l ≤ 21	
Reflections collected	9183	
Independent reflections	1857 [R(int) = 0.0893]	
Completeness to theta = 61.92	98.9 %	
Refinement method	Full-matrix least-squares on F ²	
Data / restraints / parameters	1857 / 0 / 172	
Goodness-of-fit on F ²	1.208	
Final R indices [I > 2σ(I)]	R1 = 0.1382, wR2 = 0.4080	
R indices (all data)	R1 = 0.1735, wR2 = 0.4268	
Largest diff. peak and hole	0.446 and -0.429 e. ⁻³	

Table 2. Atomic coordinates ($\times 10^4$) and equivalent isotropic displacement parameters (2×10^3) for Co-crystal 3. $U(\text{eq})$ is defined as one third of the trace of the orthogonalized U^{ij} tensor.

	x	y	z	$U(\text{eq})$
O(1)	888(12)	3984(4)	6218(3)	52(2)
O(2)	3814(14)	4722(5)	7005(4)	65(2)
O(3)	527(17)	1930(5)	8628(5)	84(3)
C(4)	-224(17)	4997(6)	6043(5)	46(2)
O(5)	7490(14)	4107(6)	9816(6)	100(3)
N(6)	7256(19)	1912(6)	7489(5)	70(2)
C(7)	-3790(16)	4999(6)	5064(5)	42(2)
C(8)	4064(18)	2919(7)	6821(5)	53(2)
C(9)	-993(17)	5006(6)	5258(5)	46(2)
O(10)	873(18)	3597(6)	8415(5)	89(3)
C(11)	2900(20)	2895(7)	9490(6)	68(3)
N(12)	3029(16)	3938(6)	9766(5)	69(3)
C(13)	5220(17)	4437(7)	9871(5)	50(2)
C(14)	2954(18)	3952(7)	6704(5)	51(2)
C(15)	6040(20)	2794(7)	7335(6)	65(3)
C(16)	3220(30)	2082(8)	6447(6)	74(3)
C(17)	6370(20)	1081(8)	7114(6)	74(3)
C(18)	1300(20)	2856(7)	8782(6)	60(3)
C(19)	4430(30)	1145(9)	6597(7)	93(4)

Table 3. Bond lengths (Å) and angles (°) for Co-crystal 3.

O(1)-C(14)	1.348(10)
O(1)-C(4)	1.467(9)
O(2)-C(14)	1.224(10)
O(3)-C(18)	1.300(11)
C(4)-C(9)	1.503(12)
O(5)-C(13)	1.199(10)
N(6)-C(15)	1.327(12)
N(6)-C(17)	1.358(13)
C(7)-C(7)#1	1.205(15)
C(7)-C(9)	1.412(11)
C(8)-C(16)	1.358(13)
C(8)-C(15)	1.359(13)
C(8)-C(14)	1.471(12)
C(9)-C(9)#2	1.382(17)
O(10)-C(18)	1.202(11)
C(11)-N(12)	1.458(12)
C(11)-C(18)	1.524(15)
N(12)-C(13)	1.268(11)
C(13)-C(13)#3	1.565(17)
C(16)-C(19)	1.386(14)
C(17)-C(19)	1.347(15)
C(14)-O(1)-C(4)	116.7(6)
O(1)-C(4)-C(9)	108.0(7)
C(15)-N(6)-C(17)	116.5(9)
C(7)#1-C(7)-C(9)	176.4(12)
C(16)-C(8)-C(15)	118.1(9)
C(16)-C(8)-C(14)	123.8(8)
C(15)-C(8)-C(14)	118.1(8)
C(9)#2-C(9)-C(7)	120.9(10)
C(9)#2-C(9)-C(4)	120.7(9)
C(7)-C(9)-C(4)	118.4(7)
N(12)-C(11)-C(18)	110.8(8)
C(13)-N(12)-C(11)	124.5(9)

O(5)-C(13)-N(12)	125.9(9)
O(5)-C(13)-C(13)#3	119.8(9)
N(12)-C(13)-C(13)#3	114.2(9)
O(2)-C(14)-O(1)	122.1(8)
O(2)-C(14)-C(8)	124.4(8)
O(1)-C(14)-C(8)	113.5(7)
N(6)-C(15)-C(8)	124.7(10)
C(8)-C(16)-C(19)	119.0(10)
C(19)-C(17)-N(6)	122.2(10)
O(10)-C(18)-O(3)	125.3(10)
O(10)-C(18)-C(11)	123.2(9)
O(3)-C(18)-C(11)	111.5(8)
C(17)-C(19)-C(16)	119.5(10)

Symmetry transformations used to generate equivalent atoms:

#1 $-x-1, -y+1, -z+1$ #2 $-x, -y+1, -z+1$ #3 $-x+1, -y+1, -z+2$

Table 4. Anisotropic displacement parameters ($\times 10^3$) for Co-crystal 3. The anisotropic displacement factor exponent takes the form: $-2\pi^2 [h^2 a^{*2} U^{11} + \dots + 2 h k a^* b^* U^{12}]$

	U ¹¹	U ²²	U ³³	U ²³	U ¹³	U ¹²
O(1)	55(4)	32(3)	70(4)	6(3)	-17(3)	-3(3)
O(2)	78(5)	35(3)	80(5)	-3(3)	-29(4)	0(3)
O(3)	118(6)	33(4)	99(6)	-6(4)	-52(5)	1(4)
C(4)	45(5)	36(5)	58(5)	-3(4)	-6(4)	4(4)
O(5)	46(4)	68(5)	186(9)	-48(6)	-15(5)	-3(4)
N(6)	82(6)	52(5)	75(6)	11(4)	-19(4)	6(4)
C(7)	43(4)	28(4)	53(5)	-8(4)	-5(4)	3(4)
C(8)	58(5)	42(5)	57(6)	2(4)	-11(4)	4(4)
C(9)	43(5)	38(5)	56(5)	0(4)	-4(4)	0(4)
O(10)	134(7)	38(4)	95(6)	4(4)	-24(5)	-9(4)
C(11)	61(6)	45(6)	98(8)	-15(5)	-16(5)	-6(5)
N(12)	50(5)	51(5)	107(7)	-20(5)	-13(4)	2(4)
C(13)	36(5)	42(5)	73(6)	-5(4)	-13(4)	-2(4)
C(14)	49(5)	48(6)	55(5)	2(4)	-5(4)	-6(4)
C(15)	73(7)	47(6)	75(7)	5(5)	-23(5)	-1(5)
C(16)	97(8)	59(7)	65(7)	-4(5)	-28(6)	6(6)
C(17)	100(8)	44(6)	78(7)	3(5)	-16(6)	11(5)
C(18)	60(6)	39(6)	81(7)	1(5)	-6(5)	8(4)
C(19)	130(11)	44(6)	102(9)	-7(6)	-46(8)	11(6)

Table 5. Hydrogen coordinates ($\times 10^4$) and isotropic displacement parameters (2×10^3) for Co-crystal 3.

	x	y	z	U(eq)
H(3)	-351	1933	8249	126
H(4A)	1130	5521	6145	56
H(4B)	-1817	5134	6329	56
H(11A)	2031	2457	9838	82
H(11B)	4738	2642	9419	82
H(12)	1515	4236	9864	83
H(15)	6571	3367	7598	78
H(16)	1863	2136	6095	89
H(17)	7141	446	7218	89
H(19)	3896	565	6342	111

Molecular Structure and Crystallography Data for Macrocycle 11

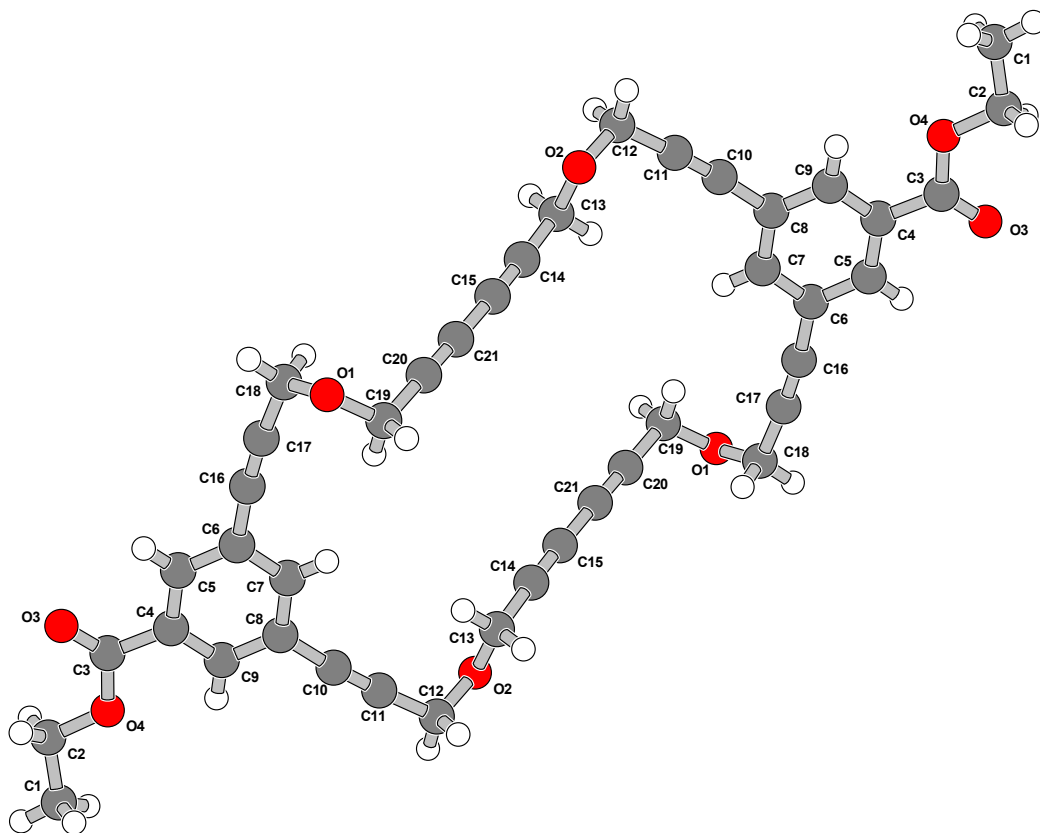


Table 1. Crystal data and structure refinement for Macrocycle 11.

Identification code	Macrocycle 11	
Empirical formula	C ₄₂ H ₃₂ O ₈	
Formula weight	664.68	
Temperature	293(2) K	
Wavelength	1.54178 Å	
Crystal system	Monoclinic	
Space group	P2(1)/n	
Unit cell dimensions	a = 4.2350(5) Å	a = 90°
	b = 44.511(5) Å	b = 98.209(11)°
	c = 9.2524(11) Å	g = 90°
Volume	1726.2(3) Å ³	
Z	2	
Density (calculated)	1.279 Mg/m ³	
Absorption coefficient	0.722 mm ⁻¹	
F(000)	696	
Crystal size	1.5 x 0.3 x 0.3 mm ³	
Theta range for data collection	3.97 to 62.25°.	
Index ranges	-4 ≤ h ≤ 4, -49 ≤ k ≤ 50, -10 ≤ l ≤ 10	
Reflections collected	19314	
Independent reflections	2682 [R(int) = 0.1149]	
Completeness to theta = 62.25	98.5 %	
Refinement method	Full-matrix least-squares on F ²	
Data / restraints / parameters	2682 / 0 / 227	
Goodness-of-fit on F ²	0.876	
Final R indices [I > 2σ(I)]	R1 = 0.0480, wR2 = 0.0904	
R indices (all data)	R1 = 0.1452, wR2 = 0.1167	
Largest diff. peak and hole	0.130 and -0.129 e. ⁻³	

Table 2. Atomic coordinates ($\times 10^4$) and equivalent isotropic displacement parameters (2×10^3) for Macrocycle 11. $U(\text{eq})$ is defined as one third of the trace of the orthogonalized U^{ij} tensor.

	x	y	z	$U(\text{eq})$
O(2)	1160(5)	1205(1)	11510(2)	71(1)
O(4)	6468(6)	2235(1)	4849(2)	84(1)
O(1)	15822(5)	357(1)	6642(3)	82(1)
C(6)	9194(7)	1213(1)	5873(3)	55(1)
C(9)	6398(7)	1746(1)	6606(3)	57(1)
C(7)	7880(7)	1235(1)	7156(3)	61(1)
O(3)	8491(7)	1978(1)	3135(3)	102(1)
C(14)	1516(9)	679(1)	11657(4)	70(1)
C(4)	7694(7)	1728(1)	5328(3)	55(1)
C(17)	11954(8)	699(1)	5426(3)	63(1)
C(3)	7633(8)	1987(1)	4304(4)	65(1)
C(18)	13547(9)	406(1)	5401(4)	76(1)
C(10)	5122(8)	1514(1)	8873(4)	60(1)
C(16)	10720(8)	936(1)	5559(3)	60(1)
C(11)	4050(8)	1505(1)	9984(4)	61(1)
C(21)	11460(8)	-181(1)	8190(3)	69(1)
C(8)	6459(7)	1500(1)	7533(3)	56(1)
C(5)	9085(7)	1461(1)	4952(3)	60(1)
C(12)	2770(8)	1481(1)	11366(3)	70(1)
C(20)	12816(9)	48(1)	8081(4)	71(1)
C(19)	14486(9)	334(1)	7949(4)	80(1)
C(13)	3326(8)	960(1)	11645(4)	81(1)
C(15)	139(8)	450(1)	11709(3)	67(1)
C(2)	6113(9)	2496(1)	3902(4)	90(1)
C(1)	5425(10)	2752(1)	4806(4)	111(1)

Table 3. Bond lengths (Å) and angles (°) for Macrocycle 11.

O(2)-C(13)	1.421(3)
O(2)-C(12)	1.421(3)
O(4)-C(3)	1.337(3)
O(4)-C(2)	1.450(3)
O(1)-C(18)	1.407(3)
O(1)-C(19)	1.410(3)
C(6)-C(7)	1.385(4)
C(6)-C(5)	1.390(4)
C(6)-C(16)	1.440(4)
C(9)-C(4)	1.375(4)
C(9)-C(8)	1.391(4)
C(7)-C(8)	1.388(4)
O(3)-C(3)	1.190(3)
C(14)-C(15)	1.180(4)
C(14)-C(13)	1.465(4)
C(4)-C(5)	1.393(4)
C(4)-C(3)	1.489(4)
C(17)-C(16)	1.191(4)
C(17)-C(18)	1.469(4)
C(10)-C(11)	1.181(4)
C(10)-C(8)	1.437(4)
C(11)-C(12)	1.463(4)
C(21)-C(20)	1.179(4)
C(21)-C(15)#1	1.387(5)
C(20)-C(19)	1.469(4)
C(15)-C(21)#1	1.387(5)
C(2)-C(1)	1.468(4)
C(13)-O(2)-C(12)	111.2(2)
C(3)-O(4)-C(2)	116.5(3)
C(18)-O(1)-C(19)	113.5(3)
C(7)-C(6)-C(5)	119.1(3)
C(7)-C(6)-C(16)	118.8(3)
C(5)-C(6)-C(16)	122.1(3)

C(4)-C(9)-C(8)	120.5(3)
C(6)-C(7)-C(8)	121.2(3)
C(15)-C(14)-C(13)	177.5(4)
C(9)-C(4)-C(5)	120.1(3)
C(9)-C(4)-C(3)	121.8(3)
C(5)-C(4)-C(3)	118.1(3)
C(16)-C(17)-C(18)	175.0(4)
O(3)-C(3)-O(4)	123.1(3)
O(3)-C(3)-C(4)	125.0(3)
O(4)-C(3)-C(4)	111.9(3)
O(1)-C(18)-C(17)	112.8(3)
C(11)-C(10)-C(8)	175.7(3)
C(17)-C(16)-C(6)	174.0(3)
C(10)-C(11)-C(12)	177.5(3)
C(20)-C(21)-C(15)#1	178.9(4)
C(7)-C(8)-C(9)	119.0(3)
C(7)-C(8)-C(10)	119.5(3)
C(9)-C(8)-C(10)	121.5(3)
C(6)-C(5)-C(4)	120.1(3)
O(2)-C(12)-C(11)	112.8(3)
C(21)-C(20)-C(19)	179.6(4)
O(1)-C(19)-C(20)	113.1(3)
O(2)-C(13)-C(14)	108.9(3)
C(14)-C(15)-C(21)#1	178.5(4)
O(4)-C(2)-C(1)	106.9(3)

Symmetry transformations used to generate equivalent atoms:

#1 -x+1,-y,-z+2

Table 4. Anisotropic displacement parameters ($\times 10^3$) for Macrocycle 11. The anisotropic displacement factor exponent takes the form: $-2p^2 [h^2 a^{*2} U^{11} + \dots + 2 h k a^* b^* U^{12}]$

	U ¹¹	U ²²	U ³³	U ²³	U ¹³	U ¹²
O(2)	77(2)	56(1)	86(2)	12(1)	31(1)	4(1)
O(4)	135(2)	52(1)	73(2)	9(1)	37(2)	15(1)
O(1)	76(2)	80(2)	89(2)	31(1)	10(2)	8(1)
C(6)	65(2)	47(2)	53(2)	0(2)	11(2)	-4(2)
C(9)	69(2)	48(2)	55(2)	-4(2)	14(2)	-2(2)
C(7)	71(2)	53(2)	58(2)	8(2)	8(2)	-6(2)
O(3)	178(3)	65(2)	75(2)	12(1)	64(2)	18(2)
C(14)	81(3)	57(2)	75(3)	13(2)	21(2)	8(2)
C(4)	74(2)	45(2)	47(2)	1(2)	13(2)	0(2)
C(17)	79(3)	54(2)	57(2)	6(2)	15(2)	-1(2)
C(3)	95(3)	51(2)	55(2)	0(2)	26(2)	1(2)
C(18)	95(3)	59(2)	78(3)	10(2)	22(2)	19(2)
C(10)	69(3)	52(2)	57(2)	1(2)	10(2)	-4(2)
C(16)	72(2)	51(2)	59(2)	2(2)	13(2)	-4(2)
C(11)	74(3)	54(2)	58(2)	6(2)	17(2)	-3(2)
C(21)	84(3)	59(2)	65(2)	12(2)	12(2)	9(2)
C(8)	67(2)	55(2)	47(2)	1(2)	11(2)	-4(2)
C(5)	71(2)	60(2)	52(2)	2(2)	17(2)	-2(2)
C(12)	91(3)	57(2)	66(2)	2(2)	28(2)	-6(2)
C(20)	84(3)	55(2)	74(3)	14(2)	12(2)	7(2)
C(19)	100(3)	68(2)	69(3)	19(2)	1(2)	-9(2)
C(13)	77(3)	64(2)	102(3)	17(2)	20(2)	10(2)
C(15)	77(3)	58(2)	66(3)	13(2)	14(2)	11(2)
C(2)	140(3)	54(2)	79(3)	14(2)	25(2)	15(2)
C(1)	162(4)	63(2)	107(3)	5(2)	16(3)	19(3)

Table 5. Hydrogen coordinates ($\times 10^4$) and isotropic displacement parameters (2×10^{-3}) for Macrocycle 11.

	x	y	z	U(eq)
H(9)	5474	1925	6853	68
H(7)	7951	1070	7777	73
H(18A)	11953	249	5338	91
H(18B)	14590	394	4535	91
H(5)	9943	1448	4083	72
H(12A)	4507	1500	12166	84
H(12B)	1300	1646	11438	84
H(19A)	12998	498	7995	96
H(19B)	16171	354	8771	96
H(13A)	4806	978	12543	97
H(13B)	4541	959	10832	97
H(2A)	4379	2465	3110	108
H(2B)	8060	2531	3489	108
H(1A)	3595	2707	5272	167
H(1B)	4999	2926	4202	167
H(1C)	7231	2789	5537	167

Molecular Structure and Crystallography Data for Compound 15

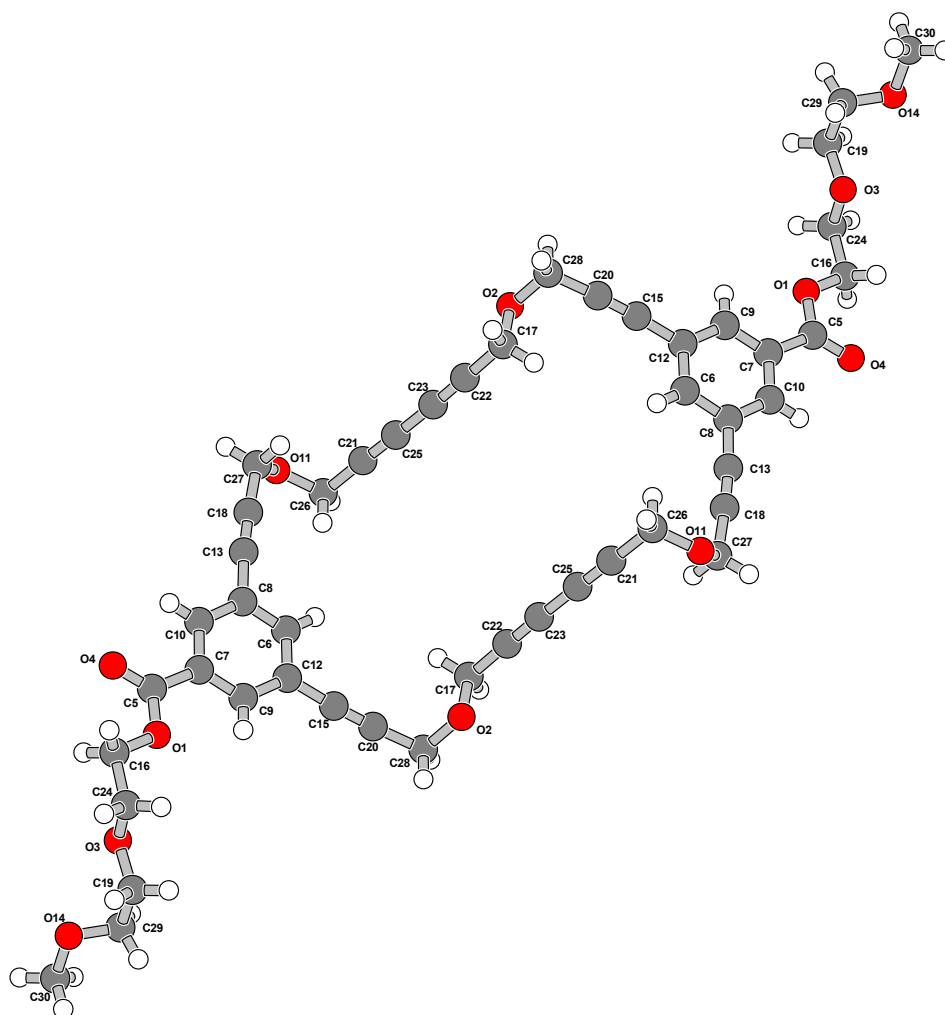


Table 1. Crystal data and structure refinement for Macrocycle 15.

Identification code	Macrocycle 15	
Empirical formula	C ₄₈ H ₄₄ O ₁₂	
Formula weight	812.83	
Temperature	293(2) K	
Wavelength	1.54178 Å	
Crystal system	Triclinic	
Space group	P-1	
Unit cell dimensions	a = 4.4321(3) Å	a = 99.344(4)°
	b = 9.2918(4) Å	b = 92.546(5)°
	c = 26.7055(14) Å	g = 96.992(5)°
Volume	1074.81(10) Å ³	
Z	1	
Density (calculated)	1.256 Mg/m ³	
Absorption coefficient	0.744 mm ⁻¹	
F(000)	428	
Crystal size	1.5 x 0.5 x 0.5 mm ³	
Theta range for data collection	4.87 to 61.71°.	
Index ranges	-5 ≤ h ≤ 4, -10 ≤ k ≤ 10, -30 ≤ l ≤ 30	
Reflections collected	23234	
Independent reflections	3308 [R(int) = 0.0665]	
Completeness to theta = 61.71	98.8 %	
Refinement method	Full-matrix least-squares on F ²	
Data / restraints / parameters	3308 / 0 / 272	
Goodness-of-fit on F ²	1.013	
Final R indices [I > 2σ(I)]	R1 = 0.0590, wR2 = 0.1428	
R indices (all data)	R1 = 0.1242, wR2 = 0.1738	
Largest diff. peak and hole	0.270 and -0.212 e. ⁻³	

Table 2. Atomic coordinates ($\times 10^4$) and equivalent isotropic displacement parameters (2×10^3) for Macrocycle 15. $U(\text{eq})$ is defined as one third of the trace of the orthogonalized U^{ij} tensor.

	x	y	z	$U(\text{eq})$
O(1)	3420(5)	3900(2)	1373(1)	73(1)
O(2)	1696(6)	2252(3)	6984(1)	82(1)
O(3)	3694(6)	3039(3)	259(1)	81(1)
O(4)	819(7)	5592(3)	1777(1)	89(1)
C(5)	1868(8)	4449(4)	1760(1)	62(1)
C(6)	1286(8)	1930(3)	2953(1)	61(1)
C(7)	1654(7)	3532(3)	2165(1)	55(1)
C(8)	12(7)	3233(3)	2996(1)	58(1)
C(9)	2941(7)	2240(3)	2129(1)	59(1)
C(10)	194(7)	4029(3)	2597(1)	60(1)
O(11)	-6215(6)	3126(3)	4400(1)	94(1)
C(12)	2774(7)	1420(3)	2523(1)	58(1)
C(13)	-1480(8)	3713(3)	3452(1)	63(1)
O(14)	1762(8)	2018(3)	-813(1)	111(1)
C(15)	4162(8)	85(4)	2501(1)	65(1)
C(16)	4171(9)	4863(4)	1006(1)	77(1)
C(17)	3657(9)	2264(5)	6574(1)	88(1)
C(18)	-2634(8)	4018(4)	3838(1)	68(1)
C(19)	5223(10)	2184(5)	-108(2)	94(1)
C(20)	5258(8)	-1002(4)	2509(1)	67(1)
C(21)	-3058(10)	1902(4)	4902(2)	80(1)
C(22)	1749(10)	2115(4)	6108(2)	80(1)
C(23)	251(10)	2022(4)	5723(2)	79(1)
C(24)	5785(9)	4052(5)	598(1)	83(1)
C(25)	-1525(10)	1946(4)	5283(2)	77(1)
C(26)	-4971(10)	1820(4)	4432(1)	93(1)
C(27)	-4053(10)	4304(4)	4322(1)	84(1)
C(28)	3341(10)	2334(4)	7450(1)	83(1)
C(29)	2937(12)	1167(5)	-493(2)	106(2)
C(30)	128(14)	1132(6)	-1254(2)	147(2)

Table 3. Bond lengths (Å) and angles (°) for Macrocycle 15.

O(1)-C(5)	1.334(4)
O(1)-C(16)	1.454(4)
O(2)-C(28)	1.401(4)
O(2)-C(17)	1.428(4)
O(3)-C(19)	1.410(4)
O(3)-C(24)	1.415(4)
O(4)-C(5)	1.206(4)
C(5)-C(7)	1.480(4)
C(6)-C(8)	1.387(4)
C(6)-C(12)	1.393(4)
C(7)-C(9)	1.382(4)
C(7)-C(10)	1.389(4)
C(8)-C(10)	1.392(4)
C(8)-C(13)	1.444(5)
C(9)-C(12)	1.396(4)
O(11)-C(26)	1.406(4)
O(11)-C(27)	1.413(4)
C(12)-C(15)	1.444(5)
C(13)-C(18)	1.181(4)
O(14)-C(29)	1.381(5)
O(14)-C(30)	1.433(5)
C(15)-C(20)	1.176(4)
C(16)-C(24)	1.483(5)
C(17)-C(22)	1.452(6)
C(18)-C(27)	1.462(5)
C(19)-C(29)	1.527(6)
C(20)-C(28)#1	1.468(5)
C(21)-C(25)	1.191(5)
C(21)-C(26)	1.469(6)
C(22)-C(23)	1.183(5)
C(23)-C(25)	1.374(6)
C(28)-C(20)#1	1.468(5)
C(5)-O(1)-C(16)	115.9(3)

C(28)-O(2)-C(17)	111.7(3)
C(19)-O(3)-C(24)	111.0(3)
O(4)-C(5)-O(1)	122.6(3)
O(4)-C(5)-C(7)	124.4(3)
O(1)-C(5)-C(7)	113.1(3)
C(8)-C(6)-C(12)	121.4(3)
C(9)-C(7)-C(10)	120.0(3)
C(9)-C(7)-C(5)	121.9(3)
C(10)-C(7)-C(5)	118.1(3)
C(6)-C(8)-C(10)	118.9(3)
C(6)-C(8)-C(13)	118.9(3)
C(10)-C(8)-C(13)	122.1(3)
C(7)-C(9)-C(12)	120.6(3)
C(7)-C(10)-C(8)	120.5(3)
C(26)-O(11)-C(27)	113.9(3)
C(6)-C(12)-C(9)	118.7(3)
C(6)-C(12)-C(15)	119.6(3)
C(9)-C(12)-C(15)	121.7(3)
C(18)-C(13)-C(8)	175.0(3)
C(29)-O(14)-C(30)	111.7(4)
C(20)-C(15)-C(12)	176.5(3)
O(1)-C(16)-C(24)	108.1(3)
O(2)-C(17)-C(22)	107.6(3)
C(13)-C(18)-C(27)	176.6(4)
O(3)-C(19)-C(29)	110.5(3)
C(15)-C(20)-C(28)#1	176.8(3)
C(25)-C(21)-C(26)	178.9(4)
C(23)-C(22)-C(17)	178.2(4)
C(22)-C(23)-C(25)	178.5(4)
O(3)-C(24)-C(16)	110.6(3)
C(21)-C(25)-C(23)	179.0(4)
O(11)-C(26)-C(21)	113.2(3)
O(11)-C(27)-C(18)	113.1(3)
O(2)-C(28)-C(20)#1	113.1(3)
O(14)-C(29)-C(19)	107.5(4)

Symmetry transformations used to generate equivalent atoms:

#1 $-x+1,-y,-z+1$

Table 4. Anisotropic displacement parameters ($\times 10^3$) for Macrocycle 15. The anisotropic displacement factor exponent takes the form: $-2p^2 [h^2 a^* U^{11} + \dots + 2 h k a^* b^* U^{12}]$

	U ¹¹	U ²²	U ³³	U ²³	U ¹³	U ¹²
O(1)	92(2)	74(2)	60(1)	26(1)	12(1)	15(1)
O(2)	89(2)	100(2)	67(2)	22(1)	8(1)	36(1)
O(3)	70(2)	111(2)	65(2)	19(1)	13(1)	17(2)
O(4)	129(2)	78(2)	69(2)	26(1)	10(2)	38(2)
C(5)	74(2)	60(2)	52(2)	9(2)	-5(2)	7(2)
C(6)	73(2)	60(2)	53(2)	16(2)	1(2)	6(2)
C(7)	64(2)	51(2)	51(2)	11(1)	-2(2)	4(2)
C(8)	60(2)	61(2)	52(2)	12(2)	-2(2)	6(2)
C(9)	65(2)	57(2)	54(2)	7(2)	0(2)	4(2)
C(10)	64(2)	58(2)	57(2)	8(2)	-4(2)	9(2)
O(11)	85(2)	116(2)	95(2)	50(2)	21(2)	21(2)
C(12)	65(2)	50(2)	58(2)	11(2)	-4(2)	2(2)
C(13)	72(2)	62(2)	59(2)	16(2)	3(2)	11(2)
O(14)	151(3)	96(2)	84(2)	16(2)	12(2)	3(2)
C(15)	77(3)	59(2)	60(2)	14(2)	3(2)	7(2)
C(16)	93(3)	81(2)	64(2)	33(2)	6(2)	5(2)
C(17)	89(3)	105(3)	77(3)	25(2)	12(2)	28(2)
C(18)	76(3)	72(2)	60(2)	18(2)	6(2)	15(2)
C(19)	90(3)	119(3)	85(3)	29(3)	20(3)	39(3)
C(20)	83(3)	61(2)	59(2)	11(2)	4(2)	14(2)
C(21)	95(3)	80(3)	72(3)	26(2)	21(2)	12(2)
C(22)	94(3)	85(3)	70(2)	27(2)	19(2)	26(2)
C(23)	95(3)	77(3)	72(3)	26(2)	22(2)	18(2)
C(24)	71(3)	113(3)	71(2)	40(2)	5(2)	10(2)
C(25)	99(3)	70(2)	69(3)	24(2)	19(2)	15(2)
C(26)	113(4)	87(3)	80(3)	29(2)	3(2)	-1(3)
C(27)	111(3)	82(3)	67(2)	22(2)	25(2)	25(2)
C(28)	108(3)	78(2)	67(2)	7(2)	2(2)	36(2)
C(29)	140(4)	108(3)	85(3)	29(3)	33(3)	53(3)
C(30)	172(5)	164(5)	84(3)	-16(3)	11(3)	-13(4)

Table 5. Hydrogen coordinates ($\times 10^4$) and isotropic displacement parameters (2×10^{-3}) for Macrocycle 15.

	x	y	z	U(eq)
H(6)	1145	1386	3216	74
H(9)	3926	1915	1840	71
H(10)	-668	4899	2620	72
H(16A)	5462	5747	1171	93
H(16B)	2327	5148	863	93
H(17A)	4863	1455	6558	105
H(17B)	5031	3179	6624	105
H(19A)	6495	1601	59	113
H(19B)	6529	2826	-284	113
H(24A)	6877	4744	413	99
H(24B)	7259	3529	748	99
H(26A)	-3758	1598	4142	112
H(26B)	-6618	1019	4412	112
H(27A)	-2479	4494	4598	101
H(27B)	-5047	5182	4333	101
H(28A)	1985	2501	7723	100
H(28B)	4926	3170	7494	100
H(29A)	3938	407	-686	127
H(29B)	1316	699	-319	127
H(30A)	1548	751	-1486	220
H(30B)	-1111	1720	-1418	220
H(30C)	-1148	330	-1154	220

Molecular Structure and Crystallography Data for Compound 21

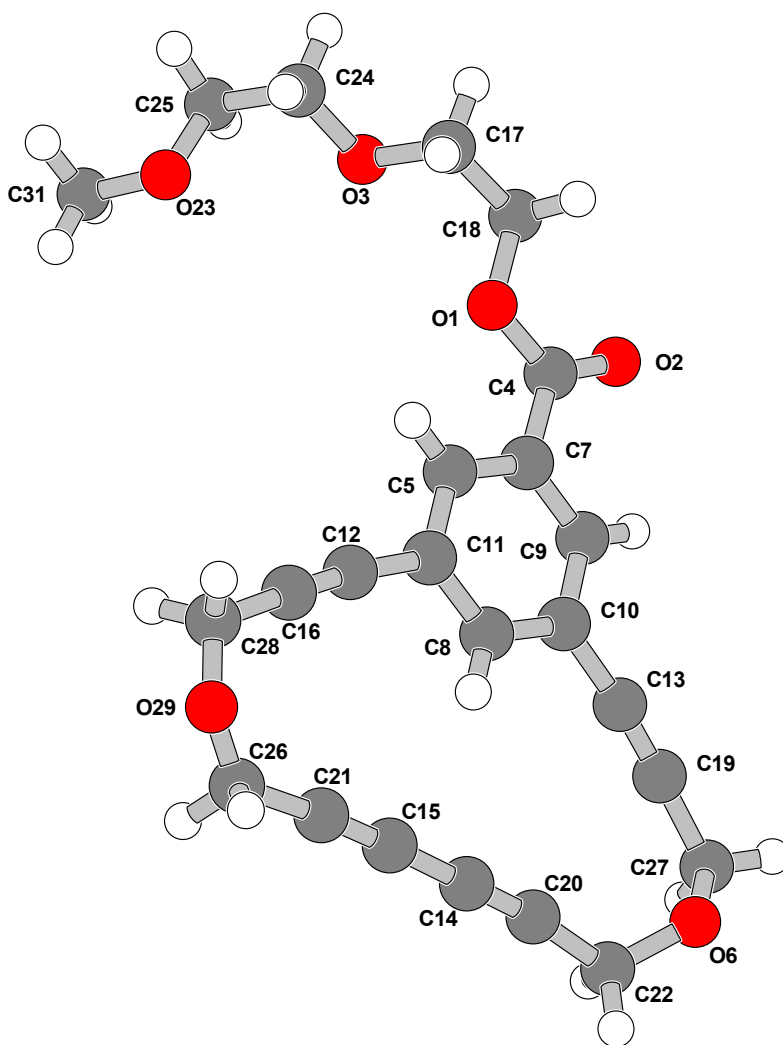


Table 1. Crystal data and structure refinement for Macrocycle 21.

Identification code	Macrocycle 21	
Empirical formula	C ₂₄ H ₂₂ O ₆	
Formula weight	406.42	
Temperature	293(2) K	
Wavelength	1.54178 Å	
Crystal system	Triclinic	
Space group	P-1	
Unit cell dimensions	a = 8.8940(7) Å	a = 114.804(7)°
	b = 10.9009(8) Å	b = 90.441(6)°
	c = 11.8202(9) Å	g = 93.051(6)°
Volume	1038.23(14) Å ³	
Z	2	
Density (calculated)	1.300 Mg/m ³	
Absorption coefficient	0.770 mm ⁻¹	
F(000)	428	
Crystal size	2 x 1 x 0.5 mm ³	
Theta range for data collection	4.12 to 73.55°.	
Index ranges	-9<=h<=10, -13<=k<=13, -14<=l<=14	
Reflections collected	15452	
Independent reflections	4086 [R(int) = 0.0457]	
Completeness to theta = 73.55	97.6 %	
Refinement method	Full-matrix least-squares on F ²	
Data / restraints / parameters	4086 / 0 / 272	
Goodness-of-fit on F ²	1.079	
Final R indices [I>2sigma(I)]	R1 = 0.0924, wR2 = 0.2630	
R indices (all data)	R1 = 0.1390, wR2 = 0.3049	
Largest diff. peak and hole	0.836 and -0.807 e. ⁻³	

Table 2. Atomic coordinates ($\times 10^4$) and equivalent isotropic displacement parameters (2×10^3) for Macrocycle 21. $U(\text{eq})$ is defined as one third of the trace of the orthogonalized U^{ij} tensor.

	x	y	z	$U(\text{eq})$
O(1)	4788(3)	12550(3)	7370(2)	58(1)
O(2)	3845(4)	13800(3)	6471(3)	77(1)
O(3)	5846(3)	13110(3)	9886(3)	61(1)
C(4)	3914(5)	12716(4)	6523(4)	56(1)
C(5)	3245(5)	10231(4)	5760(4)	54(1)
O(6)	-1341(4)	8468(3)	38(3)	73(1)
C(7)	3078(5)	11454(4)	5666(4)	52(1)
C(8)	1524(5)	9107(4)	4004(4)	56(1)
C(9)	2141(5)	11498(4)	4746(4)	56(1)
C(10)	1357(5)	10330(4)	3905(4)	55(1)
C(11)	2455(5)	9060(4)	4928(4)	54(1)
C(12)	2585(5)	7764(4)	4970(4)	62(1)
C(13)	388(5)	10300(4)	2910(4)	59(1)
C(14)	-820(5)	6301(5)	1530(4)	67(1)
C(15)	-169(5)	5587(5)	2111(5)	68(1)
C(16)	2638(6)	6647(4)	4880(4)	66(1)
C(17)	6709(5)	13323(5)	8968(4)	67(1)
C(18)	5708(6)	13731(4)	8186(4)	68(1)
C(19)	-425(5)	10114(5)	2048(5)	65(1)
C(20)	-1379(5)	6906(5)	1011(5)	71(1)
C(21)	356(6)	4938(5)	2597(5)	75(1)
C(22)	-2199(6)	7492(6)	306(6)	87(2)
O(23)	5109(6)	11417(5)	11151(4)	117(2)
C(24)	6738(6)	12867(7)	10742(6)	89(2)
C(25)	5781(9)	12720(5)	11736(5)	110(3)
C(26)	970(8)	4020(6)	3075(6)	100(2)
C(27)	-1424(6)	9808(5)	949(5)	77(1)
C(28)	2701(7)	5231(4)	4721(5)	86(2)
O(29)	1905(11)	4336(4)	3845(8)	275(6)
C(31)	4199(8)	11129(7)	11962(7)	108(2)

Table 3. Bond lengths (Å) and angles (°) for Macrocycle 21.

O(1)-C(4)	1.340(5)
O(1)-C(18)	1.446(5)
O(2)-C(4)	1.213(4)
O(3)-C(24)	1.399(5)
O(3)-C(17)	1.423(5)
C(4)-C(7)	1.477(6)
C(5)-C(11)	1.390(6)
C(5)-C(7)	1.398(5)
O(6)-C(27)	1.411(6)
O(6)-C(22)	1.420(6)
C(7)-C(9)	1.383(6)
C(8)-C(11)	1.385(6)
C(8)-C(10)	1.401(5)
C(9)-C(10)	1.389(5)
C(10)-C(13)	1.441(6)
C(11)-C(12)	1.444(5)
C(12)-C(16)	1.180(6)
C(13)-C(19)	1.184(6)
C(14)-C(20)	1.195(6)
C(14)-C(15)	1.379(7)
C(15)-C(21)	1.192(6)
C(16)-C(28)	1.480(6)
C(17)-C(18)	1.489(6)
C(19)-C(27)	1.475(7)
C(20)-C(22)	1.456(7)
C(21)-C(26)	1.465(7)
O(23)-C(31)	1.382(7)
O(23)-C(25)	1.390(7)
C(24)-C(25)	1.514(9)
C(26)-O(29)	1.155(7)
C(28)-O(29)	1.262(7)
C(4)-O(1)-C(18)	115.8(3)
C(24)-O(3)-C(17)	112.6(4)

O(2)-C(4)-O(1)	122.5(4)
O(2)-C(4)-C(7)	124.3(4)
O(1)-C(4)-C(7)	113.2(3)
C(11)-C(5)-C(7)	119.6(4)
C(27)-O(6)-C(22)	113.8(4)
C(9)-C(7)-C(5)	120.3(4)
C(9)-C(7)-C(4)	118.5(3)
C(5)-C(7)-C(4)	121.2(4)
C(11)-C(8)-C(10)	120.7(4)
C(7)-C(9)-C(10)	120.4(4)
C(9)-C(10)-C(8)	119.1(4)
C(9)-C(10)-C(13)	123.2(4)
C(8)-C(10)-C(13)	117.7(4)
C(8)-C(11)-C(5)	119.9(3)
C(8)-C(11)-C(12)	117.8(4)
C(5)-C(11)-C(12)	122.3(4)
C(16)-C(12)-C(11)	173.2(5)
C(19)-C(13)-C(10)	172.2(4)
C(20)-C(14)-C(15)	179.1(6)
C(21)-C(15)-C(14)	177.9(5)
C(12)-C(16)-C(28)	178.1(5)
O(3)-C(17)-C(18)	109.5(4)
O(1)-C(18)-C(17)	108.2(3)
C(13)-C(19)-C(27)	177.1(5)
C(14)-C(20)-C(22)	172.6(5)
C(15)-C(21)-C(26)	174.2(6)
O(6)-C(22)-C(20)	114.7(4)
C(31)-O(23)-C(25)	110.6(5)
O(3)-C(24)-C(25)	110.7(5)
O(23)-C(25)-C(24)	104.0(5)
O(29)-C(26)-C(21)	124.2(5)
O(6)-C(27)-C(19)	112.6(4)
O(29)-C(28)-C(16)	117.3(4)
C(26)-O(29)-C(28)	151.3(5)

Symmetry transformations used to generate equivalent atoms:

Table 4. Anisotropic displacement parameters ($\times 10^3$) for Macrocycle 21. The anisotropic displacement factor exponent takes the form: $-2p^2 [h^2 a^{*2} U^{11} + \dots + 2 h k a^* b^* U^{12}]$

	U ¹¹	U ²²	U ³³	U ²³	U ¹³	U ¹²
O(1)	73(2)	44(1)	55(2)	21(1)	-7(1)	-6(1)
O(2)	109(3)	45(2)	81(2)	33(2)	-20(2)	-7(2)
O(3)	60(2)	66(2)	63(2)	32(1)	-7(1)	0(1)
C(4)	73(3)	44(2)	51(2)	22(2)	1(2)	1(2)
C(5)	70(3)	44(2)	49(2)	20(2)	-1(2)	2(2)
O(6)	76(2)	81(2)	70(2)	41(2)	-13(2)	-6(2)
C(7)	64(2)	44(2)	49(2)	22(2)	4(2)	1(2)
C(8)	67(3)	44(2)	52(2)	15(2)	-1(2)	0(2)
C(9)	67(3)	46(2)	58(2)	26(2)	0(2)	0(2)
C(10)	61(3)	51(2)	55(2)	25(2)	4(2)	4(2)
C(11)	69(3)	42(2)	54(2)	21(2)	7(2)	4(2)
C(12)	81(3)	47(2)	55(2)	21(2)	-6(2)	-4(2)
C(13)	67(3)	53(2)	61(3)	27(2)	2(2)	5(2)
C(14)	65(3)	63(3)	71(3)	29(2)	-9(2)	-10(2)
C(15)	67(3)	63(3)	74(3)	31(2)	-11(2)	-9(2)
C(16)	89(3)	49(2)	62(3)	25(2)	-11(2)	3(2)
C(17)	61(3)	66(3)	63(3)	20(2)	-4(2)	-11(2)
C(18)	94(3)	49(2)	56(2)	20(2)	-11(2)	-20(2)
C(19)	61(3)	63(3)	79(3)	37(2)	-1(2)	6(2)
C(20)	68(3)	72(3)	78(3)	37(3)	-14(2)	-10(2)
C(21)	81(3)	65(3)	81(3)	34(3)	-16(3)	-9(2)
C(22)	80(4)	85(3)	105(4)	51(3)	-36(3)	-20(3)
O(23)	144(4)	102(3)	102(3)	42(3)	4(3)	-15(3)
C(24)	74(3)	112(4)	102(4)	68(4)	-29(3)	-11(3)
C(25)	216(8)	53(3)	62(3)	25(2)	-42(4)	8(4)
C(26)	143(6)	72(3)	90(4)	43(3)	-39(4)	-13(3)
C(27)	79(3)	75(3)	88(3)	44(3)	-19(3)	5(3)
C(28)	122(5)	48(2)	91(4)	35(2)	-36(3)	0(3)
O(29)	408(12)	50(2)	343(10)	71(4)	-303(10)	-49(4)
C(31)	116(5)	118(5)	117(5)	75(4)	11(4)	1(4)

Table 5. Hydrogen coordinates ($\times 10^4$) and isotropic displacement parameters (2×10^{-3}) for Macrocycle 21.

	x	y	z	U(eq)
H(5)	3882	10202	6375	65
H(8)	1005	8320	3444	68
H(9)	2036	12315	4690	67
H(17A)	7176	12497	8447	80
H(17B)	7500	14026	9371	80
H(18A)	5074	14430	8713	81
H(18B)	6309	14087	7698	81
H(22A)	-2573	6768	-474	105
H(22B)	-3065	7914	774	105
H(24A)	7489	13612	11129	107
H(24B)	7259	12047	10308	107
H(25A)	6398	12822	12454	132
H(25B)	5028	13388	12005	132
H(26A)	121	3651	3367	120
H(26B)	1335	3271	2359	120
H(27A)	-2454	9950	1214	93
H(27B)	-1150	10431	581	93
H(28A)	3742	4993	4597	103
H(28B)	2406	5194	5495	103
H(31A)	4809	11114	12630	163
H(31B)	3672	10262	11523	163
H(31C)	3485	11813	12298	163

Molecular Structure and Crystallography Data for Compound 37

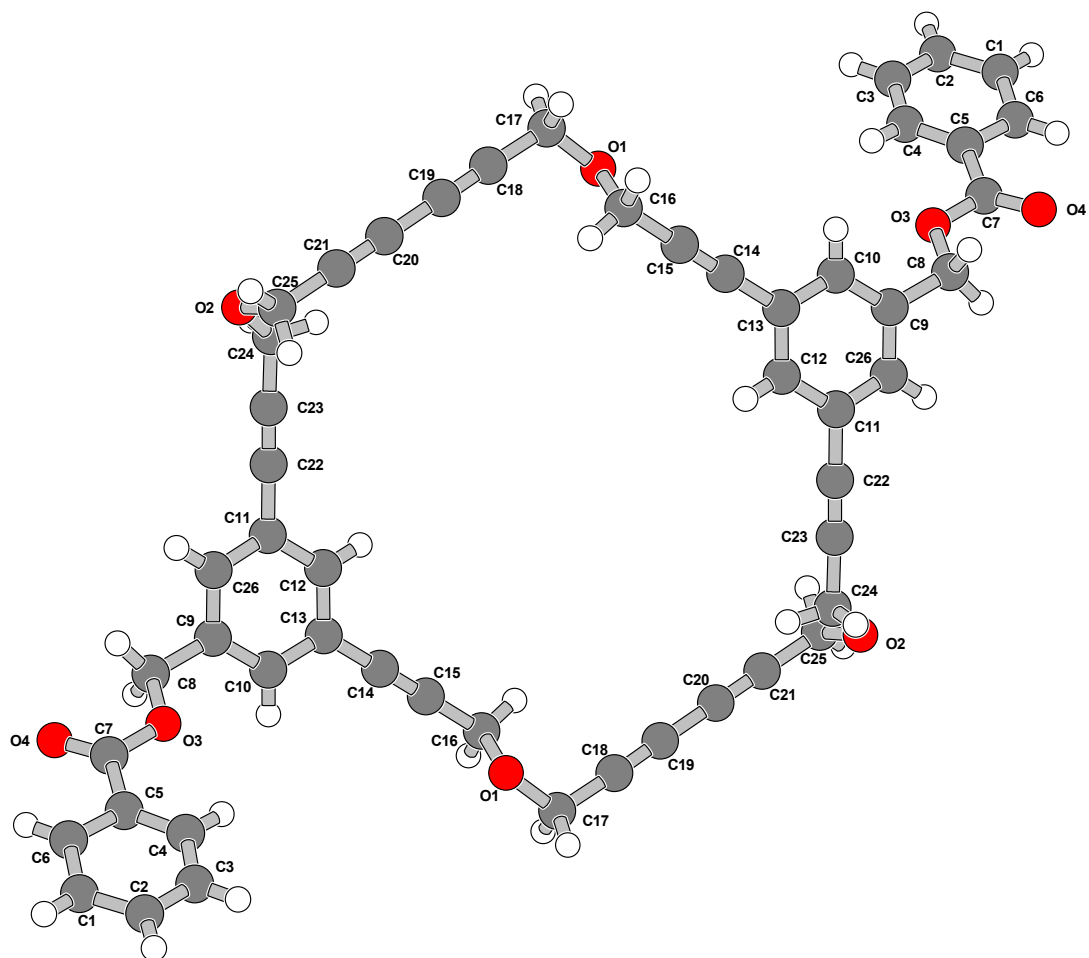


Table 1. Crystal data and structure refinement for Macrocycle 37.

Identification code	Macrocycle 37	
Empirical formula	C ₅₂ H ₃₆ O ₈	
Formula weight	788.81	
Temperature	293(2) K	
Wavelength	1.54178 Å	
Crystal system	Monoclinic	
Space group	P2(1)/c	
Unit cell dimensions	a = 10.6095(14) Å	a = 90°
	b = 21.154(2) Å	b = 95.660(12)°
	c = 9.1371(11) Å	g = 90°
Volume	2040.6(4) Å ³	
Z	2	
Density (calculated)	1.284 Mg/m ³	
Absorption coefficient	0.699 mm ⁻¹	
F(000)	824	
Crystal size	1.5 x 1 x 1 mm ³	
Theta range for data collection	4.18 to 74.39°.	
Index ranges	-12 ≤ h ≤ 13, -26 ≤ k ≤ 26, -11 ≤ l ≤ 11	
Reflections collected	21802	
Independent reflections	4075 [R(int) = 0.0866]	
Completeness to theta = 74.39	97.5 %	
Refinement method	Full-matrix least-squares on F ²	
Data / restraints / parameters	4075 / 0 / 271	
Goodness-of-fit on F ²	1.057	
Final R indices [I > 2σ(I)]	R1 = 0.1003, wR2 = 0.2998	
R indices (all data)	R1 = 0.1734, wR2 = 0.3567	
Largest diff. peak and hole	0.770 and -0.297 e. ⁻³	

Table 2. Atomic coordinates ($\times 10^4$) and equivalent isotropic displacement parameters (2×10^3) for Macrocycle 37. $U(\text{eq})$ is defined as one third of the trace of the orthogonalized U^{ij} tensor.

	x	y	z	$U(\text{eq})$
O(1)	5390(4)	1240(2)	2888(4)	92(1)
O(2)	13570(4)	2443(2)	-3513(5)	94(1)
C(11)	9592(5)	2764(2)	-1379(5)	70(1)
C(13)	7833(5)	2521(2)	-5(5)	69(1)
O(3)	8437(4)	4392(2)	1742(5)	97(1)
C(12)	8766(5)	2328(2)	-872(6)	74(1)
C(10)	7728(5)	3155(2)	335(6)	77(1)
C(9)	8551(5)	3595(2)	-148(6)	73(1)
C(21)	5386(6)	-1536(3)	2416(6)	83(2)
C(26)	9488(5)	3389(2)	-997(6)	75(1)
C(20)	5143(5)	-997(3)	2611(6)	86(2)
C(24)	12363(6)	2152(3)	-3861(7)	93(2)
C(23)	11401(5)	2383(3)	-2953(6)	80(2)
C(22)	10591(6)	2550(2)	-2252(6)	76(1)
C(16)	5279(6)	1252(3)	1315(6)	86(2)
O(4)	8483(5)	5425(2)	1234(6)	118(2)
C(8)	8415(6)	4289(2)	145(6)	89(2)
C(14)	6966(6)	2071(2)	488(6)	79(1)
C(15)	6232(5)	1705(2)	878(6)	82(2)
C(18)	4658(6)	182(3)	3104(7)	86(2)
C(17)	4445(6)	845(3)	3397(7)	93(2)
C(19)	4873(6)	-353(3)	2862(7)	87(2)
C(7)	8442(6)	5001(3)	2135(8)	98(2)
C(5)	8369(6)	5095(3)	3770(7)	91(2)
C(25)	14268(6)	2195(3)	-2242(6)	87(2)
C(6)	8546(6)	5715(3)	4275(9)	114(2)
C(4)	8111(7)	4626(3)	4689(9)	107(2)
C(2)	8241(6)	5327(3)	6704(8)	101(2)
C(3)	8049(7)	4752(4)	6127(9)	112(2)
C(1)	8490(7)	5835(3)	5826(9)	114(2)

Table 3. Bond lengths (Å) and angles (°) for Macrocycle 37.

O(1)-C(17)	1.418(6)
O(1)-C(16)	1.431(6)
O(2)-C(25)	1.416(7)
O(2)-C(24)	1.429(7)
C(11)-C(26)	1.374(7)
C(11)-C(12)	1.383(7)
C(11)-C(22)	1.459(7)
C(13)-C(10)	1.382(6)
C(13)-C(12)	1.388(7)
C(13)-C(14)	1.427(7)
O(3)-C(7)	1.338(7)
O(3)-C(8)	1.473(7)
C(10)-C(9)	1.378(7)
C(9)-C(26)	1.390(7)
C(9)-C(8)	1.502(7)
C(21)-C(20)	1.187(8)
C(21)-C(25)#1	1.453(8)
C(20)-C(19)	1.414(9)
C(24)-C(23)	1.462(8)
C(23)-C(22)	1.175(7)
C(16)-C(15)	1.476(7)
O(4)-C(7)	1.221(7)
C(14)-C(15)	1.178(7)
C(18)-C(19)	1.182(8)
C(18)-C(17)	1.450(8)
C(7)-C(5)	1.516(10)
C(5)-C(4)	1.345(9)
C(5)-C(6)	1.397(8)
C(25)-C(21)#1	1.453(8)
C(6)-C(1)	1.446(10)
C(4)-C(3)	1.349(10)
C(2)-C(3)	1.334(9)
C(2)-C(1)	1.382(9)

C(17)-O(1)-C(16)	110.5(4)
C(25)-O(2)-C(24)	114.0(4)
C(26)-C(11)-C(12)	119.0(5)
C(26)-C(11)-C(22)	121.2(5)
C(12)-C(11)-C(22)	119.7(5)
C(10)-C(13)-C(12)	119.4(4)
C(10)-C(13)-C(14)	120.5(5)
C(12)-C(13)-C(14)	120.1(4)
C(7)-O(3)-C(8)	114.1(5)
C(11)-C(12)-C(13)	120.5(5)
C(9)-C(10)-C(13)	121.0(5)
C(10)-C(9)-C(26)	118.5(5)
C(10)-C(9)-C(8)	121.9(5)
C(26)-C(9)-C(8)	119.5(4)
C(20)-C(21)-C(25)#1	177.1(7)
C(11)-C(26)-C(9)	121.6(5)
C(21)-C(20)-C(19)	179.0(7)
O(2)-C(24)-C(23)	113.0(5)
C(22)-C(23)-C(24)	177.1(7)
C(23)-C(22)-C(11)	179.3(6)
O(1)-C(16)-C(15)	107.1(5)
O(3)-C(8)-C(9)	109.2(4)
C(15)-C(14)-C(13)	178.7(7)
C(14)-C(15)-C(16)	177.8(7)
C(19)-C(18)-C(17)	177.8(6)
O(1)-C(17)-C(18)	112.4(5)
C(18)-C(19)-C(20)	178.5(7)
O(4)-C(7)-O(3)	121.7(6)
O(4)-C(7)-C(5)	125.3(6)
O(3)-C(7)-C(5)	113.0(5)
C(4)-C(5)-C(6)	121.0(7)
C(4)-C(5)-C(7)	123.5(6)
C(6)-C(5)-C(7)	115.5(6)
O(2)-C(25)-C(21)#1	112.6(5)
C(5)-C(6)-C(1)	118.2(6)
C(5)-C(4)-C(3)	119.6(7)

C(3)-C(2)-C(1)	120.7(7)
C(2)-C(3)-C(4)	123.1(8)
C(2)-C(1)-C(6)	117.4(6)

Symmetry transformations used to generate equivalent atoms:

#1 $-x+2, -y, -z$

Table 4. Anisotropic displacement parameters ($\times 10^3$) for Macrocycle 37. The anisotropic displacement factor exponent takes the form: $-2p^2 [h^2 a^{*2} U^{11} + \dots + 2 h k a^* b^* U^{12}]$

	U ¹¹	U ²²	U ³³	U ²³	U ¹³	U ¹²
O(1)	107(3)	79(2)	91(3)	-1(2)	20(2)	-17(2)
O(2)	76(3)	105(3)	103(3)	22(2)	25(2)	-1(2)
C(11)	64(3)	75(3)	71(3)	-2(2)	13(2)	0(2)
C(13)	65(3)	67(3)	76(3)	5(2)	12(2)	-1(2)
O(3)	109(3)	79(3)	107(3)	-10(2)	29(2)	-2(2)
C(12)	73(3)	67(3)	84(3)	-3(2)	13(3)	-2(2)
C(10)	68(3)	79(3)	85(3)	1(3)	23(3)	6(3)
C(9)	77(3)	64(3)	82(3)	1(2)	22(3)	0(2)
C(21)	86(4)	76(4)	90(4)	-3(3)	28(3)	-3(3)
C(26)	69(3)	72(3)	85(3)	5(2)	19(3)	-6(2)
C(20)	78(4)	101(5)	80(4)	4(3)	19(3)	-8(3)
C(24)	75(4)	122(5)	83(4)	-1(3)	20(3)	2(3)
C(23)	76(4)	92(4)	76(3)	4(3)	22(3)	1(3)
C(22)	80(4)	79(3)	71(3)	5(2)	16(3)	-4(3)
C(16)	90(4)	80(3)	92(4)	-2(3)	24(3)	-9(3)
O(4)	129(4)	84(3)	150(4)	3(3)	60(3)	-8(3)
C(8)	104(4)	71(3)	97(4)	3(3)	35(3)	-2(3)
C(14)	82(4)	66(3)	92(4)	-4(3)	24(3)	-6(3)
C(15)	84(4)	71(3)	96(4)	-3(3)	25(3)	-2(3)
C(18)	88(4)	80(4)	91(4)	2(3)	17(3)	-5(3)
C(17)	105(5)	82(4)	96(4)	9(3)	30(3)	-7(3)
C(19)	85(4)	88(4)	90(4)	2(3)	21(3)	-6(3)
C(7)	94(5)	73(4)	134(6)	3(4)	41(4)	-2(3)
C(5)	75(4)	82(4)	118(5)	-19(3)	24(3)	1(3)
C(25)	87(4)	90(4)	84(4)	0(3)	15(3)	-3(3)
C(6)	95(5)	102(5)	153(7)	3(4)	50(4)	-6(4)
C(4)	109(5)	83(4)	131(6)	0(4)	26(4)	-6(4)
C(2)	107(5)	94(4)	106(5)	-9(4)	31(4)	-1(4)
C(3)	107(5)	111(5)	117(6)	-18(4)	14(4)	5(4)
C(1)	109(5)	95(5)	142(6)	-35(4)	37(5)	-3(4)

Table 5. Hydrogen coordinates ($\times 10^4$) and isotropic displacement parameters (2×10^{-3}) for Macrocycle 37.

	x	y	z	U(eq)
H(12)	8835	1903	-1112	89
H(10)	7093	3286	899	92
H(26)	10058	3680	-1313	89
H(24A)	12452	1698	-3729	111
H(24B)	12081	2230	-4887	111
H(16A)	4435	1385	935	104
H(16B)	5435	835	931	104
H(8A)	9104	4519	-233	107
H(8B)	7624	4443	-349	107
H(17A)	3624	969	2922	112
H(17B)	4431	906	4448	112
H(25A)	13767	2232	-1414	104
H(25B)	15032	2443	-2023	104
H(6)	8695	6041	3633	137
H(4)	7977	4216	4334	128
H(2)	8207	5387	7707	121
H(3)	7864	4423	6745	134
H(1)	8617	6239	6217	137

Molecular Structure and Crystallography Data for Compound 46

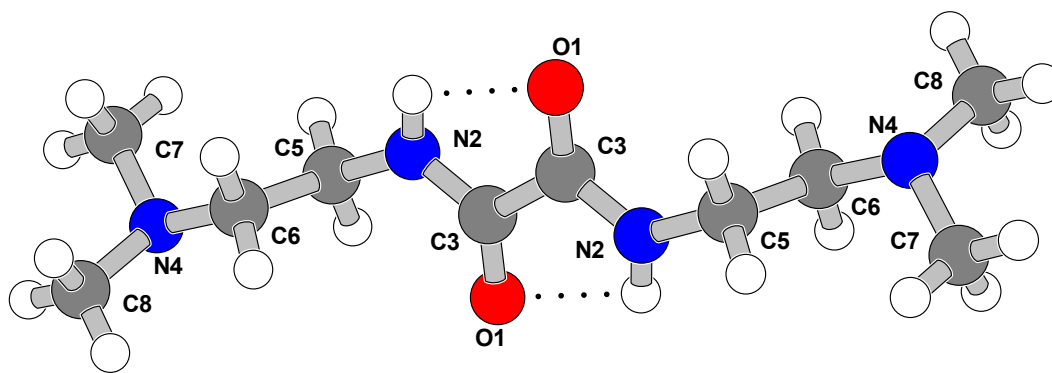


Table 1. Crystal data and structure refinement for Compound 46.

Identification code	<i>N</i> ¹ , <i>N</i> ² -bis(2-(dimethylamino)ethyl)oxalamide	
Empirical formula	C ₁₀ H ₂₂ N ₄ O ₂	
Formula weight	230.32	
Temperature	293(2) K	
Wavelength	1.54178 Å	
Crystal system	Triclinic	
Space group	P-1	
Unit cell dimensions	a = 4.7832(4) Å	a = 94.659(7)°
	b = 5.1164(5) Å	b = 94.120(7)°
	c = 14.2581(10) Å	g = 105.652(8)°
Volume	333.28(5) Å ³	
Z	1	
Density (calculated)	1.148 Mg/m ³	
Absorption coefficient	0.664 mm ⁻¹	
F(000)	126	
Crystal size	2 x 1 x 1 mm ³	
Theta range for data collection	6.26 to 61.55°.	
Index ranges	-5 ≤ h ≤ 5, -5 ≤ k ≤ 5, -16 ≤ l ≤ 16	
Reflections collected	6124	
Independent reflections	1030 [R(int) = 0.0471]	
Completeness to theta = 61.55	99.4 %	
Refinement method	Full-matrix least-squares on F ²	
Data / restraints / parameters	1030 / 0 / 75	
Goodness-of-fit on F ²	1.043	
Final R indices [I > 2σ(I)]	R1 = 0.0523, wR2 = 0.1255	
R indices (all data)	R1 = 0.0819, wR2 = 0.1442	
Largest diff. peak and hole	0.153 and -0.197 e. ⁻³	

Table 2. Atomic coordinates ($\times 10^4$) and equivalent isotropic displacement parameters (2×10^3) for Compound 46. $U(\text{eq})$ is defined as one third of the trace of the orthogonalized U^{ij} tensor.

	x	y	z	$U(\text{eq})$
O(1)	1465(4)	-2302(3)	4358(1)	60(1)
N(2)	2170(4)	2216(3)	4276(1)	48(1)
C(3)	1011(5)	-121(4)	4614(1)	42(1)
N(4)	4489(5)	3021(4)	1847(1)	66(1)
C(5)	4125(5)	2520(5)	3538(2)	52(1)
C(6)	2554(6)	2572(6)	2595(2)	67(1)
C(7)	6169(8)	5828(7)	1893(2)	93(1)
C(8)	2876(10)	2127(8)	923(2)	112(1)

Table 3. Bond lengths (Å) and angles (°) for Compound 46.

O(1)-C(3)	1.225(2)
N(2)-C(3)	1.321(3)
N(2)-C(5)	1.448(3)
C(3)-C(3)#1	1.536(4)
N(4)-C(7)	1.438(4)
N(4)-C(8)	1.450(4)
N(4)-C(6)	1.454(3)
C(5)-C(6)	1.498(4)
C(3)-N(2)-C(5)	124.01(19)
O(1)-C(3)-N(2)	125.0(2)
O(1)-C(3)-C(3)#1	121.6(2)
N(2)-C(3)-C(3)#1	113.4(2)
C(7)-N(4)-C(8)	110.5(3)
C(7)-N(4)-C(6)	111.8(2)
C(8)-N(4)-C(6)	111.1(3)
N(2)-C(5)-C(6)	111.5(2)
N(4)-C(6)-C(5)	112.8(2)

Symmetry transformations used to generate equivalent atoms:

#1 -x,-y,-z+1

Table 4. Anisotropic displacement parameters ($\times 10^3$) for Compound 46. The anisotropic displacement factor exponent takes the form: $-2p^2[h^2 a^* U^{11} + \dots + 2 h k a^* b^* U^{12}]$

	U ¹¹	U ²²	U ³³	U ²³	U ¹³	U ¹²
O(1)	90(1)	39(1)	61(1)	10(1)	28(1)	27(1)
N(2)	64(1)	38(1)	46(1)	8(1)	16(1)	18(1)
C(3)	57(1)	33(1)	38(1)	5(1)	3(1)	15(1)
N(4)	84(2)	69(2)	48(1)	11(1)	17(1)	20(1)
C(5)	60(2)	49(1)	50(1)	11(1)	14(1)	15(1)
C(6)	60(2)	83(2)	50(2)	9(1)	8(1)	8(1)
C(7)	114(3)	83(2)	83(2)	30(2)	30(2)	15(2)
C(8)	150(4)	128(3)	47(2)	6(2)	10(2)	20(3)

Table 5. Hydrogen coordinates ($\times 10^4$) and isotropic displacement parameters ($^2 \times 10^3$) for Compound 46.

	x	y	z	U(eq)
H(2)	1736	3645	4508	57
H(5A)	5001	1016	3507	63
H(5B)	5679	4201	3690	63
H(6A)	1066	851	2431	80
H(6B)	1586	4010	2639	80
H(7A)	4880	6954	1802	140
H(7B)	7479	6032	1407	140
H(7C)	7270	6371	2500	140
H(8A)	1886	215	888	168
H(8B)	4201	2436	443	168
H(8C)	1472	3136	828	168

Molecular Structure and Crystallography Data for Co-crystal 47

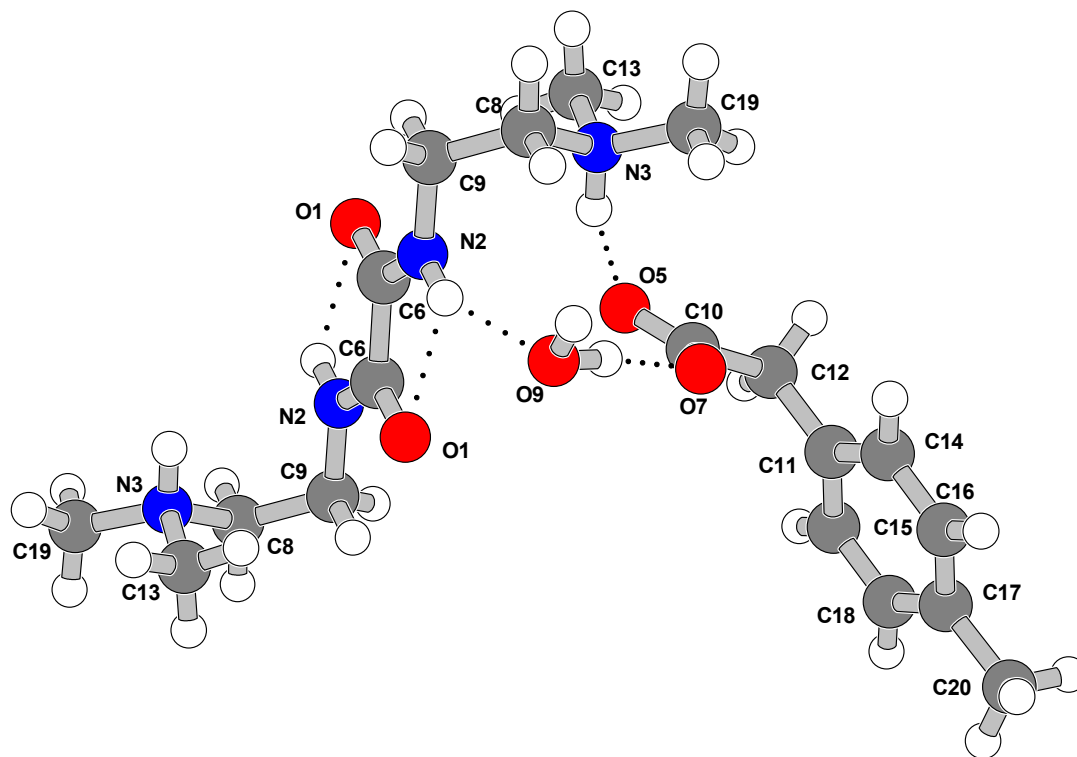


Table 1. Crystal data and structure refinement for Co-crystal 47.

Identification code	Co-crystal 47	
Empirical formula	C ₁₅ H ₂₈ N ₄ O ₄	
Formula weight	328.41	
Temperature	293(2) K	
Wavelength	1.54178 Å	
Crystal system	Triclinic	
Space group	P-1	
Unit cell dimensions	a = 5.6960(5) Å	a = 90.677(5)°
	b = 6.9614(4) Å	b = 94.021(7)°
	c = 19.4973(14) Å	g = 97.131(6)°
Volume	765.08(10) Å ³	
Z	2	
Density (calculated)	1.426 Mg/m ³	
Absorption coefficient	0.856 mm ⁻¹	
F(000)	356	
Crystal size	1.5 x 1 x 0.3 mm ³	
Theta range for data collection	4.55 to 61.69°.	
Index ranges	-6 ≤ h ≤ 6, -7 ≤ k ≤ 6, -22 ≤ l ≤ 21	
Reflections collected	4058	
Independent reflections	2333 [R(int) = 0.0204]	
Completeness to theta = 61.69	97.6 %	
Refinement method	Full-matrix least-squares on F ²	
Data / restraints / parameters	2333 / 0 / 211	
Goodness-of-fit on F ²	1.038	
Final R indices [I > 2σ(I)]	R1 = 0.0502, wR2 = 0.1145	
R indices (all data)	R1 = 0.0763, wR2 = 0.1293	
Largest diff. peak and hole	0.160 and -0.227 e. ⁻³	

Table 2. Atomic coordinates ($\times 10^4$) and equivalent isotropic displacement parameters (2×10^3) for Co-crystal 47. $U(\text{eq})$ is defined as one third of the trace of the orthogonalized U^{ij} tensor.

	x	y	z	$U(\text{eq})$
O(7)	2982(4)	6347(3)	7363(1)	67(1)
O(1)	-1160(3)	2592(2)	4818(1)	51(1)
N(2)	2434(3)	3817(2)	5322(1)	36(1)
N(3)	2466(4)	1669(3)	6618(1)	40(1)
O(5)	-152(3)	4605(3)	6831(1)	59(1)
C(6)	286(4)	3955(3)	5028(1)	35(1)
C(8)	4275(4)	1597(3)	6104(1)	41(1)
C(9)	3378(4)	1980(3)	5379(1)	41(1)
C(10)	869(5)	5632(3)	7325(1)	48(1)
C(11)	46(4)	7720(4)	8367(1)	46(1)
C(12)	-633(5)	5928(4)	7927(1)	57(1)
C(13)	373(4)	182(4)	6475(1)	51(1)
C(14)	2194(5)	8071(4)	8753(1)	54(1)
C(15)	-1486(6)	9098(4)	8400(2)	58(1)
C(16)	2772(6)	9727(5)	9153(2)	65(1)
C(17)	1239(7)	11106(4)	9191(2)	67(1)
C(18)	-909(7)	10762(5)	8807(2)	70(1)
C(19)	3561(6)	1470(4)	7326(1)	64(1)
C(20)	1864(9)	12897(5)	9647(2)	114(2)
O(9)	5811(4)	6536(3)	6267(1)	61(1)

Table 3. Bond lengths (Å) and angles (°) for Co-crystal 47.

O(7)-C(10)	1.241(3)
O(1)-C(6)	1.223(3)
N(2)-C(6)	1.329(3)
N(2)-C(9)	1.450(3)
N(3)-C(13)	1.487(3)
N(3)-C(19)	1.489(3)
N(3)-C(8)	1.492(3)
O(5)-C(10)	1.257(3)
C(6)-C(6)#1	1.533(4)
C(8)-C(9)	1.507(3)
C(10)-C(12)	1.526(4)
C(11)-C(15)	1.379(4)
C(11)-C(14)	1.384(4)
C(11)-C(12)	1.499(4)
C(14)-C(16)	1.376(4)
C(15)-C(18)	1.388(4)
C(16)-C(17)	1.380(4)
C(17)-C(18)	1.382(5)
C(17)-C(20)	1.514(4)
C(6)-N(2)-C(9)	122.09(19)
C(13)-N(3)-C(19)	110.7(2)
C(13)-N(3)-C(8)	112.47(18)
C(19)-N(3)-C(8)	110.2(2)
O(1)-C(6)-N(2)	125.4(2)
O(1)-C(6)-C(6)#1	121.0(3)
N(2)-C(6)-C(6)#1	113.5(2)
N(3)-C(8)-C(9)	113.82(18)
N(2)-C(9)-C(8)	112.52(19)
O(7)-C(10)-O(5)	124.9(2)
O(7)-C(10)-C(12)	119.1(2)
O(5)-C(10)-C(12)	116.0(2)
C(15)-C(11)-C(14)	117.2(3)
C(15)-C(11)-C(12)	120.3(3)

C(14)-C(11)-C(12)	122.5(2)
C(11)-C(12)-C(10)	117.4(2)
C(16)-C(14)-C(11)	121.3(3)
C(11)-C(15)-C(18)	121.5(3)
C(14)-C(16)-C(17)	121.7(3)
C(16)-C(17)-C(18)	117.2(3)
C(16)-C(17)-C(20)	121.3(4)
C(18)-C(17)-C(20)	121.5(4)
C(17)-C(18)-C(15)	121.1(3)

Symmetry transformations used to generate equivalent atoms:

#1 -x,-y+1,-z+1

Table 4. Anisotropic displacement parameters ($\times 10^3$) for Co-crystal 47. The anisotropic displacement factor exponent takes the form: $-2p^2 [h^2 a^{*2} U^{11} + \dots + 2 h k a^* b^* U^{12}]$

	U ¹¹	U ²²	U ³³	U ²³	U ¹³	U ¹²
O(7)	56(1)	82(1)	63(1)	-14(1)	12(1)	7(1)
O(1)	45(1)	31(1)	76(1)	-4(1)	-8(1)	1(1)
N(2)	41(1)	26(1)	41(1)	0(1)	1(1)	3(1)
N(3)	48(1)	32(1)	39(1)	2(1)	-3(1)	9(1)
O(5)	67(1)	57(1)	55(1)	-16(1)	-2(1)	16(1)
C(6)	41(1)	29(1)	36(1)	2(1)	7(1)	2(1)
C(8)	35(1)	35(1)	54(2)	4(1)	2(1)	7(1)
C(9)	46(1)	31(1)	46(1)	3(1)	11(1)	9(1)
C(10)	59(2)	39(1)	49(2)	2(1)	4(1)	15(1)
C(11)	52(2)	52(2)	36(1)	5(1)	12(1)	5(1)
C(12)	61(2)	60(2)	49(2)	-1(1)	12(1)	-1(1)
C(13)	48(2)	49(2)	54(2)	4(1)	7(1)	-2(1)
C(14)	57(2)	60(2)	47(2)	1(1)	4(1)	11(2)
C(15)	53(2)	71(2)	52(2)	9(2)	9(1)	14(2)
C(16)	74(2)	73(2)	43(2)	0(1)	-3(2)	-2(2)
C(17)	100(3)	53(2)	48(2)	-1(1)	23(2)	-3(2)
C(18)	91(3)	54(2)	72(2)	11(2)	32(2)	24(2)
C(19)	85(2)	61(2)	45(2)	4(1)	-14(2)	12(2)
C(20)	194(5)	67(2)	77(3)	-17(2)	35(3)	-13(3)
O(9)	57(1)	70(1)	54(1)	6(1)	0(1)	5(1)

Table 5. Hydrogen coordinates ($\times 10^4$) and isotropic displacement parameters (2×10^{-3}) for Co-crystal 47.

	x	y	z	U(eq)
H(2)	3291	4849	5483	43
H(3)	1950(40)	2850(40)	6594(12)	48
H(8A)	4817	330	6114	50
H(8B)	5629	2548	6236	50
H(9A)	4667	1973	5079	49
H(9B)	2148	945	5224	49
H(12A)	-2262	5929	7745	69
H(12B)	-597	4817	8222	69
H(13A)	890	-1076	6450	76
H(13B)	-441	445	6045	76
H(13C)	-681	217	6837	76
H(19A)	2445	1699	7655	96
H(19B)	4953	2397	7400	96
H(19C)	3989	186	7378	96
H(20A)	883	13864	9501	171
H(20B)	3501	13392	9613	171
H(20C)	1605	12572	10115	171
H(4)	6930(60)	5940(50)	6413(18)	85(13)
H(5)	4880(70)	6380(60)	6640(20)	124(16)
H(1)	3270(50)	7070(40)	8751(14)	62(8)
H(401)	-2070(50)	11660(40)	8806(15)	73(9)
H(301)	-2950(60)	8900(40)	8153(15)	74(10)
H(201)	4220(60)	9970(40)	9403(17)	82(10)

Molecular Structure and Crystallography Data for Co-crystal 48

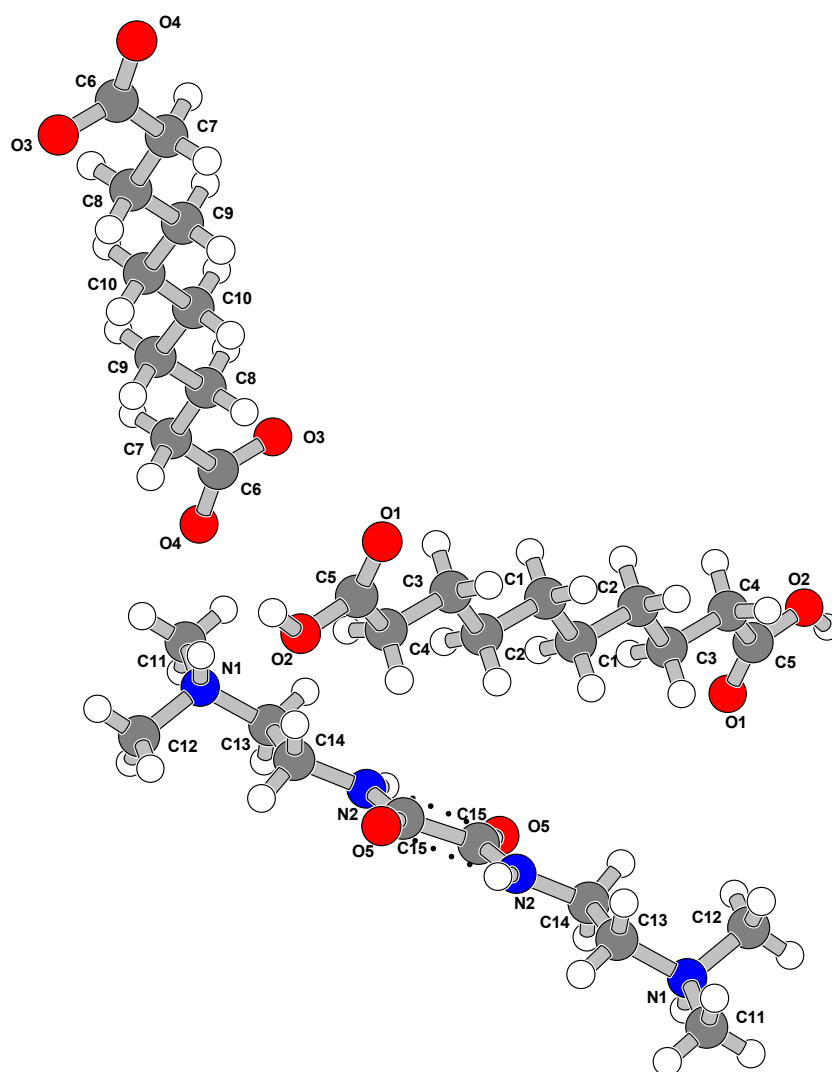


Table 1. Crystal data and structure refinement for Co-crystal 48.

Identification code	Co-crystal 48	
Empirical formula	C ₃₀ H ₅₈ N ₄ O ₁₀	
Formula weight	634.80	
Temperature	293(2) K	
Wavelength	0.71073 Å	
Crystal system	Triclinic	
Space group	P-1	
Unit cell dimensions	a = 5.4462(2) Å	a = 98.983(3)°
	b = 8.3223(3) Å	b = 90.201(4)°
	c = 19.1507(8) Å	g = 99.032(3)°
Volume	846.38(6) Å ³	
Z	1	
Density (calculated)	1.245 Mg/m ³	
Absorption coefficient	0.093 mm ⁻¹	
F(000)	346	
Crystal size	1.5 x 1 x 1 mm ³	
Theta range for data collection	3.23 to 29.54°.	
Index ranges	-7<=h<=7, -11<=k<=10, -26<=l<=26	
Reflections collected	19567	
Independent reflections	4301 [R(int) = 0.0481]	
Completeness to theta = 29.54	90.6 %	
Refinement method	Full-matrix least-squares on F ²	
Data / restraints / parameters	4301 / 0 / 209	
Goodness-of-fit on F ²	1.033	
Final R indices [I>2sigma(I)]	R1 = 0.0579, wR2 = 0.1126	
R indices (all data)	R1 = 0.1086, wR2 = 0.1371	
Largest diff. peak and hole	0.227 and -0.186 e. ⁻³	

Table 2. Atomic coordinates ($\times 10^4$) and equivalent isotropic displacement parameters (2×10^3) for Co-crystal 48. $U(\text{eq})$ is defined as one third of the trace of the orthogonalized U^{ij} tensor.

	x	y	z	$U(\text{eq})$
O(1)	6810(3)	10009(2)	2873(1)	46(1)
N(1)	3407(3)	3287(2)	2335(1)	31(1)
N(2)	1500(3)	4346(2)	4208(1)	39(1)
O(2)	5307(3)	7333(2)	2660(1)	52(1)
O(4)	11058(3)	5034(2)	1611(1)	58(1)
O(5)	-2527(3)	4618(2)	4399(1)	52(1)
C(13)	3611(3)	3623(2)	3122(1)	35(1)
O(3)	12194(3)	7729(2)	1785(1)	62(1)
C(5)	6878(3)	8606(2)	2957(1)	36(1)
C(6)	10947(3)	6423(2)	1473(1)	39(1)
C(4)	8780(4)	8122(2)	3424(1)	40(1)
C(3)	10669(3)	9508(2)	3807(1)	38(1)
C(14)	1137(4)	3818(2)	3446(1)	38(1)
C(15)	-375(4)	4708(2)	4609(1)	38(1)
C(1)	14223(3)	10291(2)	4727(1)	40(1)
C(2)	12272(3)	8937(2)	4340(1)	39(1)
C(7)	9214(4)	6557(2)	873(1)	51(1)
C(9)	6702(4)	8277(3)	263(1)	47(1)
C(8)	8429(4)	8201(2)	877(1)	45(1)
C(12)	1970(4)	1642(2)	2056(1)	43(1)
C(10)	5846(4)	9929(3)	305(1)	49(1)
C(11)	5908(4)	3449(3)	2026(1)	49(1)

Table 3. Bond lengths (Å) and angles (°) for Co-crystal 48.

O(1)-C(5)	1.210(2)
N(1)-C(11)	1.481(2)
N(1)-C(12)	1.484(2)
N(1)-C(13)	1.490(2)
N(2)-C(15)	1.325(2)
N(2)-C(14)	1.459(2)
O(2)-C(5)	1.305(2)
O(4)-C(6)	1.236(2)
O(5)-C(15)	1.225(2)
C(13)-C(14)	1.507(3)
O(3)-C(6)	1.250(2)
C(5)-C(4)	1.508(2)
C(6)-C(7)	1.512(2)
C(4)-C(3)	1.511(2)
C(3)-C(2)	1.519(2)
C(15)-C(15)#1	1.532(3)
C(1)-C(2)	1.518(2)
C(1)-C(1)#2	1.523(3)
C(7)-C(8)	1.495(3)
C(9)-C(10)	1.510(3)
C(9)-C(8)	1.519(2)
C(10)-C(10)#3	1.517(4)
C(11)-N(1)-C(12)	109.66(15)
C(11)-N(1)-C(13)	110.60(14)
C(12)-N(1)-C(13)	113.10(14)
C(15)-N(2)-C(14)	121.06(16)
N(1)-C(13)-C(14)	111.72(14)
O(1)-C(5)-O(2)	124.18(16)
O(1)-C(5)-C(4)	123.95(17)
O(2)-C(5)-C(4)	111.87(16)
O(4)-C(6)-O(3)	124.75(17)
O(4)-C(6)-C(7)	117.87(17)
O(3)-C(6)-C(7)	117.38(16)

C(5)-C(4)-C(3)	116.36(15)
C(4)-C(3)-C(2)	112.57(15)
N(2)-C(14)-C(13)	109.28(15)
O(5)-C(15)-N(2)	125.28(17)
O(5)-C(15)-C(15)#1	121.1(2)
N(2)-C(15)-C(15)#1	113.7(2)
C(2)-C(1)-C(1)#2	113.61(19)
C(1)-C(2)-C(3)	114.18(15)
C(8)-C(7)-C(6)	116.30(16)
C(10)-C(9)-C(8)	112.79(16)
C(7)-C(8)-C(9)	114.35(16)
C(9)-C(10)-C(10)#3	114.6(2)

Symmetry transformations used to generate equivalent atoms:

#1 $-x, -y+1, -z+1$ #2 $-x+3, -y+2, -z+1$ #3 $-x+1, -y+2, -z$

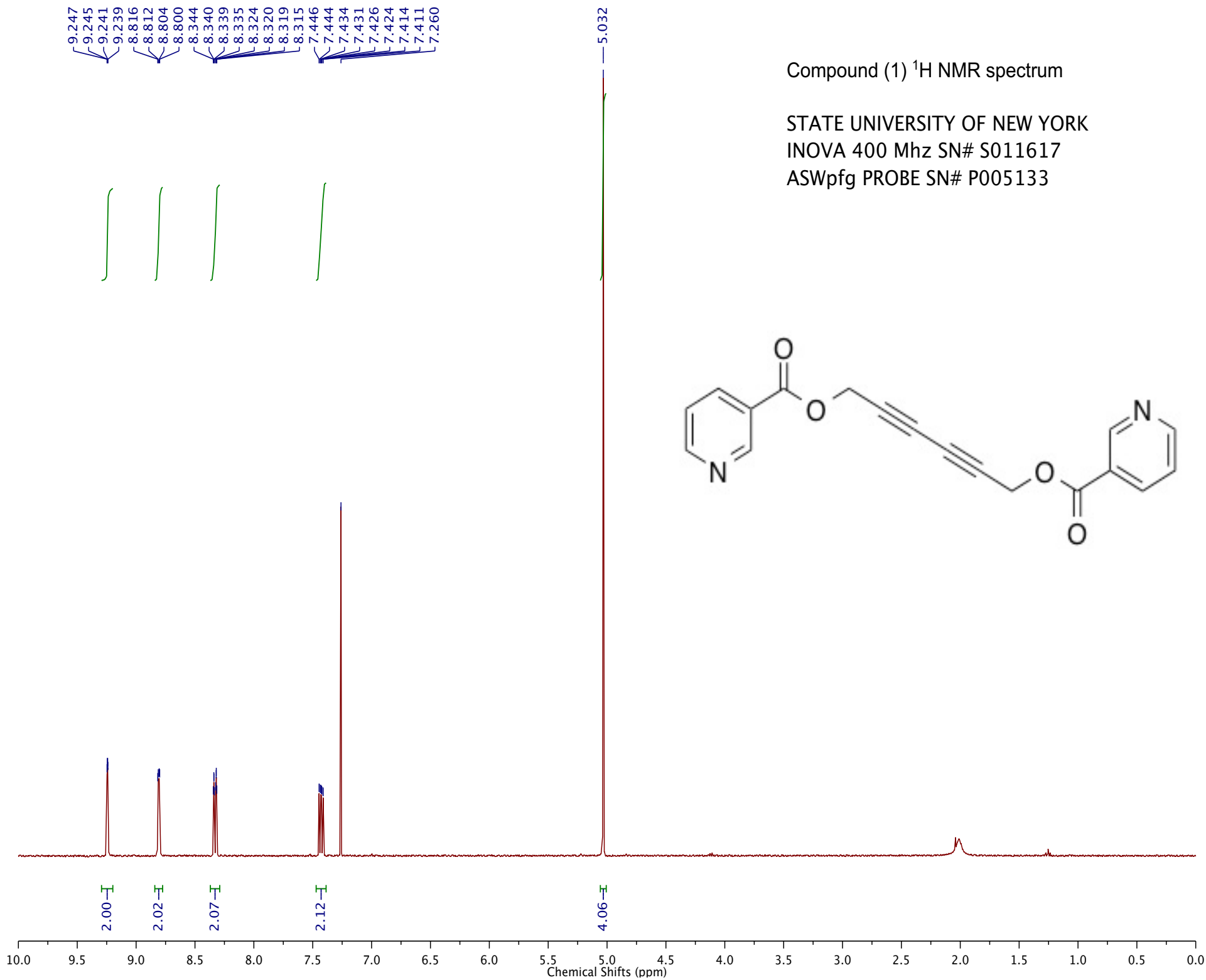
Table 4. Anisotropic displacement parameters ($\times 10^3$) for Co-crystal 48. The anisotropic displacement factor exponent takes the form: $-2\pi^2 [h^2 a^{*2} U^{11} + \dots + 2 h k a^* b^* U^{12}]$

	U ¹¹	U ²²	U ³³	U ²³	U ¹³	U ¹²
O(1)	49(1)	35(1)	56(1)	12(1)	-14(1)	6(1)
N(1)	34(1)	32(1)	29(1)	6(1)	-2(1)	9(1)
N(2)	46(1)	44(1)	27(1)	0(1)	-5(1)	11(1)
O(2)	56(1)	38(1)	59(1)	8(1)	-32(1)	-1(1)
O(4)	57(1)	43(1)	76(1)	26(1)	-28(1)	1(1)
O(5)	47(1)	72(1)	34(1)	1(1)	-7(1)	12(1)
C(13)	42(1)	36(1)	28(1)	5(1)	-6(1)	6(1)
O(3)	73(1)	41(1)	72(1)	7(1)	-45(1)	7(1)
C(5)	36(1)	38(1)	33(1)	7(1)	-5(1)	6(1)
C(6)	36(1)	39(1)	43(1)	11(1)	-8(1)	8(1)
C(4)	40(1)	37(1)	41(1)	8(1)	-14(1)	7(1)
C(3)	35(1)	37(1)	40(1)	7(1)	-9(1)	3(1)
C(14)	47(1)	41(1)	26(1)	2(1)	-4(1)	14(1)
C(15)	50(1)	32(1)	29(1)	3(1)	-3(1)	6(1)
C(1)	34(1)	44(1)	40(1)	9(1)	-9(1)	4(1)
C(2)	36(1)	42(1)	40(1)	10(1)	-8(1)	4(1)
C(7)	59(1)	40(1)	54(1)	8(1)	-29(1)	7(1)
C(9)	49(1)	52(1)	43(1)	10(1)	-13(1)	17(1)
C(8)	50(1)	49(1)	39(1)	8(1)	-13(1)	18(1)
C(12)	52(1)	35(1)	40(1)	-1(1)	-3(1)	5(1)
C(10)	53(1)	57(1)	41(1)	9(1)	-10(1)	23(1)
C(11)	40(1)	60(1)	48(1)	9(1)	8(1)	11(1)

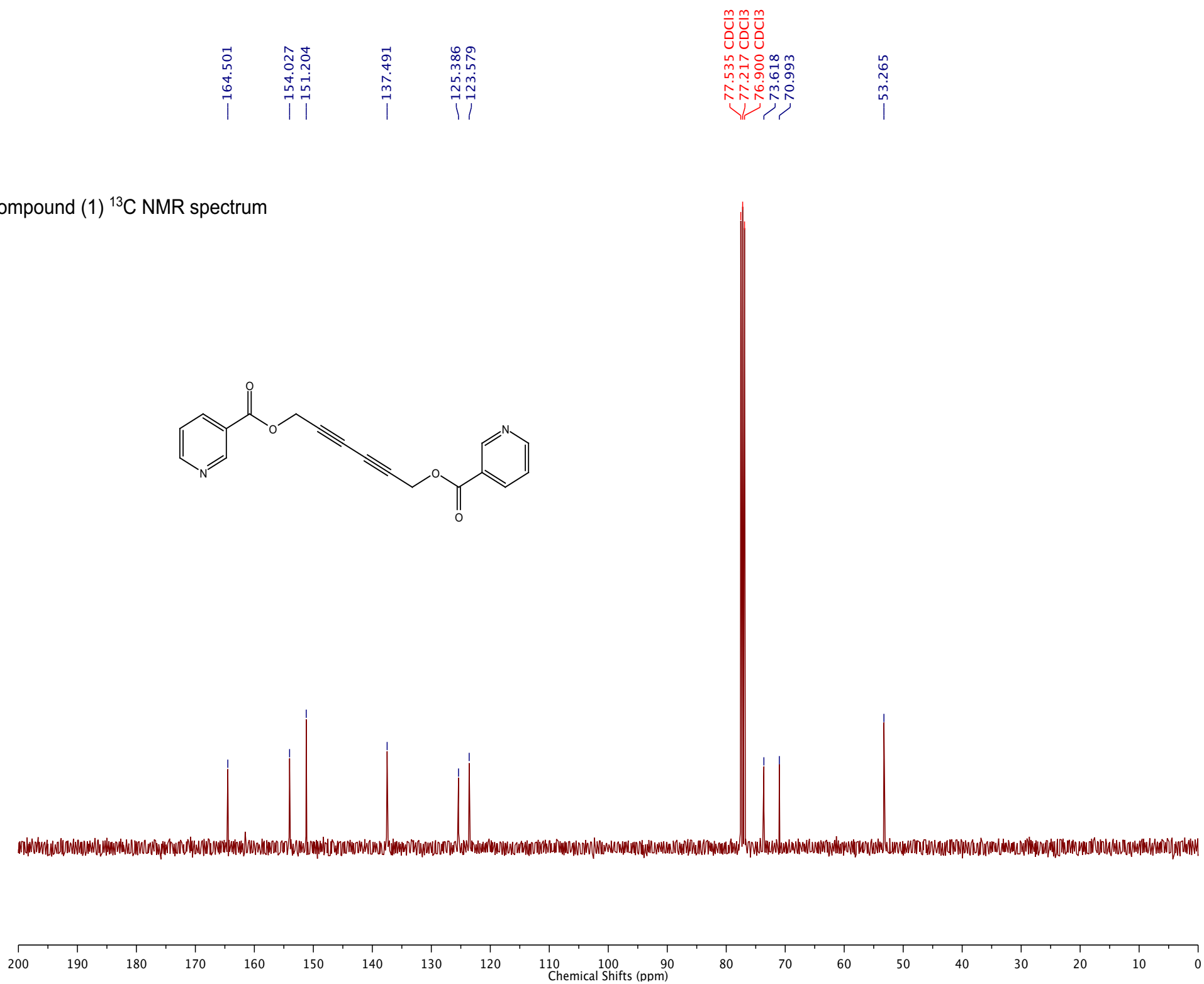
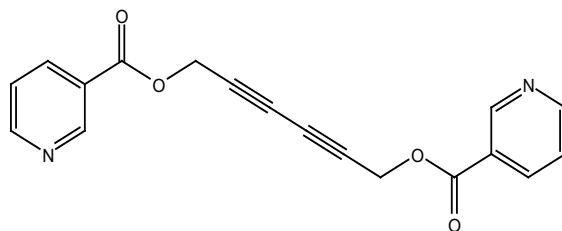
Table 5. Hydrogen coordinates ($\times 10^4$) and isotropic displacement parameters (2×10^3) for Co-crystal 48.

	x	y	z	U(eq)
H(2)	2954	4424	4398	47
H(13A)	4790	4622	3270	42
H(13B)	4240	2723	3292	42
H(4A)	9669	7350	3136	47
H(4B)	7903	7543	3775	47
H(3A)	9806	10358	4050	45
H(3B)	11731	9989	3463	45
H(14A)	405	4630	3238	45
H(14B)	12	2778	3353	45
H(1A)	13401	11170	4963	47
H(1B)	15322	10742	4384	47
H(2A)	11201	8469	4685	47
H(2B)	13101	8070	4096	47
H(7A)	10020	6268	431	61
H(7B)	7731	5745	882	61
H(9A)	7556	8050	-176	56
H(9B)	5259	7427	256	56
H(8A)	9904	9019	869	54
H(8B)	7602	8491	1316	54
H(12A)	1673	1561	1556	65
H(12B)	410	1502	2288	65
H(12C)	2899	800	2143	65
H(10A)	7298	10776	325	58
H(10B)	4974	10142	743	58
H(11A)	6794	2635	2166	74
H(11B)	6809	4529	2193	74
H(11C)	5741	3287	1520	74
H(101)	2610(40)	4060(20)	2153(10)	45(6)
H(100)	3910(60)	7540(40)	2294(16)	117(11)

Appendix 2. NMR Spectra

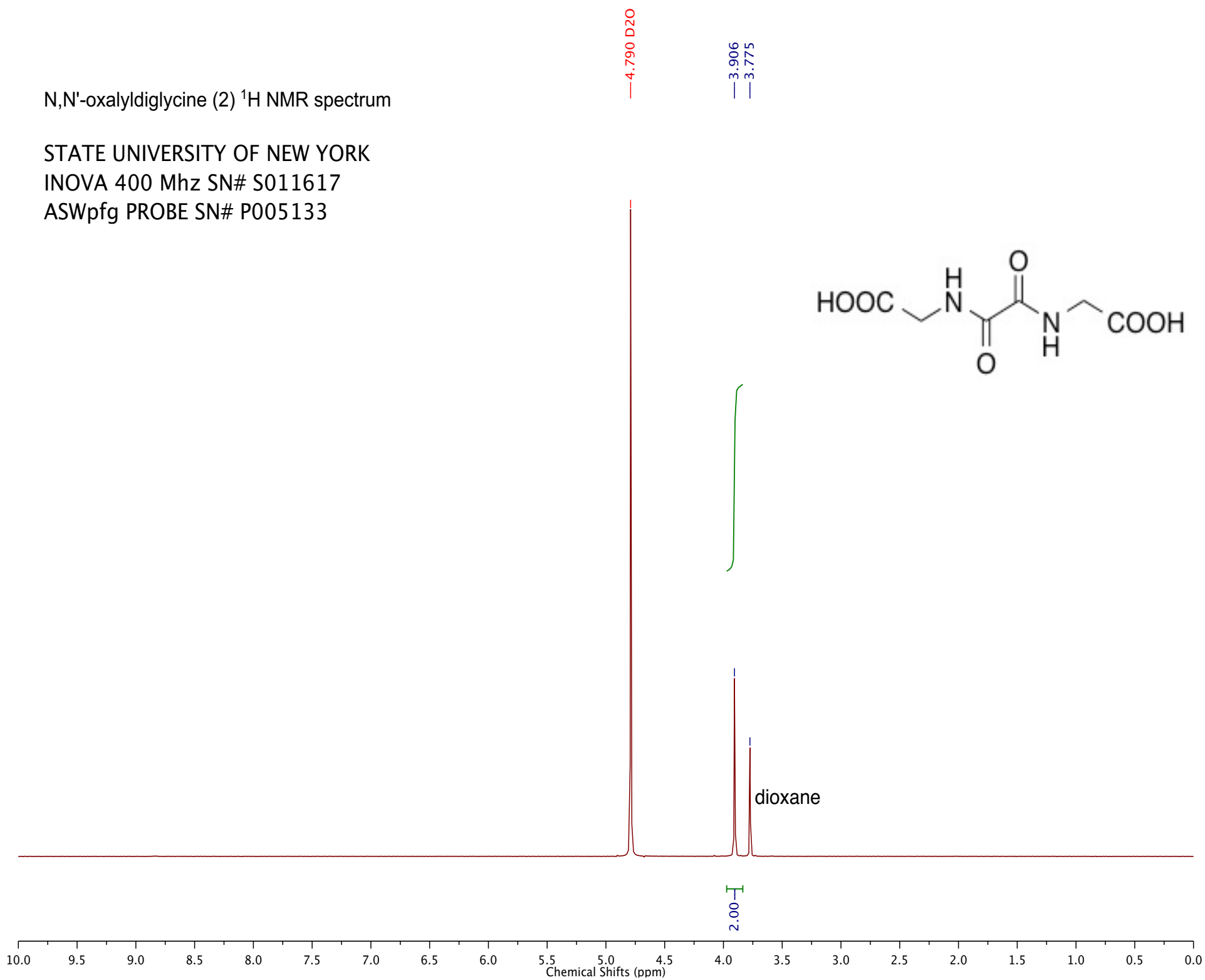


Compound (1) ^{13}C NMR spectrum

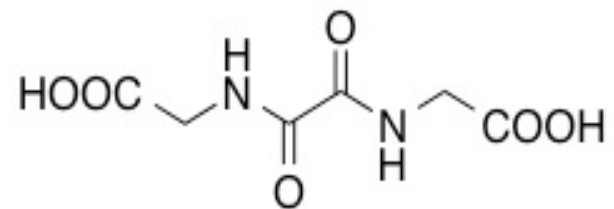


N,N'-oxalyldiglycine (2) ¹H NMR spectrum

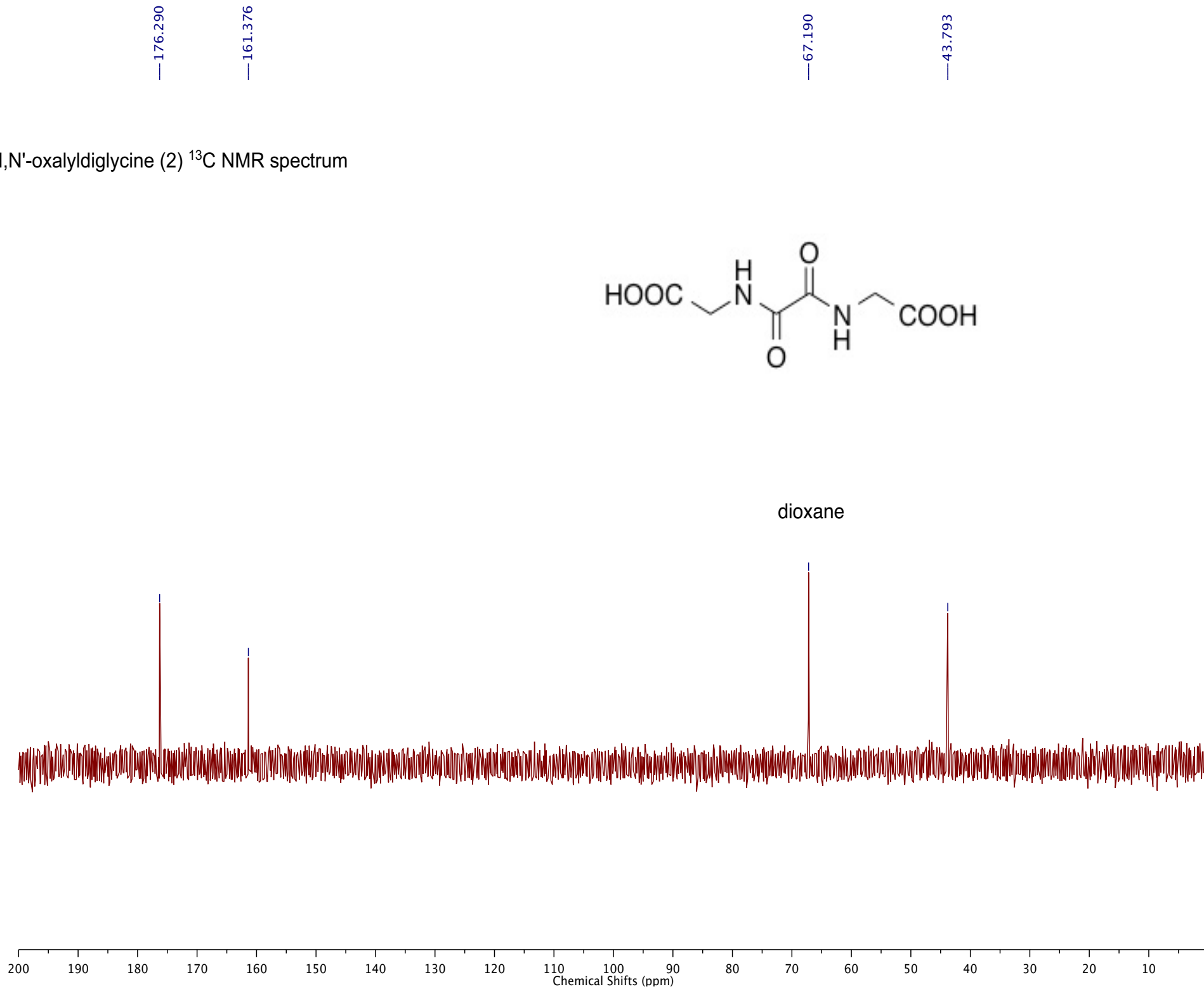
STATE UNIVERSITY OF NEW YORK
INOVA 400 Mhz SN# S011617
ASWpfg PROBE SN# P005133



N,N'-oxalyldiglycine (2) ^{13}C NMR spectrum

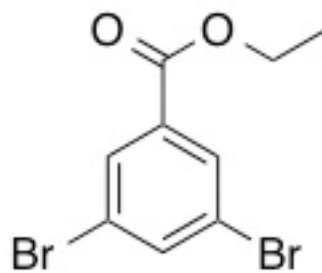


dioxane



Compound (8) ¹H NMR spectrum

STATE UNIVERSITY OF NEW YORK
INOVA 400 Mhz SN# S011617
ASWpfg PROBE SN# P005133



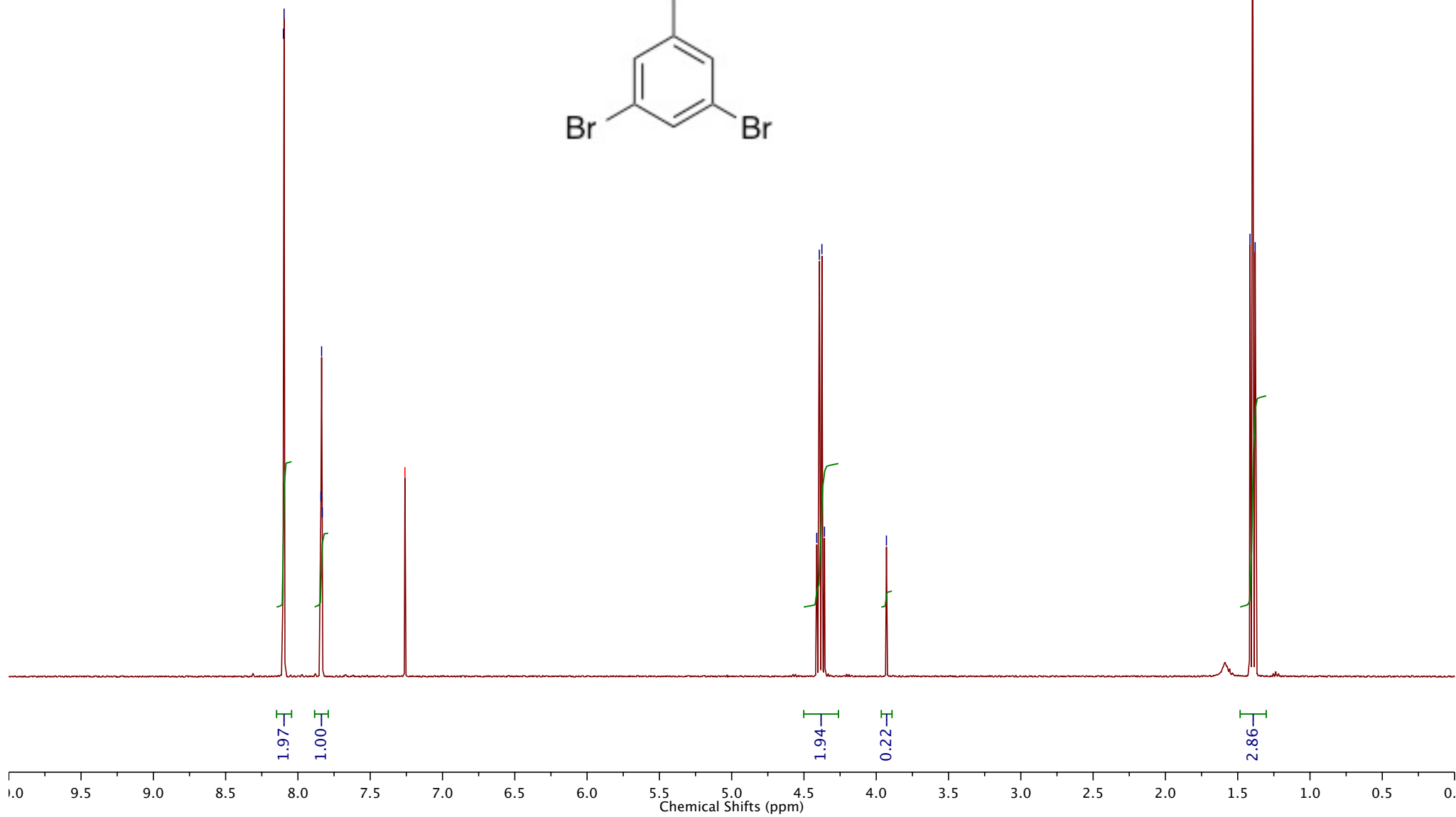
8.100
8.096
7.841
7.836
7.832

7.260 CDCl₃

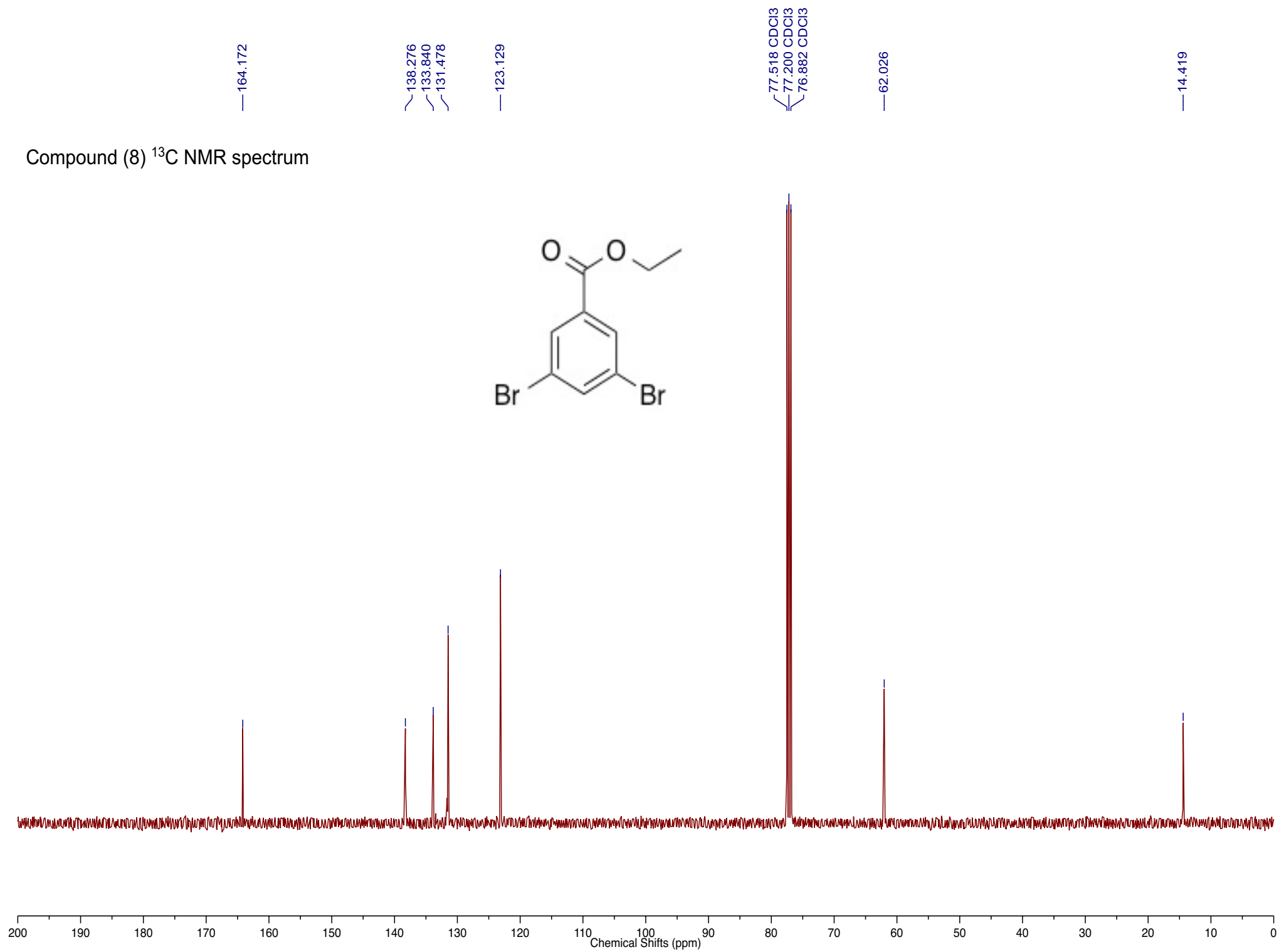
4.412
4.394
4.376
4.358

3.929

1.415
1.397
1.379



Compound (8) ^{13}C NMR spectrum



8.026
8.022
7.612
7.260

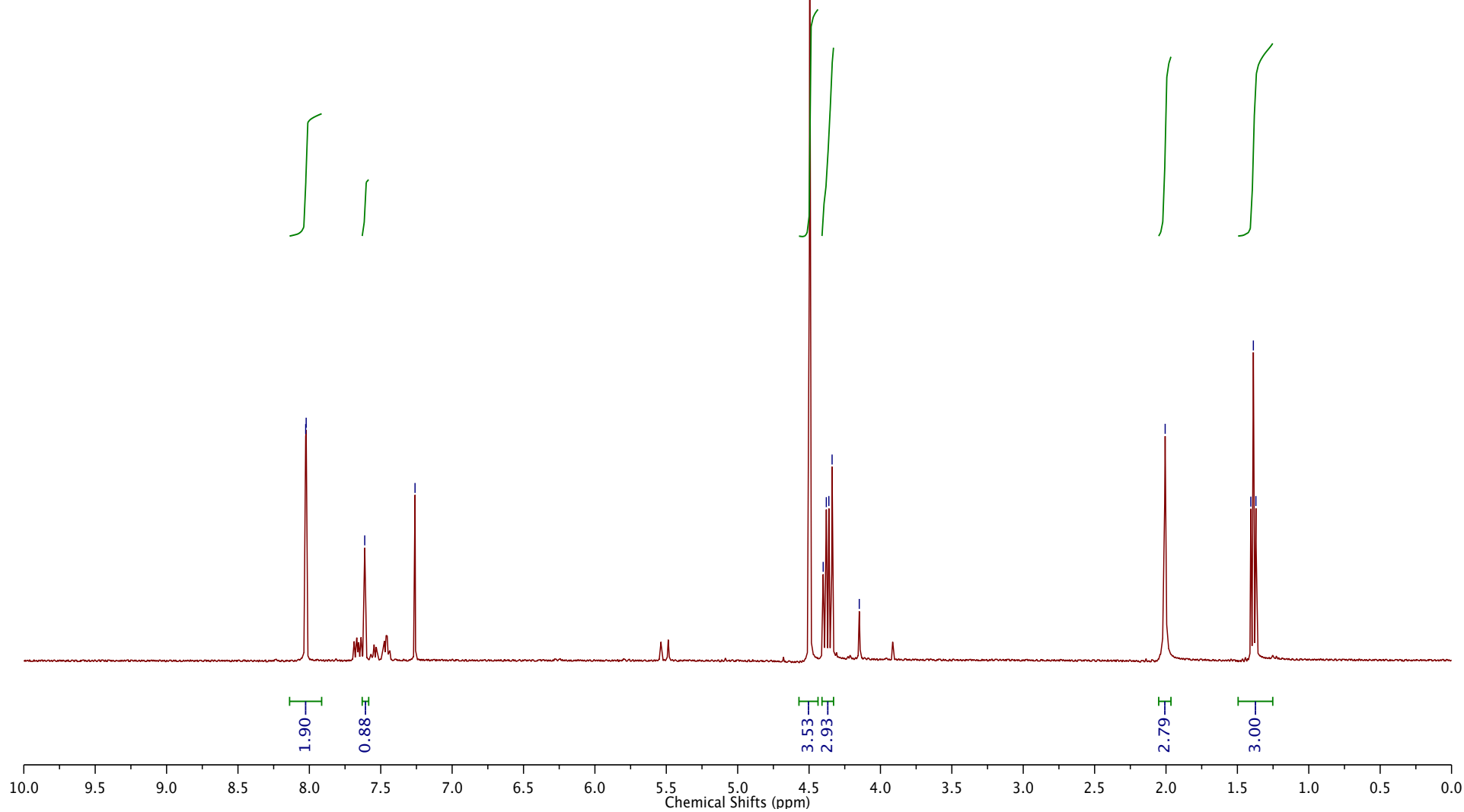
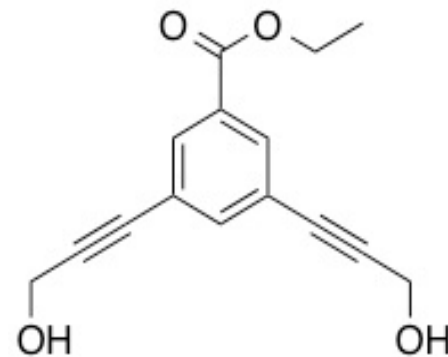
4.496
4.401
4.379
4.361
4.339
4.148

2.006

1.406
1.388
1.370

Compound (9) ¹H NMR spectrum

STATE UNIVERSITY OF NEW YORK
INOVA 400 Mhz SN# S011617
ASWpfg PROBE SN# P005133



—165.389

—138.466

—132.701

—131.278

—123.570

—89.051

—84.035

77.548

77.230

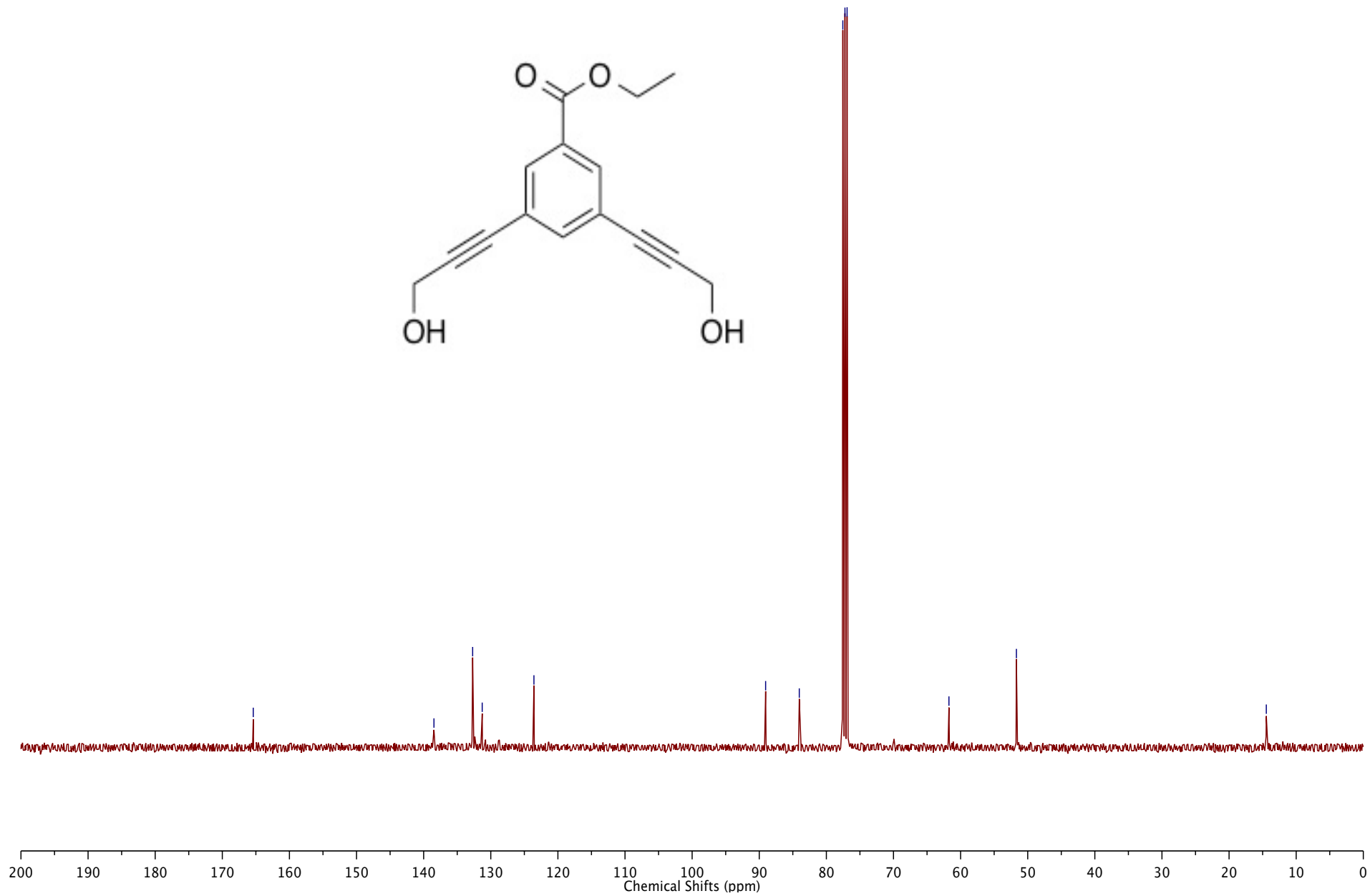
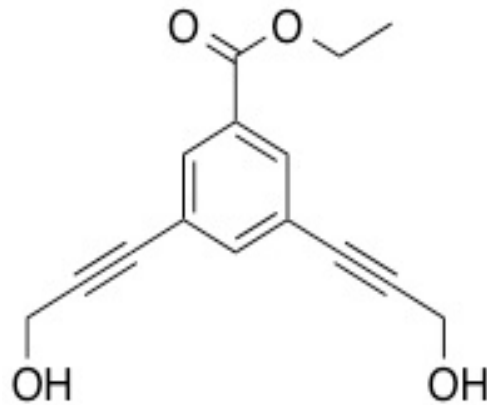
76.913

—61.738

—51.686

—14.452

Compound (9) ^{13}C NMR spectrum



8.046
8.043
7.667
7.663
7.659
— 7.260

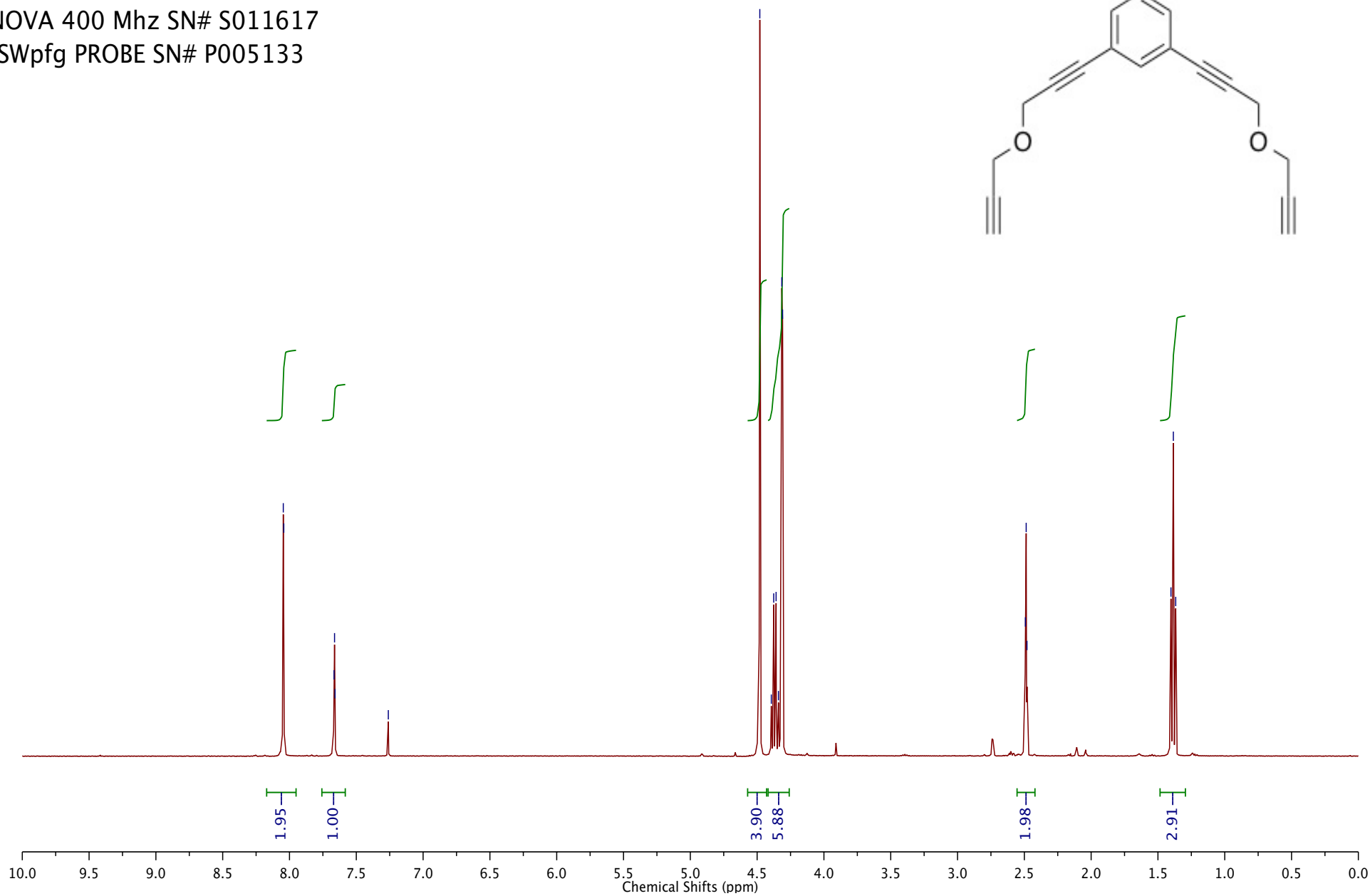
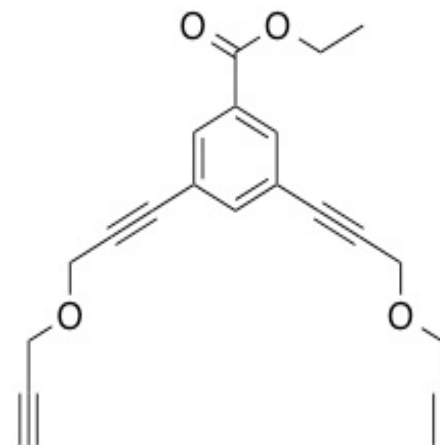
4.480
4.394
4.376
4.358
4.340
4.315
4.309

2.492
2.486
2.480

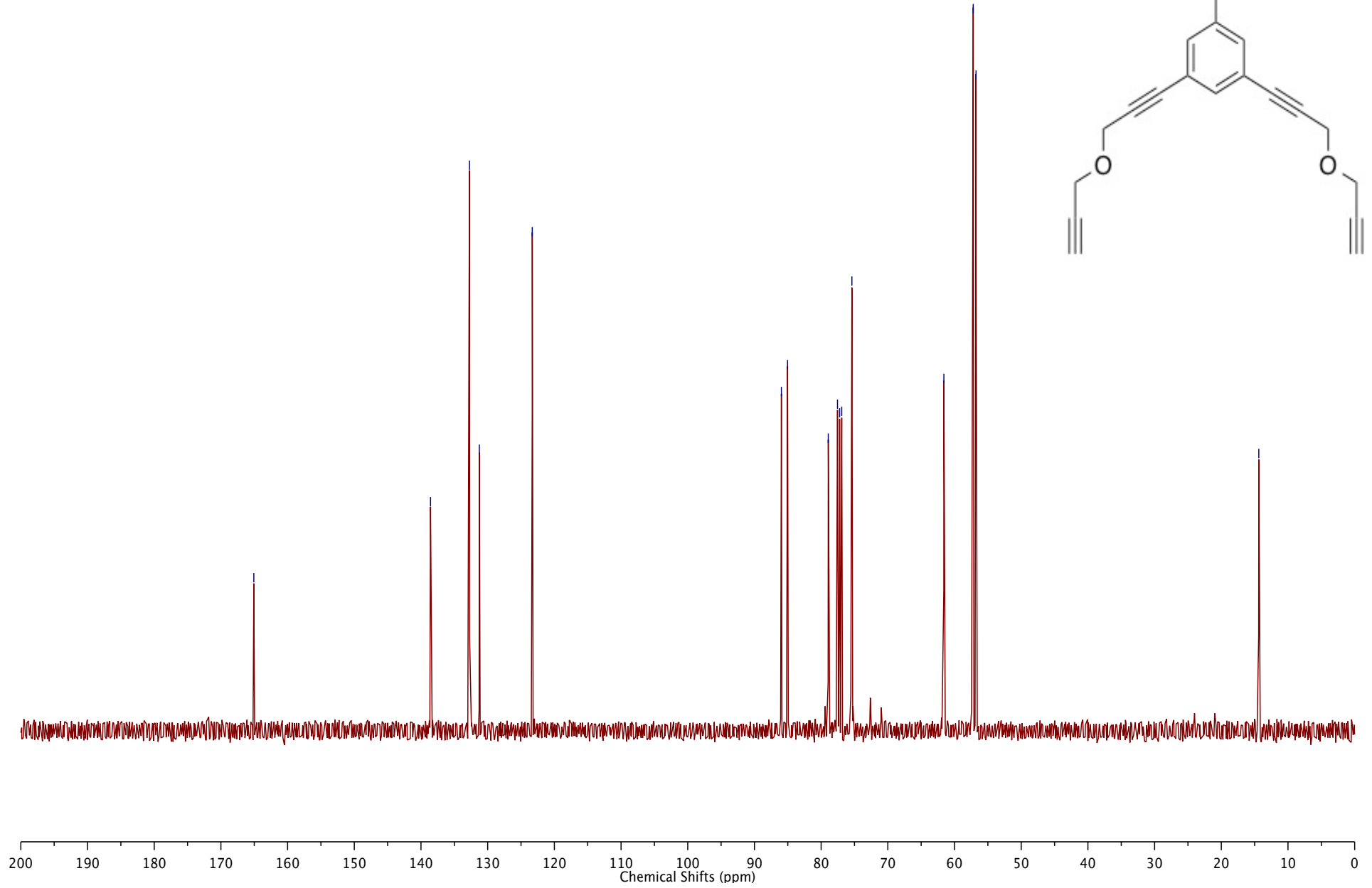
1.403
1.385
1.367

Compound (10) ¹H NMR spectrum

STATE UNIVERSITY OF NEW YORK
INOVA 400 Mhz SN# S011617
ASWpfg PROBE SN# P005133



Compound (10) ¹³C NMR spectrum



2008/10/02

new experiment

Pulse Sequence: s2pu1

Solvent: CDCl3

Temp. 25.0 C / 298.1 K

GEMINI-300BB "gem2300"

Relax. delay 1.000 sec

Pulse 7.8 degrees

Acq. time 1.998 sec

Width 4500.5 Hz

16 repetitions

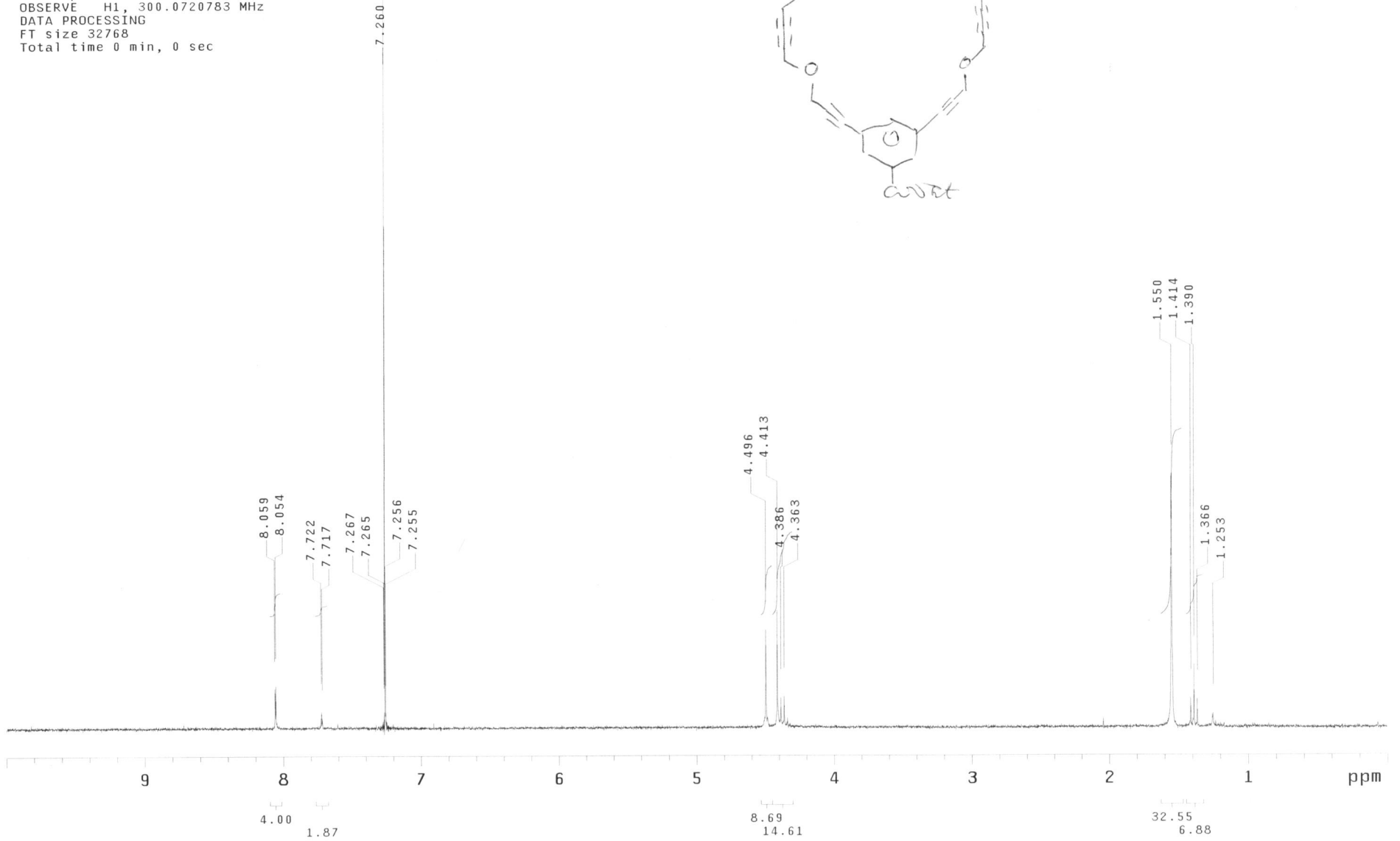
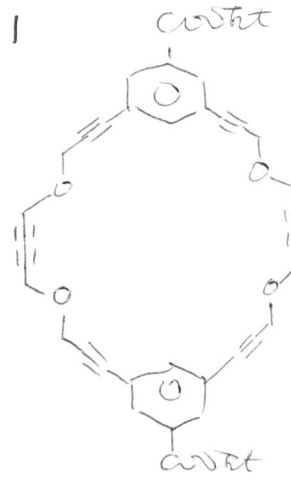
OBSERVE H1, 300.0720783 MHz

DATA PROCESSING

FT size 32768

Total time 0 min, 0 sec

Compound 11



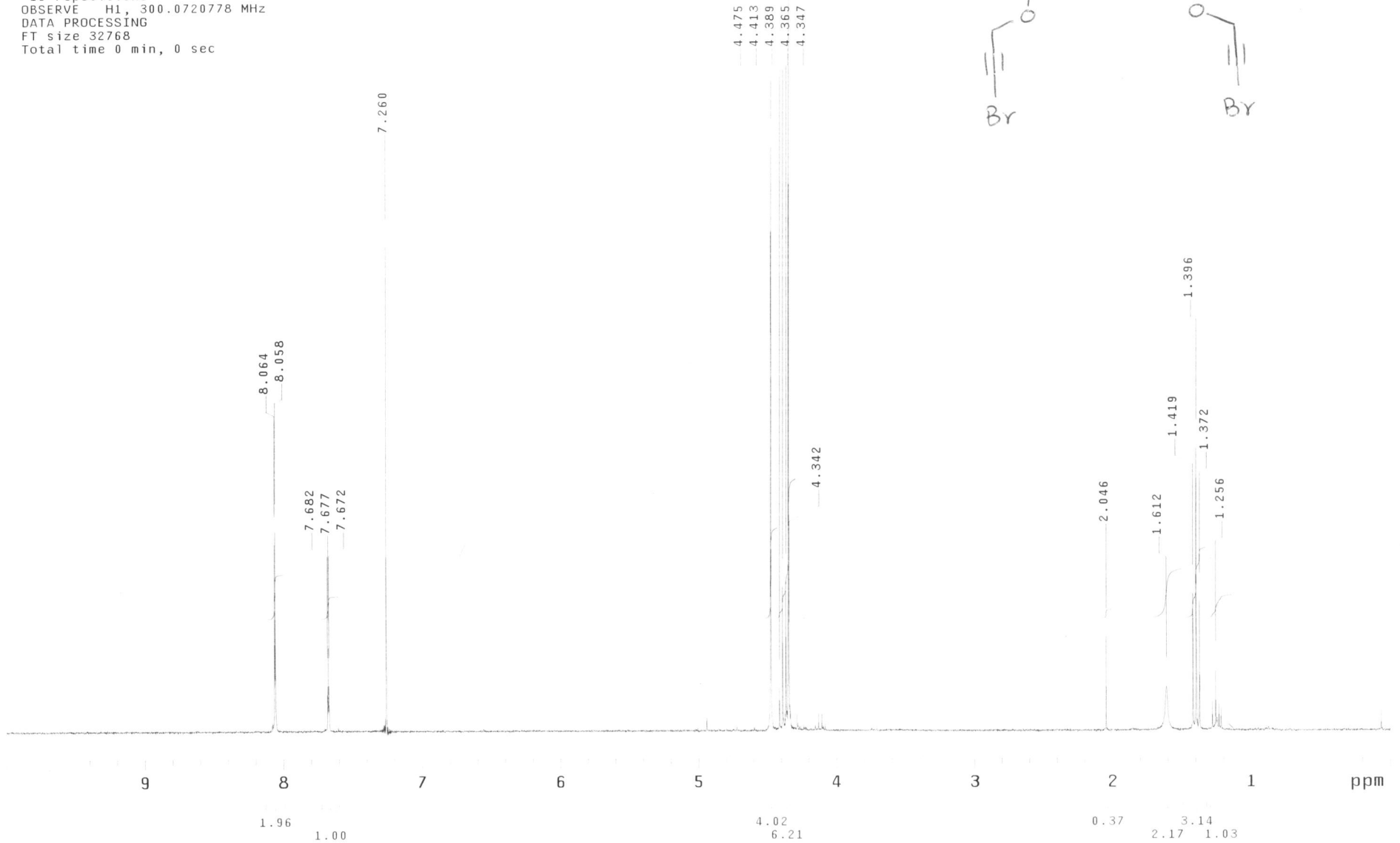
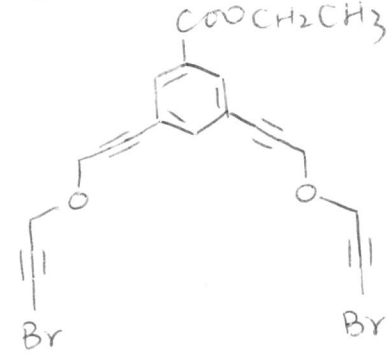
new experiment

Pulse Sequence: s2pul

Solvent: CDCl3
Temp: 25.0 C / 298.1 K
GEMINI-300BB "gem2300"

Relax. delay 1.000 sec
Pulse 7.8 degrees
Acq. time 1.998 sec
Width 4500.5 Hz
16 repetitions
OBSERVE H1, 300.0720778 MHz
DATA PROCESSING
FT size 32768
Total time 0 min, 0 sec

Compound 13



8.070
8.066
7.722
7.718
7.260

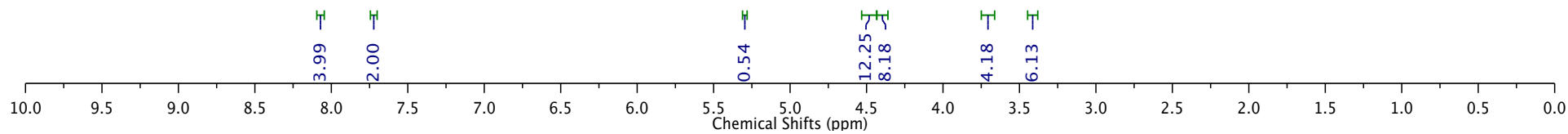
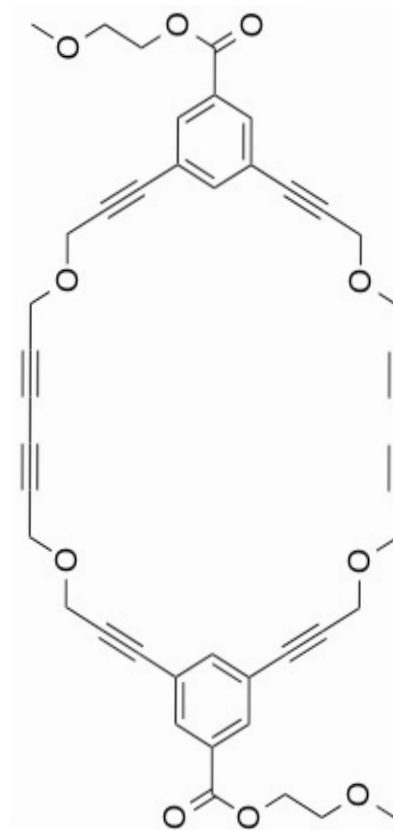
Compound (14) ¹H NMR spectrum

STATE UNIVERSITY OF NEW YORK

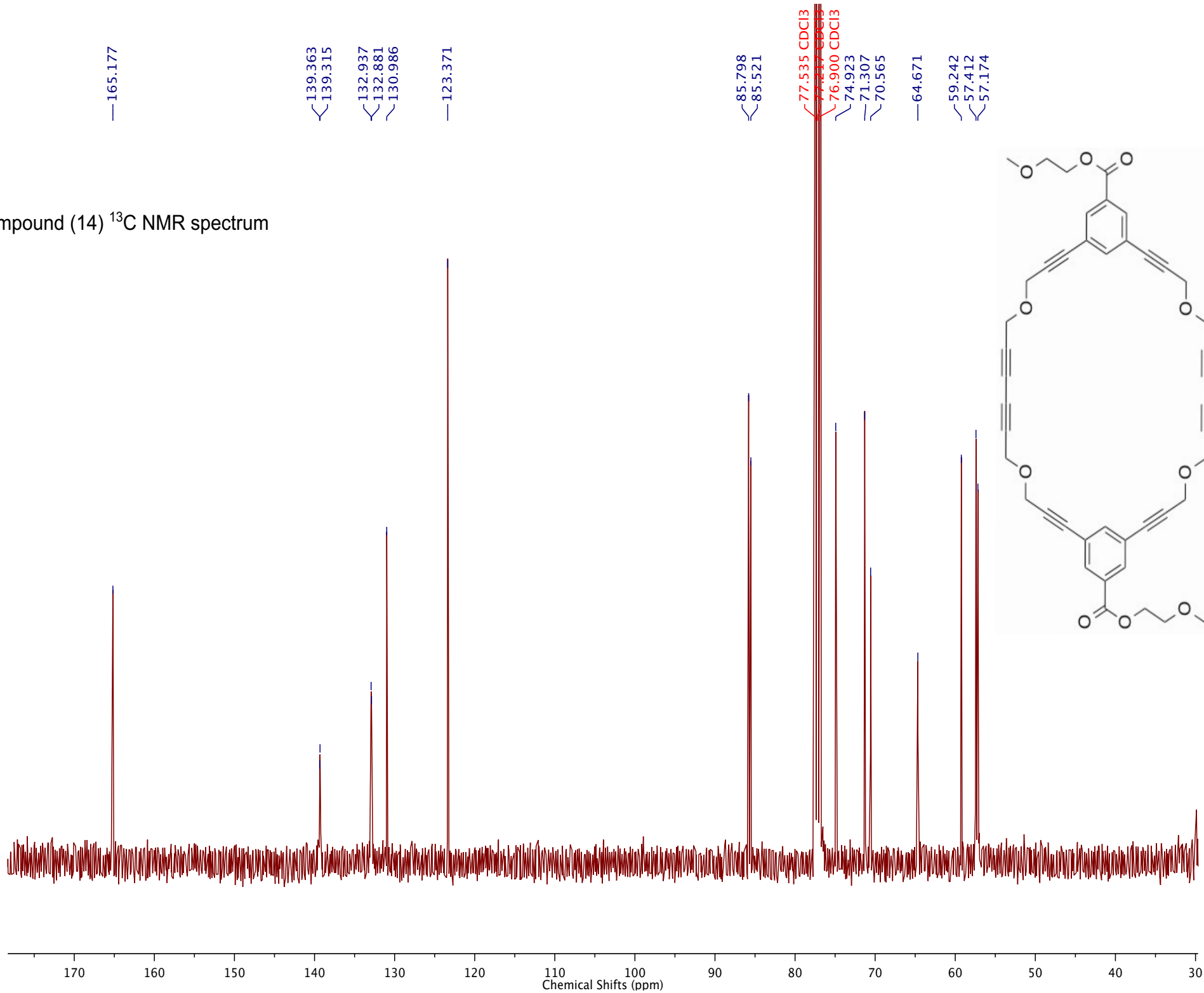
INOVA 400 Mhz SN# S011617

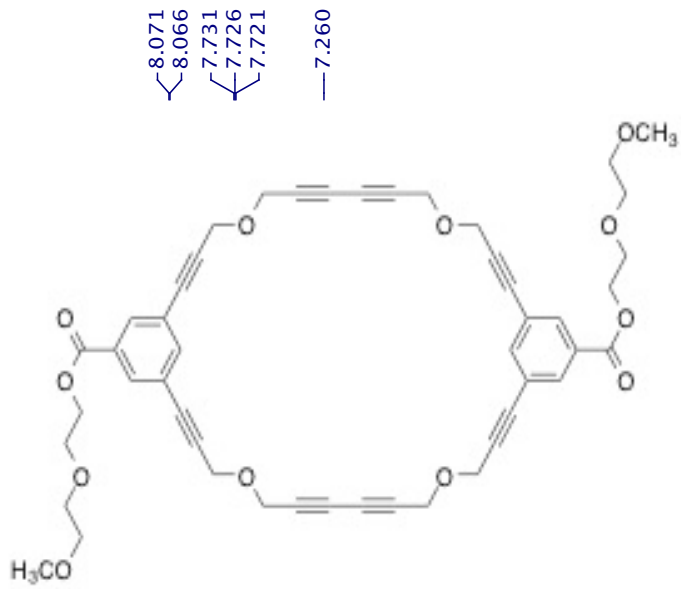
ASWpfg PROBE SN# P005133

5.293
4.490
4.475
4.463
4.452
4.407
3.721
3.709
3.697
3.418
1.248



Compound (14) ^{13}C NMR spectrum

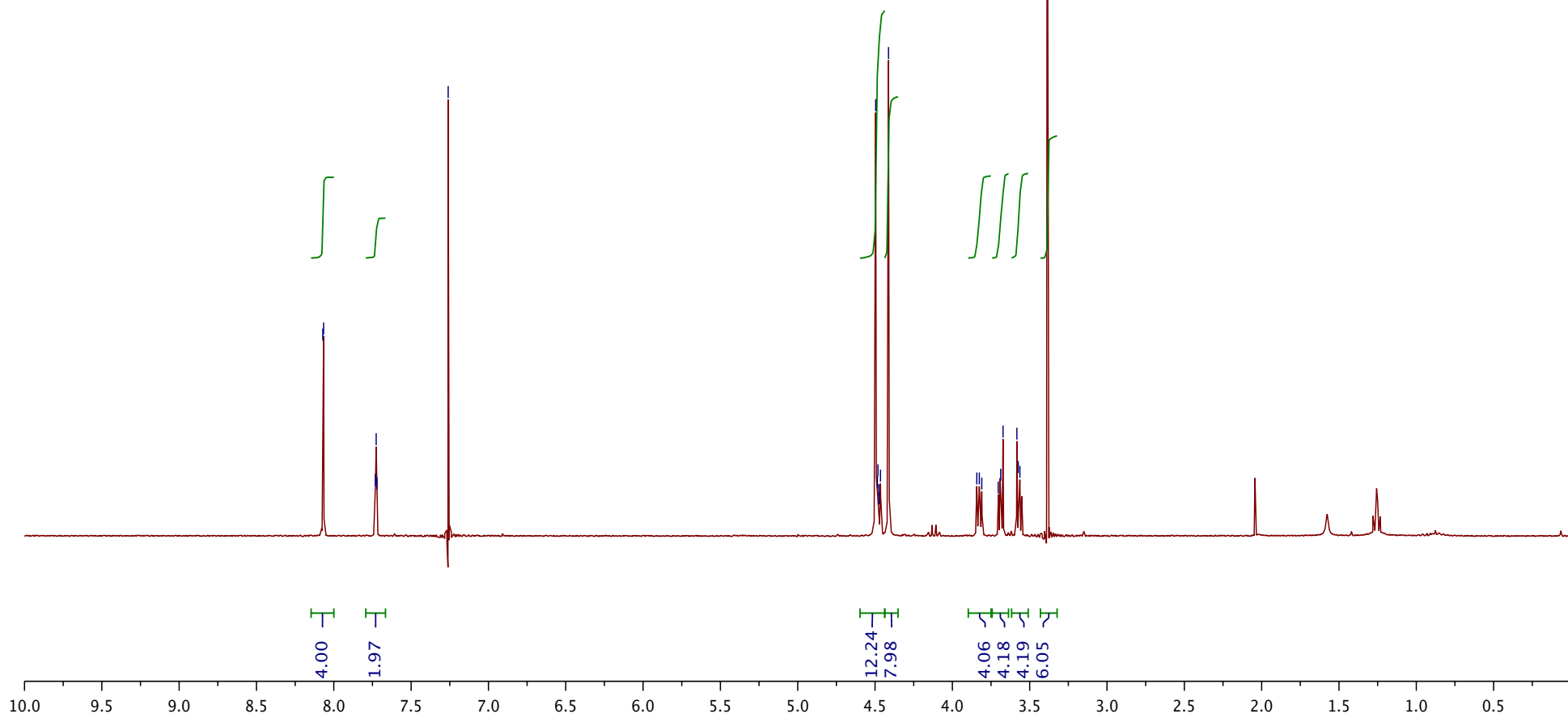




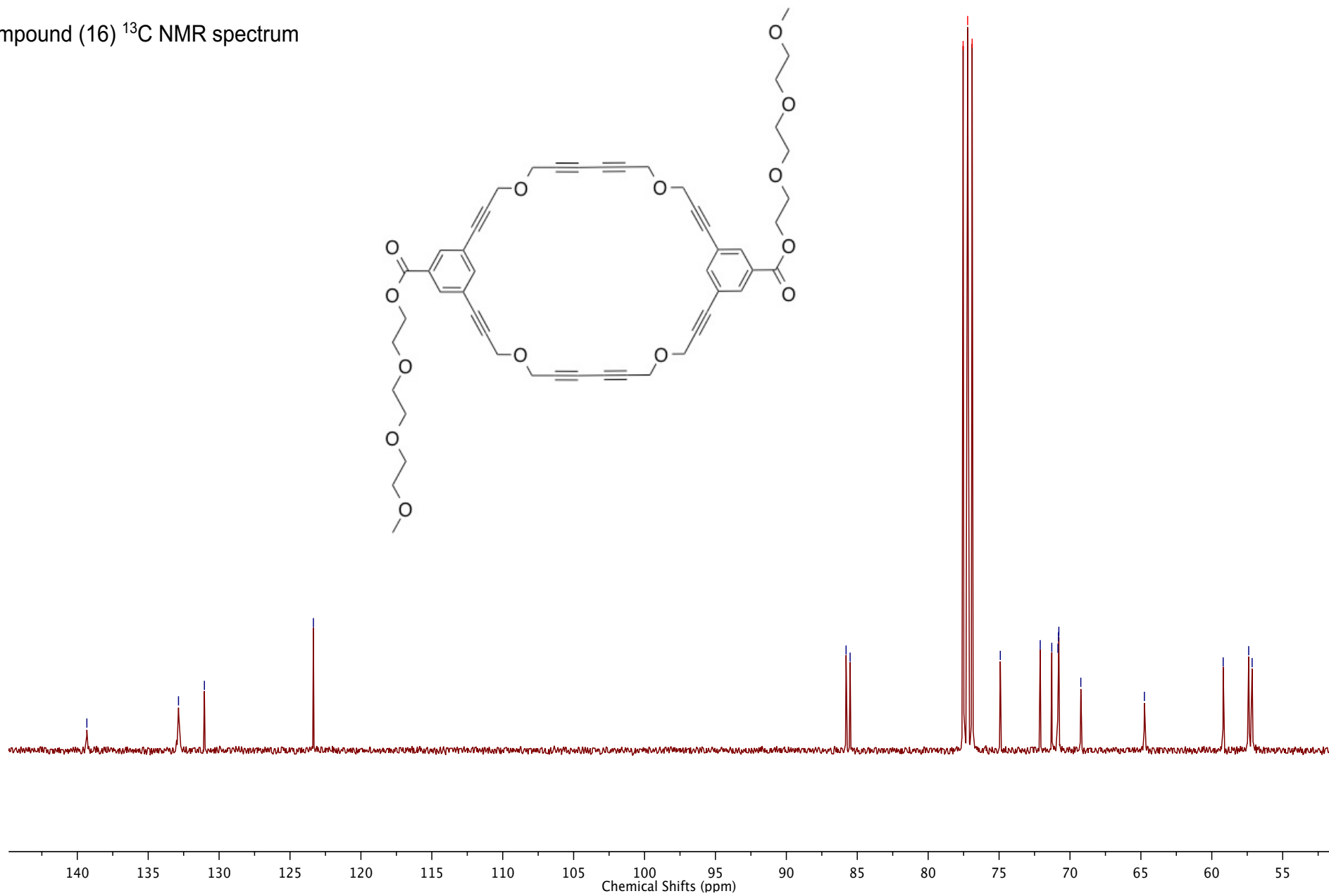
8.071
8.066
7.731
7.726
7.721
7.260

4.496
4.485
4.481
4.476
4.475
4.465
4.413
3.842
3.826
3.810
3.704
3.688
3.672
3.583
3.574
3.563
3.387

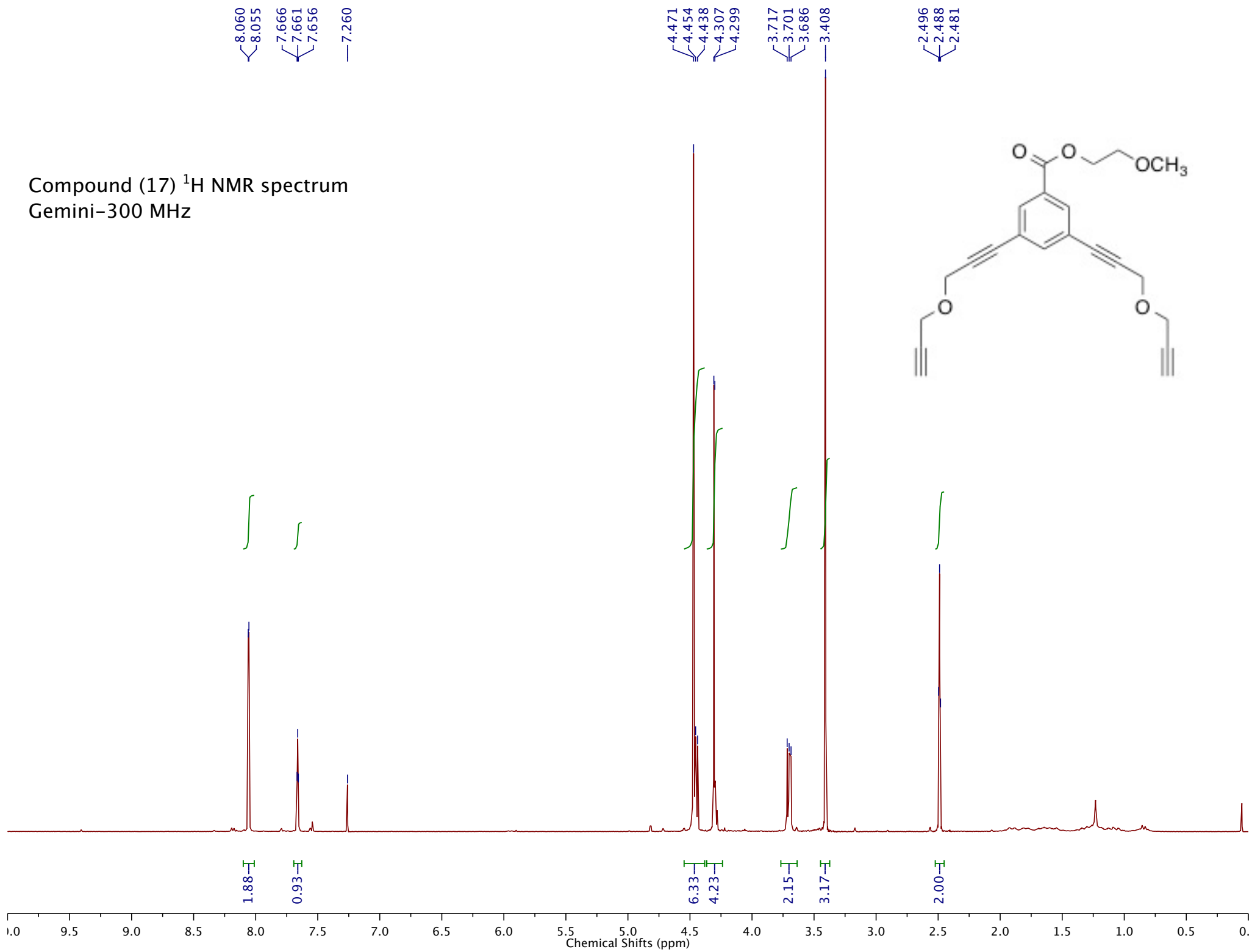
Compound (15) ¹H NMR spectrum
Gemini-300 MHz



Compound (16) ^{13}C NMR spectrum



Compound (17) ^1H NMR spectrum
Gemini-300 MHz



Compound 18

new experiment

Pulse Sequence: s2pu1

Solvent: CDCl3

Temp. 25.0 C / 298.1 K

GEMINI-300BB "gem2300"

Relax. delay 1.000 sec

Pulse 7.8 degrees

Acq. time 1.998 sec

Width 4500.5 Hz

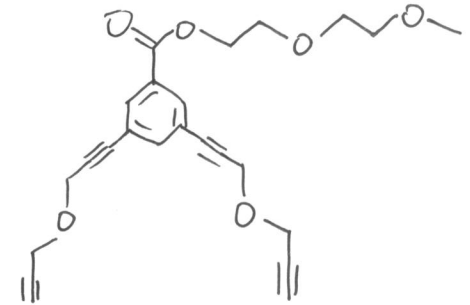
40 repetitions

OBSERVE H1, 300.0720781 MHz

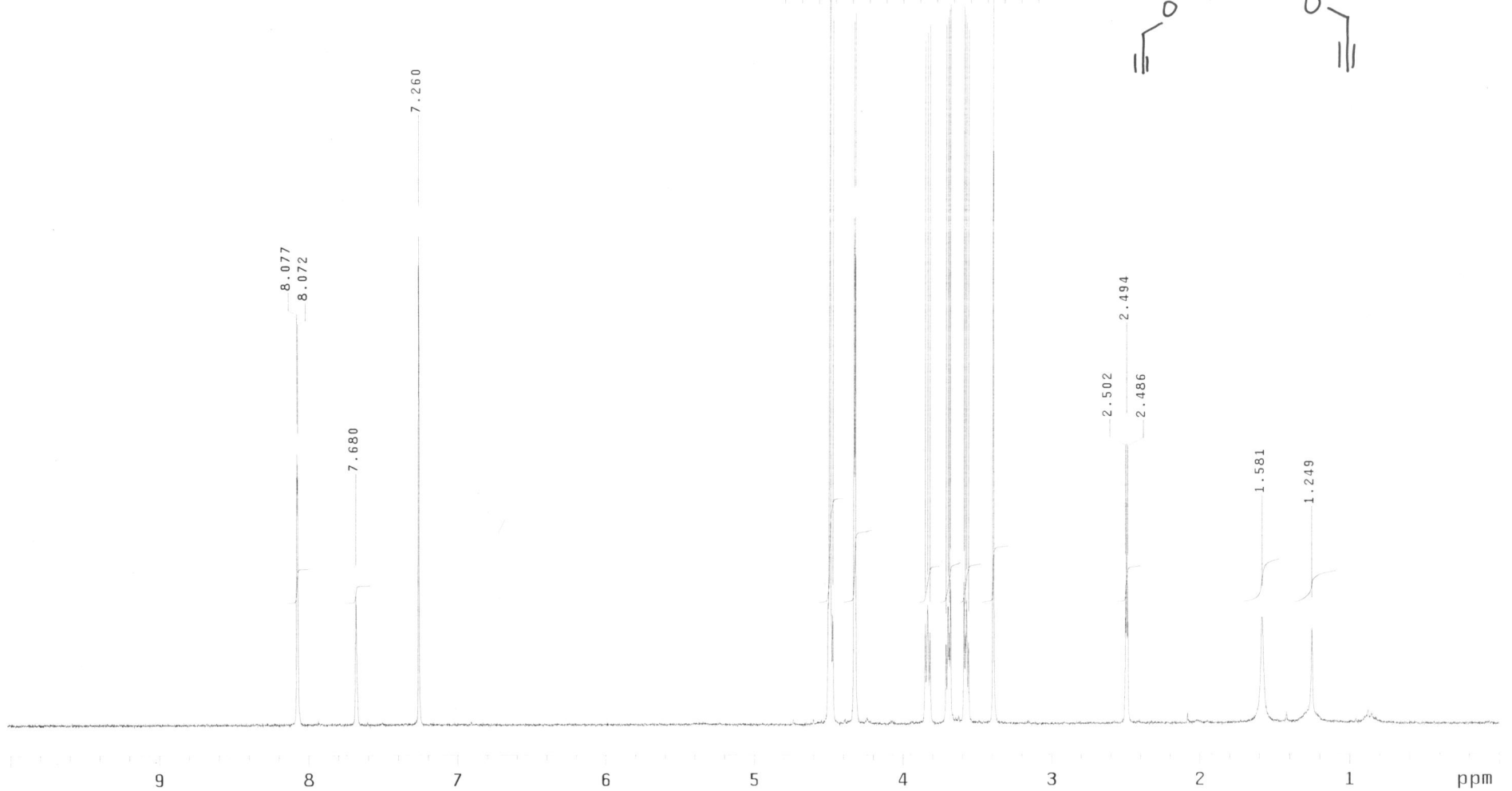
DATA PROCESSING

FT size 32768

Total time 2 min, 5 sec



4.492
4.472
4.328
4.320
3.849
3.833
3.817
3.709
3.694
3.667
3.679
3.588
3.579
3.572
3.558
3.391



1.98
1.00

6.07
4.20
2.10
2.23
2.30
3.27

2.10

2.49
1.82

new experiment

Pulse Sequence: s2pul

Solvent: CDCl3

Temp. 25.0 C / 298.1 K

GEMINI-300BB "gem2300"

Relax. delay 1.000 sec

Pulse 7.8 degrees

Acq. time 1.998 sec

Width 4500.5 Hz

20 repetitions

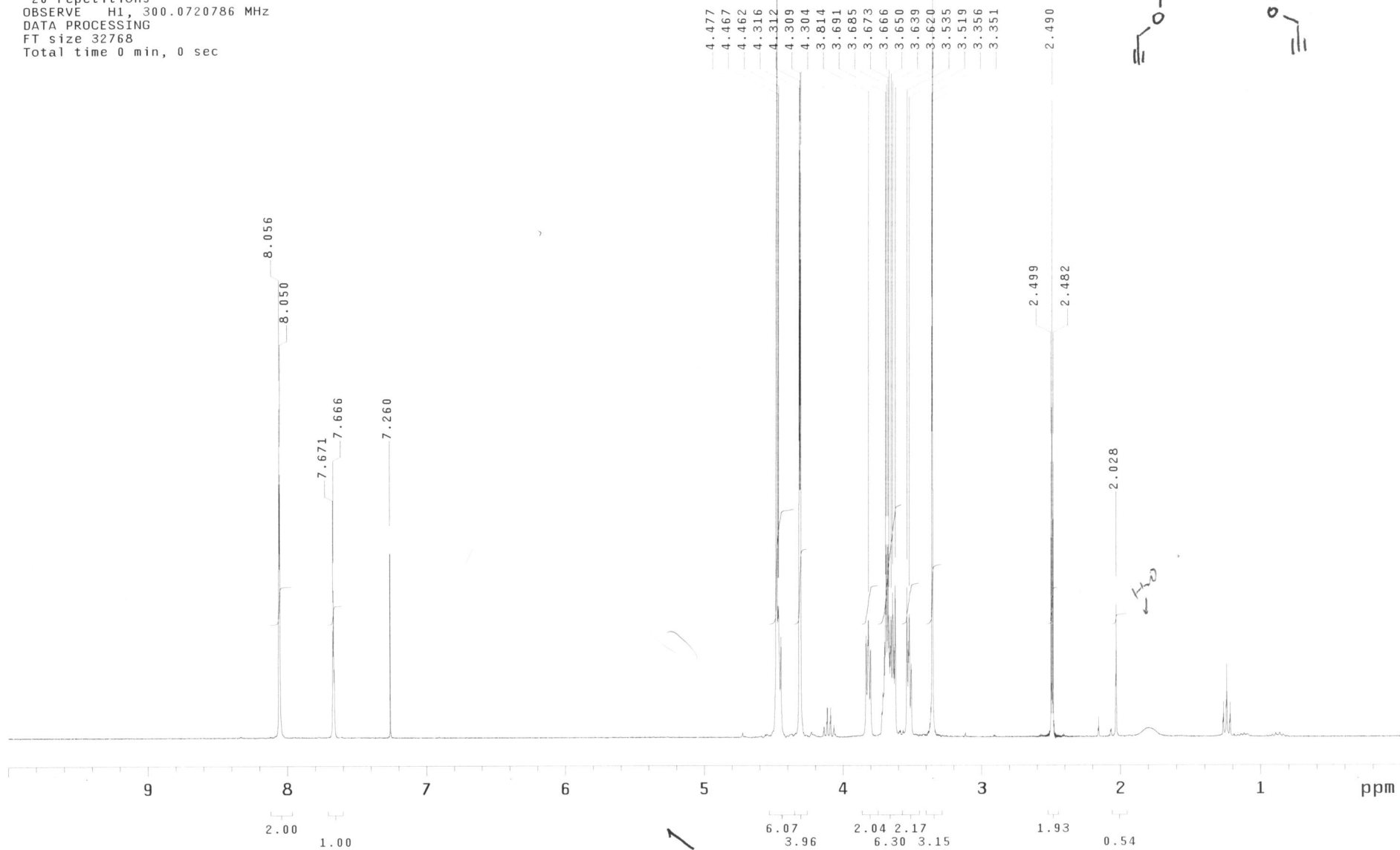
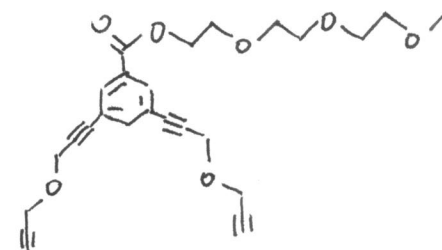
OBSERVE H1, 300.0720786 MHz

DATA PROCESSING

FT size 32768

Total time 0 min, 0 sec

Compound 19



8.294
8.290
8.286
7.957
7.953

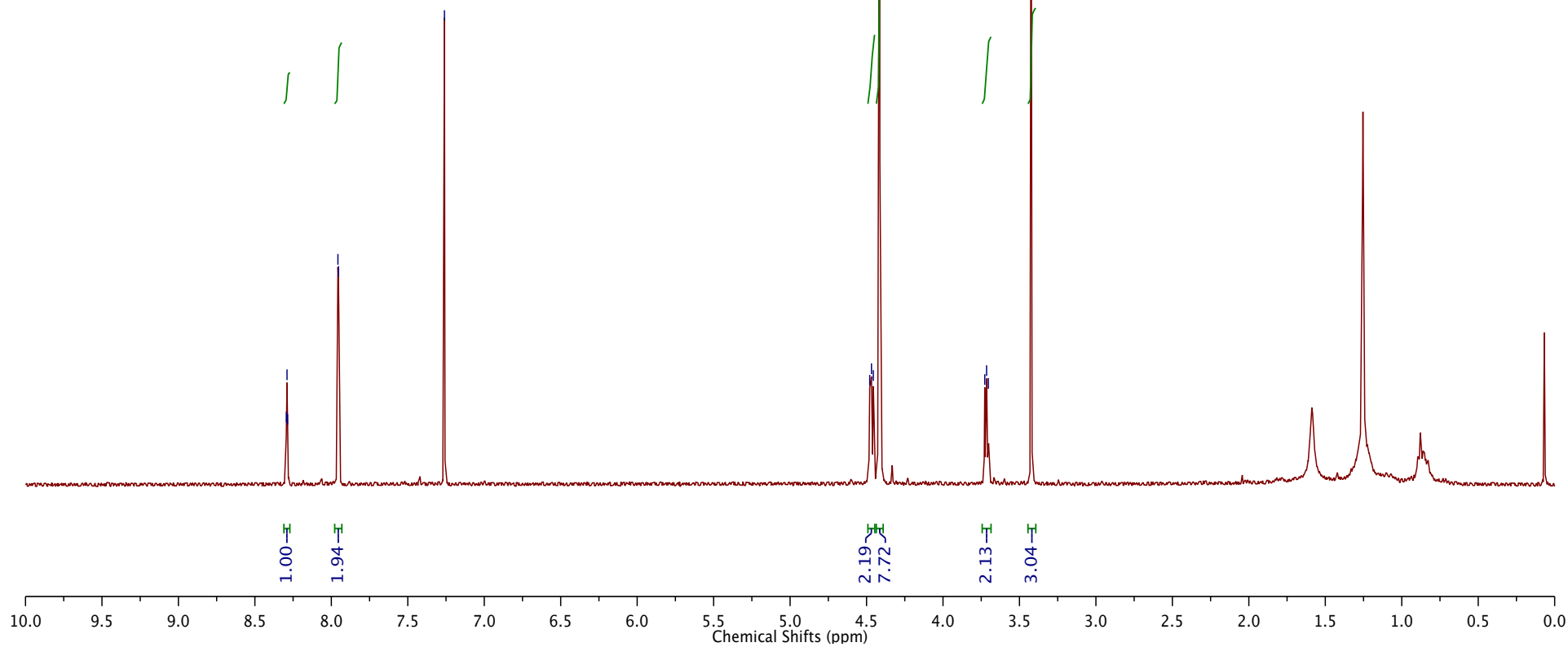
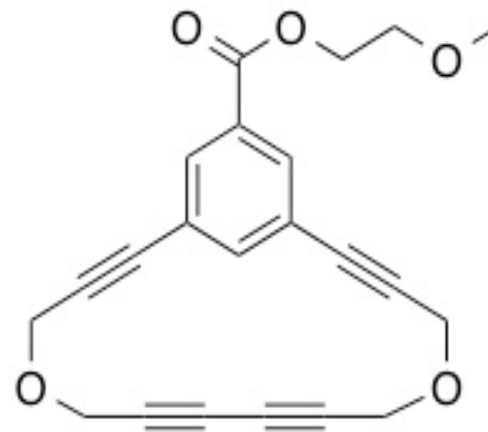
7.260

4.479
4.468
4.456
4.418
4.414

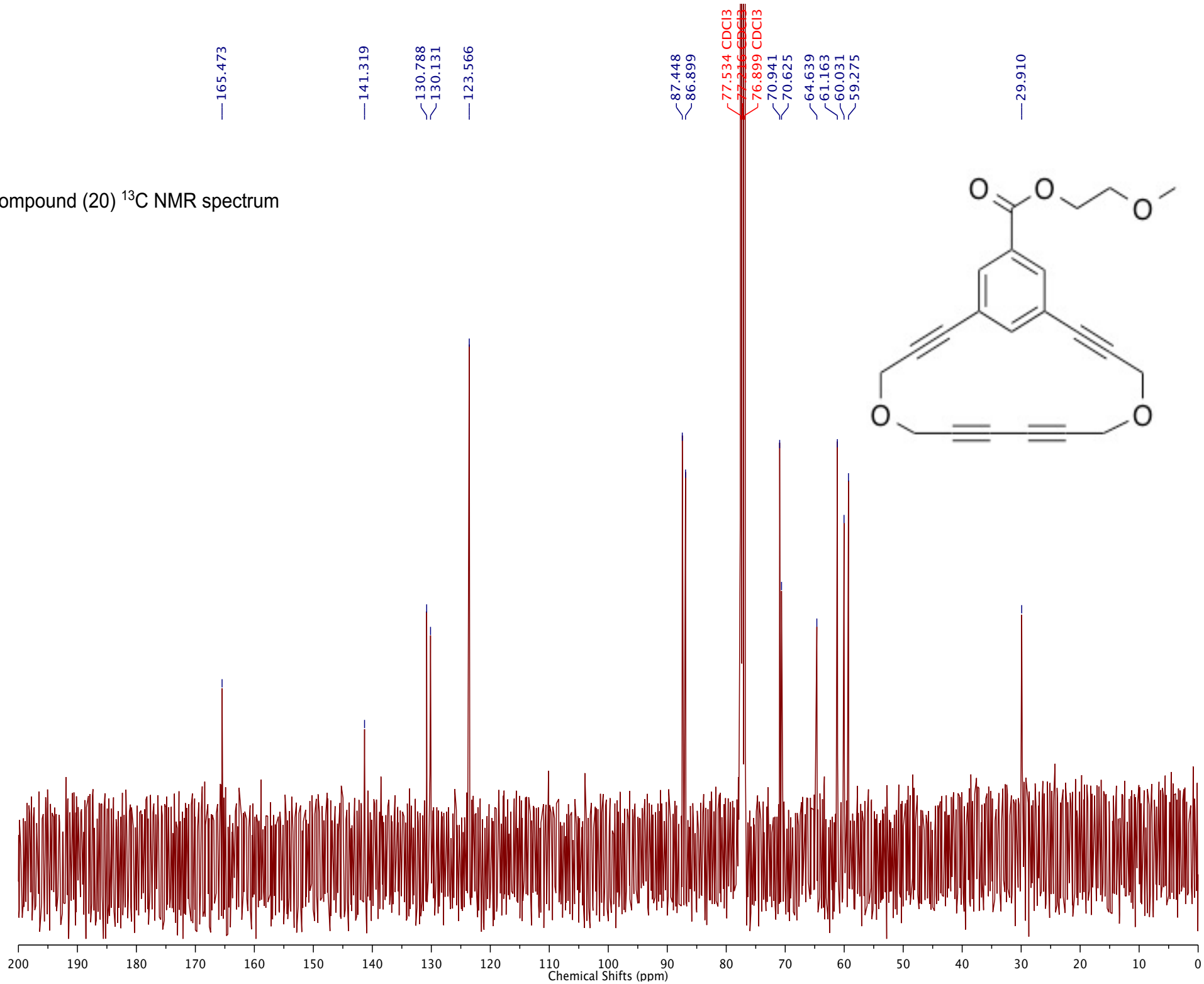
3.727
3.715
3.703
3.424

Compound (20) ¹H NMR spectrum

STATE UNIVERSITY OF NEW YORK
INOVA 400 Mhz SN# S011617
ASWpfg PROBE SN# P005133



Compound (20) ¹³C NMR spectrum



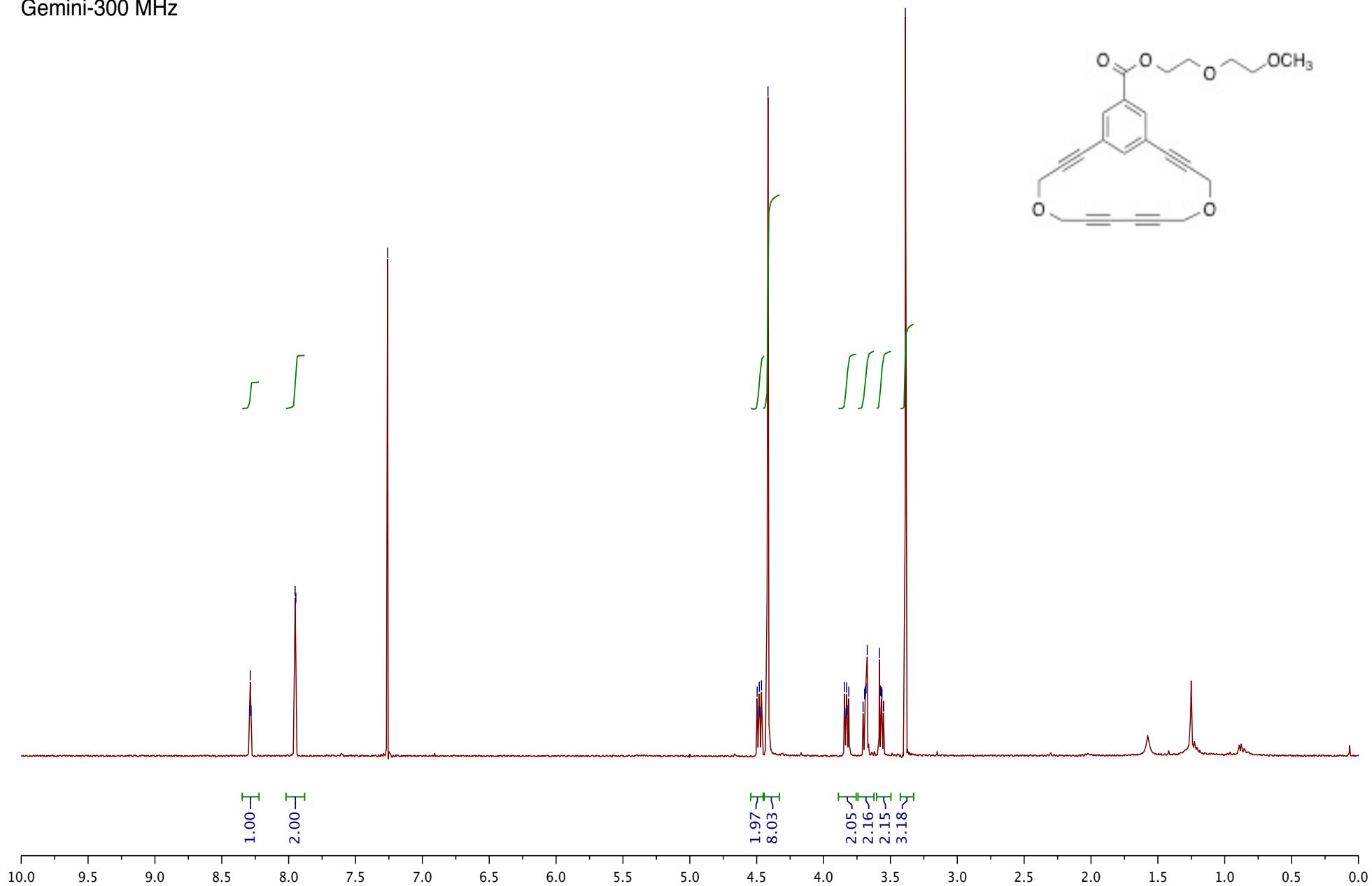
8.292
8.287
8.282
7.951
7.946

7.260

4.496
4.484
4.481
4.476
4.464
4.415
3.843
3.832
3.827
3.823
3.811
3.704
3.693
3.690
3.689
3.682
3.673
3.583
3.574
3.567
3.563
3.553
3.551
3.388

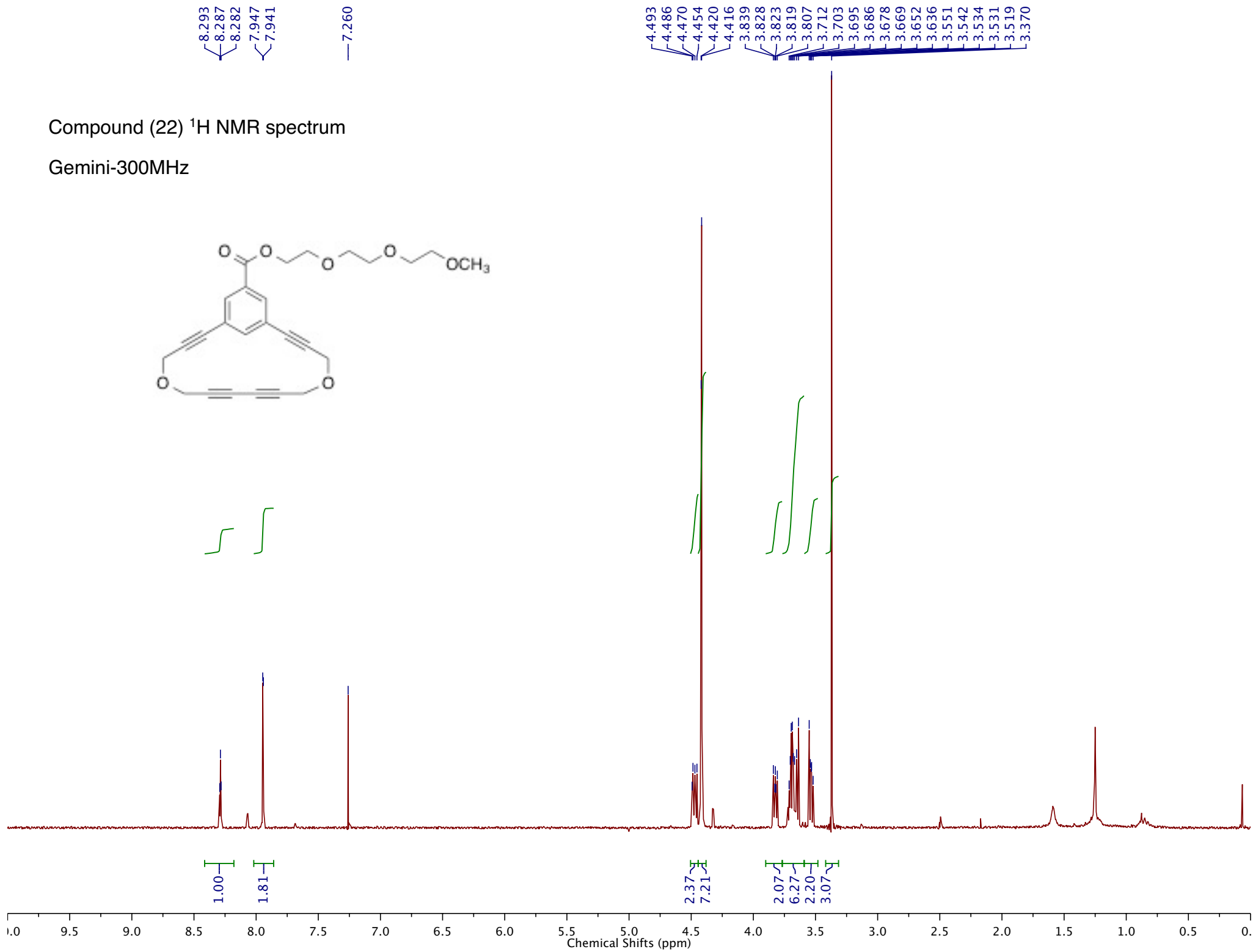
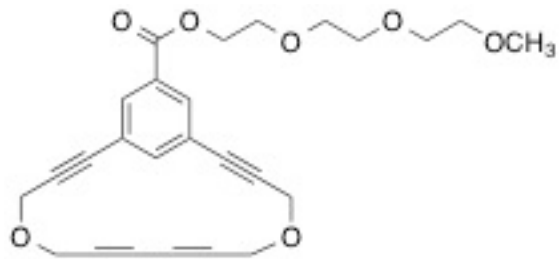
Compound (21) ¹H NMR spectrum

Gemini-300 MHz



Compound (22) ¹H NMR spectrum

Gemini-300MHz

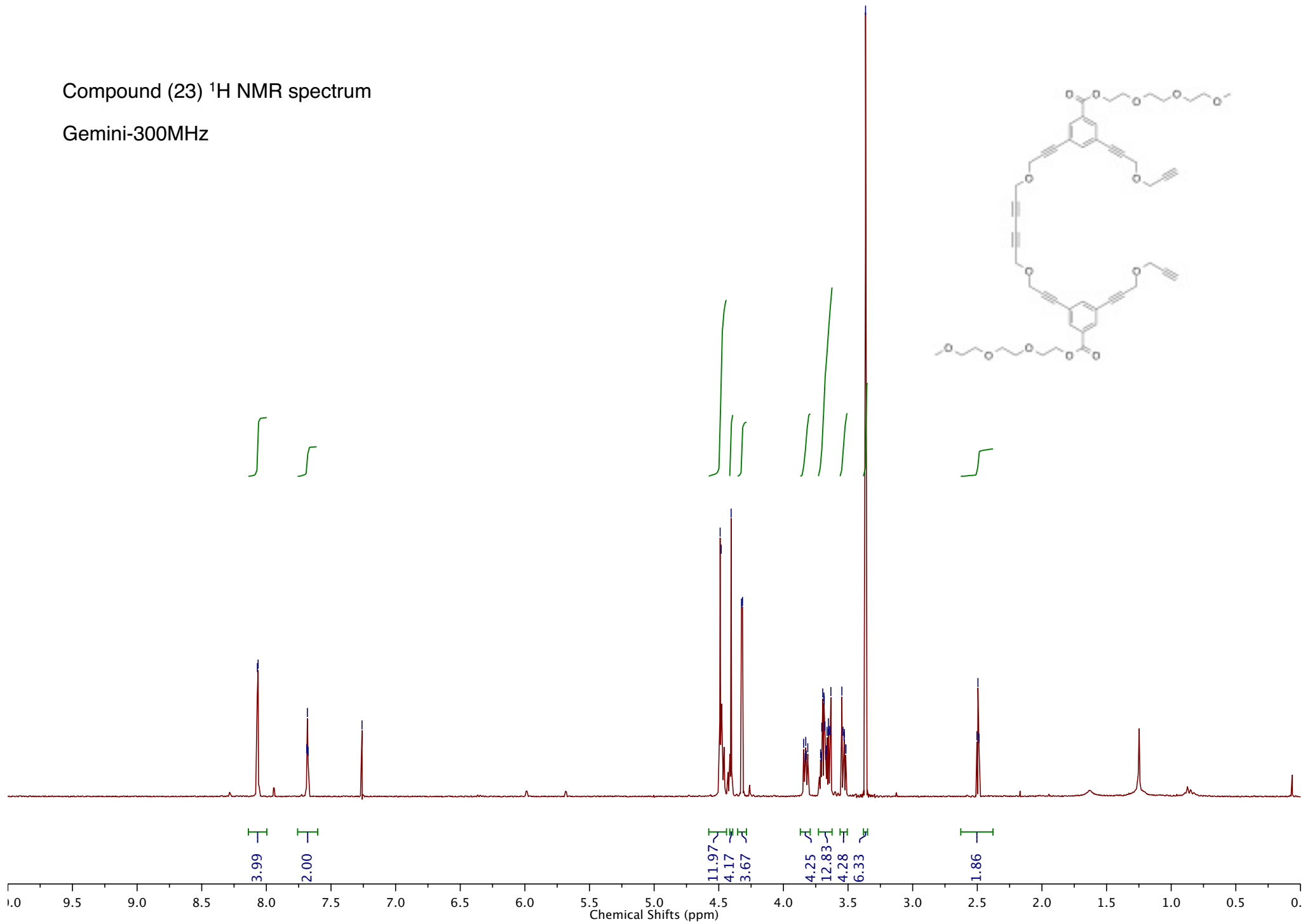
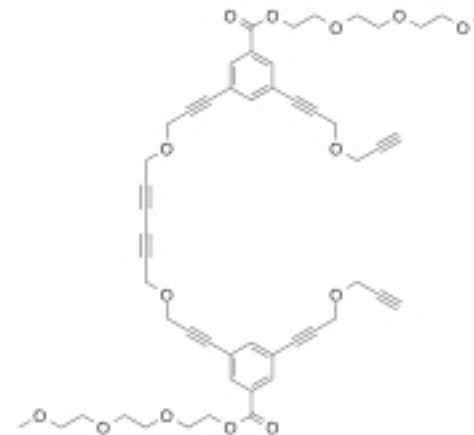


Compound (23) ¹H NMR spectrum

Gemini-300MHz

8.069
8.064
7.688
7.683
7.677
7.260

4.489
4.481
4.404
4.324
4.316
4.316
3.843
3.832
3.827
3.823
3.811
3.712
3.708
3.703
3.695
3.686
3.684
3.678
3.674
3.669
3.662
3.652
3.650
3.642
3.633
3.548
3.539
3.531
3.528
3.518
3.516
3.365
2.503
2.495
2.487

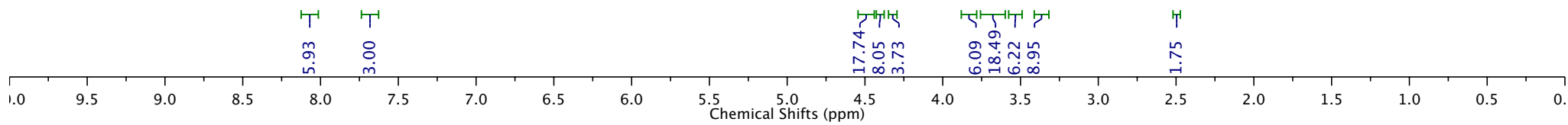
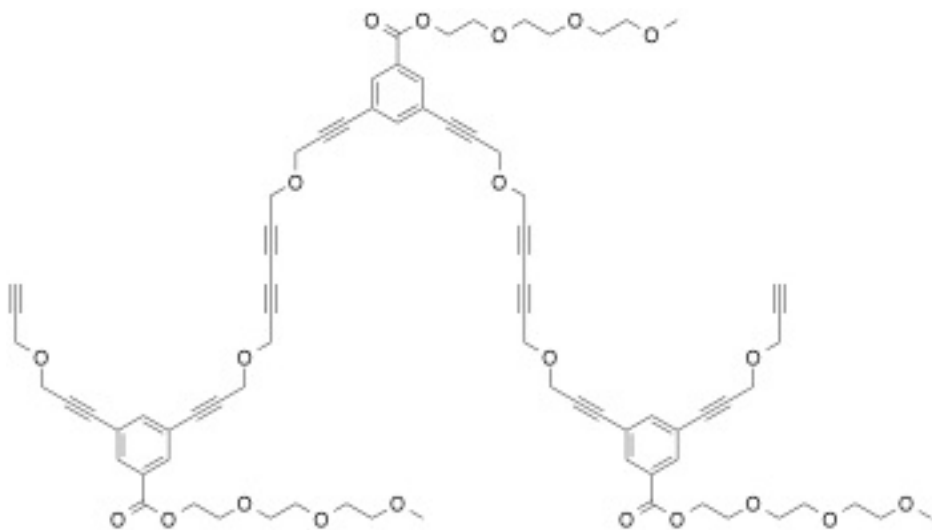


Compound (24) ¹H NMR spectrum

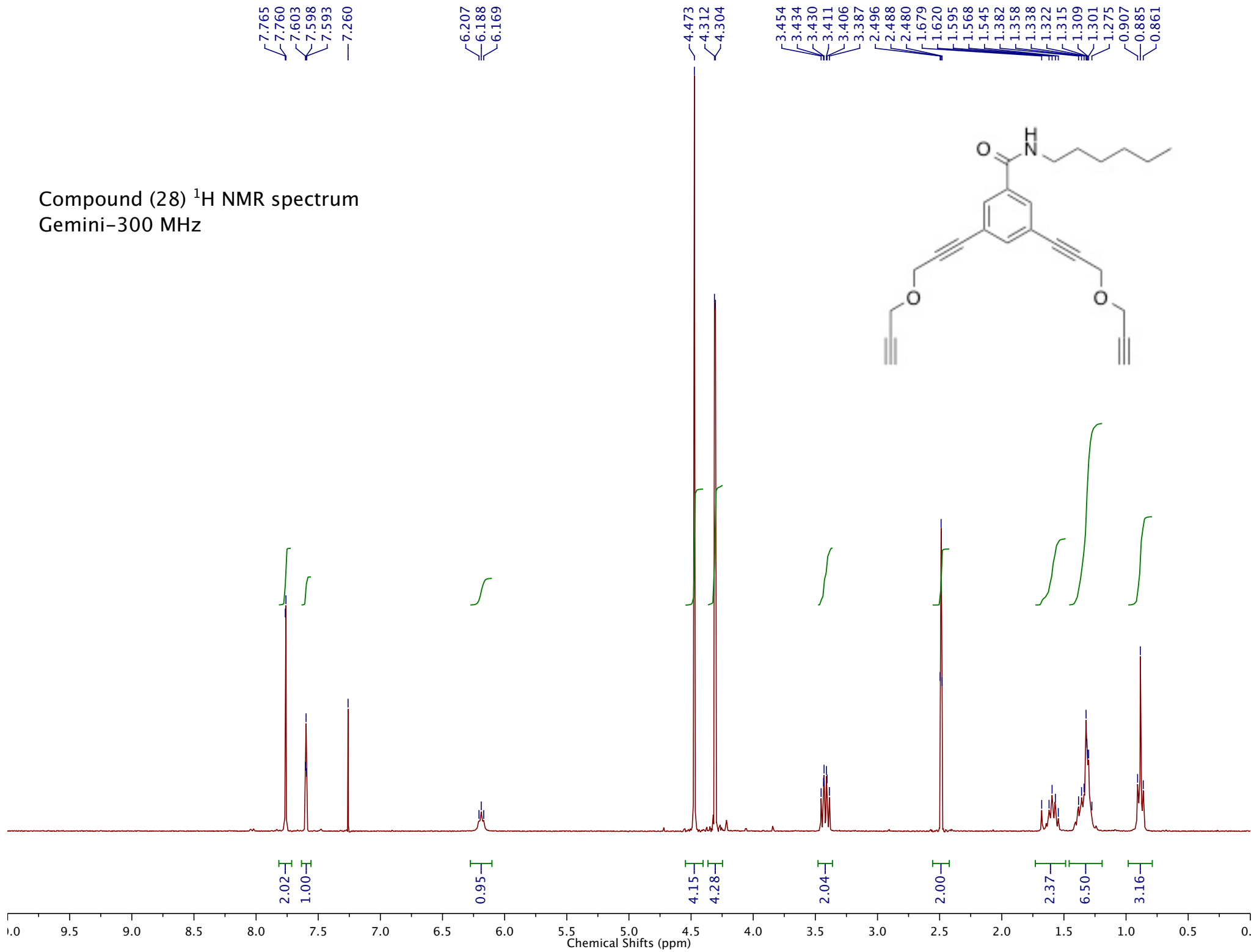
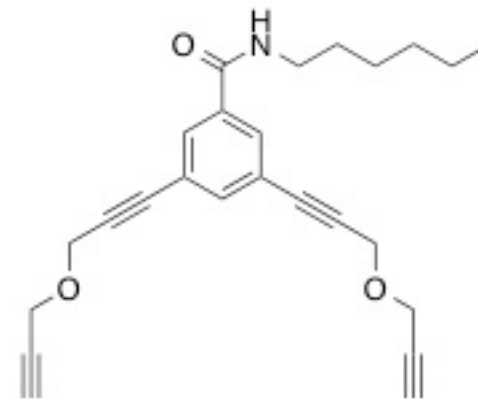
Gemini-300MHz

8.071
8.066
7.689
7.684
7.678
7.260

4.490
4.482
4.404
4.325
4.317
4.317
3.844
3.833
3.828
3.824
3.812
3.713
3.704
3.698
3.696
3.687
3.685
3.679
3.663
3.653
3.649
3.643
3.633
3.549
3.540
3.532
3.529
3.519
3.517
3.365
2.505
2.497
2.489

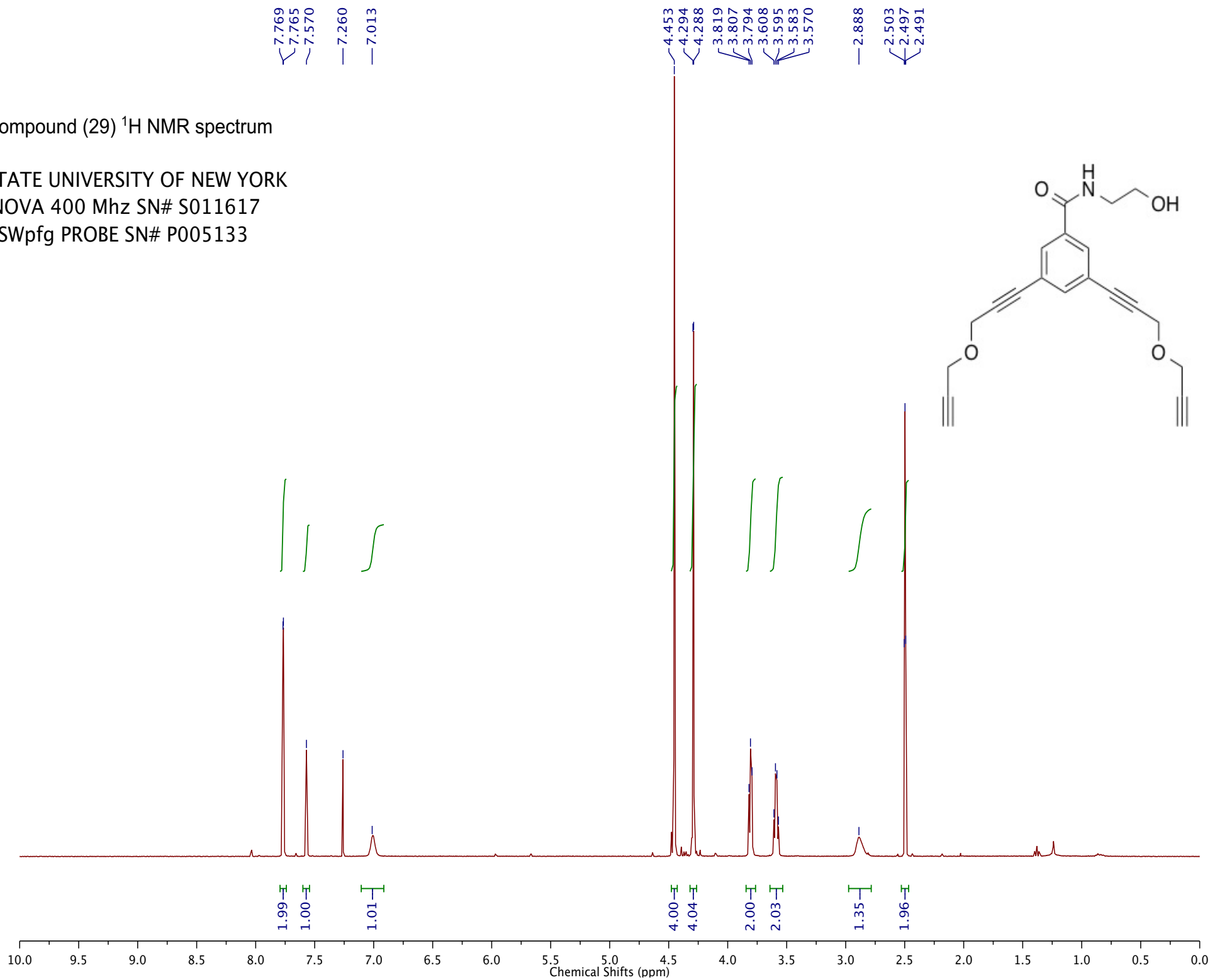
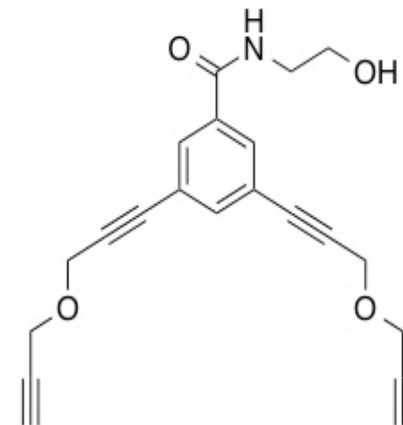


Compound (28) ¹H NMR spectrum
Gemini-300 MHz

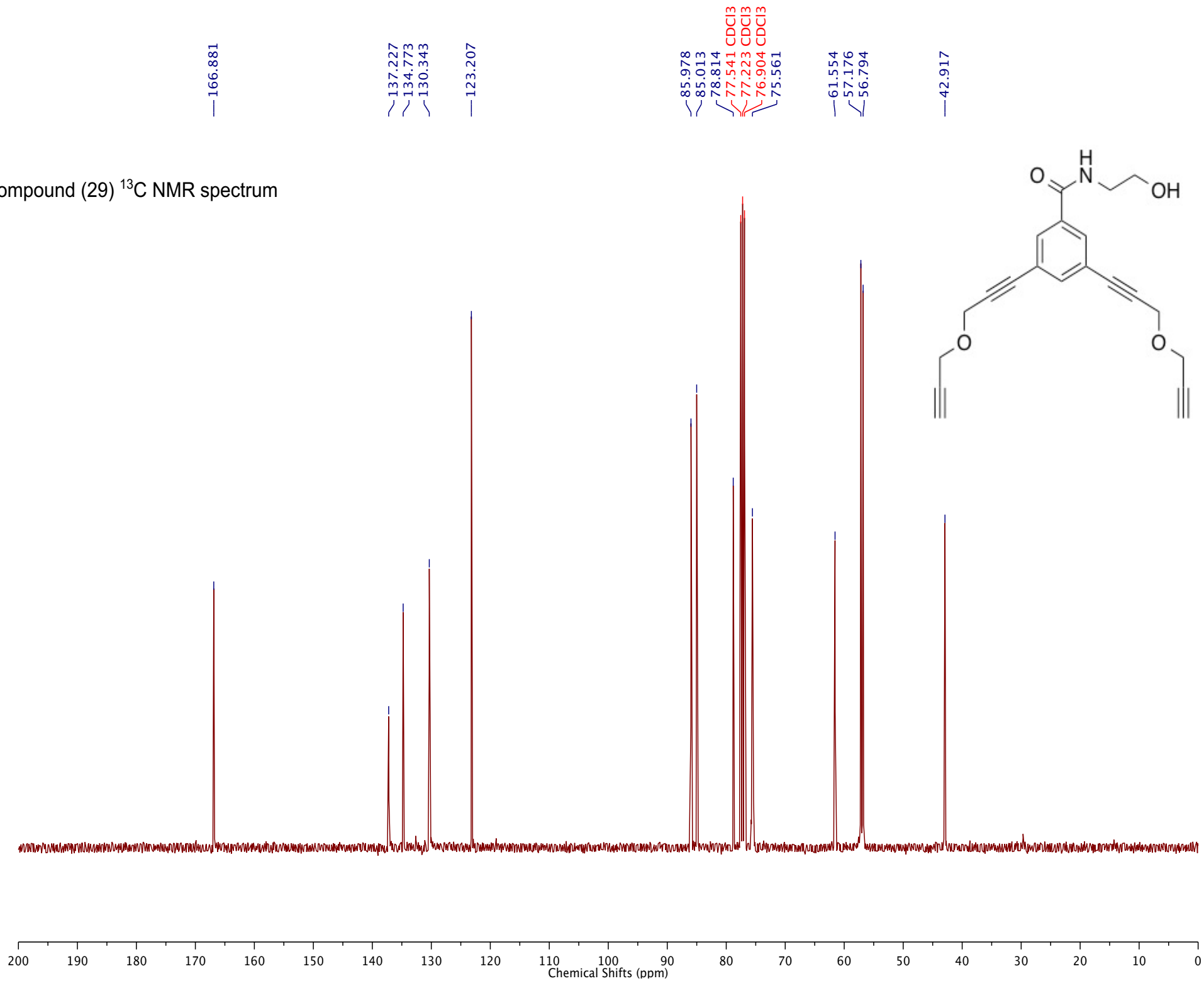


Compound (29) ¹H NMR spectrum

STATE UNIVERSITY OF NEW YORK
INOVA 400 Mhz SN# S011617
ASWpfg PROBE SN# P005133



Compound (29) ¹³C NMR spectrum



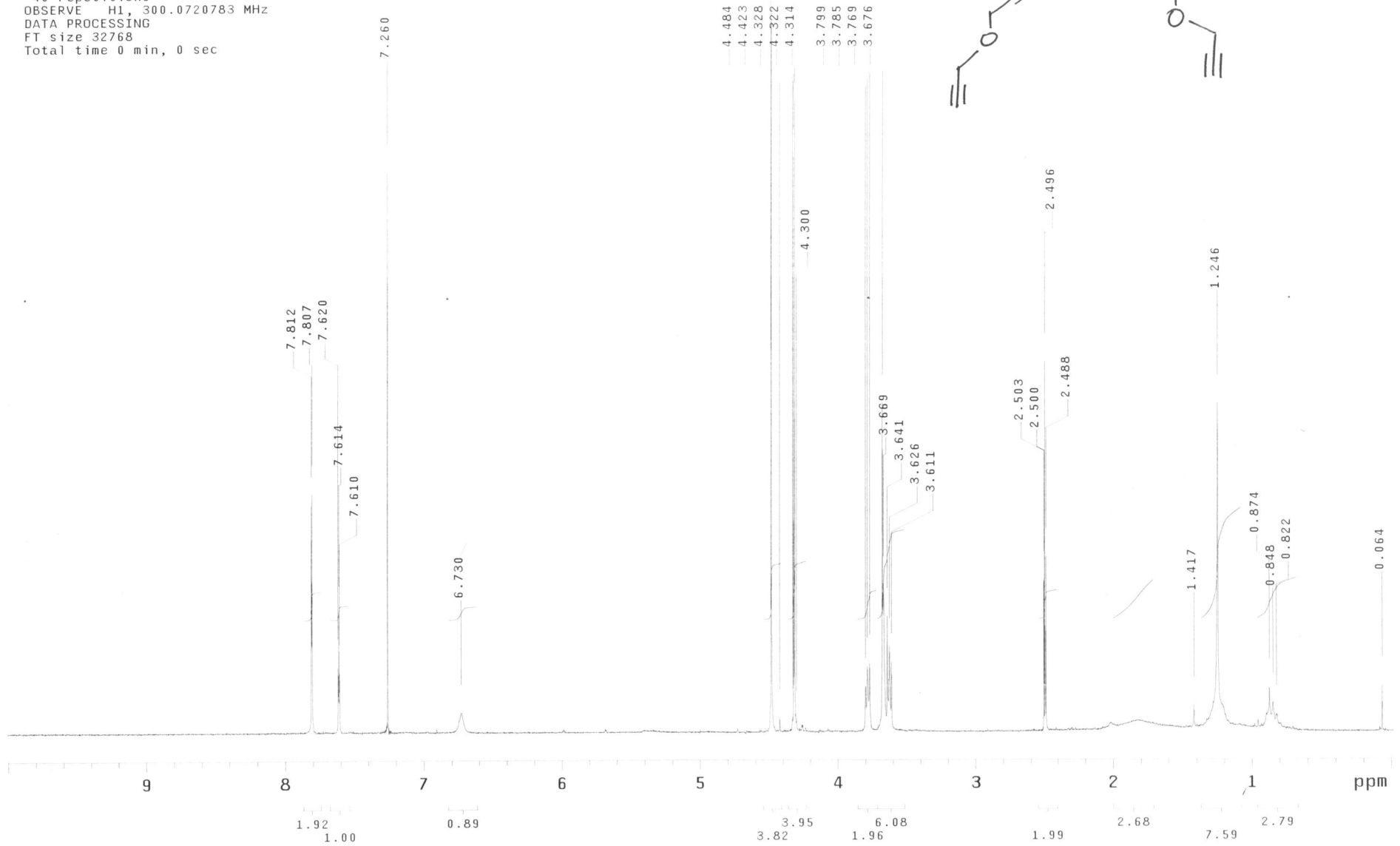
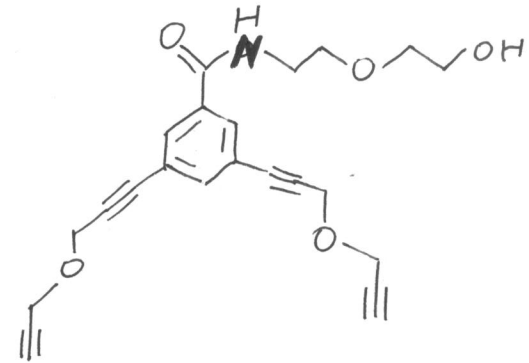
new experiment

Pulse Sequence: s2pul

Solvent: CDCl3
Temp. 25.0 C / 298.1 K
GEMINI-300BB "gem2300"

Relax. delay 1.000 sec
Pulse 7.8 degrees
Acq. time 1.998 sec
Width 4500.5 Hz
40 repetitions
OBSERVE H1, 300.0720783 MHz
DATA PROCESSING
FT size 32768
Total time 0 min, 0 sec

Compound 30



7.446
7.442
7.439
7.407
7.404
7.260

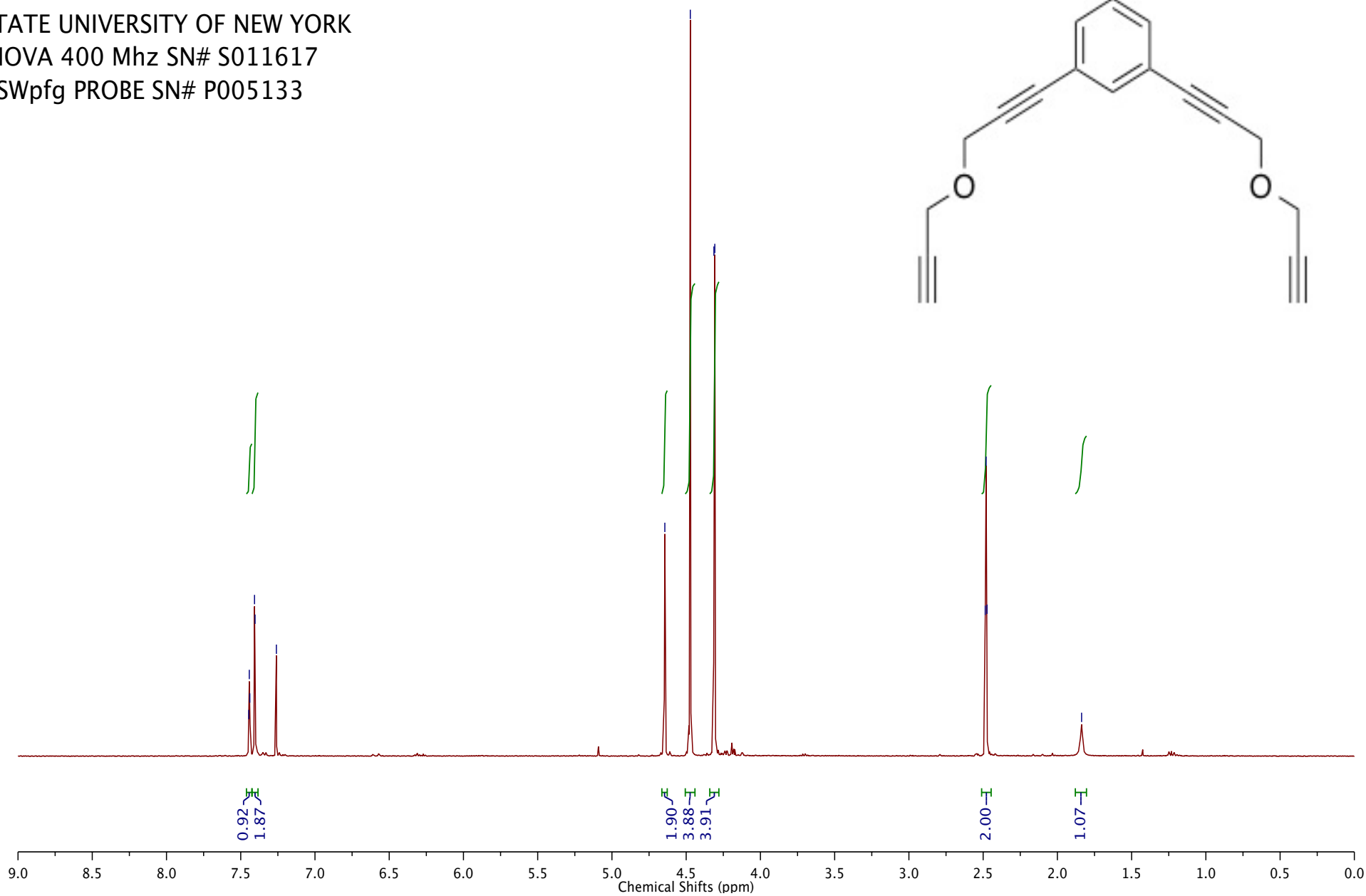
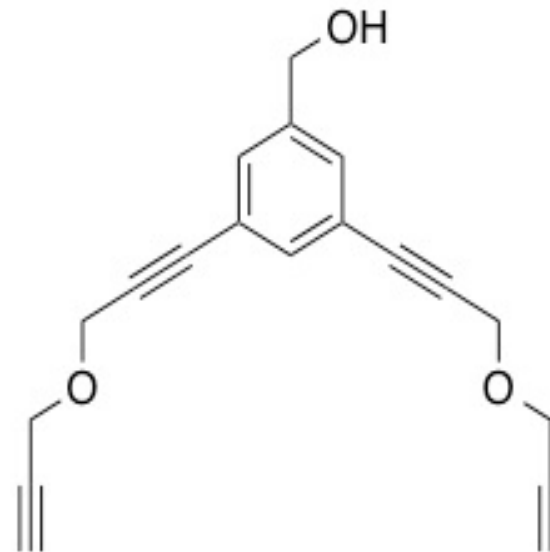
4.644
4.472
4.313
4.307

2.486
2.480
2.474

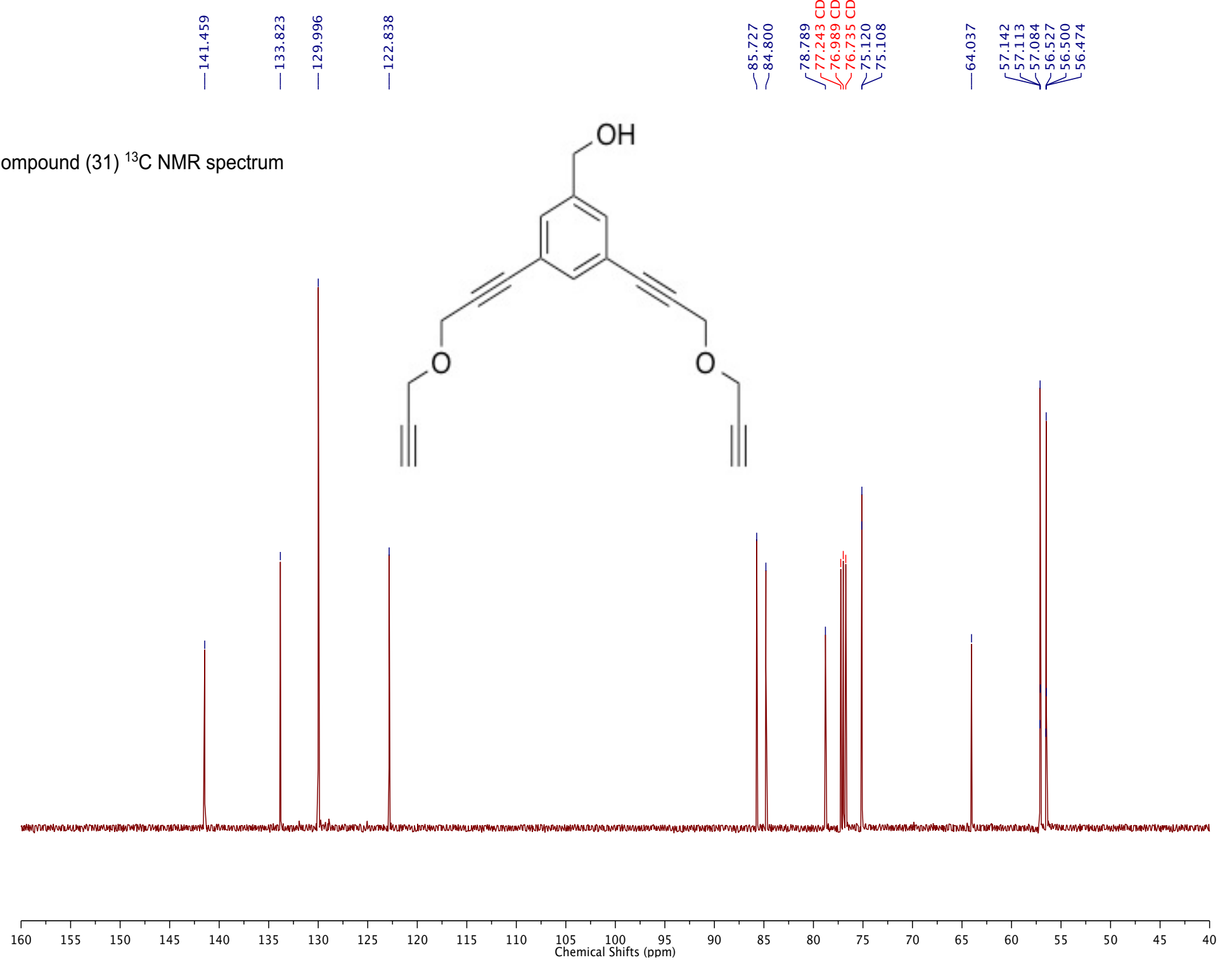
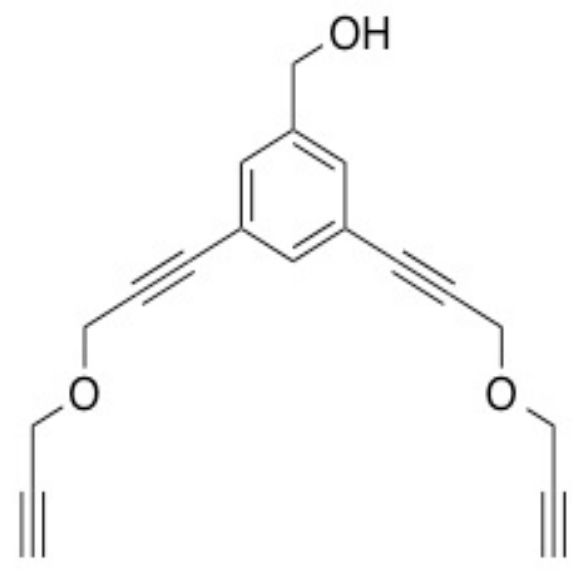
1.837

Compound (31) ¹H NMR spectrum

STATE UNIVERSITY OF NEW YORK
INOVA 400 Mhz SN# S011617
ASWpfg PROBE SN# P005133



Compound (31) ¹³C NMR spectrum



new experiment

Pulse Sequence: s2pul

Solvent: CDCl₃

Temp: 25.0 C / 298.1 K

GEMINI-300BB "gem2300"

Relax. delay 1.000 sec

Pulse 7.8 degrees

Acq. time 1.998 sec

Width 4500.5 Hz

320 repetitions

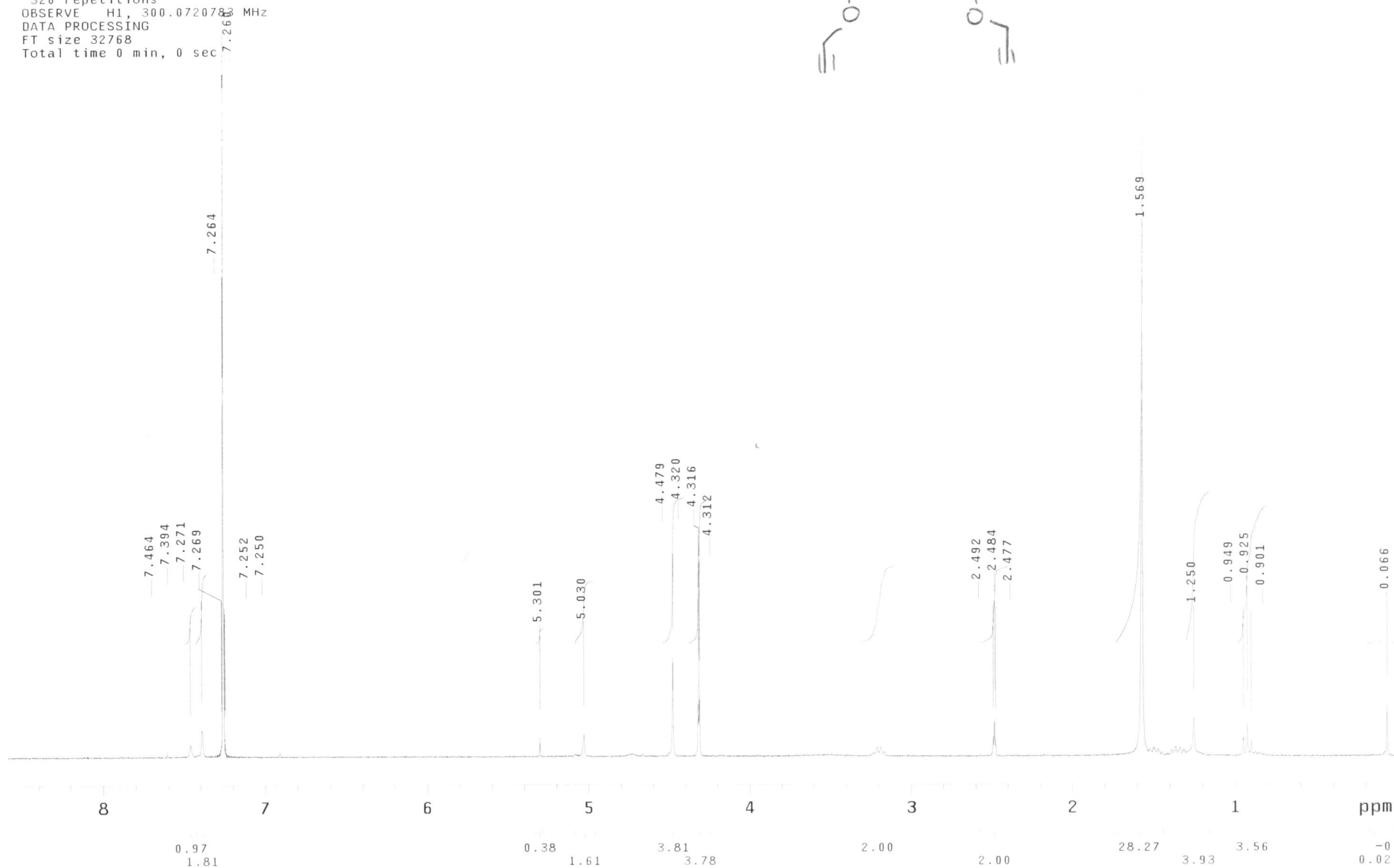
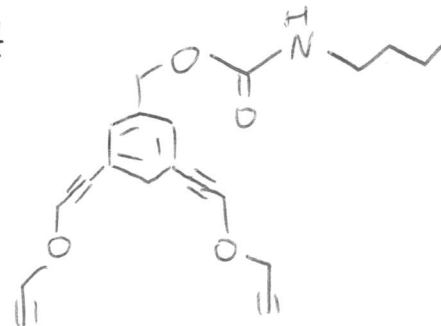
OBSERVE H1, 300.072078 MHz

DATA PROCESSING

FT size 32768

Total time 0 min, 0 sec

Compound 34



7.490
7.487
7.483
7.439
7.435
7.406
7.403
7.385
7.334
7.329
7.316
7.295
7.289
7.260
7.127
7.109
7.098
7.095
7.080
7.077
7.061
6.729

5.137

4.481
4.320
4.314

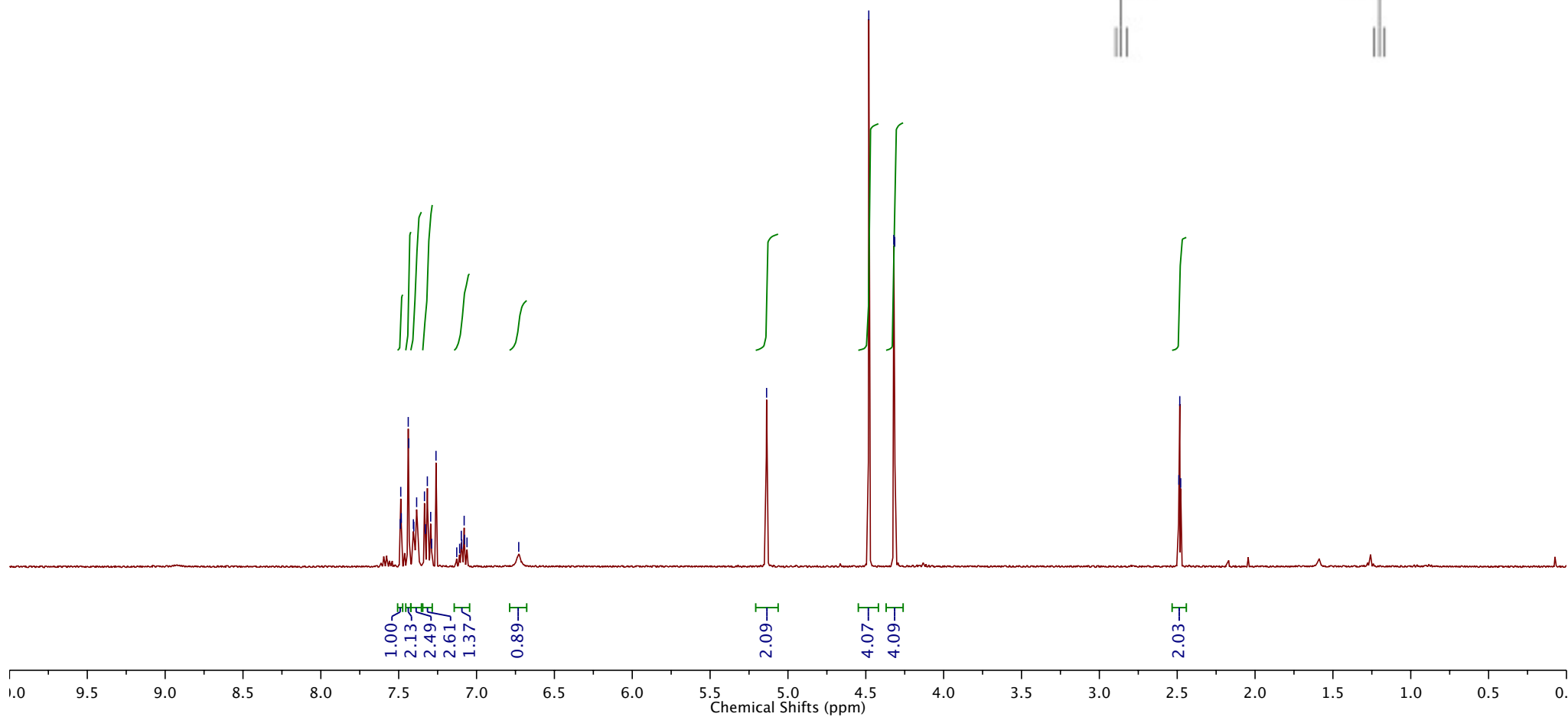
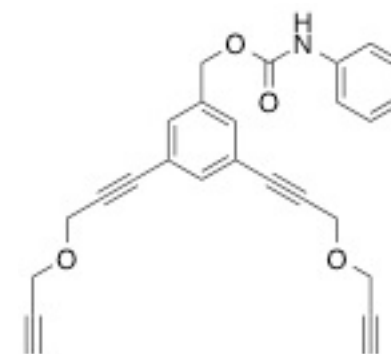
2.489
2.483
2.478

Compound (36) ¹H NMR spectrum

STATE UNIVERSITY OF NEW YORK

INOVA 400 Mhz SN# S011617

ASWpfg PROBE SN# P005133



153.674
153.326

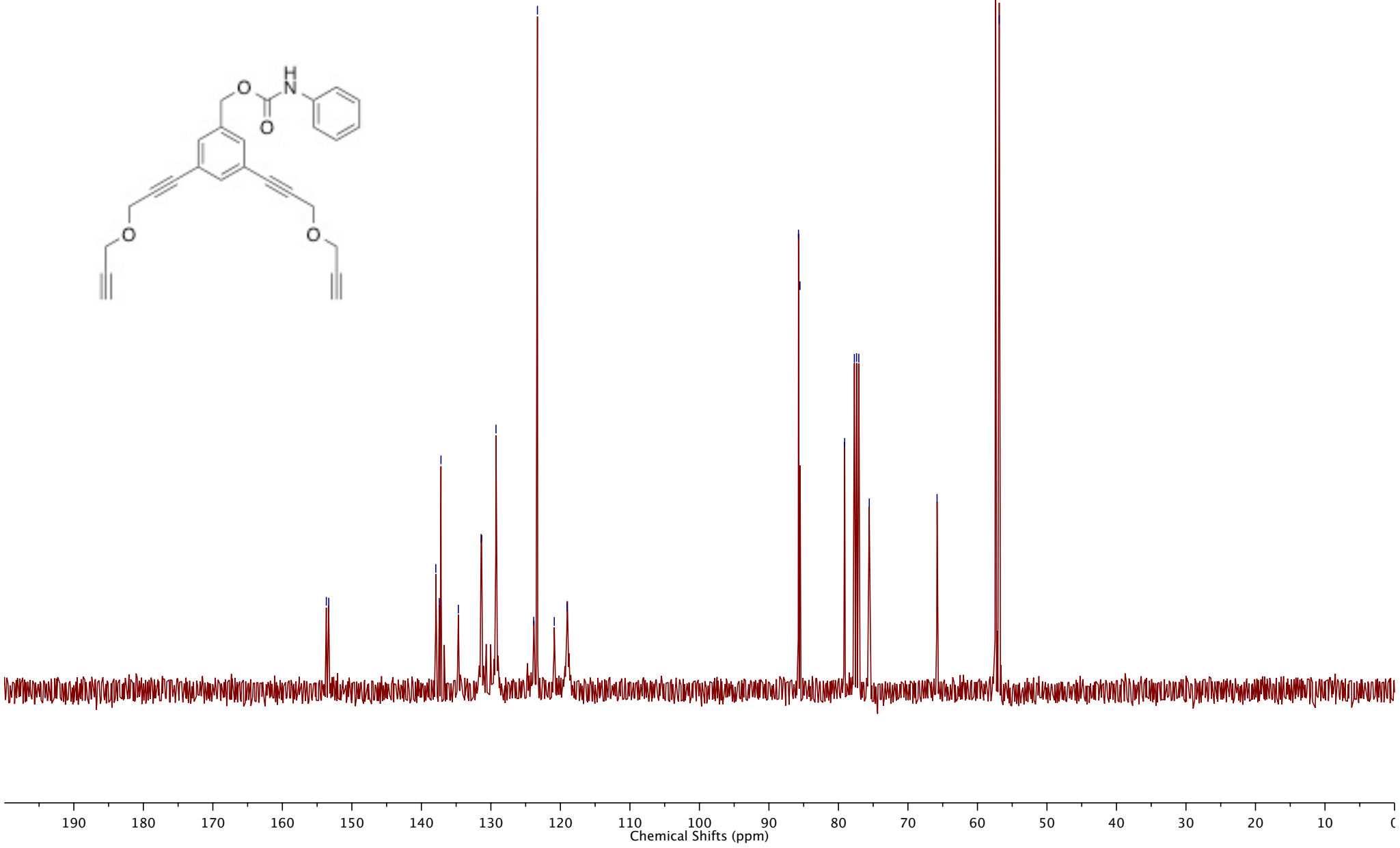
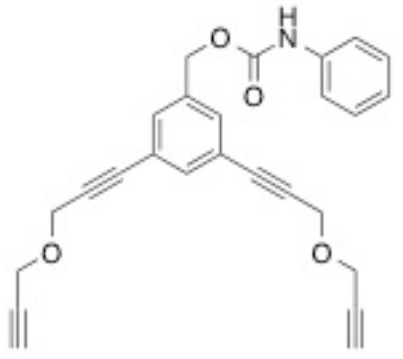
137.923
137.420
137.182
134.679
131.405
129.264
123.839
123.303
120.880
119.045

85.747
85.533
79.105
77.708
77.389
77.070
75.562

65.809

57.396
56.868

Compound (36) ¹³C NMR spectrum



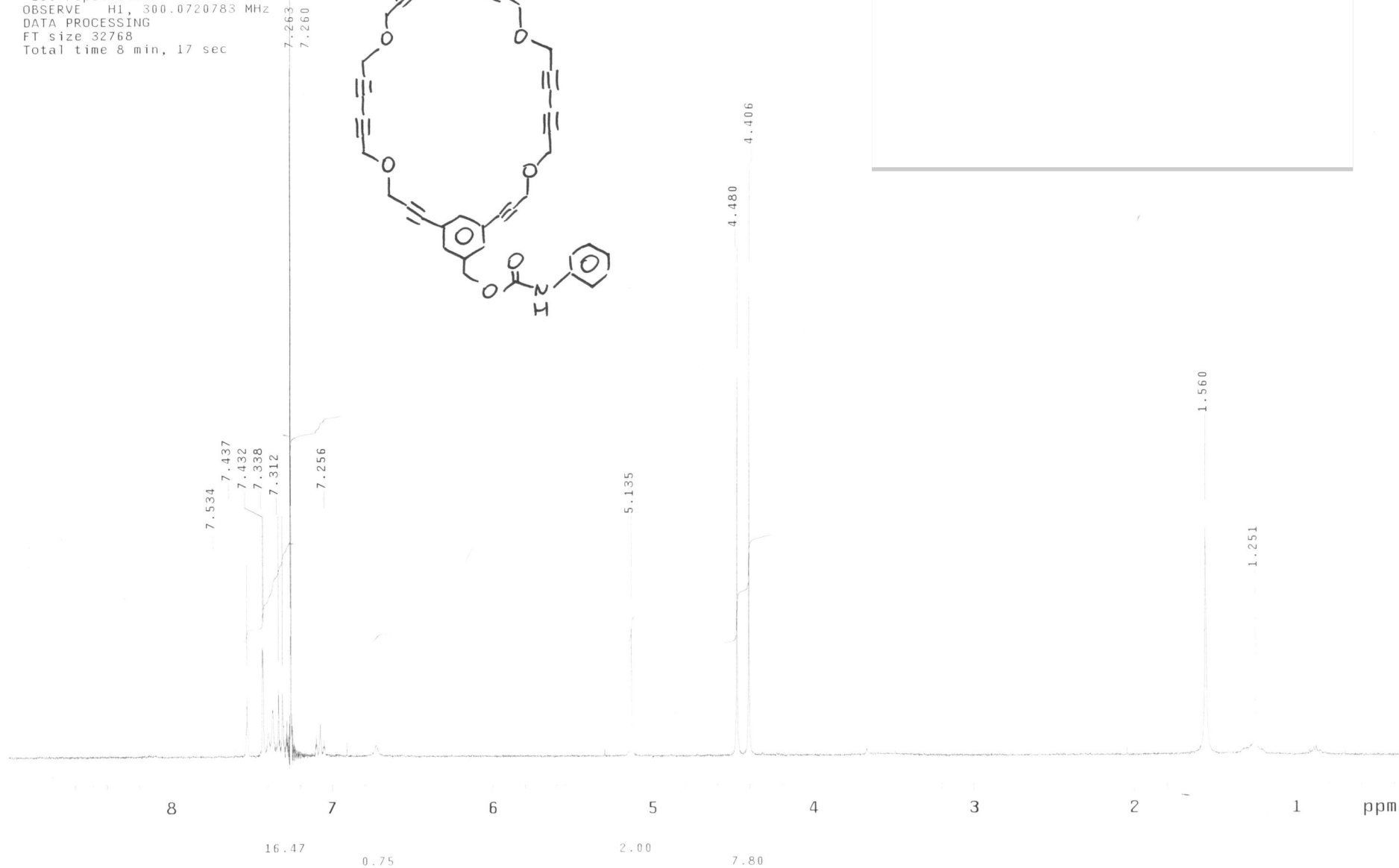
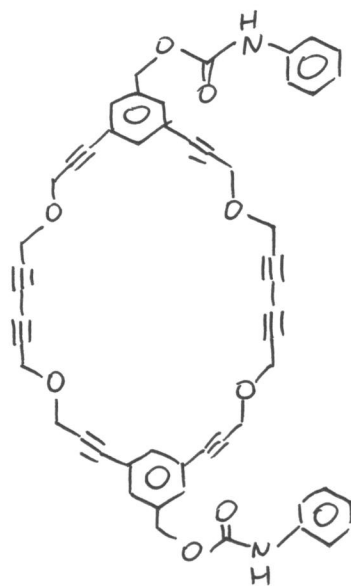
Compound 37

new experiment

Pulse Sequence: s2pul1

Solvent: CDCl₃
 Temp: 25.0 C / 298.1 K
 GEMINI-300BB "gem2300"

Relax. delay 1.000 sec
 Pulse 7.8 degrees
 Acq. time 1.998 sec
 Width 4500.5 Hz
 160 repetitions
 OBSERVE H1, 300.0720783 MHz
 DATA PROCESSING
 FT size 32768
 Total time 8 min, 17 sec



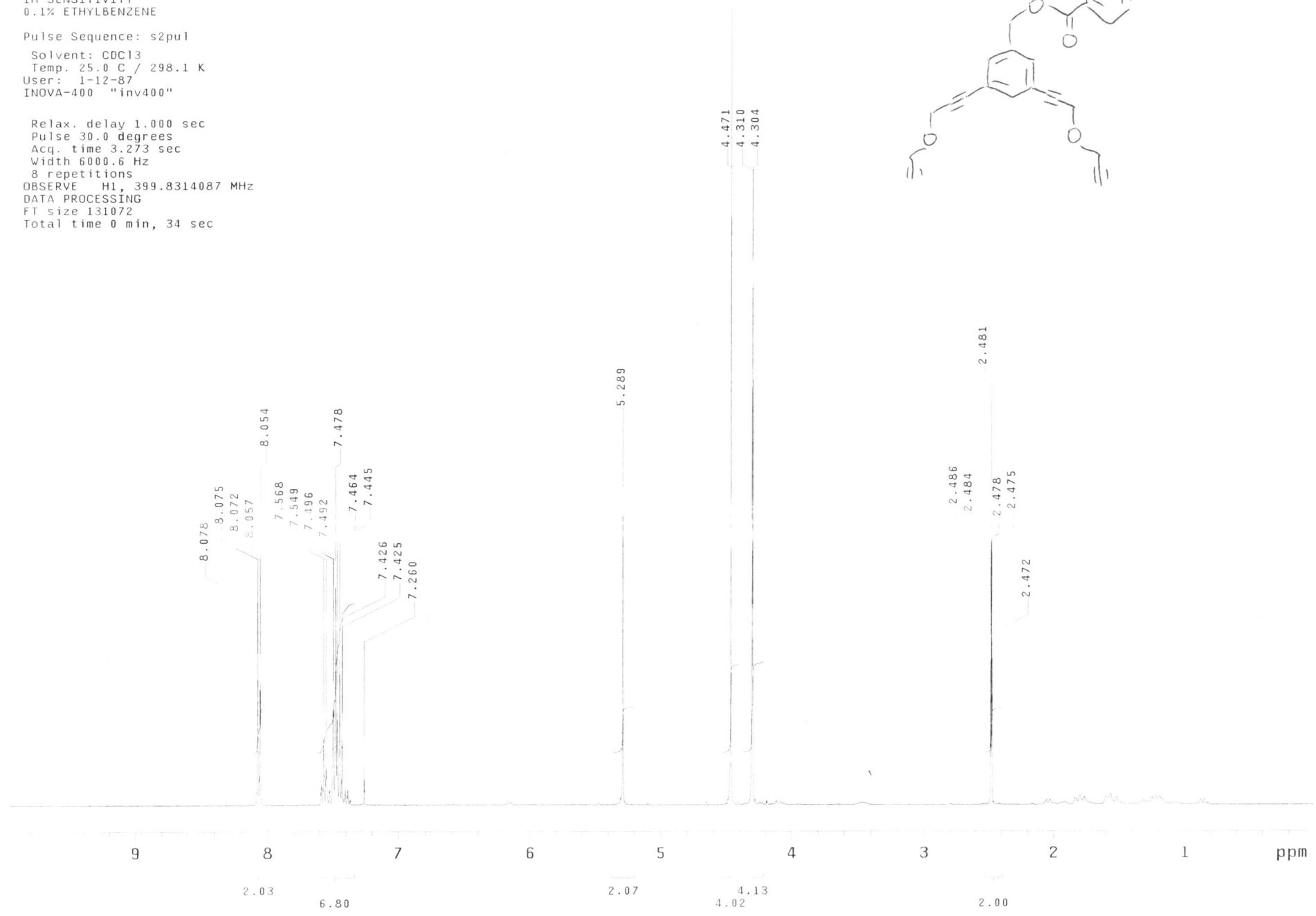
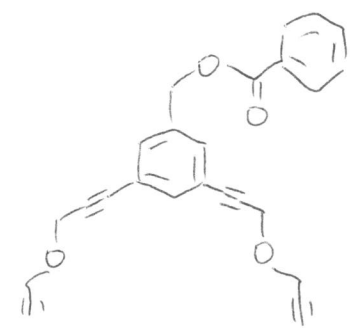
Compound 38

STATE UNIVERSITY OF NEW YORK
INOVA 400 Mhz SN# S011617
ASWpfg PROBE SN# P005133-

1H SENSITIVITY
0.1% ETHYLBENZENE

Pulse Sequence: s2pul
Solvent: CDCl3
Temp: 25.0 C / 298.1 K
User: 1-12-87
INOVA-400 "inv400"

Relax. delay 1.000 sec
Pulse 30.0 degrees
Acq. time 3.273 sec
Width 6000.6 Hz
8 repetitions
OBSERVE H1, 399.8314087 MHz
DATA PROCESSING
FT size 131072
Total time 0 min, 34 sec



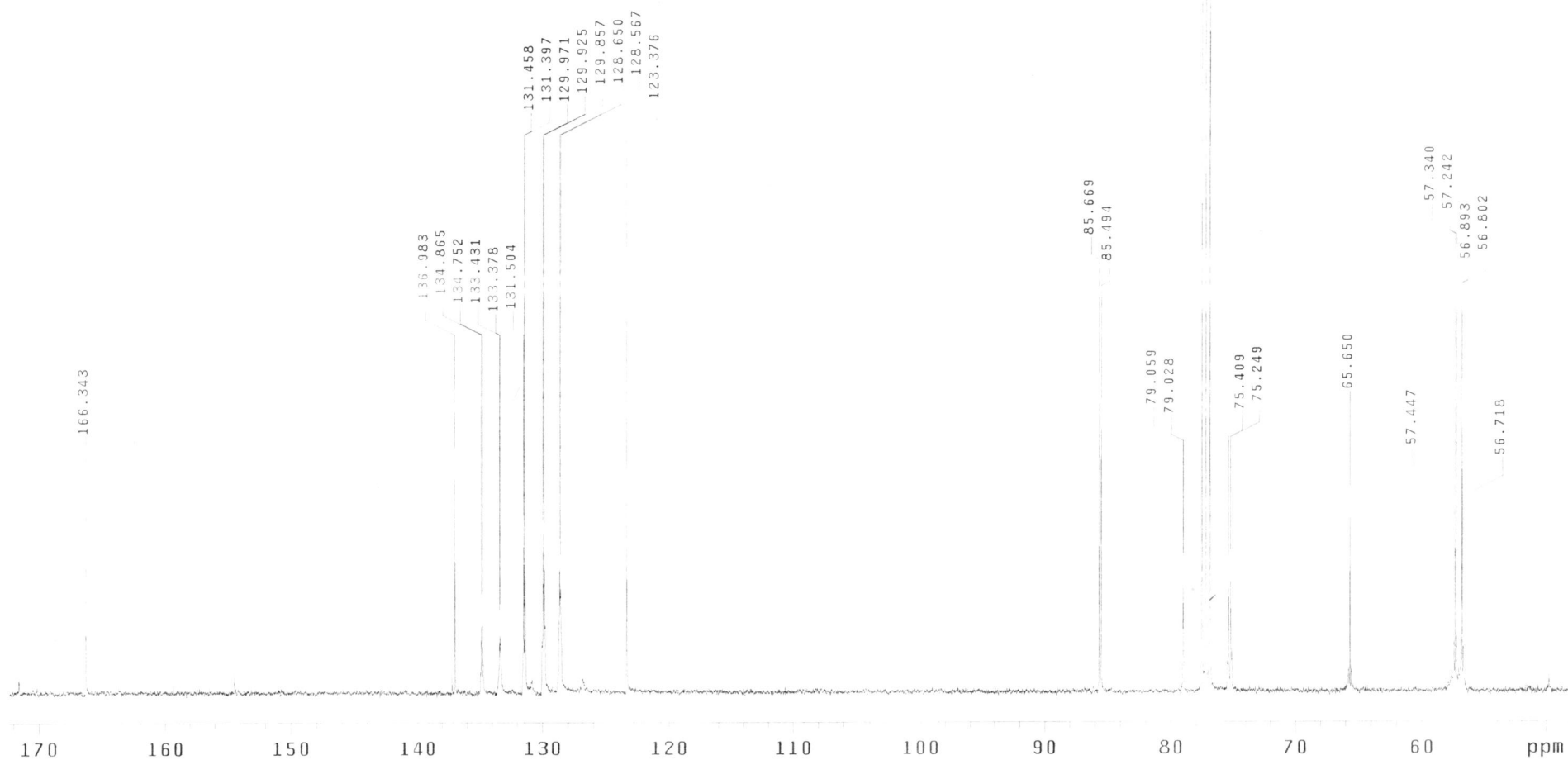
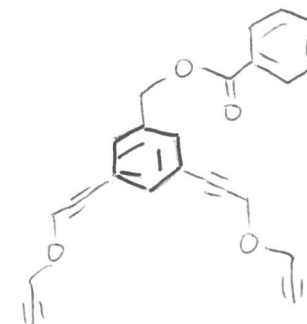
13C OBSERVE

Pulse Sequence: s2pul

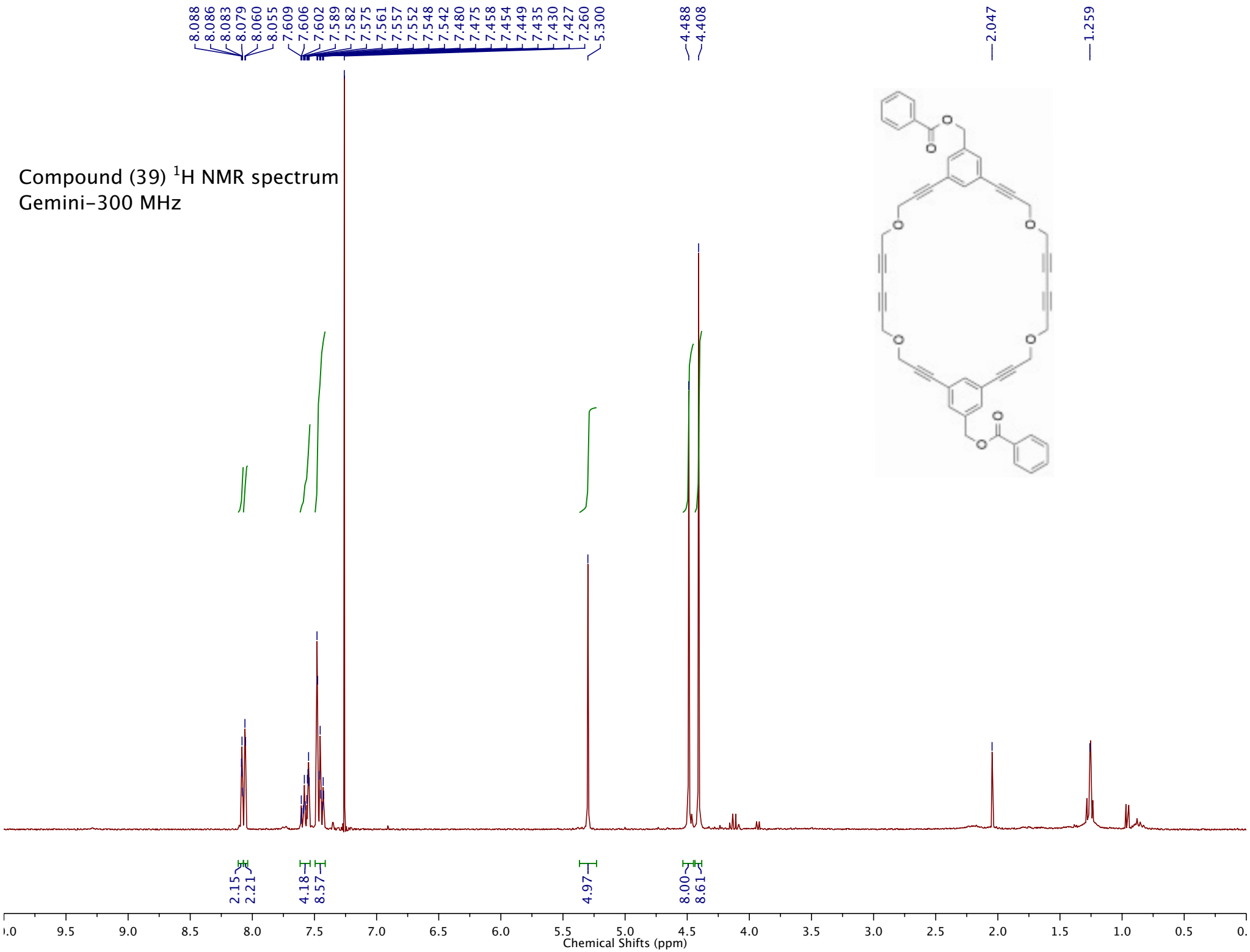
Solvent: CDCl3
Temp. 25.0 C / 298.1 K
INOVA-400 "inv400"

Relax. delay 1.000 sec
Pulse 66.3 degrees
Acq. time 1.199 sec
Width 25000.0 Hz
2560 repetitions
OBSERVE C13, 100.5376702 MHz
DECOUPLE H1, 399.8334198 MHz
Power 47 dB
continuously on
WALTZ-16 modulated
DATA PROCESSING
Line broadening 1.0 Hz
FT size 65536
Total time 6 hr, 8 min, 2 sec

Compound 38



Compound (39) ¹H NMR spectrum
Gemini-300 MHz



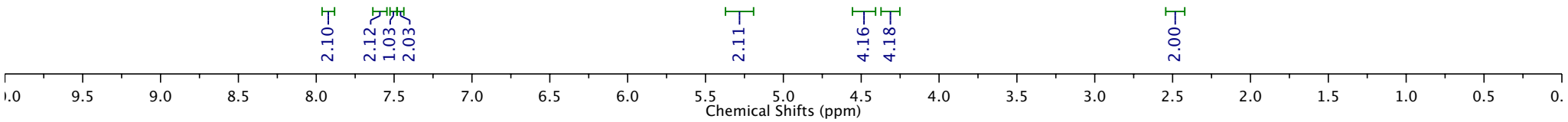
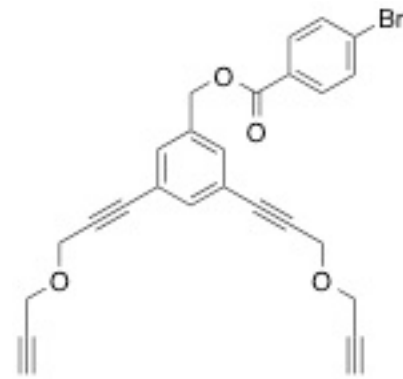
Compound (40) ¹H NMR spectrum
Gemini-300 MHz

7.944
7.937
7.930
7.914
7.907
7.900
7.612
7.605
7.598
7.582
7.576
7.568
7.508
7.503
7.498
7.465
7.460
7.261

5.279

4.477
4.316
4.308

2.493
2.485
2.477



STANDARD CARBON PARAMETERS

Data Collected on:
 inv500-inova500
 Archive directory:
 /export/home/bliu/vnmrsys/data
 Sample directory:

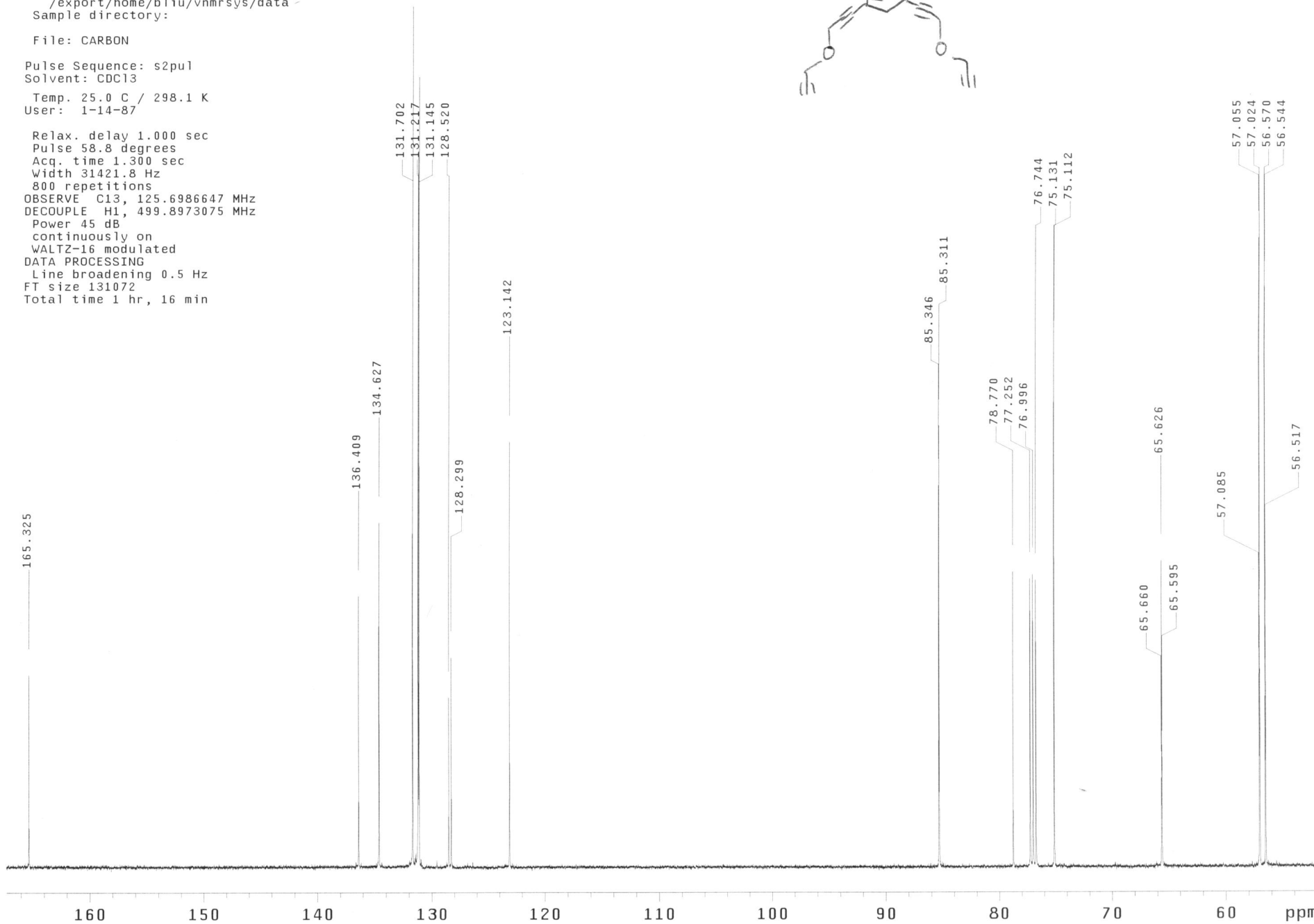
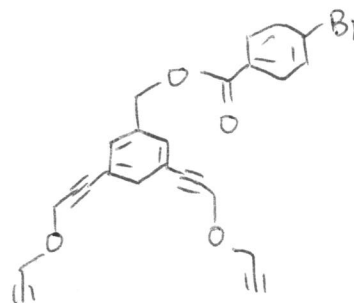
File: CARBON

Pulse Sequence: s2pul
 Solvent: CDCl3

Temp. 25.0 C / 298.1 K
 User: 1-14-87

Relax. delay 1.000 sec
 Pulse 58.8 degrees
 Acq. time 1.300 sec
 Width 31421.8 Hz
 800 repetitions
 OBSERVE C13, 125.6986647 MHz
 DECOUPLE H1, 499.8973075 MHz
 Power 45 dB
 continuously on
 WALTZ-16 modulated
 DATA PROCESSING
 Line broadening 0.5 Hz
 FT size 131072
 Total time 1 hr, 16 min

Compound 40

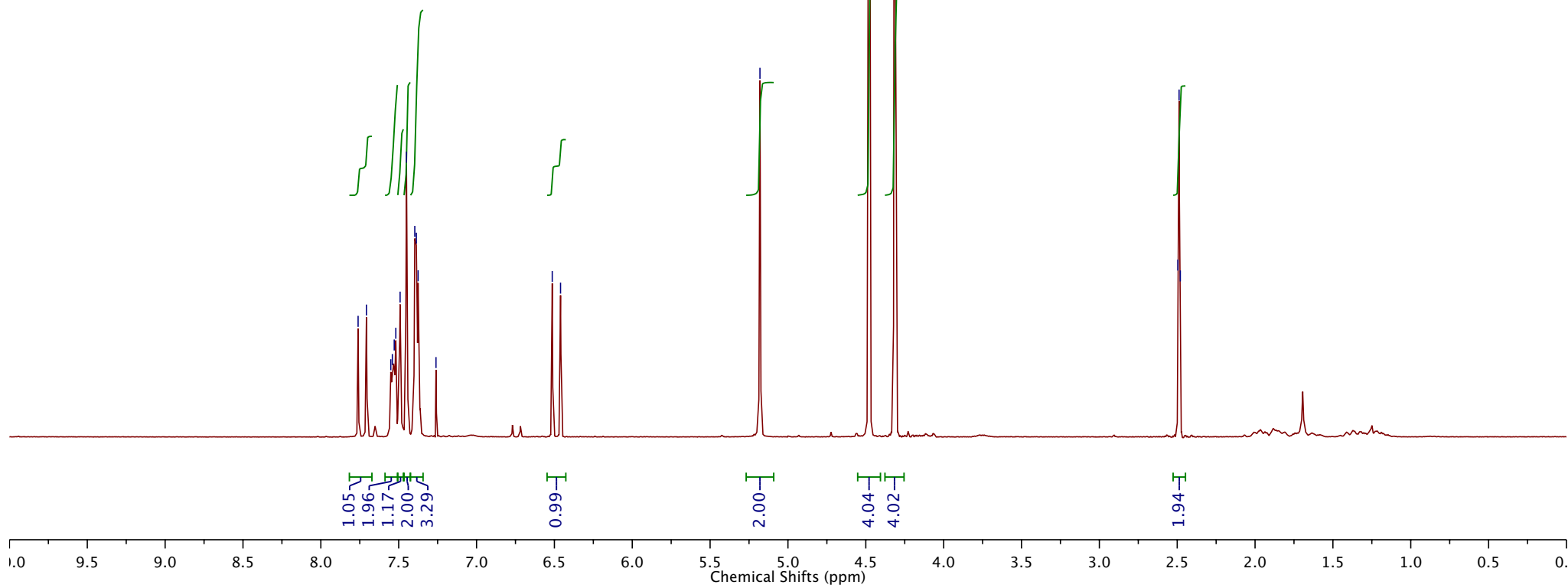
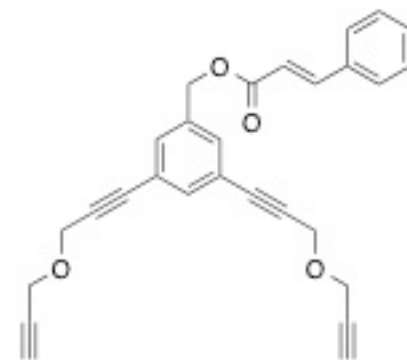


Compound (42) ¹H NMR spectrum
Gemini-300 MHz

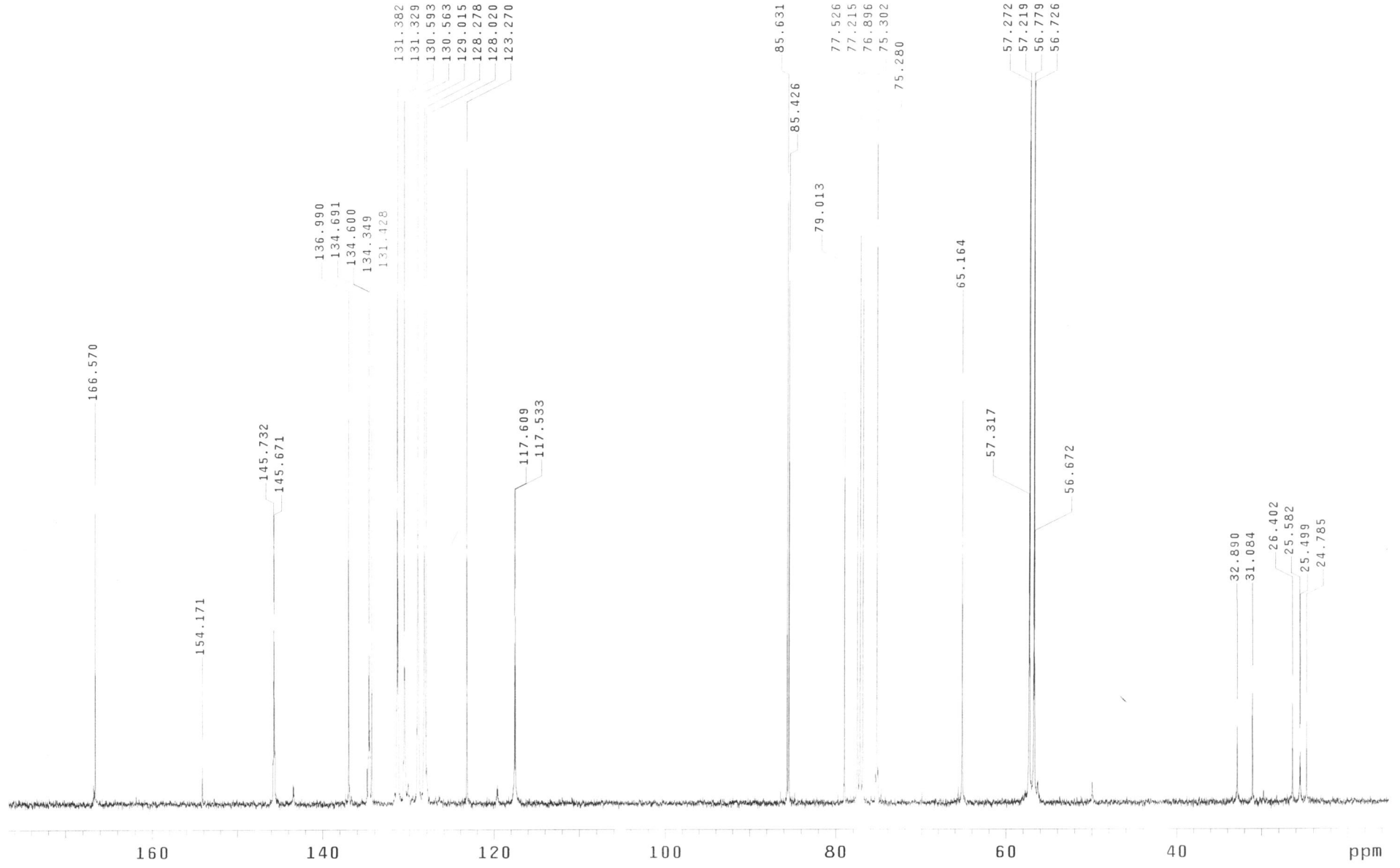
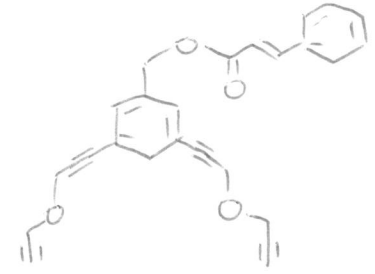
7.761
7.707
7.551
7.541
7.529
7.519
7.491
7.450
7.397
7.387
7.375
7.260
6.514
6.460

5.180
4.478
4.319
4.311

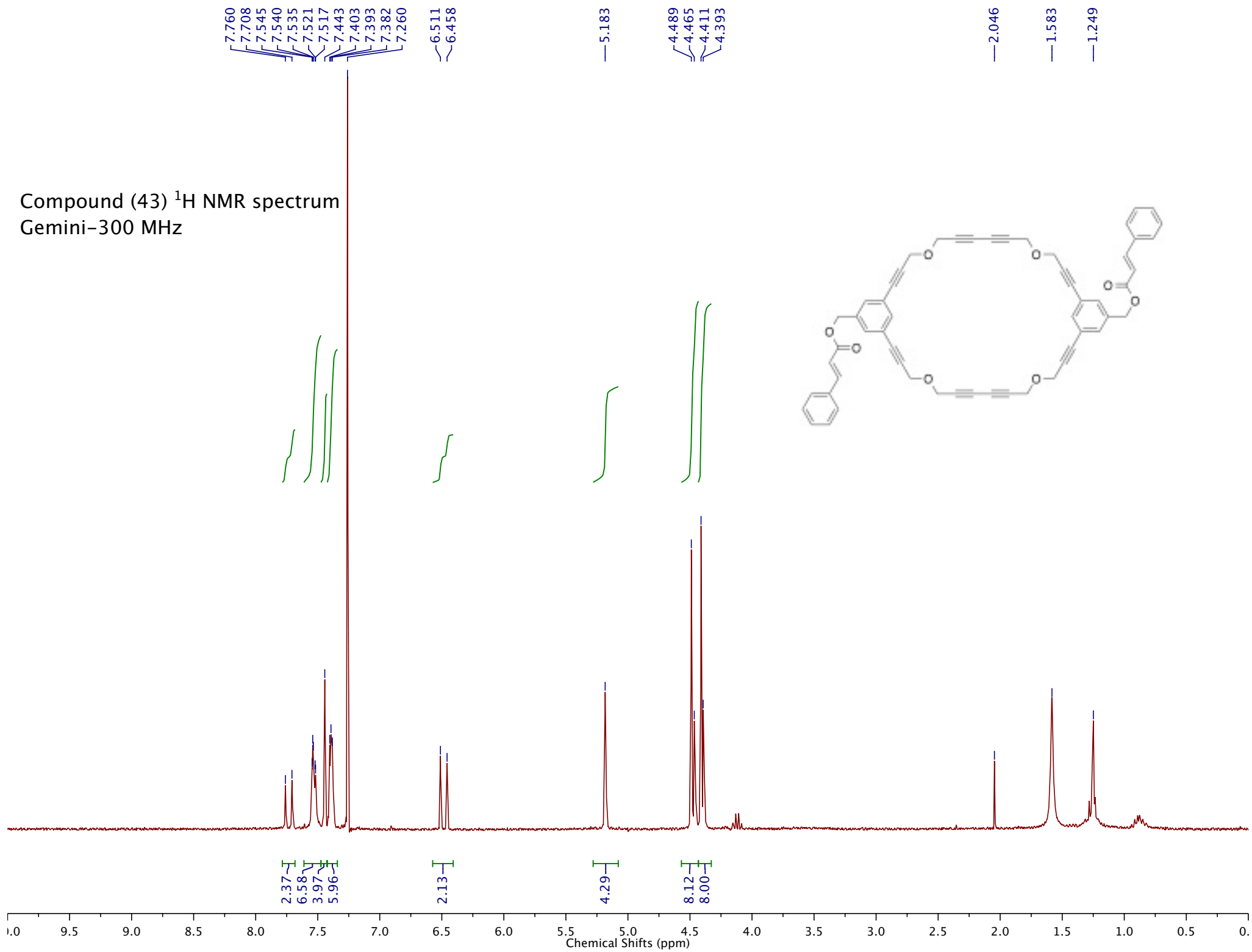
2.496
2.488
2.480



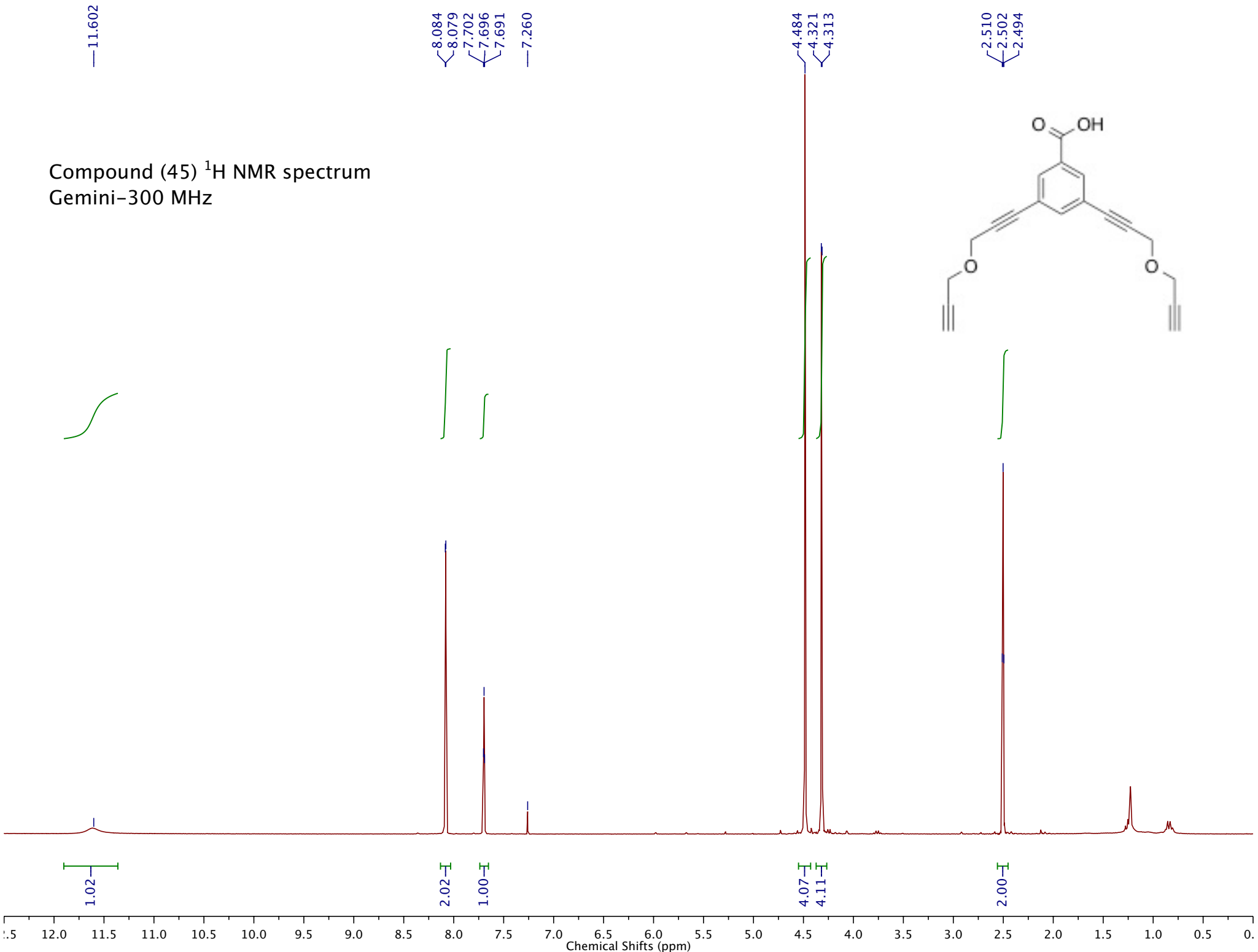
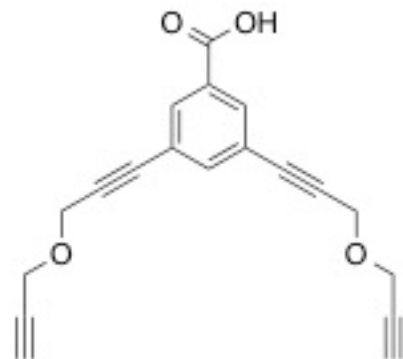
Compound 42



Compound (43) ¹H NMR spectrum
Gemini-300 MHz



Compound (45) ¹H NMR spectrum
Gemini-300 MHz



Compound 45

¹³C OBSERVE

Pulse Sequence: s2pu1

Solvent: CDCl₃
Temp. 25.0 C / 298.1 K
INOVA-400 "inv400"

Relax. delay 1.000 sec
Pulse 66.3 degrees
Acq. time 1.199 sec
Width 25000.0 Hz
128 repetitions
OBSERVE C13, 100.5376778 MHz
DECOUPLE H1, 399.8334198 MHz
Power 47 dB
continuously on
WALTZ-16 modulated
DATA PROCESSING
Line broadening 1.0 Hz
FT size 65536
Total time 1 hr, 13 min, 36 sec

